

MATURITY, OIL SOURCE ROCK AND RETORTING POTENTIAL OF PERHYDROUS COALS IN THE CENTRAL TERTIARY BASIN, SPITSBERGEN

Jacob Onyebuolise Uguna

Thesis
Submitted to the University of Nottingham
for the degree of
Doctor of Philosophy

November 2015



ABSTRACT

The occurrence of perhydrous (oil-prone) coal deposits within the Firkanten Formation of the Central Tertiary Basin (CTB) in Spitsbergen, is well documented and the oil present is reportedly sourced from the coals (Mokogwu, 2011; Marshall *et al.*, 2015a). This study uses a total of 146 coal samples covering areas of the eastern coalfield (Bassen, Breinosa and Lunckefjellet) and the western coalfield (Colesdalen) of the CTB to investigate the maturity, oil source rock potential, and retorting potential of these perhydrous coals. In addition, the controls on the oil potential of the coals are considered to provide measures that could be used to determine the optimum resource areas in the basin. Samples were provided by Store Norske Spitsbergen Kulkompani AS, and include drill cores, mine sections and outcrop sections from the Svea, Longyear, Svartepet and Askeladden seams (eastern coalfield), and the Sputnik and Verkny seams (western coalfield).

The vitrinite reflectance (VR) of the investigated coals are suppressed by bitumen impregnation and hydrogen enrichment of vitrinites; this is indicated by a general decrease in VR towards the top of the Longyear seam, which correlates with increasing Soxhlet yields towards the top of the seam, and a strong negative correlation of VR vs HI (Hydrogen Index) (R^2 between 0.73 - 0.78 in all areas), which is not maturity induced. Other evidences of VR suppression include a relatively wide range of VR values (between 0.50 - 0.79% R_o) within these seams, which are notably ≤ 2.1 m thick in all areas investigated, and wide ranges of VR distribution with bi-modal histograms observed in most samples (due to maceral effects rather than mixing of coal seams). Additionally, aliphatic biomarker and aromatic maturity parameters do not decrease towards the top of the Longyear seam (contrary to VR which decreases towards seam top), and indicates that the coals are generally in the maturity range of around 0.70% R_o or higher. T_{max}

appear suppressed, and the re-arrangements of methylphenanthrene isomers with increasing maturity also appear delayed/suppressed when there is aliphatic enrichment. True (i.e. unsuppressed) VR was estimated using the Lo (1993) method which gives thermal maturities of around 0.68, 0.78, 0.80 and 0.88% R_o in the Bassen, Lunckefjellet, Breinosa and Colesdalen areas respectively. True VR values indicate peak temperatures of around 104 °C in Bassen, 116 °C in Lunckefjellet, 118 °C in Breinosa and 125 °C in Colesdalen. Coalification gradients in the Adventdalen area equate to around 0.37% R_o /km, with an estimated geothermal gradient of approximately 55 °C/km. Peak burial depths in the Adventdalen area range from 1.9 km (up-dip), to 2.2 km (down-dip), indicating an overall overburden erosion estimate of between 0.9 – 1.2 km. In the Lunckefjellet area, peak burial depth is around 2.1 km, which implies a missing overburden of 1.1 km. In Colesdalen, peak burial depths are considerably higher at around 2.3 km, with a missing overburden estimate of 1.4 km. The implications of these results on burial and subsequent uplift and erosion are discussed.

The oil potential of the studied coals appears to be mainly due to perhydrous detrovitrinites, although other vitrinites including collotelinite, in addition to some liptinites, may have significantly contributed. Rock-Eval analysis indicates that the coals are enriched in Type II and a mixture of Types II/III kerogens with high HI (150 - 410 mg HC/g TOC), variable TOC contents (44.5 – 89.8 %), and high S2 contents (109 – 368 mg/g), all of which indicate excellent oil potential. The mean S1 contents are 6.8, 11.8, 15.0 and 14.5 mg/g for the Bassen, Lunckefjellet, Breinosa and Colesdalen coals respectively, which reflect the maturity trend across these four localities (i.e. increasing maturity from Bassen, through Lunckefjellet, to Breinosa and Colesdalen). The Bassen coals are at the onset of oil generation, while the Lunckefjellet coals are at peak oil generation/onset of oil expulsion. The

Breirosa and Colesdalen coals however, are already expelling oil (meaning they are in the effective oil window), although all samples (i.e. from all four localities) have low production index ($PI < 0.10$), which suggest that significant expulsion have not occurred. Results indicate that the Lunckefjellet coals will give the best indication of the maturity at which oil expulsion occurs in the CTB.

The oil-proneness of the coals resulted from marine influence upon the peatlands, and the consequent marine sulphur enrichment (between 0.4 – 17.7 % S in the coals). The Askeladden, Svarteper and Verkny coals generally contain more sulphur than the Longyear and Sputnik coals, and this trend is consistent with that of oil potential. Between sample localities, oil potential generally increases in the direction towards the inferred palaeocoastline. The varying sulphur contents within seams and between localities are assessed, and the implications of this variation on oil potential are examined and discussed.

In addition to the influence of sulphur on oil potential, there are other marine as well as non-marine related factors on oil potential which have been examined and discussed to help in delineating the optimum resource areas in the basin. Results indicate that greatest oil potential is mainly due to the combination of the following factors:

- a) Thermal maturity (true VR of around 0.78% R_o)
- b) Relative sea level rise leading to S contents in excess of 0.5 %
- c) Stable hydrology (i.e. relatively large/stable groundwater catchment)
- d) Fe/S ratio significantly < 0.87
- e) Optimum pH levels (alkalinity, which favours high microbial degradation)
- f) Relative distance to inferred palaeocoastline and local topography
- g) Ash content ≤ 30 %

Retorting of the CTB coals showed highest bulk yields at Lunckefjellet (160 mg/g on dry whole coal – dwc basis), with sections within seams yielding up to 240 mg/g dwc. At Breinosa and Colesdalen, bulk yields of 140 and 100 mg/g dwc respectively were measured. Lowest bulk yield was measured at Bassen (80 mg/g dwc). Residual semi-coke ranges between 60 – 75 % of starting material in all areas. Retorting yields are notably limited by coal swelling/blocking of the reactor vessel; consequently, further work involving other methods such as the Grey-King assay are required to fully measure the retorting potential in these coals. With a maximum coal resource of 3,300 Mt, of which 600 Mt is recoverable in the CTB (Orheim, 1982), maximum hydrocarbon resource via retorting would range between 3,188 – 5,394 Mbbl in place, with 580 – 981 Mbbl recoverable by mining.

ACKNOWLEDGEMENT

The University of Nottingham's Dean of Engineering Research Scholarship for International Excellence, and the financial sponsorship from Store Norske Spitsbergen Kulkompani AS are gratefully acknowledged.

Special thanks to my principal supervisor Dr David Large, firstly for securing the financial sponsorship from Store Norske. Also, Dr Large was always physically available to support me both academically and otherwise, and I cannot thank him enough for this. Many thanks to my second supervisor, Prof. Collin Snape for his support. A very important financial support from Prof. Snape in January 2015 meant I was able to meet and present my final results to Store Norske in Stavanger, which also allowed me the opportunity to present part of my research at the Norwegian Geological Society winter conference of January 2015 in Stavanger. I also thank Dr Maria Jensen, my supervisor at the University Center in Svalbard (UNIS), and gratefully acknowledge Prof. Snorre Olausen of UNIS for his interest in this project throughout.

A big thank you to Dr Andrew Carr of Advanced Geochemical Systems (AGS) Ltd for his un-ending support including recommending important references and lending me books. I have gained invaluable knowledge on organic petrography from working alongside Dr A. Carr and I am very grateful.

Many thanks to Doctors William Meredith, Clement Uguna and Chris Marshall for their support. The support from Dr W. Meredith cannot be overstated and it is very much appreciated. I also thank Dave Cliff for his support particularly in training me on preparation of polished mounts for organic petrography, and Chris Somerfield for his support with ICP-AES and coal ashing training. In addition, I

acknowledge Helen Giberson for her support particularly in processing relevant documentation for my trips to Svalbard and Norway, and for being a very reliable conduit for information flow between Dr Large and I.

Many thanks to the geology team at Store Norske including Malte Jochmann, Morten Often and Bjarki Friis for their support throughout this project, and for making my trips to Svalbard a truly great experience. Special thank you to Malte Jochmann whose enthusiasm throughout ensured samples and supporting data arrived on time when requested.

Finally, and most importantly, huge thanks to my family. Firstly, to my wife, Sandra Uguna, without whom, this study would not have been possible. Thank you San for your patience and moral support throughout. Also, special acknowledgement to my daughter Audrey who brought me good luck and continues to give me joy. A special mention of our new baby who will be arriving soon; we cannot wait to see you. Massive thanks to Joe Uguna who made it possible for me to come and study in the UK in the first place, and for his support both financially and otherwise. The support from Dr Clement Uguna cannot be overemphasised and I am very grateful to him. I thank Churchill Uguna for his all-round support whenever needed. Special thanks to my mum and dad who visited the UK in the summer of 2011 to help when Audrey was born, thereby allowing me more time for my studies; however, they had to leave before the weather became too cold. Dad, your initial wish was for me to be a medical doctor but I am now a doctor anyway, and I am very happy knowing that you are very pleased. On a final note, the Uguna family is such a big family and it will be impossible to mention everyone; however, the support and prayers from every member of this great

family, of strongly opinionated individuals, is very much appreciated. Thanks everyone and God bless.

TABLE OF CONTENTS

Abstract	I
Acknowledgement	V
Table of contents	VIII
List of figures	XV
List of tables	XXVIII
Chapter One – Introduction	1
1.1. Context	1
1.2. Aims and objectives	5
Chapter Two – Literature Review	8
2.1. Coal	8
2.1.1. Coal macerals..	9
2.1.1.1. Vitrinite group	10
2.1.1.2. Liptinite group	11
2.1.1.3. Interfinitite group	11
2.1.2. Oil-prone macerals	12
2.1.2.1. Liptinites	12
2.1.2.2. Perhydrous vitrinites	13
2.1.3. Coalification, coal rank and maturation	13
2.1.3.1. Vitrinite reflectance	15
2.2. Petroleum	17
2.2.1. Main groups of compounds in petroleum	18
2.2.1.1. Alihatic hydrocarbons..	18
2.2.1.2. Aromatic hydrocarbons	19
2.2.1.3. Asphaltenes and resins	19

2.2.2.	Bitumen	20
2.2.3.	Kerogen	20
2.2.3.1.	Type I kerogen	21
2.2.3.2.	Type II kerogen	22
2.2.3.3.	Type III kerogen	22
2.2.3.4.	Type IV kerogen	23
2.2.4.	Petroleum alteration	23
2.2.4.1.	Biodegradation	24
2.2.5.	Biological markers	25
2.3.	Pyrolysis	30
2.3.1.	Rock-eval pyrolysis vs nitrogen pyrolysis (retorting)	30
2.3.1.1.	Coking and coke potential of the CTB coals	31
2.4.	Svalbard – geography, geology and coal mining	31
2.4.1.	Geographic and physical setting	31
2.4.2.	Tectonic setting	33
2.4.3.	Stratigraphy and coal occurrence	33
2.4.4.	Coal mining in Svalbard	36
2.5.	Summary and conclusions	40
Chapter Three – Sampling and Experimental Methods/Techniques								41
3.1.	Sampling, sample distribution and sample preparation	41
3.1.1.	Sampling and sample distribution	41
3.1.2.	Sample preparation	45
3.2.	Experimental methods	46
3.2.1.	Organic petrography	46
3.2.1.1.	Sample preparation	46

3.2.1.2.	Determination of vitrinite reflectance and maceral analysis	47
3.2.2.	Organic geochemistry	50
3.2.2.1.	Soxhlet extraction	50
3.2.2.2.	Rock-Eval 6 pyrolysis	51
3.2.2.3.	Nitrogen pyrolysis (retorting)	54
3.2.2.4.	Silica-alumina adsorption column chromatography	56
3.2.2.5.	Gas chromatography (GC)	58
3.2.2.6.	Gas chromatography–mass spectrometry (GC-MS)	60
3.2.2.7.	¹³ C NMR	63
3.2.2.8.	Py-GCMS	63
3.2.3.	Inorganic geochemistry	66
3.2.3.1.	Ash measurement	66
3.2.3.2.	ICP-AES	68
3.2.3.3.	Elemental Analysis	71
3.3.	Summary and conclusions	74

Chapter Four – Vitrinite Reflectance Variations in the Central

Tertiary Basin Coals, Spitsbergen – Implications

for Local and Regional Burial Models 75

4.1.	Introduction	75
4.2.	Vitrinite reflectance assessments in areas under study	78
4.2.1.	Adventdalen	79
4.2.2.	Lunckefjellet	82
4.2.3.	Colesdalen	86

4.2.4.	Summary	88
4.3.	Geochemical assessment of maturity..	89
4.3.1.	Alkane and biomarker distribution	89
4.3.2.	Maturity assessment using terpanes	96
4.3.3.	Maturity assessment using steranes and diasteranes	98
4.3.4.	Maturity assessment using alkanes..	99
4.3.5.	Maturity assessment using aromatics	102
4.3.5.1.	How reliable are the MPI-1 estimated maturity values?	106
4.3.6.	Summary	109
4.4.	Maturity and oil potential of the Longyear coals using Rock-Eval 6 analysis	110
4.5.	Assessing VR suppression effect using ¹³ C NMR	115
4.6.	The true maturity of the CTB coals under study	115
4.7.	Thermal regime and implications for overburden models	121
4.8.	Summary and conclusions	124

Chapter Five – Oil Source Rock and Retorting Potential of Perhydrous

	Coals in the Central Tertiary Basin, Spitsbergen	128
5.1.	Introduction	128
5.1.1.	Samples and methodology	131
5.2.	Oil-prone coals – characterisation and occurrence in the CTB	131
5.2.1.	Coal maceral analysis..	132
5.2.1.1.	Peatland environment and oil potential – the Longyear and Sputnik seams	132
5.2.1.2.	Peatland environment and oil potential – the Longyear vs Svarteper seam	141

5.2.2.	Rock-Eval 6 analysis - kerogen typing and source						
	rock potential	145
5.2.2.1.	Multiple S ₂ peaks and T _{max} shift				151
5.2.3.	Assessing source rock quality using Py-GCMS					155
5.3.	Oil present in the CTB coals under study			159
5.4.	Marine sulfur and oil potential of the CTB coals under study	..					161
	5.4.1. The Longyear peatland - oil potential, sea Level						
	drop/rise and peatland transition			164
	5.4.2. Organo-sulfur compound formation in the CTB..	..					169
5.5.	Thresholds for oil generation and expulsion from the						
	CTB coals	170
5.6.	Lower Carboniferous vs Tertiary coals in Spitsbergen						
	– petrography, maturity, oil generation and expulsion	..					183
5.6.1.	Petrographic description and maceral distribution	..					183
5.6.2.	Coal maturity	189
5.6.3.	Oil generation and expulsion	190
5.7.	Retorting potential of the CTB coals		195
5.7.1.	Retorting estimates	195
	5.7.1.1. Retorting yields in various areas				195
	5.7.1.2. Comparing retorting yields between the						
	Askeladden, Svarteper, Longyear, Verkny						
	and Sputnik seams in various areas				196
	5.7.1.3. Comparing retorting yields within the Longyear						
	and Sputnik seams in various areas				197
5.7.2.	How effective is the adopted retorting technique?						200
5.7.3.	Qualitative assessment of retort oils from the						
	studied coals	203

5.7.4.	Resource estimates	208
5.8.	Summary and conclusions	211

Chapter Six - Controls on the Oil Potential of Perhydrous Coals

	In the Central Tertiary Basin, Spitsbergen				215
6.1.	Introduction	215
6.1.1.	Sample distribution and methodology				216
6.2.	Biodegradation	216
6.2.1.	Organic geochemical assessment				216
6.2.2.	Biodegradation relative to hydrology, paleoenvironment and oil potential	224
6.3.	Sulfur and iron	229
6.3.1.	Controls on S and Fe supply to the Firkanten Fm. coals						230
6.3.1.1.	The Longyear and Sputnik Seams				231
6.3.1.2.	The Svarteper seam	239
6.3.2.	Marine control on S and Fe distribution – implications for oil potential	243
6.3.2.1.	The Longyear and Sputnik Seams				243
6.3.2.2.	The Svarteper seam	250
6.3.3.	Groundwater influence on the oil potential of the Firkanten Fm. coals	254
6.3.3.1.	The Longyear and Sputnik seams				255
6.3.3.2.	The Svarteper seam	261
6.4.	The influence of proximity to inferred palaeocoastline on oil and coal potential	264
6.4.1.	Coal ash	268
6.4.1.1.	Ash content and oil potential of the CTB coals						270

6.5.	Weathering	272
6.5.1.	Effects of weathering on bitumen content					273
6.6.	Summary and conclusions	275
Chapter Seven – Summary of Conclusions and Future Work								279
7.1.	Overall conclusions	279
7.2.	Future work	283
References								286
Appendices								329

LIST OF FIGURES

Figure	Caption	Page
Figure 1.1.	Map of the island of Spitsbergen in Svalbard showing the Central Tertiary Basin (CTB), the surface extent of the late Mesozoic – Cenozoic sediments and major settlements/locations of interest in this study	2
Figure 2.1.	Cholestane (tetracycloalkane) (C ₂₇ H ₄₈)	19
Figure 2.2.	Alkyltetrahydrophenanthrene (C ₁₉ H ₂₄)	19
Figure 2.3.	Pristane (2,6,10,14-tetramethylpentadecane)	25
Figure 2.4.	Phytane (2,6,10,14-tetramethylhexadecane)	26
Figure 2.5.	Phytol	26
Figure 2.6.	C ₃₅ hopane	26
Figure 2.7.	C ₂₉ sterane	27
Figure 2.8.	C ₂₉ diasterane	28
Figure 2.9.	Demethylation of regular hopane to form 25-norhopane	29

Figure 2.10.	Geographic setting of the Svalbard Archipelago	32
Figure 2.11.	Stratigraphy of the Van Mijenfjorden group representing the sedimentary infill of the CTB, Spitsbergen	36
Figure 2.12.	Map showing currently operating coals mines in Spitsbergen and locations of interest in this study	38
Figure 3.1.	Map of the northern CTB on the island of Spitsbergen showing sampling localities and sample types	43
Figure 3.2.	Preparation of petrographic specimens	47
Figure 3.3.	Maceral analysis guide for normal and boundary cases between macerals or between maceral and mounting medium	50
Figure 3.4.	Schematic of Soxhlet extraction setup	51
Figure 3.5.	A typical Rock-Eval 6 pyrogram	52
Figure 3.6.	Schematic of the coal retorting rig	56
Figure 3.7.	Schematic of silica-alumina adsorption column chromatography	58

Figure 3.8.	Schematic of gas chromatogram	60
Figure 3.9.	Schematic of gas chromatogram – mass spectrometer	62
Figure 3.10.	Schematic of a pyroprobe for Py-GCMS	65
Figure 3.11.	Ash content determination	68
Figure 3.12.	Schematic of inductively coupled plasma – atomic emission spectrometry (ICP-AES)	69
Figure 3.13.	Acid digestion kit for ICP-AES sample preparation	71
Figure 4.1.	Photomicrographs showing the fluorescing nature of various vitrinite group macerals in the CTB coals	80
Figure 4.2.	Comparing VR profiles within the Longyear seam across the Adventdalen sub-region	81
Figure 4.3.	VR variation within the Longyear seam in Bassen	83
Figure 4.4.	Comparing VR profiles within the Longyear seam across Lunckefjellet	84
Figure 4.5.	VR variation within the Longyear seam at Lunckefjellet BH15-2011 locality	85

Figure 4.6.	VR profile in the Sputnik seam in and VR histograms of samples C6 (80.5 cm above seam base) and C8 (34.50 cm from seam base) in Colesdalen BH3-2008 locality	87
Figure 4.7.	Representative TIC of the aliphatics in Soxhlet extracts	89
Figure 4.8.	Representative m/z 191 mass chromatogram of aliphatics in Soxhlet extract	91
Figure 4.9.	Representative m/z 217 and m/z 259 mass chromatograms of aliphatic fraction in Soxhlet extract	94
Figure 4.10.	Representative TIC of aliphatic hydrocarbons fraction of Soxhlet extracts from the Longyear and Sputnik coals in main areas under investigation	100
Figure 4.11.	Aliphatic and aromatic maturity assessments of the Longyear coal in Lunckefjellet BH15-2011 locality and Mine 7	104
Figure 4.12.	Comparing the mean relative abundance of phenanthrene and 1- 2- 3- and 9-methylphenanthrenes in the Longyear and Sputnik coals	105
Figure 4.13.	T_{max} vs HI of the Longyear and Sputnik coals	111

Figure 4.14.	VR vs HI of the Longyear and Sputnik coals	112
Figure 4.15.	Comparing trends of Soxhlet yield (dry whole coal basis) with VR from base to top of the Longyear seam in Mine 7 and Bassen	114
Figure 4.16.	Model for correcting the suppression of VR	118
Figure 5.1.	Comparing trends of detrovitrinite and Soxhlet yield in the Longyear seam at Bassen	133
Figure 5.2.	Photomicrographs of coals from Breinosa BH4-2009 locality	137
Figure 5.3.	Coal facies plot of the Longyear coals from Bassen, Lunckefjellet and Breinosa, and the Sputnik coals from Colesdalen	140
Figure 5.4.	The inertinite profiles of the Svarteper and Longyear seams at Lunckefjellet BH15-2011 locality	144
Figure 5.5.	Comparing TPI and Soxhlet yield (dwc) from base to top of the Longyear seam in Lunckefjellet BH15-2011 locality	145
Figure 5.6.	van Krevelen plot of 67 coals from the Askeladden, Svarteper, Longyear, Verkny and Sputnik seams from the four main areas under investigation	146

Figure 5.7	TOC vs S2 plot of 67 coals from the Askeladden, Svarteper, Longyear, Verkny and Sputnik seams from the four main areas under investigation	147
Figure 5.8.	Map showing variation in the mean Pristane/Phytane values across the CTB	151
Figure 5.9.A-D.	Rock-Eval 6 pyrograms showing multiple S2 peaks	153-154
Figure 5.10.	Representative TIC and <i>m/z</i> 69-71 from the Py-GCMS analysis of investigated coals (sample Ba1) showing selected components used to determine petroleum type and source rock organic facies	156
Figure 5.11.	(A) Composition of kerogen pyrolysates according to the chain length distribution of total resolved C ₁ - C ₅ , C ₆ - C ₁₄ <i>n</i> -alkanes plus <i>n</i> -alkenes and C ₁₅₊ <i>n</i> -alkanes plus <i>n</i> -alkenes. (B) Composition of kerogen pyrolysates of C ₅₊ fraction according to the proportion of <i>n</i> -alkyl moieties, aromatic moieties and resolved unknowns	158
Figure 5.12.	Photomicrographs of sample Br1 - the top 19 cm coal from Askeladden seam in Breinosa BH4-2009	163
Figure 5.13.	The sulphur trend from the base to top of the Longyear seam in Bassen	164

Figure 5.14.	Comparing the profiles of A) Sulphur contents, B) Soxhlet yield (dwc), C) Rock-Eval S1, D) Rock-Eval HI, from base to top of the Longyear seam at Bassen	167
Figure 5.15.	Comparing the profiles of Soxhlet yield from base to top of the Longyear seam in Bassen, Lunckefjellet and Mine 7, and the Sputnik seam in Colesdalen	168
Figure 5.16.	T_{max} vs Bitumen Index and the inferred rank threshold for oil and gas generation in the investigated coals	172
Figure 5.17.	T_{max} vs Quality Index and the inferred rank threshold for oil expulsion from the investigated coals	173
Figure 5.18.	Photomicrographs from coals in Breinosa BH4-2009 locality	174
Figure 5.19.	Photomicrographs from Longyear coals in Lunckefjellet BH6A-2007 locality	175
Figure 5.20.	Photomicrographs showing oil expulsion with Newton's rings from cracks on perhydrous vitrinites in coals from Breinosa BH4-2009 locality	176
Figure 5.21.	Comparing the Py-GCMS aliphatic traces of coals from the eastern and western coalfields of the CTB	178

Figure 5.22.	Comparing HI, S1 and Soxhlet yield in the Longyear seam in Bassen and the Sputnik seam in Colesdalen	180
Figure 5.23.	An east-west cross section through the Lower-Middle Carboniferous of Central Spitsbergen	185
Figure 5.24.	Map showing location of the Lower Carboniferous coal sample of this study (Pyramiden) relative to the cross section in Figure 5.23	186
Figure 5.25.	Photomicrographs of oil-prone Lower Carboniferous coal from Pyramiden, Spitsbergen	187
Figure 5.26.	Photomicrographs of oil-prone Lower Carboniferous coal from Pyramiden, Spitsbergen	188
Figure 5.27.	VR histogram of the Lower Carboniferous coal from Pyramiden	190
Figure 5.28.	<i>m/z</i> 69-71 from the Py-GCMS analysis of the Lower Carboniferous coal from Pyramiden	192
Figure 5.29.	T_{max} vs Quality Index plot of the L. Carboniferous coal from Pyramiden	193
Figure 5.30.	Mean bulk retorting yields from all areas of the CTB under study	196

Figure 5.31.	Comparing the retorting yields from base to top of seam for the Longyear coals in Bassen and Lunckefjellet BH15-2011, and Sputnik coals in Colesdalen BH3-2008	198
Figure 5.32.	Retorting yields vs Rock-Eval S1+S2 contents for the coals under study	201
Figure 5.33.	Soxhlet yields vs Free Swelling Index of the Sputnik coals under study	202
Figure 5.34.	Spitsbergen retort oils vs global crude oils	204
Figure 5.35.	Comparing representative TIC of aliphatic hydrocarbons between Soxhlet extracts and retort oil	207
Figure 6.1.	Comparing the profiles of Isoprenoid/ <i>n</i> -alkane ratios and Rock-Eval S1 from base to top of the Longyear seam in Mine 7	217
Figure 6.2.	Comparing the profiles of Isoprenoid/ <i>n</i> -alkane ratios and Rock-Eval S1 from bottom to top of the Longyear seam in Lunckefjellet BH15-2011 locality	218
Figure 6.3.	TIC of severely biodegraded oil seep from the western coalfield of the CTB	219

Figure 6.4.	Comparing sterane distribution in Soxhlet extracts from a Colesdalen coal with that of the biodegraded oil seep in Figure 6.3 as both samples are from the western coalfield of the CTB	220
Figure 6.5.	Comparing sterane distribution in the Soxhlet extracts from a Svarteper coal with that of a Longyear coal in Lunckefjellet BH15-2011 locality	221
Figure 6.6.	Comparing terpane distribution in the Soxhlet extracts from a Sputnik coal with that of the biodegraded oil seep, as both samples are from the western coalfield of the CTB	223
Figure 6.7.A-B.	Comparing sulphur vs diasterane/sterane plots of the Greta coals from Sydney Basin in George <i>et al.</i> (1994) with those of the Longyear coals under study	226
Figure 6.8.	Comparing sulphur vs diasterane/sterane, and ash vs diasterane/sterane plots of the Askeladden and Svarteper coals under study	227
Figure 6.9.	S vs Fe contents of the CTB coals under study	230
Figure 6.10.	Comparing the profiles of; Soxhlet yield, S content, Fe content and Fe/S ratio, within the Longyear seam in Bassen	245

Figure 6.11.	Comparing the profiles of; Soxhlet yield, S content, Fe content and Fe/S ratio, within the Longyear seam in Lunckefjellet BH15-2011	246
Figure 6.12.	Comparing the profiles of; Soxhlet yield, S content, Fe content and Fe/S ratio, within the Longyear seam in Lunckefjellet BH6A-2007	247
Figure 6.13.	Comparing the profiles of; Soxhlet yield, S content, Fe content, Fe/S ratio, within the Longyear seam in Lunckefjellet BH10-2009	248
Figure 6.14.	Comparing the profiles of; Soxhlet yield, S content, Fe content and Fe/S ratio, within the Sputnik seam in Colesdalen BH3-2008	249
Figure 6.15.	Comparing the profiles of; Soxhlet yield, S content, Fe content and Fe/S ratio, within the Svarteper seam in Lunckefjellet BH15-2011	251
Figure 6.16.	Comparing the profiles of; Soxhlet yield, S content, Fe content and Fe/S ratio, within the Svarteper seam in Lunckefjellet BH10-2009	252
Figure 6.17.	Fe and S discrimination relative to Soxhlet yield between the Longyear and Svarteper coal seams at Lunckefjellet	254

Figure 6.18.	Comparing the profiles of; A) Soxhlet yield on dwc basis, B-E) Groundwater controlled elements, in the Longyear seam in eastern Lunckefjellet (BH15-2011)	257
Figure 6.19.	Comparing the profiles of; A) Soxhlet yield on dwc basis, B-E) Groundwater controlled elements, in the Longyear seam in northern Lunckefjellet (BH6A-2007)	258
Figure 6.20.	Comparing the profiles of; A) Soxhlet yield on dwc basis, B-E) Groundwater controlled elements in the Longyear seam in Bassen	259
Figure 6.21.	Comparing the profiles of; A) Soxhlet yield on dwc basis, B-E) Groundwater controlled elements in the Sputnik coal in Colesdalen BH3-2008	260
Figure 6.22.	Comparing the profiles of; A) Soxhlet yield on dwc basis, B-E) Groundwater controlled elements, in the Svarteper seam in Lunckefjellet BH15-2011	262
Figure 6.23.	Comparing the profiles of; A) Soxhlet yield on dwc basis, B-E) Groundwater controlled elements in the Svarteper seam in southern Lunckefjellet BH10-2009	263

Figure 6.24.A.	The Longyear seam thickness map for the eastern CTB showing the influence of proximity of coal resource to inferred palaeocoastline during period of relative sea level drop	265
Figure 6.24.B.	The Longyear seam thickness map for the eastern CTB showing the influence of proximity of coal resource to inferred palaeocoastline during the period of relative sea level rise	266
Figure 6.25.	Variations in resource quality and quantity relative to the distance from inferred palaeocoastline along the Lunckefjellet N-S sampling cross section in Figure 6.24.A and B	267
Figure 6.26.	Soxhlet yield vs ash content discrimination between the Askeladden/Svarteper/Verkny and Longyear/Sputnik coals	270
Figure 6.27.	Comparing the ash and Soxhlet yield within the Svarteper seam (top) and the Longyear seam (bottom) in Lunckefjellet BH15-2011 locality	271

LIST OF TABLES

Table	Caption	Page
Table 2.1.	Summary of macerals in hard coal	10
Table 3.1.	Sample distribution	44
Table 3.2.	Grinding and polishing stages of petrographic specimen (mount) preparation	47
Table 3.3.	Reproducibility data of Rock-Eval 6 pyrolysis	54
Table 3.4.	Selected aromatic components from Py-GCMS (shown in Figure 5.10) used to determine petroleum type and source rock organic facies	66
Table 3.5.	SARM18 standard and reproducibility data for ICP-AES analysis	73
Table 3.6.	SARM19 standard and reproducibility data for ICP-AES analysis	74
Table 4.1.	Vitrinite reflectance and alkane parameters used to assess the source and maturity of the Firkanten Fm. coals under study	92

Table 4.2.	Vitrinite reflectance, hopane, sterane and aromatic biomarker parameters used to assess the source and maturity of the Firkanten Fm. coals under study	95
Table 4.3.	Comparing MPI-1 and MPDF estimated maturities in the four main areas of the CTB under investigation	108
Table 4.4.	Comparing data from various measures of thermal maturity for the CTB coals in the Bassen and Breinosa areas	119
Table 4.5.	Comparing data from various measures of thermal maturity for the CTB coals in the Lunckefjellet, Svea Nord and Colesdalen areas	120
Table 5.1.A	Maceral distribution of the Longyear coals from the Bassen and Lunckefjellet BH15-2011 localities	135
Table 5.1.B.	Maceral distribution of the Longyear coals from the Breinosa BH4-2009 and Mine 7 localities, and the Sputnik coals from Colesdalen BH3-2008 locality	136
Table 5.2.	Geochemical data from Marshall <i>et al.</i> (2015a), which compares oil potential between the Svea, Longyear, Svarteper and Askeladden coals	139

Table 5.3.	Comparing the maceral distribution of the Svarteper coals, the Upper Longyear (100 – 210 cm from seam base) coals and the Lower Longyear coals (0 – 90 cm above seam base) in Lunckefjellet BH15-2011 locality	143
Table 5.4.	Rock-Eval data of the Bassen and Breinosa coal samples under study	148
Table 5.5.	Rock-Eval data of the Lunckefjellet, Svea Nord and Colesdalen coals under study	149
Table 5.6.	Calculated percentages of the main resolved classes and parameters used to determine petroleum type and source rock organic facies from open Py-GCMS	157
Table 5.7.	Soxhlet yields of the Firkanten Fm coals under study	160
Table 5.8.	Sulphur data of the Firkanten Fm. coals under study	162
Table 5.9.	Comparing the <i>n</i> -alkanes + <i>n</i> -alkenes chain length distributions and VR of coals from the main areas under investigation	179
Table 5.10.	Maceral composition of the Lower Carboniferous coal from Pyramiden	184

Table 5.11.	Comparing geochemical data between the L. Carboniferous and Tertiary coals in Spitsbergen	192
Table 5.12.	Comparing the retorting yields and Rock-Eval S1+S2 contents of 44 CTB coals under study	199
Table 5.13.	Aliphatic, aromatic and polar contents of Soxhlet extracts and oils from retorting	205
Table 5.14.	Coal and liquid hydrocarbon resource estimate of the CTB coals	210
Table 6.1.	Summary of bulk <i>n</i> -alkane and isoprenoid ratios of the Longyear and Sputnik coals under study	218
Table 6.2.	Comparing the sulphur, ash and diasterane/sterane data from George <i>et al.</i> (1994) and this study	228
Table 6.3.	Bulk S and Fe contents, and Fe/S ratios of the CTB Coals Under study	230
Table 6.4.	Guideline for interpreting the strength of coefficient of correlation (R) as applied in this study	231
Table 6.5.	Major element distributions in the Longyear seam in Lunckefjellet	232

Table 6.6.	Correlation matrices of major elements in the Longyear seam in Lunckefjellet	234
Table 6.7.	Major element distribution in the Longyear seam in Bassen	236
Table 6.8.	Comparing the contents of major elements in coals of the Adventdalen area between current and previous studies	236
Table 6.9.	Correlation matrix of major elements in the Longyear seam in Bassen	237
Table 6.10.	Major element distribution in the Sputnik seam in Colesdalen	237
Table 6.11.A.	Correlation matrix of major elements in the Sputnik seam in Colesdalen	238
Table 6.11.B.	Correlation matrix of major elements in the Sputnik seam in Colesdalen after excluding an outlier	239
Table 6.12.	Major element distribution in the Svarteper seam in Lunckefjellet	240
Table 6.13.	Correlation matrices of major elements in the Svarteper seam in Lunckefjellet	242

Table 6.14.	Comparing Soxhlet yield, coal thickness and sulphur contents at Lunckefjellet and Bassen	267
Table 6.15.	Ash data of the Firkanten Fm. coals under study	269

INTRODUCTION

The main aims of this PhD study is to investigate the maturity, oil source rock potential and retorting potential of perhydrous coals in the CTB in Spitsbergen, Svalbard (Figure 1.1). The controls on the oil potential of the coals are also examined to provide measures that could be used in the delineation of optimum resource areas in the basin. Additionally, the Lower Carboniferous and Tertiary coals in Spitsbergen are compared with respect to oil potential.

1.1. Context

Oil prone coals are generally perhydrous, and they show a general trend of increasing hydrogen content with increasing sulfur content (e.g. Petersen, 2006). Over the past 20 to 30 years, there are numerous publications discussing various important aspects of coal as a source rock of liquid hydrocarbons (e.g. Saxby and Shibaoka, 1986; Bertrand *et al.*, 1986; Fleet and Scott, 1994; Powell and Boreham, 1994; Iglesias *et al.*, 2002; Boreham *et al.*, 1999; Petersen, 2005; 2006); this subject is extensively reviewed by Wilkins and George (2002). There are two types of oil-prone coals in Svalbard, they include;

- a) The Lower Carboniferous coals previously mined at Pyramiden (Figure 1.1) (Abdullah *et al.* 1988, Nøttvedt *et al.* 1993, Harland *et al.* 1997, Moi, 2008; Tangedal, 2011). These coals represent the oil-prone coals formed at the equator (van Koeverden *et al.*, 2010, van Koeverden *et al.*, 2011, Bojeson-Koefoed *et al.*, 2012, Macgregor, 1994), and their oil-proneness is attributed to their high liptinite content.

- b) The Lower Palaeogene coals from the Central Tertiary Basin (CTB) in Svalbard (Figure 1.1). These coals represent the oil-prone coals formed in

high latitude regions (Sandison *et al.* 2002, Vu *et al.* 2009, Killops *et al.* 1994). Their oil-proneness is inferred to result from their perhydrous vitrinite content (Marshall *et al.*, 2015a; Marshall *et al.*, 2015b) and they are the main focus of this study.

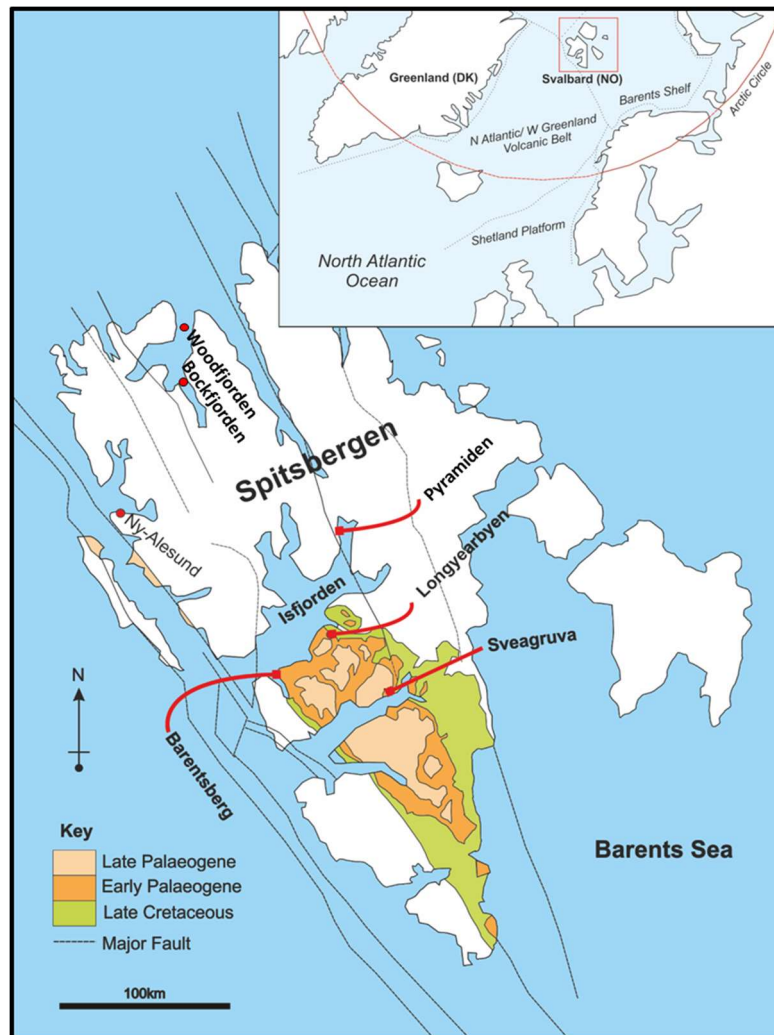


Figure 1.1. Map of the island of Spitsbergen in Svalbard showing the Central Tertiary Basin, the surface extent of the late Mesozoic – Cenozoic sediments and major settlements/locations of interest in this study (modified from Marshall, 2013).

Liquid hydrocarbon generation from coals and coaly source rocks is known from many parts of the world, especially in the Australasian region (MacGregor 1994;

Todd *et al.* 1997). Although oil prone coals from the Taranaki Basin, New Zealand (Killops *et al.*, 1998) and from the Danish North Sea (Petersen, 2005) have been broadly characterised, the CTB coals present an invaluable opportunity to understand the processes and conditions required for oil prone coal formation in the high Arctic, with Marshall (2013) suggesting that the unique temperate high latitude Palaeocene climate of Svalbard played a significant role. Coal mining in Spitsbergen has been a primary activity throughout the last century; Cretaceous coals in Advent City and Carboniferous coals in Pyramiden have been mined in the past (Harland *et al.*, 1997), while the Palaeocene coals within the CTB which constitute the basis of this PhD study are currently exploited. Orheim (1982) used the Monte Carlo simulation to estimate coal resource of 3,300 Mt, of which 600 Mt was recoverable within the CTB.

In the vitrinite reflectance (VR) records of the CTB, apparent gaps and inversions (large decrease and/or increase in VR within a relatively small depth range) appear common, particularly between the Triassic-Jurassic boundary and Cretaceous-Basal Tertiary strata (Paech and Koch, 2001). Orheim *et al.* (2007) also reported a VR gap within the basal Tertiary Firkanten Fm. coal seams, which stratigraphically, are only 40 meters apart, and proposed it is due to VR suppression by bitumen enrichment and/or thermal insulation from underlying seams. This study utilises high resolution sampling from various areas of the CTB to examine whether reported VR variation could be replicated. Additionally, organic biomarkers, Rock-Eval 6 and aromaticity were utilised to provide alternative estimates of maturity. Assuming VR values of the coals do not represent the true maturity within the CTB, previous thermal regime and overburden erosion estimates (Manum and Thronsen, 1978), would need to be re-evaluated.

Tertiary coals from the Kings Bay (Ny-Alesund) region (Figure 1.1) were reported by Hoel (1925) to have been successfully retorted by low temperature distillation at a small scale during the 1920's, producing average hydrocarbon yields of 180 – 214 mg/g coal. Retorting of the Firkanten Formation CTB coals from the Breinosa area was simulated using nitrogen pyrolysis on bulk samples to produce yields between 175 – 195 mg/g while leaving a potentially valuable residual coke (Wang, 2011). The Kings Bay and CTB, now geographically separate are thought to have been formed synchronously (Harland *et al.*, 1976); thus, the yields from retorting coals from the Breinosa area may be a basin wide feature and would represent a significant oil resource. Therefore, with coal resource in excess of 3,000 Mt (Orheim, 1982), the CTB may represent an unconventional hydrocarbon province. However, any form of gaseous/liquid hydrocarbon exploitation technique, be it in-situ or ex-situ, would depend on the distribution of oil prone materials and oil quality. Consequently, this study uses high resolution sampling in an attempt to confirm and expatiate on the oil source rock and retorting potential of the CTB coals, and to find out whether documented yields can be replicated in different areas of the basin.

The perhydrous nature of coals is highly dependent on sulphur; H₂S combines with organic matter to form organosulfur compounds – OSC (e.g. Sandison, 2001), which in turn allows the preferential preservation of hydrogen rich plant components (Sinninghe Damsté and de Leeuw, 1990; Sandison, 2001; Sandison *et al.*, 2002), and ultimately leads to the formation of perhydrous coals. The sulfur content in peat is closely related to its depositional environment; peats accumulating in a freshwater environment will generally have lower sulfur content than peats accumulating under the influence of seawater (Chou, 2012). Considering the CTB coals are influenced by seawater (e.g. Orheim *et al.*, 2007;

Marshall *et al.*, 2015a), coal sulphur contents and distribution are expected to vary between areas of the CTB in relation to distance from inferred palaeocoastline. Also, considering sulphate reducing bacteria will produce H₂S (in anaerobic conditions) to levels which exceed iron supply in order for a depositional environment to allow the formation of OSC (Sandison, 2001), the relative contents and distribution of sulfur and iron in different areas of the CTB will significantly influence the variation of oil potential in the basin. Consequently, a geochemical study of sulfur and iron will provide invaluable information that will help in delineating areas of optimum hydrocarbon resource in the CTB. This constitutes another major aspect of this study.

1.2. Aims and Objectives

The main aims of this PhD study are as follows:

- a) Investigate the true maturity of the Firkanten Fm. coals in the CTB
- b) Assess the source rock and retorting potential of the coals
- c) Assess whether there is a basin wide variation in oil potential.
- d) Assess and understand possible controls on oil potential to allow delineation of potential areas of optimal coal and hydrocarbon resource.

To achieve the above aims, the following objectives are met within various chapters as follows:

- Chapter 2 discusses the relevant aspects relating to the main concepts and keywords of this PhD study including coal, petroleum, retorting and the geology of Svalbard.

- Chapter 3 gives details of sampling and sample locations, the adopted methods/techniques utilised and demonstrates the reliability of data obtained.
- Chapter 4 investigates the maturity of the Firkanten Fm. coals. This was achieved by assessing the bulk and high resolution vitrinite reflectance (VR) measurements to examine whether reported VR variability within and between the Firkanten Fm. coal seams of the CTB (e.g. Orheim *et al.*, 2007) is replicated. Other maturity parameters such as organic biomarkers, Rock-Eval 6 and aromaticity were utilised to provide alternative estimates of maturity. Results from both sections were reconciled and related to oil potential to determine the true maturity of the Svalbard coals. This chapter goes on to examine the implications of VR variability on thermal regime and overburden estimates.
- Chapter 5 focuses on the source rock and retorting potential of the CTB coals. Firstly, coal maceral analysis, Rock-Eval analysis, Soxhlet extracts and sulfur contents were used to investigate whether there are variations in oil potential in the basin. Rock-Eval analysis and Py-GCMS were then applied to assess kerogen type and quality. The Tertiary and Lower Carboniferous coals in Spitsbergen are then compared in terms of oil potential using organic petrography and geochemical assessments. Finally, coal retorting potential was assessed in different areas of the basin leading to hydrocarbon resource estimates.
- Chapter 6 examines controls on oil potential within and between coal seams in different areas of the basin through the use of coal maceral

analysis, and organic and inorganic geochemical analyses. Findings from this chapter provides useful information that will help in delineating optimum resource areas.

- Chapter 7 summarises the main goals of this study, and discusses the conclusions drawn with particular attention to how oil potential varies within the CTB. It also highlights key indicators and controls on oil potential. This chapter concludes by discussing the future work.

Findings from this study will be invaluable for the short and long term planning for prospecting and mining not just in Lunckefjellet, where a new mine is scheduled to commence production when the Svea Nord coal deposits becomes depleted, but in Svalbard at large. Notably, geochemical and petrographic data will become available for areas which have not been previously investigated such as the western coalfield of the CTB as the investigation of the Verkny and Sputnik coal seams from this part of the basin will possibly allow the identification of their eastern CTB equivalent.

LITERATURE REVIEW

This chapter discusses relevant aspects of coal, petroleum, retorting and the geology of Svalbard.

2.1. Coal

Coal is derived from the rapid accumulation and burial of terrestrial/land derived plant materials in depositional environments in sedimentary basin. The original sediment formed during coal formation process is a damp, spongy material called peat. This later becomes dried, compressed and modified both in composition and texture due to the overburden pressure associated with burial (Ward, 1984). The conversion of plant materials to peat is called peatification or peat diagenesis, while the development from peat through the different stages or ranks of coal is called coalification (Taylor *et al.*, 1998). Peat formation is facilitated by the presence and rapid accumulation of large amounts of plant materials; the conditions necessary for the formation of thick peats are summarised by Teichmüller and Teichmüller (1982) as follows:

- *A slow, steady and continuous rise of the groundwater table i.e. subsidence.*
- *Adequate protection of the swamp area by features such as sand bars, against major floods by sea and rivers.*
- *A low energy relief which would restrict the supply of river sediments which could hinder the peat formation process.*

Previous studies by Dallmann (1993) revealed that these kinds of conditions operated in the early Svalbard basin; however, coal seam formation generally depends on the palaeogeographical and structural interactions within the

sedimentary region (Teichmüller and Teichmüller, 1982). Different kinds of peat originate as a result of varying original material and burial conditions, which eventually leads to the formation of different kinds of coals, although the ultimate peat characteristics are determined by the type and composition of the parent plant (Tissot and Welte, 1984). In a situation where the peat is derived from abundant hydrogen-rich land-plant components such as spores, cuticles and resins, such peat will mature to perhydrous coals that will have the capacity to generate liquid hydrocarbons. This is believed to be the case of the coals in Svalbard and some Australian coals (Scott and Fleet, 1994).

2.1.1. Coal Macerals

Macerals are the basic organic constituents of coals which can be recognised at the microscopic scale (Kearey, 2001). Macerals can be compared with minerals in inorganic rocks but there is a difference; whereas a mineral is characterised by a fairly well-defined chemical composition due to the uniformity of its substance, and by the fact that minerals are crystalline, a maceral of coal varies widely in its chemical composition and physical properties and is not crystalline (Stach, 1982). Table 2.1 shows the three main maceral groups in coals; these groups can be subdivided into macerals and sub-macerals. According to Teichmüller (1989), the degree, length and depth of burial (which signifies rank) of coal forming materials is pivotal for the microscopic appearance of macerals, although the parent plant materials and climate are also influential. Stach (1982) reported that as rank increases, macerals vary and their physical, chemical and technological properties are altered; hence, coal technologists have established the presence of a clear relation between the reflectance of a coal maceral and the coal rank. Coal structure and reflectance under incident light are the main parameters used

to differentiate macerals and maceral groups under the microscope. The three main maceral groups and macerals in coals are further discussed below.

Maceral group	Maceral sub-group	Maceral	Hydrocarbon potential
Vitrinite	Telovitrinite	Telinite	Hydrogen poor; mainly precursors for gas, except detrovitrinite which is perhydrous
	Detrovitrinite	Collotelinite	
		Vitrodetrinite	
	Gelovitrinite	Collodetrinite	
Liptinite		Corpogelinite	Hydrogen-rich; precursors for oil and gas
		Gelinite	
		Sporiite	
		Cutinite	
		Resinite	
		Fluorinite	
		Alginite	
		Suberinite	
		Liptodetrinite	
		Bituminite	
Inertinite		Chlorophyllinite	Very hydrogen-poor; largely inert, but may produce gas at very late stages of maturation
		Exsudatinite	
		Fusinite	
		Semifusinite	
		Funginite	
		Secretinite	
		Macrinite	
Micrinite			
Inertodetrinite			

Table 2.1. Summary of the macerals in hard coal (ICCP, 1998; Boreham and Powell, 1993; Taylor *et al.*, 1998)

2.1.1.1. Vitrinite Group

Vitrinites are by far the most frequent, complex and abundant maceral group occurring in bituminous coals (e.g. Scott, 2002). They originate mainly from humic substances, which are dark coloured compounds of complex composition. These substances are largely alteration products of lignin and cellulose from plant cell walls, and also from tannings which permeate cell walls and fill cell lumens Teichmüller (1989). Beyond containing true plant material, this group also contains detrital materials and chemical precipitates. The main morphological distinction between the members of this group is made between the cell wall (telinites), gels (gellinites/collinites) and the detrital material (detrinites) (ICCP, 1998). When

compared with other macerals, vitrinites have an intermediate reflectance which is lowest in high volatile coals and increases with rank. Hydrogen rich vitrinites are regarded as oil-prone and are very important in source rock studies (Wilkins and George, 2002, Marshall *et al.*, 2015a; b and references within). It is well documented that vitrinites are the most abundant maceral group in the CTB coals (Ćmiel and Fabianska, 2004; Marshall, 2013; Orheim *et al.*, 2007) with detrovitrinite macerals dominating.

2.1.1.2. *Liptinite Group*

This group is often referred to as the exinite group. Some of the most characteristic macerals of this group include sporiite, cutinite, resinite, alginate, suberinite, liptodetrinite, and chlorophyllinite. Others include fluorinate, bituminite and exsudatinitite whose first recognition was relatively late (Taylor *et al.*, 1998). Liptinites originate from hydrogen-rich plant organs as well as from decomposition products and algal and bacterial substances (Teichmüller, 1989). They are the least abundant, lightest and most volatile macerals (Scott, 2002); their hydrogen rich nature makes them important as oil-prone macerals despite their limited distribution (Hunt, 1991; Boreham and Powell, 1993). Crelling (1987) stated that the most outstanding petrographic property of the liptinite group is that they have a reflectance that is lower than that of the vitrinites and inertinites in the same coal sample. Liptinite contents of 2 – 3 vol %, dominated by sporonite, liptodetrinite and cutinite have been reported in some Longyear and Svea coals in the CTB (Orheim *et al.*, 2007).

2.1.1.3. *Inertinite Group*

Inertinite is obtained from the word 'inert' meaning they are typically unreactive (Stach, 1982). The distinguishing properties of inertinites include high reflectance,

little or no fluorescence, high carbon and low hydrogen contents (Scott, 2002); hence they are quite unimportant with regards to their oil-proneness but are relevant in classifying coals in a general sense. The chemical and botanical precursors of inertinites are mainly the same as those of vitrinites namely cellulose and lignin from cell walls of plants. However, these constituents experience a quite different history, which has been described as fusinitization (e.g. Taylor *et al.*, 1998). Fusinitization produces substances with relatively high carbon contents, low hydrogen contents and, for the same H/C ratio, a higher O/C ratio than for vitrinite. With regards to the “inert” nature of inertinites in general, Stach (1982) observed that the maceral micrinite is not inert and in fact, differs in its origin from the rest of the inertinites with reports (e.g. Taylor *et al.*, 1998) suggesting it is a remnant of oil generation. However, it is still grouped under the inertinite group which is a very diverse group. In the CTB, significant difference in inertinite concentration has been reported between the Longyear coals (7 vol %) and the Svea coals (45 – 51 vol %) (Orheim *et al.*, 2007).

2.1.2. Oil-Prone Macerals

Liptinites and perhydrous vitrinites have been identified as the two main groups of oil-prone macerals (e.g. Boreham and Powell, 1993; Wilkins and George, 2002).

2.1.2.1. Liptinites

The hydrogen rich nature of liptinites makes them important as oil prone macerals despite their limited distribution (Hunt, 1991; Boreham and Powell, 1993). There have been several attempts at estimating the minimum volume percentage level of liptinite in a coal for it to be considered capable of generating oil (Snowdon, 1991); however, it has become apparent that not all liptinitic macerals are of the same quality for petroleum generation. Based on the abundance of aliphatic

carbons in ^{13}C NMR spectra of a suite of purified macerals, Qin *et al.* (1993) proposed the potential of liptinite macerals to form hydrocarbons was in the order alginite, resinite, cutinite, sporinite, and suberinite.

2.1.2.2. *Perhydrous Vitrinites*

Certain vitrinites, such as those from marine-influenced coals, have an increased 'wax-resin' component (Stach *et al.*, 1982; Taylor *et al.*, 1998); these vitrinites are characterised by a reddish-brown fluorescence under blue light excitation, high fluidity and swelling properties in coking tests. The visible fluorescence of these vitrinites is commonly taken to be a strong indicator of a hydrogen-rich composition when chemical analyses are not available and are called perhydrous vitrinites (Taylor *et al.*, 1998). The reason for the oil-prone nature of perhydrous vitrinite is not clear; Shanmugam (1985) suggested it is due to the destruction of liptinite during petroleum generation, Taylor *et al.* (1998) reported it is due to dispersed sub-microscopic lipids, while Killops *et al.* (1994) attributes it to the oil-proneness of detrovitrinite.

2.1.3. Coalification, Coal Rank and Maturation

Following the deposition of peat, a combination of geochemical and geologic processes eventually paves the way for coalification; this is the physical and chemical conversion of peat into various types of coal due to the action of temperature, pressure, time and biochemical interactions (Taylor *et al.*, 1998; Orem and Finkelman, 2003). The terms peat, brown coal (lignite), sub-bituminous coal, bituminous coal and anthracite coal represent various stages of the coalification series. These stages of coalification are referred to as levels of rank which serve as an indication of the progression of peat all the way to anthracite coal (Teichmüller and Teichmüller, 1982; Tissot and Welte, 1984 and references

within). The main ranks of coal exhibit some physiochemical characteristics as outlined by Kearey (2001) as follows:

- Peat – this is considered to be the precursor of coal and has a dark brown appearance.
- Lignite (brown coal) – this is the lowest rank of coal. It is soft and has a fixed carbon content of 40 – 60 %.
- Sub-bituminous – this displays properties of sub-bituminous coal range from those of lignite to those of bituminous coal with a fixed carbon content of 40 – 60 %.
- Bituminous - this is considered intermediate between brown coal and anthracite and generally rich in volatile hydrocarbons.
- Anthracite – this is the highest rank of coal with a high carbon content and very low content of volatile materials.

According to Taylor *et al.* (1998), increasing rank (i.e. from peat to anthracite) is not only characterised by chemical and physical, but also petrographic changes and all changes vary in the different rank stages. The main chemical reactions include condensation, polymerisation, aromatisation and the loss of functional groups containing oxygen, sulfur and nitrogen. The carbon content increase but not linearly. The main physical changes are those of porosity, density and hardness. In terms of petrographic changes (i.e. microscopic observation), the translucency of macerals, which depends on their refractive and absorptive indices, decreases, the reflectance and bireflectance (anisotropy) of huminites/vitrinites and liptinites increases, while the fluorescence properties of liptinites and huminites/vitrinites change in a characteristic way. Increase in reflectance is one of the most characteristic changes during progressive coalification of huminites/vitrinites (Taylor *et al.*, 1998); as the coals under study

are of bituminous rank, the focus will be on the reflectance of vitrinite which is further discussed in Section 2.1.3.1.

Coalification and maturation follow the same trend, i.e. the loss of functional groups and of oxygen and an increase in carbon content (Taylor *et al.*, 1998). The process of maturation is what converts the immature organic matter source rocks to oil and gas, and for coals this would occur during the initial stages of coalification (Hunt, 1991; 1995). During the coal maturation process, mobile products such as gas and crude oil are expelled from the coal lattice with subsequent aromatisation and condensation of the solid residual product (coal) taking place (van Krevelen, 1984). Petroleum generation from coal organic matter begins under the pressure, temperature and time conditions when the coals pass through the sub-bituminous stage and end when the coals have reached a medium-bituminous rank. The degree of bituminisation is synonymous with the maturity of the crude oil generated by the coal and this serves as the basis for measuring the maturity at which coals can expel crude oil (Teichmüller, 1989).

2.1.3.1. Vitrinite Reflectance (VR)

The term maturation is used for the diagenetic development of organic matter that leads to the formation of petroleum and natural gas from source rocks (Taylor *et al.*, 1998). Thus, thermal maturity is established as the route to petroleum generation and VR serves as a correlating tool for determining the maturity at which source rocks will generate and expel oil (Killops *et al.*, 1998; 2002). Understanding the process of coal maturity is important in characterising oil-prone coals and the degree of maturation can be measured by different parameters including vitrinite reflectance. R_o is a measure of the percentage of incident light

(546 nm wavelength) that is reflected off the surface of a vitrinite maceral in a polished mount of kerogen, coal or whole rock, under an oil-immersion microscope objective (e.g. Taylor *et al.*, 1998; Peters *et al.*, 2005). Reflectance measurement is usually done on the vitrinite maceral because vitrinites show a moderately consistent increase in reflectance with increasing rank (Crelling *et al.*, 1988). VR ranges of 0.5 - 0.6% R_o to 1.30 - 1.35% R_o has been suggested as the maturity threshold for which coals will generate oil (e.g. Hunt, 1991).

A major limitation in the use of VR to determine maturity was reported by Teichmüller and Teichmüller (1967); these workers noted certain important disconformities or jumps in VR ranges with increase in rank. The first jump is between the range of 0.6 - 0.7% R_o and the second is between the range of 1.3 - 1.4% R_o ; these were referred to as the first and second coalification jumps respectively. The first jump coincides approximately with the start of oil generation from kerogen. The second jump is caused by a marked loss of oxygen (as CO_2 and H_2O) during coalification process, and by the beginning of hydrogen release in the form of methane, correlating approximately with the 'death line' for oil generation (Taylor *et al.*, 1998).

Another limitation in the use of VR for maturity determination is the suppression of VR due to the adsorption of hydrogen rich components by vitrinites (Diessel and Gammidge, 1998; Carr, 2000 and references within). Petersen and Rosenberg (1998) referred to hydrogen-enriched vitrinite as having retarded reflectance, but retardation applies to the the inhibition of the maturation process due to high pressures (Carr 2000; Carr *et al.*, 2009; Uguna *et al.*, 2012, 2015). The effect of VR suppression is the reduction of VR values in very hydrogen rich coals. Consequently, coals experiencing VR suppression may generate oil at maturity

levels less than 0.50% R_o . Although Orheim *et al.* (2007) reported VR values averaging 0.71% R_o for the Longyear seam in the CTB indicating that they are in a maturity range for petroleum generation, the perhydrous nature of these coals (Mokogwu, 2011, Marshal, 2013; Marshall *et al.*, 2015a; b) implies the measured VR values may not reflect their true maturity. Consequently, the VR gap within the Longyear coal seam (Orheim *et al.*, 2007) may be due to suppression and will be further investigated in this study.

2.2. Petroleum

Petroleum is defined as a mixture of hydrocarbons containing small quantities of oxygen, nitrogen, and sulphur bearing compounds, and traces of metallic constituents. Its physical state may be gaseous, liquid or solid, depending on the nature and on the proportion of the different compounds of which it is constituted, and also on the existing conditions of temperature and pressure (Tissot and Welte, 1984). Littke and Leythaeuser (1993) cited by Wilkins and George (2002), summarised observations that indicate there could have been important petroleum generation from coals:

- Coals may contain significant quantities of the hydrogen-rich and hydrocarbon-generating macerals
- When heated, coals produce petroleum-like pyrolysis products.
- Bituminous coals contain bitumen that can be easily released by extraction using common solvents.
- Coals are a major source of methane.
- Some gas and oil accumulations occur in close proximity to coal seams.
- The maturation sequence of terrestrial organic matter through peat, bituminous coal and anthracite implies a significant loss of volatile products, including hydrocarbons.

2.2.1. Main Groups of Compounds in Petroleum

Petroleum is composed mainly of aliphatic hydrocarbons, aromatic hydrocarbons, resins and asphaltenes (Tissot and Welte, 1984) and the relative abundance of these groups have been used in compositional and qualitative assessments of petroleum from coals (Horsfield, 1989 and references within). The distribution of aliphatic hydrocarbons (i.e. long vs short chain lengths) is useful in assessing the oil generation potential of coals (e.g. Isaksen *et al.*, 1998; Petersen *et al.*, 2009). Also, important maturity parameters are assessed using certain aromatic components of coal including methylated naphthalenes and phenanthrenes (e.g. Radke *et al.*, 1982a; b); this will be particularly useful in the maturity assessments of the CTB coals believed to be experiencing VR suppression. Therefore, in this study, solvent extracts are fractionated into these main groups of compounds (aliphatic, aromatic and NSO compounds) to allow the above assessments. Additionally, aliphatic chain length distributions from Pyrolysis-GCMS (Py-GCMS) are used to support the results from solvent extracts.

2.2.1.1. Aliphatic Hydrocarbons

Aliphatic hydrocarbons comprise of normal and branched alkanes (paraffins), and cycloalkanes (Tissot and Welte, 1984). They are usually the most important hydrocarbons in crude oils, except in degraded oils that may have partly or completely lost their *n*-alkanes, and a few immature oils rich in heavy constituents and naphthenoaromatics. Aliphatic hydrocarbons may reach up to about 60 % in paraffinic-naphthenic crude oils, 40 – 45 % in more aromatic type of crude oil, and 20 – 25 % in degraded heavy oils and tars that have lost part or all of their *n*-alkanes (Tissot and Welte, 1984). Figure 2.1 shows a cycloalkane.

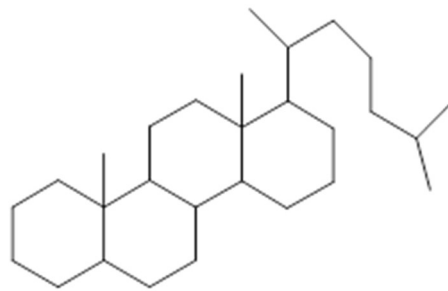


Figure 2.1. Cholestane (tetracycloalkane) ($C_{27}H_{48}$)

2.2.1.2. Aromatic Hydrocarbons

Aromatic hydrocarbons include pure aromatics, cycloalkanoaromatics or naphthenoaromatics molecules, and usually cyclic sulphur compounds (Petrov, 1987). They are classified as hydrocarbons, which contain aromatic rings, side chains and aliphatic bridges and may be distinguished as mono-, bi-, tri- and poly-aromatics (Bestougeff, 1967). Figure 2.2 is an example of an aromatic compound.

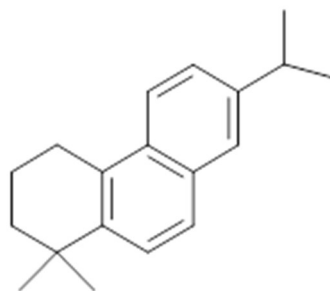


Figure 2.2. Alkyltetrahydrophenanthrene ($C_{19}H_{24}$)

2.2.1.3. Asphaltenes and Resins

Asphaltenes and resins are made up of the high molecular mass polycyclic fraction of crude oil comprising nitrogen, sulphur and oxygen atoms (Bestougeff,

1967). Asphaltene is the fraction of moderate, heavy and extra heavy oils that are insoluble in light alkanes such as pentane (Ignasiak *et al.*, 1977). Within the asphaltene structure, aliphatic hydrocarbons called biological markers are covalently bound to aromatic rings (Behar *et al.*, 1984; Bergmann *et al.*, 2000). In biodegraded oils, these aliphatic hydrocarbons preserve information about the parent oil (Peters and Moldowan, 1993). Although resins are more soluble than asphaltenes, they are likewise very polar. Both compounds usually range from 0 – 40 % in non-degraded crude oils; depending on genetic type and thermal maturity, their content is usually high in shallow immature petroleum and decreases with increasing depth and subsequent cracking. They may reach 25 – 60 % in heavy oils and tars resulting from alteration by microbial activity, water washing and oxidation (Tissot and Welte, 1984).

2.2.2. Bitumen

Bitumen is a naturally occurring solid or liquid hydrocarbon deposit that is soluble in an organic solvent such as carbon disulphide (Killops and Killops, 2005). Bitumen is composed of three main fractions, asphaltenes, resins and hydrocarbons (Tissot and Welte, 1984; Killops and Killops, 2005). Asphaltenes and resins are heavy nitrogen, sulphur and oxygen containing molecules with high molecular weights (Tissot and Welte, 1984)

2.2.3. Kerogen

Kerogen is the organic constituent of sedimentary rocks that is neither soluble in aqueous alkaline solvents nor in the common organic solvents (Tissot and Welte, 1984). It is the polymeric material from which hydrocarbons are produced with increasing burial and heating (Killops and Killops, 2005). Kerogen occurs in sedimentary rocks mostly in the form of finely disseminated organic macerals, and

it is by far the most abundant form of organic carbon in the earth's crust. An insoluble material in young sediments known as humin is believed to be the precursor of kerogen (Tissot and Welte, 1984; Killops and Killops, 2005). Kerogen is composed mainly of the elements carbon and hydrogen, with hydrogen varying between 500 - 1800 atoms for every 1000 carbon atoms depending on the type and the evolution of the organic matter. Oxygen is the next abundant element amounting to only 25 - 300 atoms, with nitrogen (5 - 30) atoms and sulphur (10 - 35) atoms per every 1000 carbon atoms also present (Tissot and Welte, 1984; Killops and Killops, 1993). Kerogens can be distinguished into types I, II, III and IV (Tissot and Welte, 1984). These kerogens are broadly equivalent to the maceral groups; liptinites, vitrinite and inertinite (Killops and Killops, 1993). Type I kerogen comprises mostly liptinite while type III is an equivalent of humic coal. Type II kerogen has an intermediate property between types I and III kerogens and type IV kerogen is recognized by their extremely low hydrogen and oxygen contents (Killops and Killops, 2005).

2.2.3.1. *Type I Kerogen*

This refers to kerogen with a high initial H/C atomic ratio (≥ 1.5) and a low initial O/C ratio (< 0.1) (Killops and Killops, 1993). Type I kerogen contains low amounts of aromatic units and heteroatoms when compared to other types of kerogen, the amount of oxygen is small and is present in the form of ester bonds (Killops and Killops, 1993). The fresh water alga *botryococcus braunii* appears to be a major contributor to some type I kerogen (Killops and Killops, 2005). Type I kerogen comprises mainly of lipid materials particularly aliphatic chains, and it is thought to have a high oil potential (Tissot and Welte, 1984; Killops and Killops, 1993). Examples of type I kerogen includes torbanites of Scottish oil shales, the

Eocene Green River oil shale of Colorado, Utah and Wyoming (Killops and Killops, 1993).

2.2.3.2. *Type II Kerogen*

This is the most commonly occurring kerogen; it has a relatively high H/C and low O/C ratios, although they are generally lower than that found in type I kerogen (Killops and Killops, 1993). Type II or liptinite-type kerogens typically has a moderate to high sulphur content, more polyaromatics nuclei, heteroatomic ketones, carboxylic acid groups and ester bonds compared to Type I (Killops and Killops, 1993). The saturated materials in this type of kerogen contain aromatic and naphthenic rings and aliphatic chains of moderate length (up to C₂₅) (Tissot and Welte 1984; Killops and Killops, 2005). Type II kerogen can also be further classified as type II-S, which are sulphur rich (containing 8 - 14 % organic S) and have atomic S/C ratio greater than 0.04 (Killops and Killops, 1993). Type II kerogen is usually related to marine organic matter deposited in a reducing environment, and the oil and gas potential are lower than observed for type I kerogen (Tissot and Welte, 1984; Killops and Killops, 1993).

2.2.3.3. *Type III Kerogen*

Type III or vitrinite-type kerogen has a low H/C (<1.0) and a high O/C (up to 0.2 - 0.3) ratio, and contains mostly condensed polyaromatics and oxygenated (ketone and carboxylic acid) functional groups, but lacks ester groups (Killops and Killops, 1993). This type of kerogen contains minor amounts of aliphatic chains, dominated by methyl and other short chains, often bound to oxygen containing groups (Killops and Killops, 1993). A few long chains are also present in type III kerogen, originating from higher plant waxes and cutin (Killops and Killops, 1993). Type III kerogen is essentially formed from vascular plants and contains

much identifiable plants debris, so vitrinite macerals predominate (Killops and Killops, 2005). The oil potential is lower than that of types I and II but may still generate abundant gas at greater depth (Killops and Killops, 2005). Humic coal is predominantly composed of Type III kerogen (Taylor *et al.*, 1998).

2.2.3.4. Type IV Kerogen

This is a residual type of kerogen exhibiting a very low H/C and a relatively high O/C ratio, comprising primarily black opaque debris largely composed of carbon in the form of inertinite. This kind of kerogen cannot generate any hydrocarbons, and is considered as a form of dead carbon in the sense of petroleum generation. It may consist of reworked, oxidized organic material, or inertinitic material originating from subaerial weathering or biological oxidation (Tissot and Welte, 1984; Killops and Killops, 1993).

2.2.4. Petroleum Alteration

Several authors have reported petroleum alteration (Connan *et al.*, 1975; Price 1980; Pande *et al.*, 1994; Bost *et al.*, 2001; Akinlua *et al.*, 2006), with the most common alteration processes being biodegradation, thermal alteration, deasphalting, gas diffusion and water washing (Tissot and Welte, 1984; Killops and Killops, 2005). Ratios of pairs of hydrocarbons can be used to investigate the extent of the various processes; among the most useful group of compounds are the gasoline-range hydrocarbons (Halpern, 1995). Oil-prone coal formation is reported to be associated with high microbial degradation, (e.g. Vu *et al.*, 2009); thus this section further examines biodegradation.

2.2.4.1. Biodegradation

Biodegradation is the microbial alteration of crude oil by selective utilization of certain types of hydrocarbons by micro-organisms, leading to the formation of heavier oils (Tissot and Welte, 1984). Biodegradation is thought to occur when reservoirs are close to the surface (Tissot and Welte, 1984), and has been classified as aerobic (caused by aerobic bacteria) or anaerobic (caused by anaerobic bacteria) (e.g. Larter *et al.*, 2006). Aerobic biodegradation occurs when bacteria are introduced into an oil pool with oxygen rich meteoric waters; the bacteria apparently utilize this dissolved oxygen and metabolize preferentially certain types of hydrocarbons (Tissot and Welte, 1984). Anaerobic degradation can take place via sulphate-reducing bacteria and methanogens (Killops and Killops, 2005; Peters *et al.*, 2005). The non-hydrocarbon contents of crude oils particularly asphaltenes increases with biodegradation (Bailey *et al.*, 1973a; b). Hydrocarbons and biomarkers show different resistance to biodegradation; according to Peters and Moldowan (1993), the resistance of hydrocarbons and biomarkers to biodegradation generally increase from *n-alkanes* to *isoprenoids* to *steranes* to *hopanes* to *diasteranes* to *aromatic steroids* to *porphyrins*. Crude oils that have been biodegraded are characterised by gas chromatograms with broad humps known as the unresolved complex mixture (UCM) of compounds (Killops and Killops, 2005 and references within). The Conditions necessary for the biodegradation of crude oils in reservoirs (Connan, 1984; Peters and Moldowan, 1993; Peters *et al.*, 2005) include;

- Access to surface recharge waters containing oxygen and nutrients (nitrate, phosphate) to sustain aerobic bacteria, although the degradation of hydrocarbons under anaerobic conditions is now known (e.g. Wilkes *et al.*, 2000).
- Temperatures of between 65 - 80 °C.

- The petroleum must be free of H₂S, which suppresses the bacteria.

2.2.5. Biological Markers

Preserved lipid components found within kerogen, oil and source rocks are called biological markers (biomarkers) or geochemical fossils because they can be unambiguously linked with biological precursor compound (Cranwell, 1982). According to Peters *et al.* (2005), they are complex organic compounds composed of carbon, hydrogen and other elements, and they show little or no change in structure from their parent organic molecules in living organisms. Biomarkers are in relatively small amounts in oils (usually <1 wt %), and although these trapped compounds may provide a diagenetic source of hydrocarbons, during catagenesis they are progressively diluted by new hydrocarbons (Killops and Killops, 2005). Some biomarkers reported to date include acyclic isoprenoids, hopanes, steranes, diasteranes, aromatic steroids, and porphyrins (Mackenzie, 1984). For the purpose of this study, the emphasis will be on acyclic isoprenoids, hopanes, steranes, diasteranes and 25-norhopanes.

i. Acyclic Isoprenoids

The common isoprenoid alkanes normally observed in sedimentary rocks and petroleum are pristane (C₁₉) and phytane (C₂₀) (Mackenzie, 1984; Killops and Killops, 2005). Pristane (Figure 2.3) and phytane (Figure 2.4) share a common precursor called phytol (Figure 2.5); pristane is believed to arise via oxidation and decarboxylation of phytol, while phytane could result from dehydration and reduction of phytol (Ikan *et al.*, 1975).

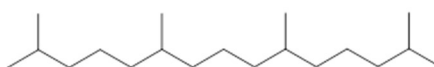


Figure 2.3. Pristane (2,6,10,14-tetramethylpentadecane)

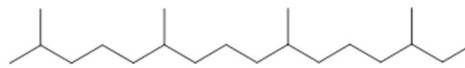


Figure 2.4. Phytane (2,6,10,14-tetramethylhexadecane)

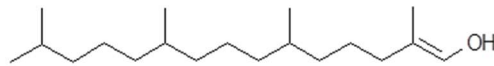


Figure 2.5. Phytol

ii. *Hopanes*

Hopanes are pentacyclic triterpenoids which are abundant in sediments, sedimentary rocks and petroleum; they range from C₂₇ to C₃₅₊ excluding a regular C₂₈ member (Mackenzie, 1984; Peters and Moldowan, 1991). According to Peters *et al.* (2005), bacteria appear to be the major source of hopanoids in sediments, rocks and petroleum hence these alkanes are believed to originate from bacteriohopanoids. It has also been suggested that bacteriohopanepolyols found in bacteria, such as bacteriohopanetetrol are the precursors of the extended hopanes (homohopanes C₃₁ - C₃₅; Figure 2.6) (Mackenzie, 1984; Peters and Moldowan, 1991).

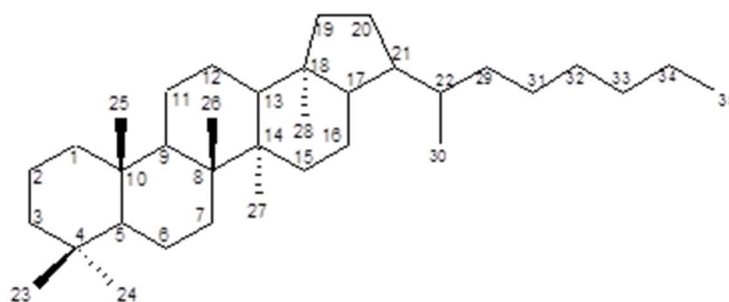


Figure 2.6. C₃₅ hopane

The biologically inherited isomeric configuration of the hopanes in immature sediments is 17 β (H),21 β (H)-22R ($\beta\beta$ hopanes); with increasing maturity it isomerises at C-17, C-21 and C-22 to a more stable 17 α (H),21 β (H)-22R and 17 α (H),21 β (H)-22S ($\alpha\beta$ hopanes) mixtures, and 17 β (H),21 α (H) moretanes ($\beta\alpha$ hopanes). At a higher level of maturity, the $\beta\alpha$ hopanes also converts to $\alpha\beta$ hopane mixtures, which is the more stable isomer of the hopanes (Mackenzie, 1984; Peters and Moldowan, 1991).

iii. Steranes

Steranes belong to the group of compounds called steroids; the sterols found in the lipid membranes of eukaryotic organisms, are precursors to the steranes in sediments, rocks and petroleum (Peters and Moldowan, 1993). Sterane compositions within higher land plants are typically dominated by C₂₉ steranes (Figure 2.7), whereas C₂₇ and C₂₈ steranes are characteristic of marine sediments (e.g. Peters *et al.*, 2005).

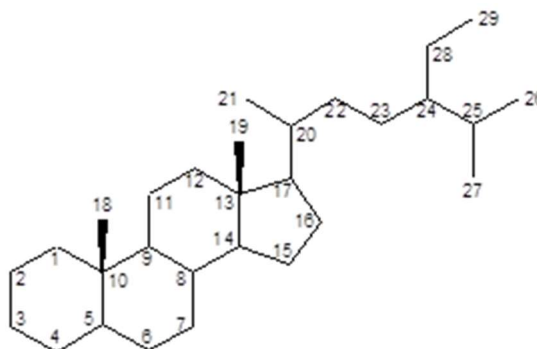


Figure 2.7. C₂₉ sterane

Steranes can be found in a number of configurations whose relative abundance is largely controlled by thermal maturity (Moldowan *et al.*, 1991); hence they can

be useful in assessing the maturity of source rocks. There is a large number of asymmetric centers in sterols, although only some of the asymmetric positions, particularly those at C-14, C-17, and C-20, are of greater importance to the geochemist than others. The 5 α (H),14 α (H),17 α (H),20R configuration (aaaR) inherited from living organisms is unstable during catagenesis and results in isomerisation to geological configurations ($\alpha\beta\beta$ S, $\alpha\beta\beta$ R and aaaS) (Peters and Moldowan, 1993).

iv. *Diasteranes (Rearranged Steranes)*

Diasteranes are believed to be hydrocarbons, which originate from the acidic promoted re-arrangement (carbonium-ionic re-arrangement) of the regular C₂₇ - C₂₉ steranes in the presence of aluminosilicates, and as such they are not biological products. The re-arrangement of the regular steranes to give diasteranes proceeds by the migration of methyl groups at C-10 and C-13 in the regular steranes to C-5 and C-14 in diasteranes (Petrov, 1987) (Figure 2.8).

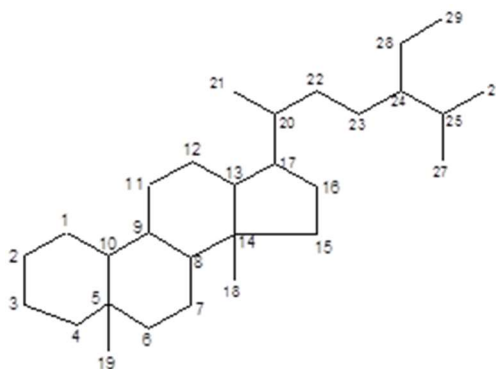


Figure 2.8. C₂₉ diasterane

The most stable epimers of diasteranes normally have a 10 α , 13 β , 17 α , 20R and 20S as well as a 10 α , 13 α , 17 β , 20R and 20S configuration. These diasteranes

occur in two basic modes; the 13 β , 17 α -configuration ($\beta\alpha$) which is a major petroleum constituent, and the 13 α , 17 β -configuration ($\alpha\beta$) which is a minor petroleum constituent, and they range in carbon number from C₂₇ - C₂₉ as they are derived from the C₂₇ - C₂₉ regular steranes. The diasteranes show diagnostic ion profiles at *m/z* 149,189,217 and 259 (Seifert and Moldowan, 1979). Figure 2.8 shows the C₂₉ diasterane.

v. 25-Norhopanes (10-desmethylhopanes)

The 25-norhopanes are a series of compounds present in many heavily biodegraded oils and are believed to be derived by the removal of a methyl group at C-10 of the A/B ring (Figure 2.9) of the regular hopanes (Reed, 1977; Seifert and Moldowan, 1979; Rullkötter and Wendisch, 1982; Volkman *et al.*, 1983). These compounds have also been found in crude oils, which contain *n*-alkanes and thus interpreted to result from the mixing of degraded and non-degraded oils (Howell *et al.*, 1984). The identification of 25-norhopanes in source rocks and in un-altered oils (Horstad *et al.*, 1991) has made the origin of these compounds a controversial issue. It is also important to note that biodegradation of hopanes commonly occurs without the formation of 25-norhopanes (Peters and Moldowan, 1993).

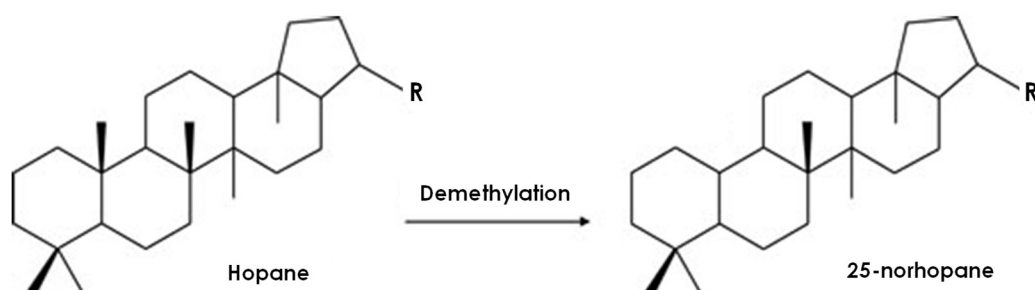


Figure 2.9. Demethylation of regular hopane to form 25-norhopane

2.3. Pyrolysis

Pyrolysis is the thermal decomposition of organic matter through the application of heat. Studies have demonstrated that the pyrolysis of coals and kerogen have the ability to simulate hydrocarbon maturation (Monthioux *et al.*, 1985; Monthioux *et al.*, 1986; Michels *et al.*, 1994). Other studies have shown pyrolysis to be able to generate hydrocarbons (Blanc and Connan, 1992; Price and Wenger, 1992; Michels *et al.*, 1995) and expel oil from coals, kerogen and petroleum source rocks (Lewan *et al.*, 1979; Behar *et al.*, 2003). Pyrolysis techniques have also been used for the evaluation of petroleum source rocks (Peters, 1986). Important biological marker compounds of geochemical interest have been generated and liberated from asphaltenes and kerogens through the use of pyrolysis techniques (Love *et al.*, 1995). Pyrolysis techniques have also been employed for hydrocarbon cracking experiments (Weres *et al.*, 1988; Enguehard *et al.*, 1990; Domine, 1991). For the purpose of this study discussions will be focussed on Rock-Eval pyrolysis and nitrogen pyrolysis (retorting).

2.3.1. Rock-Eval Pyrolysis vs Nitrogen Pyrolysis (Retorting)

Rock-Eval pyrolysis is applied to evaluate the petroleum source rock potential of the CTB coals, while nitrogen pyrolysis is applied to simulate retorting of these coals. The S1 and S2 parameters of Rock-Eval pyrolysis respectively represent the quantity of free hydrocarbons present and the amount of hydrocarbons produced during the thermal cracking of the insoluble organic matter (kerogen) (Lafargue *et al.*, 1998 and references within). Nitrogen pyrolysis (retorting) seeks to generate and expel liquid hydrocarbons via cracking of kerogen. Thus, the hydrocarbon yields from both methods/techniques would be complementary in estimating the liquid hydrocarbon resource potential of the CTB coals. Further discussion is done in the experimental sections of Chapter 3.

2.3.1.1. Coking and Coke Potential of the CTB Coals

Coke has been defined as a solid fuel produced by heating coal in the absence of air so that the volatile components are driven off (OD, 2015). This definition however is not a strict one as further discussion within this paragraph reveal. The industrial manufacture of coke from coal commenced in early 17th century by heaping coal into circular mounds in the open, covering them with earth, clay or ash, and slowly burning them to produce heap of coke (Taylor *et al.*, 1998). This led to the evolution of a number of coke oven designs which mainly includes “non-recovery” and “by-product” ovens (Sandercock, 1975). In the non-recovery ovens, heat is supplied by combustion of the gas evolved from the coal charge together with a limited supply of air. However, in the by-product oven, no air is admitted into the coking chamber. Therefore, the above definition of coke is only applicable to “by-product coking” which is simulated in this study by employing nitrogen gas in an open system. The Longyear, Svarteper and Askeladden coal seams in the CTB, due to their high vitrinite content (e.g. Orheim *et al.*, 2007; Marshall, 2013) are considered suitable for coking as vitrinite is the maceral group that contributes most to the formation of coke, although Taylor *et al.* (1998) noted that vitrinite alone would not produce the best coke. Other important coking qualities of coal including but not limited to the free swelling index (range between 4 – 9) are indicative that the coals under study have a medium to high coking potential (Marshall, 2013).

2.4. Svalbard – Geography, Geology and Coal Mining

2.4.1. Geographic and Physical Setting

The CTB is located on the island of Spitsbergen, the largest of three islands which constitute the Svalbard Archipelago. The archipelago is located mid-way

between the northernmost point of Europe and the North Pole at a distance of about 650 km north of Norway (Figure 2.10). The main islands of the Svalbard archipelago (Spitsbergen, Nordaustlandet and Edgeøya) lies between latitude 76° and 81° north, and longitude 10° and 35° east, and roughly centred on latitude 78° north and longitude 20° east. The archipelago covers an area of about 62,049 km², and Spitsbergen accounts for more than half of the land mass covering a 39,044 km² area (Dallmann *et al.*, 1988; Harland *et al.*, 1997).

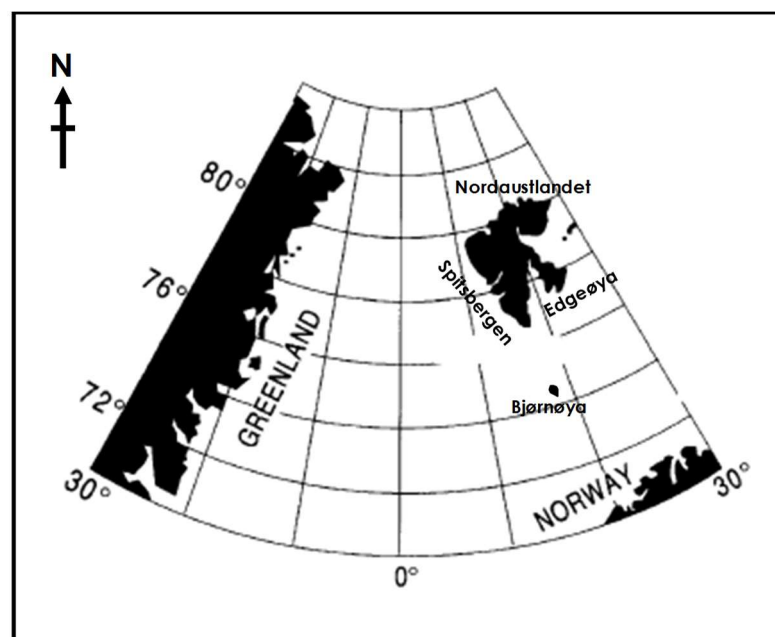


Figure 2.10. Geographic setting of the Svalbard Archipelago (Modified from Nagy, 2005)

The Svalbard climate is arctic with extensive glaciations covering about 60 % of the region (Svendsen *et al.*, 2002). The summer air temperature at sea level averages 4 - 5 °C. The winter temperature is about -12 °C and mostly down to -20 °C in the west. Extreme conditions may range between -50 to 20 °C. Temperatures are lower towards the north and east (Harland *et al.*, 1997). With annual ambient mean temperature of -5 °C, the sea routes are ice capped for 6

months of the year (Orheim *et al.*, 2007). Heavy glaciations and the northern latitude generally choke up arable land hindering the growth of trees and shrubs on the island (Harland *et al.*, 1997); hence the sediments/rocks are free from vegetative cover thereby making Svalbard a unique and interesting location for geological studies.

2.4.2. Tectonic Setting

The Svalbard archipelago represents an uplifted part of the Barents Sea Shelf; its evolution is associated with the North Atlantic continental movement consisting of numerous episodes of uplift/subsidence with corresponding lateral re-deposition of reworked sediments briefly interrupted by episodes of volcanism with basalts and dykes (Harland *et al.*, 1997). The Svalbard platform is a broad NW-SE trending syncline with a steeper limb (fold belt) to the west and a gently rising limb towards the east. Much of central and southern Spitsbergen forms part of the CTB which occurs within the central part of this syncline (Figure 1.1). The syncline is bounded to the east and west by the Billefjorden Fault Zone and West Spitsbergen fold and thrust belt respectively; it formed in response to the onset of compression related West Spitsbergen foreland fold and thrusting, and prior to the strike-slip separation of Svalbard and Barents Shelf from Greenland (Harland *et al.*, 1997; Tessensohn, 2001).

2.4.3. Stratigraphy and Coal Occurrence

The islands of the Svalbard Archipelago are composed of sedimentary, metamorphic and igneous rocks of Precambrian to Quaternary ages, and are closely related to the north-eastern part of Greenland and the Canadian Arctic Islands (Harland *et al.*, 1997). Tertiary sediments in the Svalbard archipelago exist only on Spitsbergen and Prins Karls Forland (Ny-Alesund area) (Figure 1.1), and

Paleogene coal bearing strata occur in three main basins in these areas (Harland *et al.*, 1997), these are:

- The Central Basin – this occupies the middle part of Spitsbergen area, and the Todalen Mbr. bears multiple coal seams of economic quantity (Figure 2.10).
- The Forlandsundet Basin – this occurs on the east side of Spitsbergen and exposes the Balanuspynten Fm. whose Sarsbukta Mbr. contains coal and plant fragments defining thin seams of up to 0.15 meters. There is no prospect of coal mining.
- The Calypsostranda Basin - in the Skilvika Fm. contains many thin coal horizons, which were the basis of short-lived exploitation at Calypsobyen. The Seams are mostly thin, and three of them attained only 0.5 – 0.6 m thickness.

It is noted that the occurrence of some Devonian (Famennian) coals in Svalbard have been reported (Harland *et al.*, 1997); these coals occur at Bjornoya (Figure 2.10), the southernmost island located 235 km south of mainland Spitsbergen. The Central Basin is further discussed below as it is the main focus of this study.

In the CTB, the Mid-Eocene to Paleocene Van Mijenfjorden Group is the main Tertiary sequence; it is up to 2.3 km thick (Harland *et al.*, 1997; Ćmiel and Fabianska, 2004; Nagy, 2005) and it is divided into six lithologic formations (Figure 2.11). The CTB contains the majority of the economic coal deposits on Svalbard, with mining concentrated within the Firkanten Formation (Orheim *et al.*, 2007) generally dated as early Paleocene (e.g. Harland *et al.*, 1997; Nagy, 2005). The Firkanten Formation is a 100 - 170 m thick overall transgressive unit comprising three to eight coastal/deltaic successions with conglomerate commonly

occurring at its base (Orheim *et al.*, 2007). In the NE Central Tertiary Basin, the Firkanten Formation comprises two sub-units; the lowermost Todalen Member and the overlying Endalen Member representing a sequence of paralic coal bearing tidal sediments overlain by laminated or heavily bioturbated marine sandstones (Dallmann *et al.*, 1999). The base of the Firkanten Formation is marked by a low angle unconformity with the Lower Cretaceous Carolinefjellet Formation, sometimes marked by a basal conglomerate known as the Grønfjorden bed. To the west, there is an additional offshore unit known as the Kolthoffberget Member (Dallmann *et al.*, 1999; Harland *et al.*, 1997). The Todalen Member represents the main coal bearing unit within the Van Mijenfjorden Group (Figure 2.11); it consists of siltstone-sandstone-coal successions representing increased subsidence and the infilling of the Cretaceous peneplain (Dallmann *et al.*, 1999; Harland *et al.*, 1997). Five main coal seams are commonly cited within the Todalen Member; the Svea, Todalen, Longyear, Svarteper and Askeladden Seams (Harland *et al.*, 1997; Dallmann *et al.*, 1999, Orheim *et al.*, 2007). To the west of the CTB, there are only three coal seams present with a different naming system (Nidzny, Verkny and Sputnik seams). Western seams to the south of Barentsburg (Figure 1.1 and 2.11) are inferred to be associated with fan deposits from the newly forming West Spitsbergen Fold and Thrust Belt (Worsley *et al.*, 1986). Although the relationship between the coal seams of the Western and Eastern sides of the basin is not well known, many of the reconstructions indicate that the western coalfields of Barentsburg and Colesdalen are a continuation of the more extensive eastern coalfield (Steel *et al.*, 1981; Steel and Worsley, 1984; Nøttvedt, 1985; Worsley *et al.*, 1986; Nagy, 2005; Lüthje, 2008). This study will attempt to draw correlations between the eastern and western coal seams of the CTB.

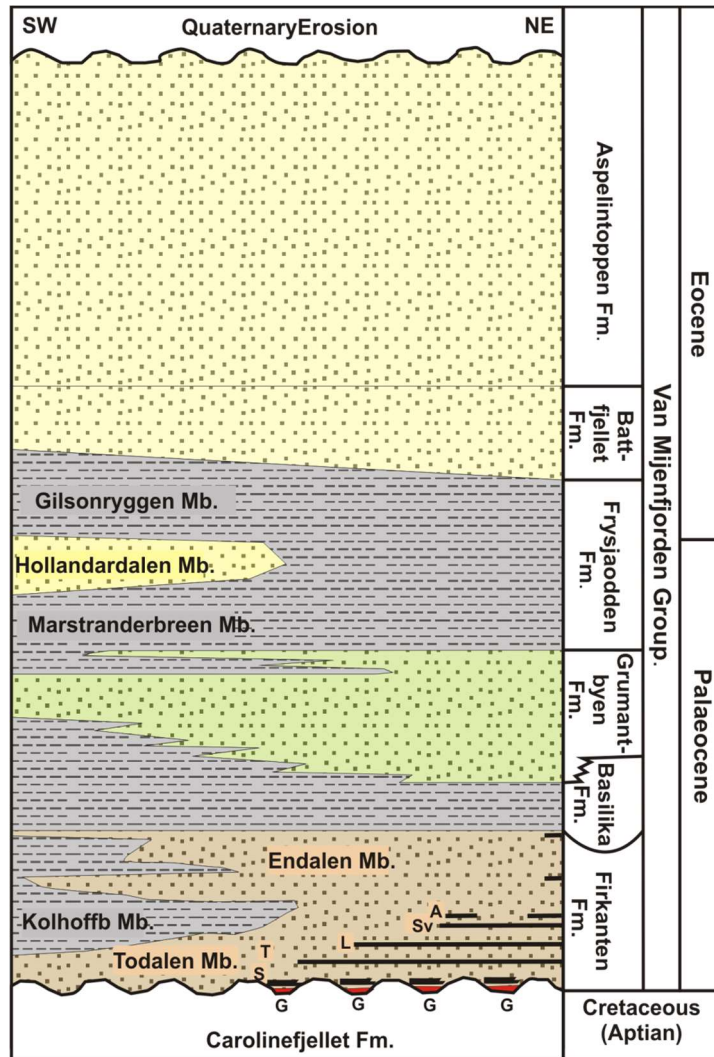


Figure 2.11. The Van Mijenfjorden Group representing the sedimentary infill of the CTB, Spitsbergen (Adapted from Marshal *et al.*, 2015b). Note: multiple coal seams occurring within the basal Todalen Member. S = Svea, T = Todalen, L = Longyear, Sv = Svarteper, A = Askeladden.

2.4.4. Coal Mining in Svalbard

According to the Store Norske AS website, coal mining in Svalbard commenced before 1916 and was mainly carried out by a US owned Arctic Coal Company. In November 1916, Store Norske AS was formed, and took over coal mining operations in Longyearbyen from the Arctic Coal Company. Since then, Store Norske has operated coal mines on Svalbard continually, with the exception of a

period during World War II. Store Norske is 99.9 percent owned by the Norwegian State. With a population of around 2,600 people in Svalbard, Store Norske is the largest employer in Svalbard with 320 employees. The company is a paramount contributor to a stable and robust community in Longyearbyen.

Store Norske carries out both geological mapping and exploration drilling. Owing to Svalbard's strict environmental laws, the drilling is done in the winter between January and June. During this period, the ground is frozen and covered with snow so that the activity leaves no permanent traces. The cold, the darkness, and drilling through permafrost and glaciers creates huge challenges for the teams and their equipment. Over time, the company has however developed the expertise and technology that permits the mastery of these conditions. The main focus of the exploration activities is coal deposits in the CTB, Spitsbergen. Store Norske currently operates three coal mines on Svalbard: Svea Nord, Lunckefjellet and Mine 7 (Figure 2.12).

a) Svea Nord Mine

Currently, principal operations of Store Norske are in the Svea Nord mine, which is about 60 km south of Longyearbyen. Most of the company's employees work in Svea. Svea Nord has been in normal commercial operation since 2002 and accounts for most of the company's production; annual production in 2012 was about 1.2 million tonnes of coal.



Figure 2.12. Map showing currently operating coal mines and locations of interest in the northern Central Tertiary Basin, Spitsbergen (After NPI, 2015)

b) Mine 7

Mine 7 (also known as Gruve 7 mine) lies 15 km from Longyearbyen and has been in production since 1975. About 25 people are employed in the mine, which produces approximately 70,000 tonnes of coal annually. Some 25,000 tonnes of this are delivered to Longyearbyen Energiverk, a coal-fired power plant which provides electricity and heating in Longyearbyen. The rest of the coal is sold largely to the foundry industry in Germany.

c) Lunckefjellet Mine

The Lunckefjellet Mountain lies northeast of the Svea Nord mine and bears an estimated 8.4 million tonnes of saleable coal. This Lunckefjellet mine is new and the main production will commence when the Svea Nord core becomes depleted under the current production plans.

Store Norske supplies coal for a variety of purposes, but the largest area is energy production. Half the coal is sold to coal-fired power plants on the European Continent. The largest recipient is Germany, followed by Denmark, with delivery also done to France, the UK, Spain, and Norway. In addition to coal for energy production, Store Norske has for several years supplied the steel-making industry. Other customers for Store Norske coals include cement, lime kilns, foundries and chemical enterprises. The coal is shipped from the port at Kapp Amsterdam in Svea by 30,000 tonne (handysize) and 70,000 tonne (panmax) vessels. Hamburg and Rotterdam are important recipient ports.

Whilst there are mining plans for the next 15 years (as per Store Norske), the coal resource which is main economic strength of Svalbard is gradually running out. The oil-prone nature of the CTB coals implies that they may be of considerably

greater economic value, and from a geological basin view point; the CTB may represent an unconventional hydrocarbon province.

2.5. Summary and Conclusions

In Chapter 1, the previous work on the oil potential of the Firkanten Fm. coals have been discussed in details, which lead to the aims and objectives upon which this current study is based. This Chapter (2) has covered the relevant aspects relating to the main concepts and keywords of this PhD study including coal, petroleum, biodegradation, pyrolysis/retorting, the geology of Svalbard, and coal mining in Svalbard. The foregoing (Chapters 1 and 2) will therefore serve as a base to understand and interpret data from inorganic and organic geochemistry, and the organic petrographic studies of the coals under investigation.

SAMPLING AND EXPERIMENTAL METHODS/TECHNIQUES

3.1. Sampling, Sample Distribution and Sample Preparation

3.1.1. Sampling and Sample Distribution

To achieve the aims of this research, a wide sample spread was required; thus, a total of 146 coal samples was provided by Store Norske Spitsbergen AS and investigated. Sample locations cover four main areas of the CTB including Bassen, Lunckefjellet, Breinosa and Colesdalen. The rationale behind selection of sample locations are:

- a) Because of the strong influence of marine sulphur contents on the oil potential of coals (e.g. Diessel and Gammidge, 1998; George *et al.*, 1994; Wilkins and George, 2002; Sykes and Snowdon, 2002; Sykes *et al.*, 2004; 2014; Marshal *et al.*, 2015a), these four areas are sampled to reflect varying levels of marine influence as they are of varying distances from the inferred palaeocoastline in the northern CTB (Marshall, 2013).
- b) Besides the marine influence on oil potential, another important control on source rock potential is thermal maturity. The four areas sampled would reflect varying maturities from the present day north-eastern basin margin (Bassen) toward basin Centre (Colesdalen) (e.g. Throndsen, 1982; Harland *et al.*, 1997).
- c) Both the eastern coalfield (Bassen, Breinosa and Colesdalen) and the western coalfield (Colesdalen) of the CTB are represented.

Main areas and sample distribution is presented in Figure 3.1 and summarised in Table 3.1, and further described below. A comprehensive list of all 146 samples is presented in Appendix 1, which shows the designated sample ID for every

sample, location, sample type, coal seam, drill depth, sample position above seam base and general comments (i.e. coal, ash-rich coal or mudstone).

Bassen – represents the north-eastern margin of the CTB, Spitsbergen. The Bassen samples were sampled from outcrops of the Longyear seam on the eastern mountain side during field work. Samples were wrapped in paper with the sample identification and orientation marked on the covering to ensure preservation. This was then wrapped within a plastic sample bag, which was marked again with the sample name, orientation and sample interval. Samples were sub-sampled to higher resolution (4 - 9 cm intervals) at the University of Nottingham to obtain 32 coal samples and assigned sample IDs ranging from Ba1 – Ba32.

Lunckefjellet – represents the eastern margin of the CTB, Spitsbergen. Samples are from 4 x boreholes; BH15-2011 in the east while BH10-2009, BH10-2007 and BH6A-2007 are from the west, and in an orientation reflecting the direction toward the eastern margin of the basin i.e. away from palaeocoastline (Marshall, 2013). Both the Longyear and Svarteper coals were sampled from all 4 cores and assigned sample IDs in the range of L1 – L55.

Breinosa – represents sediments which are down-dip of the eastern margin of the CTB, and roughly 1/3 the distance from basin margin to center. Samples are from the Askeladden, Svarteper, Longyear and Svea seams at BH4-2009, BH5-2009 and Mine 7 localities. An unknown coal occurring between the Svarteper and Longyear seam at BH4-2009 locality was also sampled. Samples are numbered Br1 - Br42. All mine 7 and Svea Nord data in this study are as per Pers. Comm. Chris Marshall, 28th January, 2015.

Colesdalen – represents the western coalfield and center of the CTB; samples are from the Verkny and Sputnik seam in Synndalen BH3-2008 locality. Sample IDs range from C1 - C9.

In addition to the four main areas above, the Svea coals were sampled from the Svea Nord mine (Samples S1 - S6) which is ~2.5 km south of Lunckefjellet. A Lower Carboniferous coal from Pyramiden (Sample P1) was also sampled during field work. High resolution sampling within seams will account for possible variations in the petrographic and geochemical characteristics arising from variations in levels of marine influence upon peatland (e.g. Marshall *et al.*, 2015a and references within), and for all analytical techniques, sample selections within localities were done at intervals to reflect these possible variations.

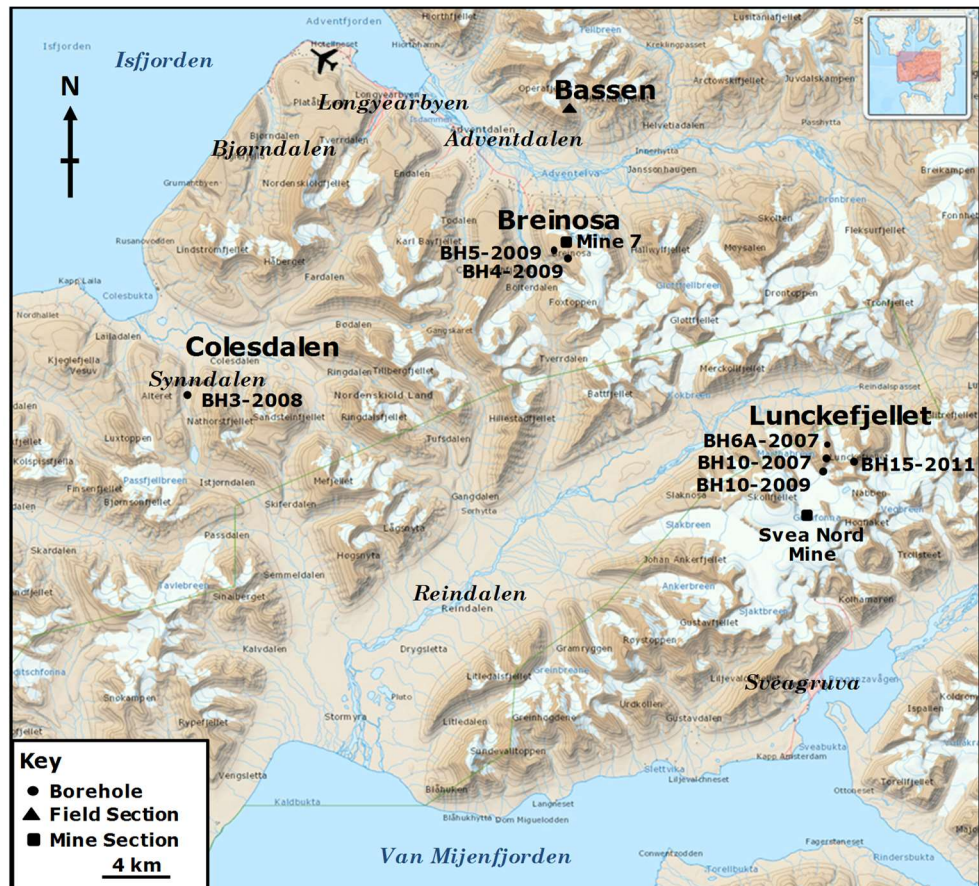


Figure 3.1. Map of the northern Central Tertiary Basin on the island of Spitsbergen showing sampling localities and sample types (Modified from <http://toposvallbard.npolar.no/>)

Sample ID	Area	Location and sample type	Seam	Age	No. of samples	Sample length (cm)			
						Mean	Minimum	Maximum	Median
Ba1 – Ba32	Bassen	Outcrop section	Longyear	Palaeocene	32	6.0	4.0	9.0	6.0
Br1 – Br3	Breinosa	BH4-2009	Askeladden	Palaeocene	3	18.7	4.0	33.0	19.0
Br4 – Br8	Breinosa	BH4-2009	Svarteper	Palaeocene	5	23.8	23.0	24.0	24.0
Br9	Breinosa	BH4-2009	Unknown	Palaeocene	1	24.0	24.0	24.0	24.0
Br10 – Br17	Breinosa	BH4-2009	Longyear	Palaeocene	8	18.3	16.0	21.0	18.0
Br18	Breinosa	BH5-2009	Askeladden	Palaeocene	1	-	-	-	-
Br19 – Br20	Breinosa	BH5-2009	Svarteper	Palaeocene	2	-	-	-	-
Br21 – Br24	Breinosa	BH5-2009	Svea	Palaeocene	4	-	-	-	-
Br25 – Br42	Breinosa	Mine 7 section	Longyear	Palaeocene	18	8.3	3.0	18.0	7.5
L1 – L8	Lunckefjellet	BH15-2011	Svarteper	Palaeocene	8	10.0	10.0	10.0	10.0
L9 – L27	Lunckefjellet	BH15-2011	Longyear	Palaeocene	19	10.0	10.0	10.0	10.0
L28 – L32	Lunckefjellet	BH10-09	Svarteper	Palaeocene	5	22.0	20.0	27.0	21.0
L33 – L36	Lunckefjellet	BH10-09	Longyear	Palaeocene	4	23.5	21.0	30.0	21.5
L37 – L38	Lunckefjellet	BH10-2007	Svarteper	Palaeocene	2	38.0	35.0	41.0	38.0
L39 – L44	Lunckefjellet	BH10-2007	Longyear	Palaeocene	6	24.0	19.0	25.0	25.0
L45 – L47	Lunckefjellet	BH6A-2007	Svarteper	Palaeocene	3	37.3	34.0	39.0	39.0
L48 – L55	Lunckefjellet	BH6A-2007	Longyear	Palaeocene	8	25.0	25.0	25.0	25.0
S1 – S2	Svea Nord	Mine section	Svea	Palaeocene	2	Bulk	-	-	-
C1	Colesdalen	BH3-2008	Verkny	Palaeocene	1	16.0	16.0	16.0	16.0
C2 – C9	Colesdalen	BH3-2008	Sputnik	Palaeocene	8	23.1	18.0	25.0	23.0
P1	Pyramiden	Outcrop section	Unknown	Lower Carboniferous	1	Bulk	-	-	-

Table 3.1. Sample distribution (summary) showing designated sample ID for all samples investigated throughout this study. A comprehensive table of sample distribution is shown in Appendix 1.

3.1.2. Sample Preparation

All drill core and mine samples were cleaned, sub-sampled, bagged and labelled by/at Store Norske Spitsbergen AS. The Bassen Outcrop sections were sub-sampled at the University of Nottingham using an electric diamond tipped bench mounted circular saw. The samples were then washed, air dried, wrapped in foil and placed in a plastic sample bag. Samples were further crushed using a metal pestle and mortar, which were cleaned using industrial methylated spirits (IMS) after each use to prevent cross contamination. Because of the mismatch between the samples sizes received (Table 3.1) and the sample sizes required for the different analytical techniques (e.g. 1 g from petrographic analysis), the coarse crushed coals were subsequently sub-sampled by cone and quarter to reduce the samples from the received to analytical sizes, and obtain coal to be retained, coal to be used for organic petrology and coal to be milled for organic and inorganic geochemical analysis. Coal to be used for organic petrology were further crushed using a metal pestle and mortar, sieved to a particle size of <1 - 0.15 mm and saved in fresh sample bags. To prevent cross contamination; the sieve was brushed and cleaned using IMS after each sample. Coal for organic and inorganic geochemical analysis were ground in an Agate TEMA mill for 2 - 3 minutes to obtain a fine powder (<100 μm). Milled samples were placed in glass bottles and stored in a freezer. The Agate TEMA mill was thoroughly washed with water, air dried, cleaned with IMS and again, air dried after each sample to avoid cross contamination.

3.2. Experimental Methods

3.2.1. Organic Petrography

3.2.1.1. Sample Preparation

The <1 - 0.15 mm particle sized fraction of coals previously separated were used to prepare polished specimens for organic petrology in two main stages; the first of which involves preparation of coal samples in moulds. This involves the following steps:

- Step 1: <1 to 0.15 mm particle sized coals was poured into circular moulds of 30 mm diameter (Figure 3.2).
- Step 2: Synthetic resin was prepared by mixing epofix resin with hardener (25:3 vol./vol.) and poured up to $\frac{1}{2}$ the internal depth of each mould containing the coal particles.
- Step 3: The mixture of coal grains and epofix resin/hardener was thoroughly and slowly mixed to ensure grains are separated by resin and avoid generation of too much air bubbles.
- Step 4: The mould and its contents were then transferred to a pressure chamber for about 30 minutes to extract air bubbles.
- Step 5: More epofix resin/hardener mixture was added up to $\frac{3}{4}$ of the depth of the moulds and left overnight to dry.

After drying, specimens were removed from the mould for grinding and polishing in 5 sub-stages (Table 3.2.) using a Rotopol/Pedemat machine (Figure 3.2.B).

Stages	Grinding/polishing material
Stage 1	25 mm grit diamond plate
Stage 2	15 mm grit diamond plate
Stage 3	6 μm grit on cloth
Stage 4	3 μm grit on cloth
Stage 5	0.0 4 μm colloidal silica on cloth

Table 3.2. Grinding and polishing stages of petrographic specimen preparation

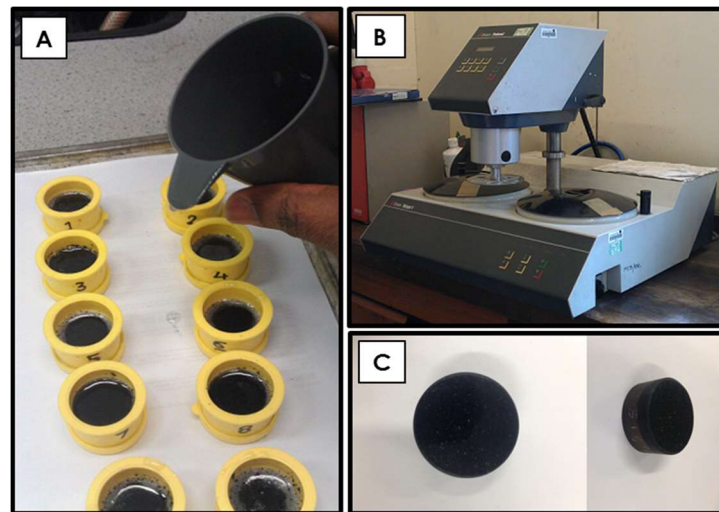


Figure 3.2. Preparation of petrographic specimens. A – Mixing coal particles with synthetic resin in in circular moulds. B – Rotapol/Pedemat grinding and polishing machine. C - Prepared specimens ready for petrographic analysis.

3.2.1.2. Determination of Vitrinite Reflectance (VR) and Maceral Analysis

In Section 2.1, a detailed discussion on the use of VR as a tool for determining the maturity of source rocks was covered. Also in Section 2.1, coal macerals were discussed with particular attention to oil-prone macerals. Hence, this section will give details of the methods utilised for measuring VR and coal maceral analysis.

a) Vitrinite Reflectance (VR)

VR determination is in accordance with ISO 7404-5:1994. A Leitz Ortholux microscope fitted with oil immersion objectives was employed; a 12 V 100 W

quartz halogen lamp was used for white light, and a 100 W HBO high pressure mercury lamp was used for UV light. VR measurements were taken using an attached photomultiplier, and using a green filter with a peak transmission of 546 nm and a 16 μm^2 measuring aperture. Calibration was done using a 1.24% R_O glass prisma standard, and a blank (0% R_O). The calibration was checked using a third standard (YAG) with a reflectance of 0.89% R_O to ensure a linear calibration. Random reflectance (R_{Or}) measurements for 100 points were taken for each sample.

R_{Or} are measurements taken in non-polarised light, and it is different from maximum reflectance (R_{Omax}) as the latter is taken in polarised light whilst rotating the microscope stage. When readings are taken in non-polarised light (as in R_{Or}), they represent an integration of values in all directions (through 360°) in which incident light is vibrating, i.e. the reflectance in all directions is integrated into the R_{Or} reading regardless of the stage orientation. On the other hand, R_{Omax} is obtained when the reflected light is aligned with the vibration direction of incident light (Taylor *et al.*, 1998). Vitrinite has a uniaxial negative optical indicatrix; thus, when the stage is rotated through 360°, 2 to 3 maxima are obtained per particle, which is used to calculate the R_{Omax} value (Taylor *et al.*, 1998). This procedure is repeated 100 times per coal sample to obtain a very accurate measure of the rank of that sample. Thus, whereas a series of R_{Omax} taken on a particulate sample should have only a small standard deviation, similar series of R_{Or} will demonstrate a wider range of values. In this study, there was no access to a computer system set up for R_{Omax} measurement; hence, R_{Or} was measured. However, it is noted that the closely spaced sampling (high sampling resolution), would reduce the error margins associated with measuring R_{Or} .

b) Maceral Analysis

Maceral analysis was done in accordance with ISO 7404-3:1994, and using the same microscope set-up as used for VR measurement. A 12 V 100 W quartz halogen lamp was used for white light illumination and a 100 WHBO, high pressure mercury lamp was used for blue light. Macerals were counted under the ocular for 500 points using an automatic point counter which ensures one count per maceral (Taylor *et al.*, 1998). The automatic point-counting equipment was employed to avoid the potential statistical problem associated with taking multiple counts in a field (Taylor *et al.*, 1998). The microscope ocular contains a single cross hair, and the entities which come to coincide with this point are recorded. Pressing any button on the automatic point counter not only records a count for the particular constituent, but also causes the stage to move a pre-set incremental distance to the next grid point. Whenever the grid point appears to coincide with a particle or maceral boundary, quadrants of the field of view were examined in turn according to Figure 3.3, commencing at the top right and proceeding clockwise. If the boundary line in question extends from the grid point into the first quadrant, subsequent quadrants were examined until one is found in which the boundary line does not occur; the maceral adjacent to the grid point in that quadrant is then recorded.

c) Photomicrograph

Taking of photomicrographs and additional petrographic examination were done using a LEICA DM4500P microscope fitted with oil immersion objectives. The white light source was a 12 V 100 W halogen lamp with a LED illumination slider 29 x 11.5 mm in the incident light axis. A LED 450 nm was used for fluorescence. Examination of samples, analysis and data collection were done via the Hilgers Fossil Man software.

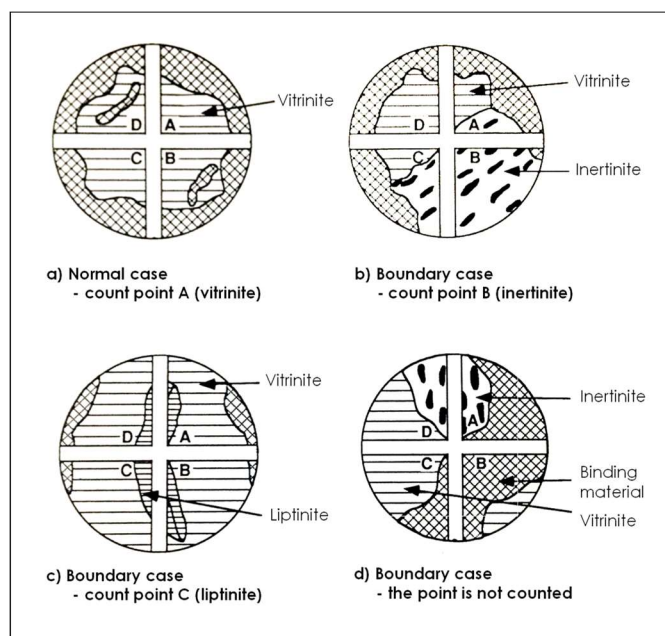


Figure 3.3. Maceral analysis guide for normal and boundary cases between macerals or between maceral and mounting medium. Note: width of cross hairs is exaggerated for clarity (Adapted from ISO 7404-3:1994; Taylor *et al.*, 1998)

3.2.2. Organic Geochemistry

3.2.2.1. Soxhlet Extraction

Free bitumen plus oil present in all coals under study were solvent extracted using a Soxhlet extraction technique. The Soxhlet extraction setup comprises of four main parts; condenser, Soxhlet, flask and heat source (Figure 3.4). Approximately 2 g of milled coal (<100 μm) was weighed and transferred to a cleaned cellulose thimble and capped with cleaned cotton wool to stop samples from spilling out. The thimble and contents was then placed in the Soxhlet (Figure 3.4). Extraction was carried out using about 190 ml DCM/methanol mixtures (93:7 vol/vol) for a period of 3 to 8 days until a clear solvent mixture is achieved within the thimble chamber of the Soxhlet, while the bitumen is collected alongside solvent mixture in the flask. After extraction, the DCM/Methanol mixture was evaporated (almost

to dryness) using a rotary evaporator, and then transferred to a vial of known weight and left under a stream of dry nitrogen for evaporation to continue until constant weight is achieved which implies only bitumen plus oil content is left.

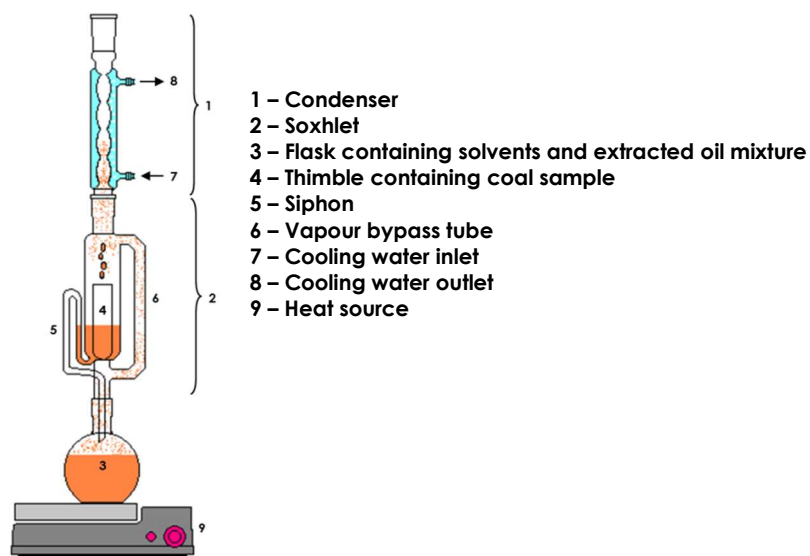


Figure 3.4. Schematic of Soxhlet extraction setup

3.2.2.2. Rock-Eval 6 Pyrolysis

The characterization of the organic matter from sedimentary rocks is one of the main objectives of organic geochemistry and is now widely recognized as a critical step in the evaluation of hydrocarbon potential. The use of pyrolysis methods to provide data on the potential, maturity and type of the source rocks in sedimentary basins is well documented (Barker, 1974; Claypool and Reed, 1976; Clementz *et al.*, 1979; Larter and Douglas, 1982; Horsfield, 1985; Peters, 1986). Among these techniques, Rock-Eval pyrolysis has been widely used in the industry as a standard method in petroleum exploration. The Rock-Eval 6 machine is the newest version of the Rock-Eval technique; whilst it is generally similar to previous versions, it shows minor but significant improvements some of which are

particularly relevant to coal; hence, it is utilised in this study. For example, in Rock-Eval 6, the final pyrolysis temperature is 850 °C rather than 600 °C. Pyrolysis at high temperatures up to 850 °C is necessary for complete thermal degradation of terrestrial Type III kerogen as previous studies have shown that thermal cracking of terrestrial organic matter is not always complete at 600 °C; consequently, the resulting HI in Rock-Eval 6 is more representative (Lafargue *et al.*, 1998) leading to a better evaluation of the oil potential of Type III kerogen. Rock-Eval 6 generally consists of the temperature programmed heating of a small amount of rock (100 mg) in an inert atmosphere (helium/nitrogen) so as to allow measurements illustrated in Figure 3.5. Some of the measurements are:

- The quantity of free hydrocarbons in the sample (S1 peak) expressed in mg HC/g rock.
- The amount of hydrocarbons produced from the cracking of heavy hydrocarbons and from the thermal breakdown of insoluble organic matter (kerogen) in the rock (S2 peak) expressed in mg HC/g rock.
- The temperature at which S2 reaches maximum is the T_{max} .

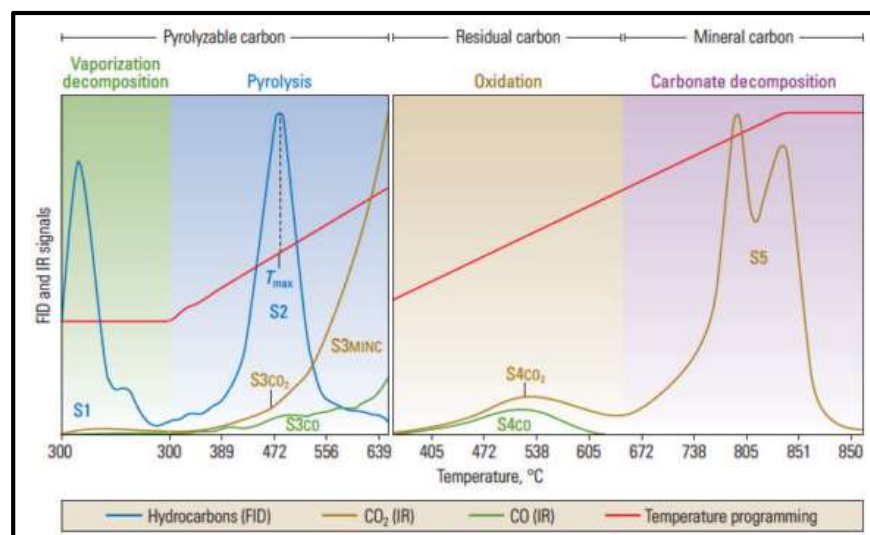


Figure 3.5. A typical Rock-Eval 6 pyrogram (after McCarthy *et al.*, 2011). The pyrolysable carbon (PC) is computed from S1, S2, S3co and S3co₂. Residual carbon (RC) is computed from S4co and S4co₂. Mineral carbon (MINC) is computed from S5 and S3MINC. TOC is calculated by summation of PC and RC

With increasing maturity during catagenesis, hydrocarbons are generated in increasing quantity, so the S2 measurement decreases, while S1 increases (in the absence of migration). The values of T_{max} also increases with increasing maturity (Teichmüller and Durand, 1983) and reflects the increasing thermal energy that is required to break the remaining bonds in kerogen associated with hydrocarbon generation (Killops and Killops, 2005). Thus, T_{max} can be used as a maturity parameter, although it is affected by the type of organic matter because of variation in the thermal energy required to break the different types of bonds present (Peters *et al.*, 2005).

The Total Organic Carbon (TOC) content of the rock is calculated by the summation of pyrolysed carbon (PC) and residual carbon (RC). Hydrogen Index (HI) is the quantity of pyrolysable organic compounds or hydrocarbons from S2 relative to the TOC in the sample, and is computed as $(S2 * 100)/TOC$ expressed in mg HC/g TOC. HI provides an indication of the likely quantitative importance of oil among the total hydrocarbons generated. Generally, a source rock sample just approaching the onset of petroleum generation is considered to have only gas potential if its HI value is ≤ 150 mg/g, but to be mainly oil prone if $HI > 300$ mg/g (Killops and Killops, 2005). However; according to Petersen (2005), $HI > 150$ mg/g is indicative of oil potential for coals. Another useful Rock-Eval parameter applied in this study is the oxygen index (OI) which is used alongside HI to assess kerogen types (e.g. Killops and Killops, 2005). OI is calculated as $(S3 * 100)/TOC$ expressed in mg CO_2/g TOC, where S3 represents the amount of CO and CO_2 generated from the rock expressed in mg $(CO + CO_2)/g$ rock.

76 of the CTB coals under investigation were selected for Rock-Eval 6 analysis at the Center for Environmental Geochemistry, British Geological Survey in Keyworth,

Nottingham. The high organic content of coal lithologies are a potential source of error as the high concentration of pyro-products generally overloads the Rock-Eval FID if the standard sample load of 100 mg is used; thus, a nominal load size of 10 mg is generally recommended for coals and coaly shales (Sykes and Snowdon, 2002). The Rock-Eval 6 analyser was configured in standard mode (pyrolysis and oxidation as a serial process). As per the recommendation of Sykes and Snowdon (2002), between 8 - 9.5 mg (dry wt) of coal were heated from 300 to 650 °C at 25 °C/min in an inert atmosphere of N₂ and the residual carbon oxidised from 300 to 850 °C at 20 °C/min (hold for 5 minutes). Hydrocarbons released during the two stage pyrolysis were measured using a flame ionization detector while CO and CO₂ were measured using an Infrared cell. The performance of the instrument was checked every 10 samples against the accepted values of the Institut Français du Pétrole (IFP) standard (IFP 160 000, S/N1 5-081840). The error on the T_{max} is about ±6 °C in general, and Table 3 shows data is reproduced (<3 % standard deviation).

Sample ID	Area	Location and sample type	Seam	T _{max} (°C)		
				Initial	Repeat	STDEV
Ba1	Bassen	Field sample	Longyear	430	429	0.71
Br16	Breinosa	BH4-2009	Longyear	445	442	2.12
L1	Lunckefjellet	BH15-2011	Svarteper	433	437	2.83
L27	Lunckefjellet	BH15-2011	Longyear	437	434	2.12
L45	Lunckefjellet	BH6A-2007	Svarteper	431	434	2.12
C8	Colesdalen	BH3-2008	Sputnik	443	442	0.71

Table 3.3. Reproducibility data for Rock-Eval 6 analysis using T_{max}

3.2.2.3. Nitrogen Pyrolysis (Retorting)

Pyrolysis of coal can be achieved by heating pulverised coal extremely rapidly (flash pyrolysis); the feed coal passes through a plastic stage beginning at

approximately 350 °C during which the fusible macerals soften and decompose into tarry liquids (considered as the product) in addition to gas and solid char (Taylor *et al.*, 1998). In a commercial plant, the tars have to be hydrogenated to produce heavy or light oil as required. Process efficiency can also be improved by employing a hydrogen atmosphere for the thermal devolatilization of the coal (hydropyrolysis) under conditions of rapid heating to high temperatures and short residence time (Taylor *et al.*, 1998). A nitrogen pyrolysis method using a low nitrogen pressure (2 bars) as applied in this study is designed to replicate a simple retorting approach with the aim of generating and expelling liquid hydrocarbons. This method is adopted from a documented hydropyrolysis technique (Love *et al.*, 1995; Meredith *et al.*, 2004) which involves pyrolysis assisted by high hydrogen gas pressures (150 bars) at the University of Nottingham, UK. The use of low nitrogen gas pressure instead of high hydrogen gas pressure presents an economically viable approach in assessing the retorting potential of the CTB coals as these coals show HI in excess of 250 mg/g (e.g. Marshall *et al.*, 2015a)

A total of 44 CTB coals from all seams excluding the Svea were selected for retorting. Sample preparation involves mixing approximately 0.25 g of milled coal (<100 µm) with 95 % silica sand (ratio 1:20 wt/wt) before introduction in the reactor tube (Figure 3.6) to avoid blockage of nitrogen gas flow due to swelling. It is noted that the silica sand was initially cleaned overnight by solvent Soxhlet extraction as described in Section 3.2.2.1, air dried, and then heated in a furnace at 550 °C for 6 hours to avoid contamination. Figure 3.6 shows the schematic of the nitrogen pyrolysis method; the coal samples were resistively heated in the reactor tube from ambient temperature to 250 °C at 300 °C/min, and further heating to 520 °C at 8 °C/min where it was held for 2 minutes. The experiments were carried out under a nitrogen pressure of 2 bars with flow rate of 1 l/min; a

continuous flow of the nitrogen gas through the reactor bed is maintained to ensure the residence times of generated volatiles are kept at minimum (few seconds), and the product was collected in a dry-ice cooled trap containing silica (Meredith *et al.*, 2004). The products were recovered from silica via elution with DCM/methanol mixture (50:50 vol/vol) and subsequently fractionated into aliphatic and aromatic hydrocarbons, and polar compounds (Section 3.2.2.4) for further analysis. The semi-coke residue and sand mixture was collected from the reactor tube for quantification.

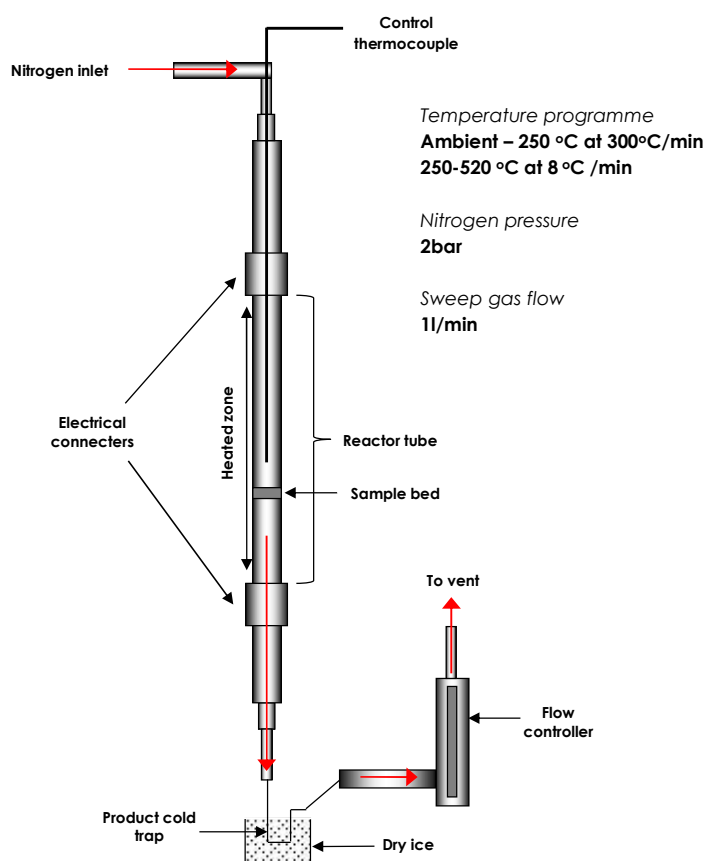


Figure 3.6. Schematic of the coal retorting rig

3.2.2.4. Silica-alumina adsorption column chromatography

When bitumen is mixed with a light hydrocarbon (e.g. pentane) it separates into a soluble fraction (maltenes) and an insoluble fraction (asphaltenes). The maltenes

can then be separated chromatographically into hydrocarbons and resins on the basis of the greater polarity of the resins. The hydrocarbon fraction can further be separated into aliphatic and aromatic sub-fractions, again on the basis of greater polarity of the aromatics (Killops and Killops, 2005). In a strict sense, the term hydrocarbon should only apply to H and C containing compounds, but there are usually other compounds present in the hydrocarbons fraction that contain an atom of N, S or O, generally in the aromatics sub-fraction. Hence, Soxhlet extracts and oil from coal retorting were fractionated into aliphatic, aromatic and NSO polar compounds using silica-alumina adsorption column chromatography to allow qualitative assessments and GC-MS analysis.

The chromatography set-up (Figure 3.7) comprises of a standard 5 ml burette packed with cotton wool at the base followed by alumina and silica packed respectively in $\frac{1}{4}$ and $\frac{3}{4}$ volumes of the graduated area of burette, and represents the stationary phase. The top area of the burette is left unpacked to allow for introduction of samples and solvents, and represents the mobile phase. Soxhlet extracts from 37 coals, and retort oils from 13 coals under study were fractionated. For sample preparation, extracts were weighed, dissolved in DCM and pre-absorbed onto silica and left under a stream of dry nitrogen for solvent to evaporate. The Soxhlet extract and silica mixture is subsequently introduced into the fractionation column by pouring directly from their containing vials into the unpacked zone and then fractionated into aliphatic, aromatic and NSO fractions using successive elutions of 15 ml *n*-hexane, 15 ml *n*-hexane/DCM mixture (9:6 vol/vol) and 15 ml DCM/methanol mixture (7.5:7.5 vol/vol). The amount of each fraction obtained was determined by firstly evaporating the solvents from the mixtures of solvents and fractionated compounds under a stream of dry nitrogen

in pre-weighed vials, and then re-weighing the vials plus fractionated compounds until constant weight is achieved.

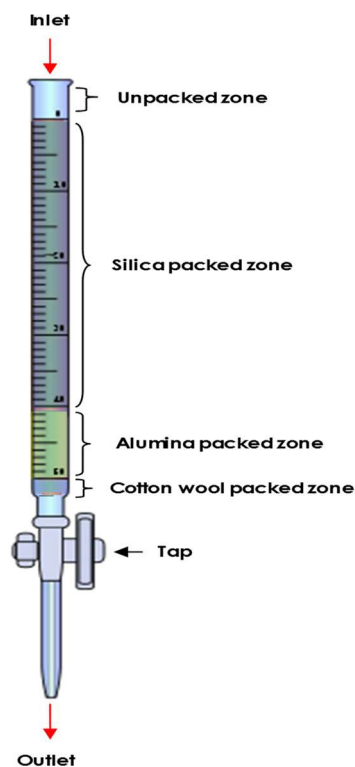


Figure 3.7. Schematic of silica-alumina adsorption column chromatography

3.2.2.5. Gas Chromatography (GC)

The main idea behind chromatography is the separation of a mixture of compounds by using two auxiliary phases; a static one and a mobile one (Simanzhenkov and Idem, 2003). GC is generally divided into two main types; gas-liquid chromatography (GLC) in which the stationary phase is a high boiling liquid and gas-solid chromatography (GSC) in which the stationary phase is a solid. Carrier gases (mobile phase) commonly used include nitrogen, helium and hydrogen, the choice depending on the type of column (packed or capillary), cost and the detector to be used. Helium and hydrogen are the preferred gases

for capillary columns because chromatographic efficiency diminishes more slowly with increasing flow rate above the optimum with these gases than with nitrogen, thus facilitating faster separations. Niessen (2001) stated that the sample introduction is a very critical step in the operation of the GC, reason being that the complete sample ought to be introduced in a narrow band at the top of the column without thermal degradation and/or component discrimination which arises from to differences in volatility. Therefore, samples which must be thermally stable at the operating temperature (usually from ambient to over 400 °C, programmed to suit the elution process), are introduced into the gas flow via an injection port located at the top of the column (Figure 3.8). The column is usually a coil of stainless steel, glass or fused silica tubing which may be 1 - 100 m long and have an internal diameter of between 0.1 - 3 mm. A continuous flow of gas elutes the components from the column in order of increasing distribution ratio from where they pass through a detector (which monitors the carrier gas as it emerges from the column and respond to changes in its composition as solutes are eluted) connected to a recording system.

Gas chromatography has very widespread use, almost entirely for organic materials; its main application is in the analysis of complicated mixtures of many components (100 or more components). It is essentially popular because it has the ability to analyse small sample amounts and the possibility to analyse compounds in trace amounts (as small as 0.5 cm³ for a gas sample and 10 mg for a liquid sample mixtures). Special GCs have been developed to handle samples under 1 mg (Grob and Barry, 2004). GC is useful for both qualitative and quantitative analysis (e.g. Pecsok *et al.*, 1968; Fifield and Kealey, 2000). Other important advantages of gas chromatography include its ability to analyse samples relatively quickly (few minutes to 1 hour) and samples are not destroyed

during analysis (Pecsok *et al.*, 1968; Fifield and Kealey, 2000; Simanzhenkov and Idem, 2003). Compounds analysed in a GC must be in the gaseous phase or should be able to evaporate into the gaseous phase (e.g. Simanzhenkov and Idem, 2003).

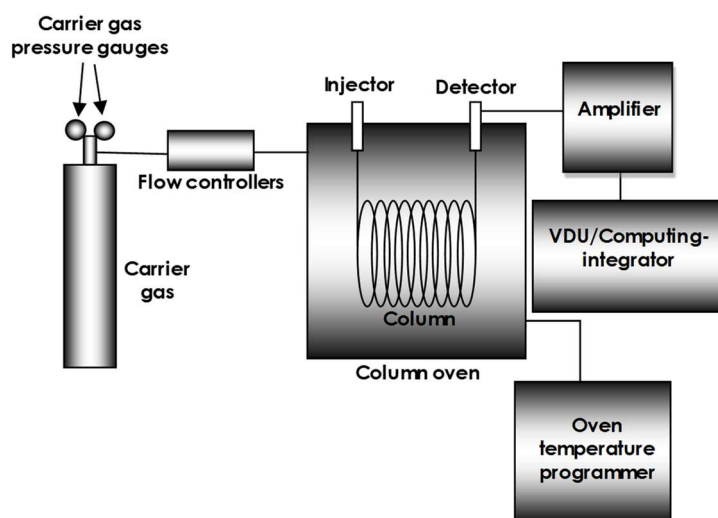


Figure 3.8. Schematic of gas chromatograph

3.2.2.6. Gas Chromatography-Mass Spectrometry (GC-MS)

A GC-MS equipment comprises of a gas chromatograph (described in Section 3.2.2.5) coupled to a mass spectrometer. According to Peters and Moldowan (1993), a typical GC-MS performs six functions namely;

- a) Compound separation (takes place in the GC; Figure 3.9)
- b) Transfer of separated compounds into the ionizing chamber of the mass spectrometer (i.e. interface between the GC and the MS in Figure 3.9)
- c) Ionization
- d) Mass analysis
- e) Detection of the ions by the electron multiplier
- f) Acquisition, processing and display of the data by a computer

The principle of a mass spectrometer (MS) is the production of gas phase ions that are subsequently separated according to their mass-to-charge (m/z) ratio and detected (e.g. Niessen, 2001). The resulting mass spectrum is a plot of the m/z vs response at a constant scan number (related to time), while the mass chromatogram is a plot of the scan number vs response at a constant m/z ratio (Peters and Moldowan, 1993). Each mass spectrum consists of a series of fragment ions that can be used to help elucidate the structure of a single compound, whereas a mass chromatogram can be used to monitor a series of compounds of various molecular weights that will all fragment to form a particular ion (Peters and Moldowan, 1993). Identification of separated components in GC-MS is achieved by feeding the effluent gases from the GC column directly to the MS (Figure 3.9). The carrier gas usually helium is pumped away with the aid of a jet-orifice separator (usually for parked columns) while allowing the sample vapours to pass on into the mass spectrometer (Hsu and Drinkwater, 2001). Eluted components can be detected by either monitoring in full scan (FS) mode, or selected ion monitoring (SIM). FS mode is the sum of the currents generated by all the fragment ions of a particular compound, and is proportional to the instantaneous concentration of that compound in the ionizing chamber of the mass spectrometer, while SIM involves monitoring the ion current for a selected mass fragment (m/z) value characteristic of a particular compound or group of compounds (Hsu and Drinkwater, 2001). Detection by SIM can be made very selective and often specific; it is more sensitive than FS and is therefore particularly useful in trace analysis (Hsu and Drinkwater, 2001). The technique of GC-MS is now well established as one of the most powerful analytical tools available for the study of complex samples (e.g. Fifield and Kealey, 2000). In the petroleum industry, it is suitable for analysing fractions of natural gas to vacuum gas oil with boiling point up to 650 °C, for analysing whole crude oil, pre-

asphalting prior to GC-MS analysis can avoid or reduce contamination at the injector (Hsu and Drinkwater, 2001).

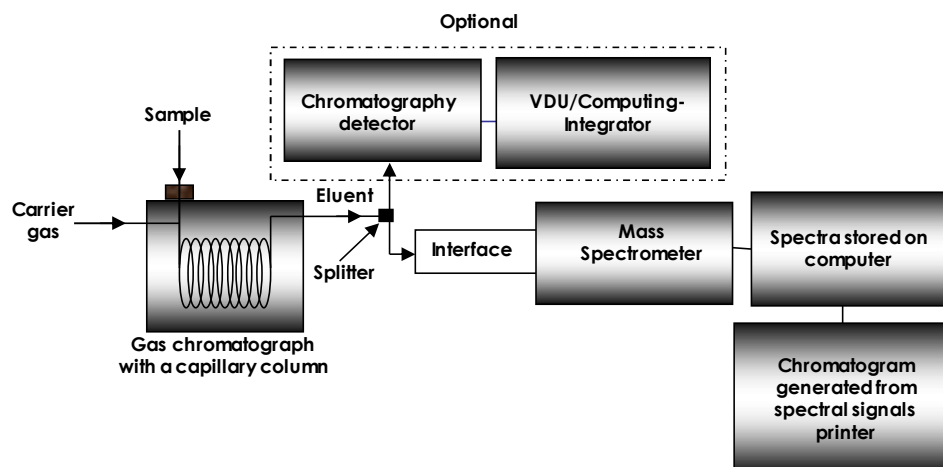


Figure 3.9. Schematic of gas chromatograph – mass spectrometer

Biomarkers present in the aliphatic and aromatic fractions of Soxhlet extracts from 37 coals, and retort products of 11 coals were analysed via GC-MS. Analysis was performed on a Varian Instrument 3800 gas chromatograph interfaced to a 1200 Quadrupole mass spectrometer (ionising energy 70 eV, source temperature 280 °C). Separation was performed on a fused silica capillary column (50 m x 0.25 mm i.d.) coated with BPX5 phase (0.25 µm thickness), using helium as the carrier gas, and an oven programme of 50 °C (hold 2 minutes) increasing to 300 °C at the rate of 4 °C/min (hold 20.5 minutes). FS and SIM modes were used to examine mass range 50 – 450 m/z . Peaks were identified from relative retention times, elution patterns, fragmentation patterns and comparison with published mass-spectra (Bechtel, 2002a; 2002b; 2003; 2004; 2005; Peters *et al.*, 2005). For the integrations of peak area data throughout this study, the ions used are: m/z 71 for *n*-alkanes, pristane and phytane, m/z 191 for regular hopanes, m/z 271 for steranes

and m/z 259 for diasteranes. The Identification of 25-norhopanes was done using m/z 177.

3.2.2.7. ^{13}C NMR (Nuclear Magnetic Resonance Spectrometry)

^{13}C NMR is the application of nuclear magnetic resonance (NMR) spectroscopy to carbon. It is analogous to proton NMR (^1H NMR) and allows the identification of carbon atoms in an organic molecule just as proton NMR identifies hydrogen atoms. Hence it is an important tool in chemical structure elucidation in organic chemistry. ^{13}C NMR detects only the ^{13}C isotope of carbon, whose natural abundance is only 1.1 %; this is due to the fact that ^{12}C , the main carbon isotope, is not detectable by NMR since it has zero net spin (Breitmaier and Bauer, 1984). High resolution solid state 50 MHz ^{13}C NMR analysis of the Longyear and Svea coal samples were carried out in a BrukerAvance 200 spectrometer using the cross polarisation (CP) sequence in conjunction with magic angle spinning (MAS). For CP-MAS analysis, the acquisition time was 0.05 s, the relaxation delay was 1.5 s and the contact time was 1 ms. Samples were packed tight into a cylindrical (7 mm o.d.) zirconia rotor with a cap made of a homopolymer of chlorotrifluoroethene (Kel-F) and spun at the magic angle (54.7356°) with a spinning rate of approximately 5 kHz. Tetrakis (trimethylsilyl) silane (TKS) was added to the samples as an internal standard. The number of scans was 2500 and the free induction decays were processed using a line broadening factor of 50Hz.

3.2.2.8. Pyrolysis-GCMS

The equipment used for flash Py-GCMS was a CDS 5000 pyroprobe (Figure 3.10), connected to an HP 5890 gas chromatograph (GC), with an Agilent 7890B GC with 5977A MSD analyser. The GC was equipped with a 25-m HP-1 column (0.2 mm i.d., film thickness 0.33 μm). The oven of the gas chromatograph was

operated under the following program: isothermal for 5 min at 0 °C, temperature programmed at 5°/min to 300 °C, and then isothermal for 15 min. The MSD was operated in full scan mode (50-550 Da, 0.86 scan/s, 70 eV ionization voltage). 14 coals including the Longyear and Sputnik coals in the CTB, and the Lower Carboniferous coal from Pyramiden were analysed. Approximately 0.5 mg of coal was weighed into a quartz tube and inserted in the middle of the platinum coil (Figure 3.10), and then pyrolysed at 750 °C in a flow of helium. Peak identification was based on mass spectra, GC retention times, with reference to literature (Radke *et al.*, 1982b; 1990; Douglas *et al.*, 1991; Hartgers *et al.*, 1992; Sinninghe Damste *et al.*, 1989, 1992, 1993; Han and Kruger, 1999). The major identified components are the C₅+ *n*-alkanes plus *n*-alkenes (*m/z* 69+71), benzene (*m/z* 78) plus 10 alkylbenzenes (*m/z* 92+106+120), phenol plus 8 alkylphenols (*m/z* 94+108+122) and naphthalene plus 13 alkylnaphthalenes (*m/z* 128+142+156+170) (Table 3.4; Figure 5.9). All other major resolved peaks are also shown on the TIC (Figure 5.9).

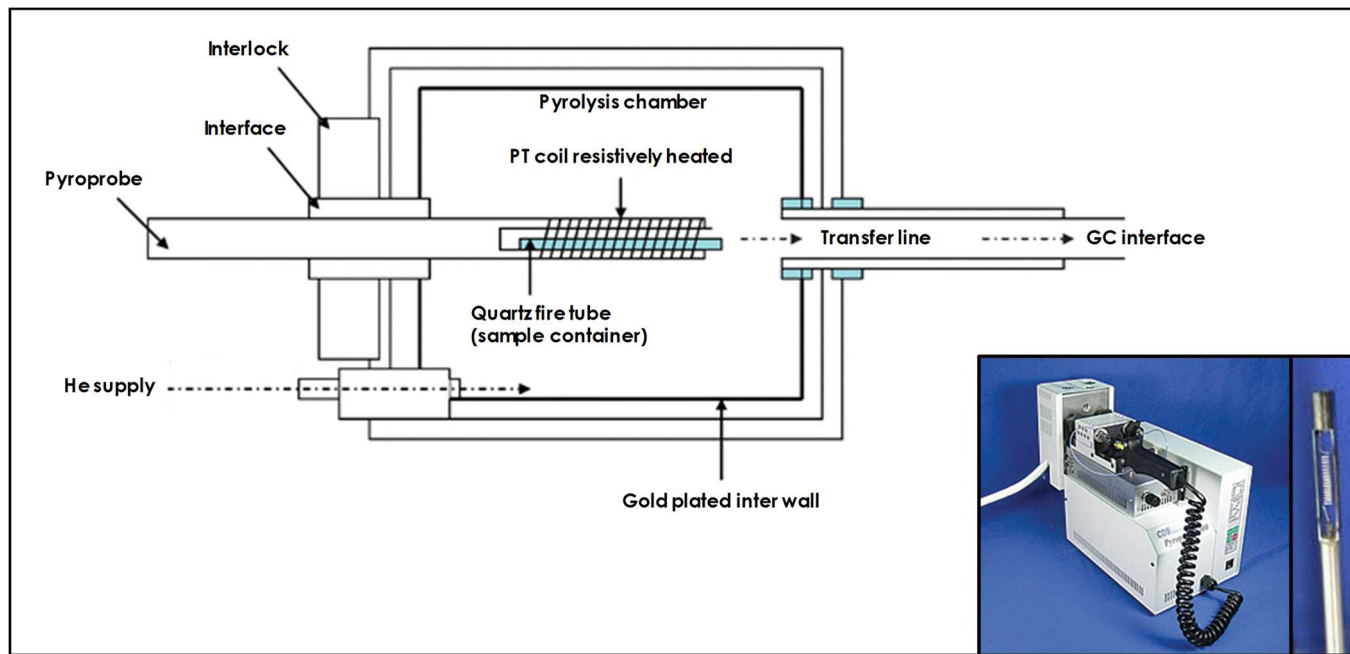


Figure 3.10. Schematic of a pyroprobe. Insert shows a pyroprobe CDS 5000 machine (left) and the probe with platinum coil within which samples (loaded in quartz tube) are inserted and pyrolysed (right).

ID	Compounds	m/z
B	Benzene	78
T	Methylbenzene (Toluene)	92+106+120
B1	Ethylbenzene	92+106+120
B2	1,3-dimethylbenzene	92+106+120
B3	1,4-Dimethylbenzene	92+106+120
B4	Propylbenzene	92+106+120
B5	1-ethyl-3-methylbenzene	92+106+120
B6	1,2,3-trimethylbenzene	92+106+120
B7	1-ethyl-3-methylbenzene	92+106+120
B8	1,2,3-trimethylbenzene	92+106+120
B9	1,2,3-trimethylbenzene	92+106+120
P	Phenol	94+108+122
P1	2-methylphenol	94+108+122
P2	4-methylphenol	94+108+122
P3	2,5-dimethylphenol	94+108+122
P4	2-ethylphenol	94+108+122
P5	3,4-dimethylphenol	94+108+122
P6	4-ethylphenol	94+108+122
P7	3,5-dimethylphenol	94+108+122
P8	2,5 or 2,3-dimethylphenol	94+108+122
N	Naphthalene	128+142+156+170
N1	2-methylnaphthalene	128+142+156+170
N2	1-methylnaphthalene	128+142+156+170
N3	1,7-dimethylnaphthalene	128+142+156+170
N4	1,7-dimethylnaphthalene	128+142+156+170
N5	1,7-dimethylnaphthalene	128+142+156+170
N6	1,7-dimethylnaphthalene	128+142+156+170
N7	1,7-dimethylnaphthalene	128+142+156+170
N8	1,4-dimethylnaphthalene	128+142+156+170
N9	1,6,7-trimethylnaphthalene	128+142+156+170
N10	2,3,6-trimethylnaphthalene	128+142+156+170
N11	1,6,7-trimethylnaphthalene	128+142+156+170
N12	1,6,7-trimethylnaphthalene	128+142+156+170
N13	1,6,7-trimethylnaphthalene	128+142+156+170

Table 3.4. Selected aromatic components from Py-GCMS used to determine petroleum type and source rock organic facies in Chapter 5. The IDs represent the numbering of the compounds labelled from the left to right hand side of Figure 5.9.

3.2.3. Inorganic Geochemistry

3.2.3.1. Ash Measurement

Coal ash content determination is based on the amount of residue (ash) left behind after heating coal in a muffle furnace at high temperatures (USOCR, 1967). A muffle furnace has an externally heated chamber, the walls of which radiantly heat the contents of the chamber, so that the material being heated has no contact with the flame. According to USOCR (1967), muffle furnaces are

designed to maintain an ample supply of air at all times to ensure complete oxidation and removal of combustion products formed during ignition of sample.

Ash procedure employed in this study is as follows:

- Milled coal samples (<100 µm) in bottles (without lids) and empty crucibles were oven-dried overnight at 60 °C to remove moisture.
- Sample bottles were removed hot, and lids were replaced immediately and left to cool to room temperature. Crucibles were left to cool to room temperature inside the switched off oven with the oven door closed.
- 1 ± 0.1 g of oven dried sample was weighed onto each crucible ensuring samples are well spread out in crucibles.
- Crucibles containing samples were loaded into a room temperature carbolite muffle furnace (Figure 3.11.A) and heated up to 825 °C in approximately 2 hours where it was held for a minimum of 3 hours before switch off.
- The furnace door was then opened to allow cooling to room temperature.
- Crucibles plus ashes (3.11.B) were re-weighed immediately after cooling to avoid ignition losses of coal ashes (i.e. moisture or CO₂ that may be absorbed by ashes if left for long periods after cooling) although such losses are generally low, ranging from 0.1 to 0.3 % (USOCR, 1967). The empty crucibles are also re-weighed.
- Ash percent is calculated as:

$$\text{Ash \%} = \frac{(\text{wt of ash and crucib} \quad \text{of crucible}) * 100}{\text{wt of coal}} \quad (3.1)$$

To check precision and errors due to flying ashes, samples were loaded into the furnace in duplicates alongside 2 coal reference materials (SARM18 and SARM19)

and blanks (Figure 3.8.B). Errors on duplicates were monitored throughout to ensure they are;

- a) less than 0.1 % for ash content of ≤ 15 wt %
- b) less than 0.2 % for ash content of ≥ 15 wt %



Figure 3.11. Ash content determination. A) Carbolite muffle furnace with coal samples in crucibles before heating, B) Crucibles containing ash and empty crucibles (blanks) after heating

3.2.3.2. ICP-AES

One of the principal methods of analysing the elemental composition of geochemical samples is inductively coupled plasma - atomic emission spectrometry (ICP-AES); this method provides a rapid and precise means of monitoring up to 50 elements simultaneously for minor and trace levels (Templeton, 1994; Lajunen and Peramaki, 2004). When the sample solution is introduced into the spectrometer (Figure 3.12), it becomes atomized into a mist-like cloud; this mist is carried into the argon plasma with a stream of argon gas.

The plasma (ionized argon) produces temperatures close to 7,000 °C, which thermally excites the outer-shell electrons of the elements in the sample. The relaxation of the excited electrons as they return to the ground state is accompanied by the emission of photons of light with an energy characteristic of the element. As the sample contains a mixture of elements, a spectrum of light wavelengths is emitted simultaneously. The spectrometer uses a grating to disperse the light, separating the particular element emissions and directing each to a dedicated photomultiplier tube detector. The more intense this light is, the more concentrated the element. A computer converts the electronic signal from the photomultiplier tubes into concentrations. The determination portion of the process takes approximately 2 minutes to complete (Templeton, 1994).

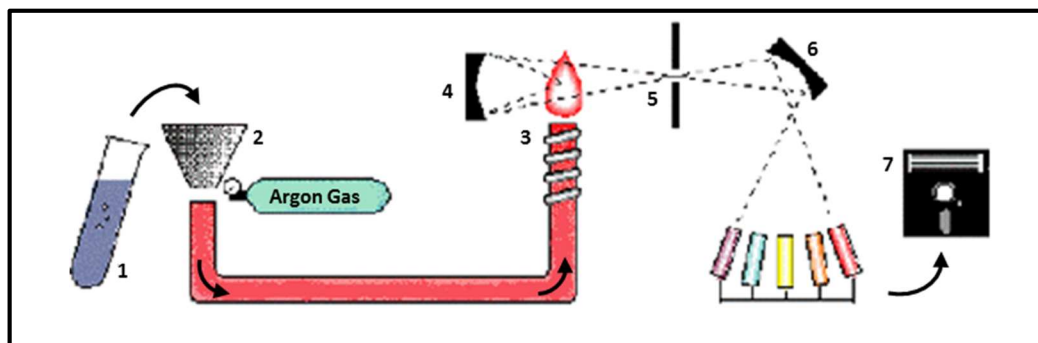


Figure 3.12. Schematic of inductively coupled plasma - atomic emission spectrometry. Note: Aqueous sample (1) is pumped and atomized with argon gas (2) into the hot plasma (3). The sample is excited, emitting light wavelengths characteristic of its elements. A mirror (4) reflects the light through the entrance slit of the spectrometer (5) onto a grating (6) that separates the element wavelengths onto photomultiplier detector (7) (Modified from USGS, 2015).

Major and trace elements determination in the samples under investigation was done at the University of Nottingham, UK. Sample preparation involves drying milled coal (<100 µm) in an oven overnight at 60 °C, followed by total digestion of samples in acids in the following steps:

- 1) Between 0.45 and 0.55 g of dried coal samples were weighed into microwave pressure vessels (Figure 3.13).

2) Total digestion of samples in acids

2a) Addition of nitric acid (69 % w/v)

- 30 ml of concentrated nitric acid was added to the samples in the vessels.
- Vessels were then capped and tightened in the cradle (Figure 3.13) using a torque wrench and placed in a CEM MARS5 sealed vessel microwave digestion system (after Laban and Atkins, 1999). Microwaving was done using the following programmes:

Ramp to 550 p.s.i. and 190 °C in 15 minutes, and then hold for 30 minutes. (Note: allow microwave to cool down to 50 °C before opening pressure vessels)

2b) Addition of hydrochloric acid (36 % w/v) and hydrofluoric acid (40 % w/v)

- Following stage 2a, 8 ml of concentrated hydrochloric acid and 2ml of concentrated hydrofluoric acid were added to the samples in the vessels.
- Vessels were then capped and tightened in the cradle using a torque wrench and placed in the microwave for microwaving using the following programme:

Ramp to 550 p.s.i. and 190 °C in 15 minutes, then hold for 20 minutes. (Note: allow microwave to cool down to 50 °C before opening pressure vessels.)

2c) Addition of 4% boric acid (4 % w/v)

- Following stage 2b, 15 ml of 4 % boric acid was added to the samples in the vessels.
- Vessels were then capped and tightened in the cradle using a torque wrench and placed into the microwave for microwaving using the following programme:

Ramp to 550 p.s.i. and 170 °C in 10 minutes, then hold for 5 minutes. (Note: allow microwave to cool down to 50 °C before opening pressure vessels)

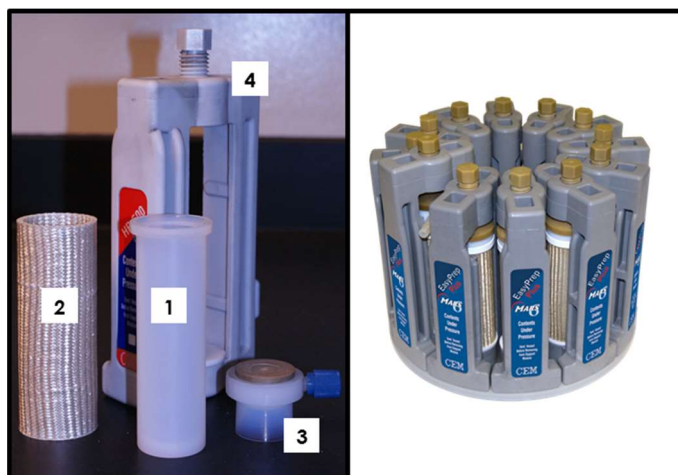


Figure 3.13. Acid digestion kit for ICP-AES sample preparation. Left – A pressure vessel and components. 1) Vessel, 2) Sleeve, 3) Cap, 4) Cradle. Right – A set of 12 vessels

3) Transfer of digested samples

Following digestion, vessels were removed from the cradles and sleeves and contents poured into labelled 100 ml volumetric flask. Vessels were then rinsed with several small volumes of 'ultrapure' water and added to the volumetric flask ensuring the 100 ml mark on the flask is reached. The volumetric flask contents were then transferred into labelled polypropylene bottles for storage, in readiness for ICP-AES analysis.

Following acid digestion, measurement of major and trace element contents was done using the ICP-AES Perkin-Elmer Optima 3300DV emission spectrometer. Accuracy and data reliability was checked by duplicating 1 sample, alongside 1 SARM18 coal reference material in every batch of 12 specimens. This was done to ensure deviation was consistently less than 10 %. Data quality was evaluated by

examining the standard deviation values for sample repeats, and comparing the measured and reported data of SARM18 standard (Table 3.5). The deviation for measured and reported SARM18 values is less than 10 % for all elements with the exception of phosphorus (P). Although, the reported SARM18 data are generally reproduced, the relatively low values of measured P were a cause for concern as values of up to 14 ppm less than reported values resulted in up to 45 % deviation. Consequently, SARM19 standard material was analysed and used as a check; although this showed relatively lower deviation for P (19 %), the deviation is still higher than acceptable (10 %) (Table 3.6). It was therefore concluded that P is generally under-detected in both standards because its concentration in solution for SARM18 in particular is very low (i.e. at or below detection limit). Consequently, the concentration of measured P will have large errors. Questions may arise as to why manganese with similarly low concentration in these standards, show very low deviation (Tables 3.5 and 3.6); this is because different elements have different detection limits. Mn can be measured at much lower concentrations than P as the detection limit for Mn is in the order of 50 - 100 times lower than P (Lajunen and Peramaki, 2004). With regards to the CTB coals under study, the perceived under-detection of P was not a cause of major concern as its concentration is generally low and often below detection in the Longyear, Svarteper and Askeladden seams (e.g. Orheim *et al.*, 2007; Marshall, 2013), which are the seams of main concern in this study.

Elements	SARM18 measurements x 7 (ppm)					SARM18 reported (ppm)			Deviation of SARM 18 measured from reported (%)
	Minimum	Maximum	Mean	Median	STDEV	Minimum	Maximum	Mean	
Al	11224	13389	12253	12199	1032	13443	13813	13628	10.1
Ca	1276	1458	1387	1407	82	1215	1358	1286	7.9
Fe	1966	2028	1993	1990	26	1958	2028	1993	0
K	1108	1161	1143	1152	24	1162	1245	1204	5.1
Mg	563	655	614	618	42	603	663	633	3
Mn	22	23	22	22	1	21	23	22	0
Na	123	129	126	125	3	130	130	130	3.1
P	10	23	17	17	6	26	36	31	45.2
S	5675	5757	5730	5744	37	5300	6200	5750	0.3
Ti	662	684	676	680	10	665	695	680	0.6

Table 3.5. SARM18 standard and reproducibility data for ICP-AES analysis. Note: relatively high percent deviation of phosphorous. SARM18 reported data are as per SARM18 Certificate of Analysis from the Council for Mineral Technology (MINTEK), South Africa.

Elements	SARM19 measured (ppm)	SARM19 reported (ppm)	Deviation of SARM19 measured from reported (%)
Al	39767	42366	6.1
Ca	9735	9934	2
Fe	12245	12205	0.3
K	1875	2034	7.8
Mg	1180	1266	6.8
Mn	157	156	1.3
Na	2084	2188	4.8
P	99	122	18.9
S	14596	14850	1.7
Ti	2034	2038	0.2

Table 3.6. SARM19 standard and reproducibility data for ICP-AES analysis. Note: percent deviation of phosphorous is greater than accepted (>10 %). SARM19 reported data are as per SARM19 Certificate of Analysis from the Council for Mineral Technology (MINTEK), South Africa.

3.3. Summary and Conclusions

This chapter explains the rationale behind the selection of sample locations. It explains in detail, the working principles of adopted techniques and methods, and discusses why these were adopted in this study. The systematic approaches to sample preparation for various methods are also highlighted. Thus, data obtained are considered to be of acceptable standards for further analysis.

**VITRINITE REFLECTANCE VARIATIONS IN THE CENTRAL TERTIARY BASIN COALS,
SPITSBERGEN - IMPLICATIONS FOR LOCAL AND REGIONAL BURIAL MODELS**

4.1. Introduction

In the vitrinite reflectance (VR) records of the Central Tertiary Basin (CTB), apparent gaps and inversions (i.e. large decrease and/or increase in VR within a relatively small depth range) appear common, notably between the Triassic-Jurassic boundary and Cretaceous-Basal Tertiary strata (Paech and Koch, 2001). Orheim *et al.* (2007) also reported a VR gap (sudden change from 0.94 to 0.71% R_o) within the Basal Tertiary Firkanten Fm. coal seams; considering these seams are stratigraphically only 40 m apart, this would imply a VR gradient in excess of 5.0 R_o /km which is not the case. Consequently, Orheim *et al.* (2007) provided two possible explanations for the VR variations within the Tertiary coals; namely an insulation effect of an underlying seam and the suppression of VR by bitumen enrichment. Tertiary VR data forms a key part of many estimates regarding geothermal gradient, maximum burial depth and overburden loss (Major and Nagy, 1972; Manum and Throndsen, 1978; Throndsen, 1982; Paech and Koch, 2001). Assuming the VR gaps are caused by suppression of VR, the replacement of suppressed VR values with their non-suppressed equivalent may therefore imply re-evaluation of existing estimates of erosion.

In the Adventdalen area (Figure 3.1), elevated heat flows during burial have been implied in a number of studies (Major and Nagy, 1972; Manum and Throndsen, 1978; Throndsen, 1982; Paech and Koch, 2001; Braathen *et al.*, 2012). The presence of bentonite beds in the Van Mijenfjorden Group sediments and a dolerite sill in the Bjørndalen area near Longyearbyen (Pers. Comm. Trygvason Eliassen, 2014 cited in Marshall *et al.*, 2015b) indicates the CTB was subject to

volcanic activity in the Tertiary. Additionally, there are several basaltic Quaternary-age volcanoes on north-western Spitsbergen (Bockfjorden and Woodfjorden areas) associated with the Breibogen-Bockfjorden fault system (Jamtveit *et al.* 2006; Salvigsen and Høgvard 2007), which runs along Bockfjorden and extends southwards to Isfjorden (Figure 1.1) near Longyearbyen (Treiman, 2012). The lateral/vertical extent of temperature effects associated with igneous intrusions on country rocks depends on a number of factors including but not limited to the intrusion thickness and lithology, coal rank within the country rock at the time of intrusion and porewater volume (degree of compaction) of country rock (Jones and Creaney, 1977; Clayton and Bostick, 1986; Raymond and Murchison, 1988, George, 1992; Bishop and Abbot, 1995; Farrimond *et al.*, 1996). Reeckmann *et al.* (1985) reported that temperatures of at least 110 – 130 °C occurred up to 3 km from thin doleritic dikes and sills in porous sandstones; pre-intrusion temperatures were around 40 °C, with evidence of increased temperature also apparent 26 km from intrusion. These workers postulated that efficient vertical and lateral heat transfer occurred by movement of hot waters through the sedimentary rocks over large distances away from the igneous bodies. Schutter (2010), however suggested that most shallow igneous intrusions are volumetrically too small to affect a large volume of rock, and even flood basalts cool too quickly to have a marked effect, and that most thermal effects are due to regional heating or hydrothermal circulation. Thus, hot waters associated with intrusions may be important in elevating thermal regime both locally and regionally, although VR appears to be less sensitive to heat pulses of short duration, even in situations where temperatures greater than 110 °C occurred (Reeckmann *et al.*, 1985). While the increase of VR with rising temperature is different for “burial heating” and “hydrothermal heating” (Barker and Goldstein, 1990; Mukhopadhyay and Dow, 1994), it is unclear whether either

of these cases could lead to VR gaps and inversions within relatively small depth intervals as observed in the CTB.

VR suppression by bitumen is well documented in oil source rocks including coals (Price, 1985; Wilkins *et al.*, 1992; Lo, 1993; George *et al.*, 1994; Diessel and Gammidge, 1998; Carr, 2000; Barker *et al.*, 2004; Barker *et al.*, 2007; Bostick, 2011; Kalinowski and Gurba, 2014); the presence of fluorescent (perhydrous) vitrinite enriched in hydrogen rich material suppresses the VR values and it is an indicator of oil potential (Diessel and Gammidge, 1998 and references within). As VR is an indirect measure of aromaticity (Miknis *et al.*, 1981; Russell *et al.*, 1983; Davidson, 1986; Carr and Williamson, 1990; Kalkreuth *et al.*, 1991; Suggate and Dickinson, 2004), any excess aliphatic material will lead to suppression of VR values. Orheim *et al.*, (2007) observed that some Firkanten Fm. coals in Svalbard fluoresce under UV light, producing droplets of oil during preparation. In addition, Marshall *et al.* (2015a) showed that some of these coals produce up to 40 % hydrocarbons when a mixture of Soxhlet solvent extraction and hydrous pyrolysis was applied. This would indicate that the coals have at least some oil potential and therefore VR suppression by bitumen may present a reasonable explanation. The effect of bitumen suppressing vitrinite reflectance has been investigated by Barker *et al.* (2007), who found that vitrinite reflectance suppression did not appear to be caused by bitumen, as the vitrinite reflectance after solvent extraction for 48 hours using chloroform did not produce an increase in the reflectance of the solvent-extracted samples compared with the samples that had not been extracted. These findings are consistent with the results obtained in a study of suppressed Pennsylvanian coals and shales, where solvent extraction did not increase the reflectance of the extracted samples compared with the initial samples (Wenger and Baker, 1987). However, there is a problem with chloroform

extraction in that the amount of extract can be significantly increased using pyridine and hydrolysis, as physically-trapped and covalently-bonded components were removed from the polymeric structure of the vitrinite that were not removed by chloroform extraction (Love *et al.*, 1991; 1996). This potential inability of the chloroform extract method led Carr (2000) to suggest that bitumen impregnation together with hydrogen-rich vitrinites and high liptinite concentrations were all plausible models to account for the occurrence of VR suppression. The oil-prone nature of the CTB coals have been linked to bitumen impregnated vitrinites with HI values of around 300 - 400 mg/g TOC measured in the coals (Marshall *et al.*, 2015a). Because these coals are generally low in liptinites with mean values ≤ 10 vol % (Ćmiel and Fabiańska, 2004; Orheim *et al.*, 2007; Marshall *et al.*, 2015a), bitumen impregnation and hydrogen-rich vitrinites would most likely account for VR suppression if occurring in these coals.

Therefore, this chapter investigates the bulk and high resolution VR measurements to examine whether reported VR variability could be replicated. Additionally, other maturity parameters such as organic biomarkers, Rock-Eval 6 and aromaticity were utilised to provide alternative estimates of maturity from the coals. Focussing upon the role of oil potential on VR suppression, the Rock-Eval HI values were compared with VR to attempt to correct for possible suppression effect. The implications for the thermal regime and missing overburden estimates are then discussed.

4.2. Vitrinite Reflectance Assessments in Areas under Study

The use of vitrinite reflectance (VR) as a tool for rank and maturity determination has been discussed (Sections 2.1.3.1 and 3.2.1.2); thus this section will discuss the measured VR of the coals under investigation. VR values measured from two bulk

samples of Svea and Longyear coal seams are 0.78 and 0.65% R_o respectively (Table 4.1) which replicates the VR gap reported by Orheim *et al.*, (2007). Therefore, to gain further understanding of the main cause of the VR gap and the extent of the VR variations, the Longyear seams are examined at higher resolution in coals from three sub-regions; Adventdalen (Bassen and Breinosa), Lunckefjellet and Colesdalen (Figure 3.1)

4.2.1. Adventdalen

Coals from the Adventdalen sub-region are vitrinite dominated (Tables 5.1) with the exception of the Svea coal which is relatively inertinite rich (Orheim *et al.*, 2007; Marshall, 2013; Marshall *et al.*, 2015a). The vitrinites exhibit dull orange/brown fluorescence under blue light excitation (Figures 4.1.1, 4.1.2, 5.2, 5.11, 5.18 and 5.19). VR measurements show a wide range of values between 0.50 - 0.79% R_o ; consistently high values are observed within the Svea coals in Breinosa (0.76 – 0.79% R_o), while the upper Longyear coals in Mine 7 show the lowest values (0.50 – 0.57% R_o) (Figure 4.2; Table 4.1). The Longyear coals from Bassen and Mine 7 show similar range of VR values (0.54 – 0.73 and 0.5 – 0.79% R_o respectively; Figure 4.2), which is unexpected as the Bassen samples are up-dip of the Breinosa samples, and therefore should have lower maturities. There is a distinct difference between the upper and lower Longyear seam in Mine 7 and Bassen in that the VR values in upper seam are generally lower than values in the lower seam; Figure 4.2). Unlike the Mine 7 and Bassen samples, the VR values from the BH4-2009 locality show relatively less variation (0.59 – 0.69% R_o ; Figure 4.2), which is perhaps the product of a more homogenous composition.

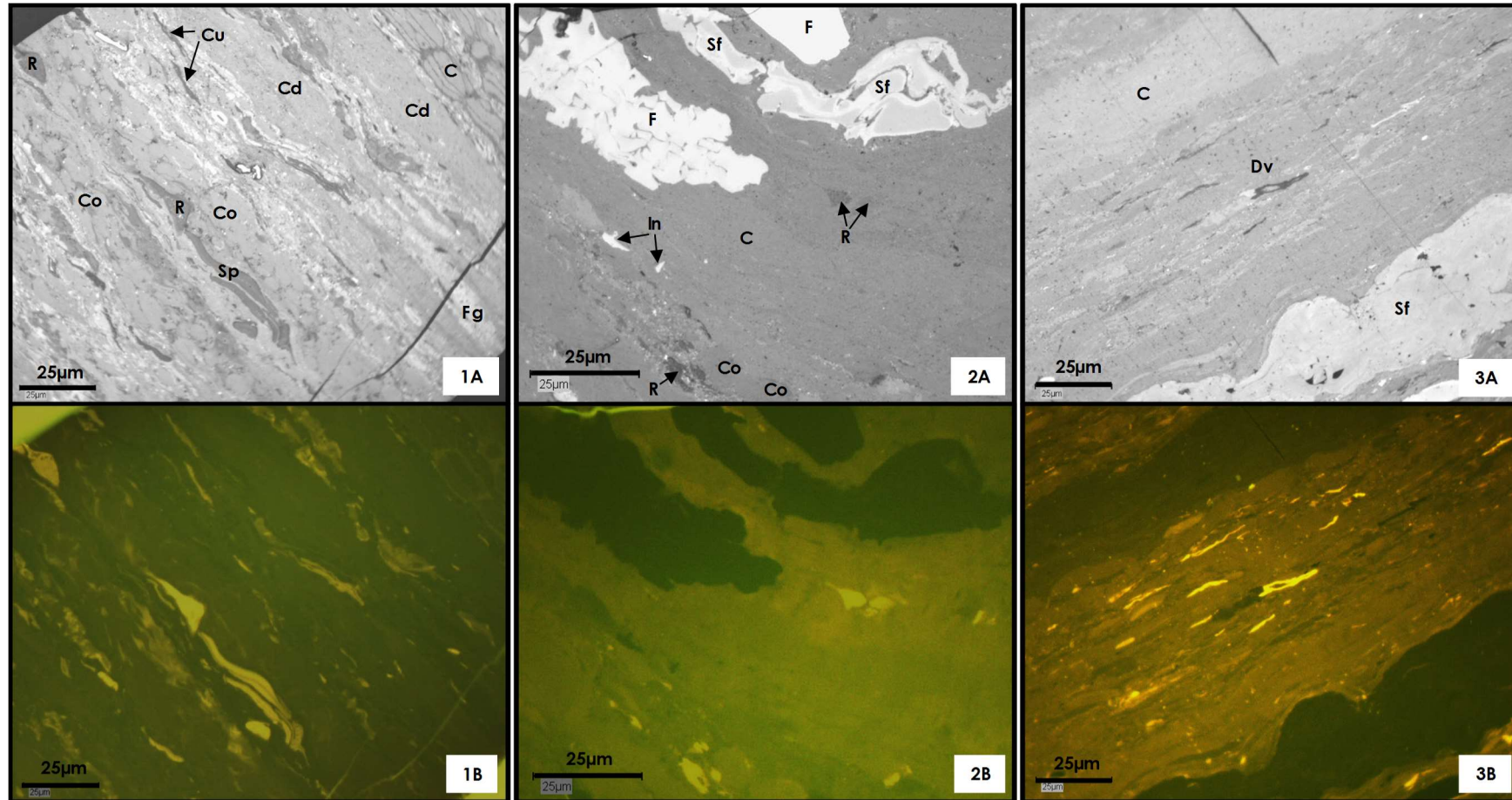


Figure 4.1. Photomicrographs showing the fluorescing (perhydrous) nature of various vitrinite group macerals in the CTB coals. A) Bassen sample Ba1, B) Breinosa sample Br12, C) Colesdalen sample C3. (A - white light, B - blue light). Note: Photomicrographs from Lunckefjellet samples are shown in Figure 5.18. In 3, the vitrinites show varying fluorescence intensities with the detrovitrinite (Dv) displaying stronger fluorescence than the collotelinite (C). Co = corpogelinite, Cd = collodetrinite, Sp = sporinite, R = resinite, Fg = funginite, In = inertodetrinite, F = fusinite, Sf = semifusinite.

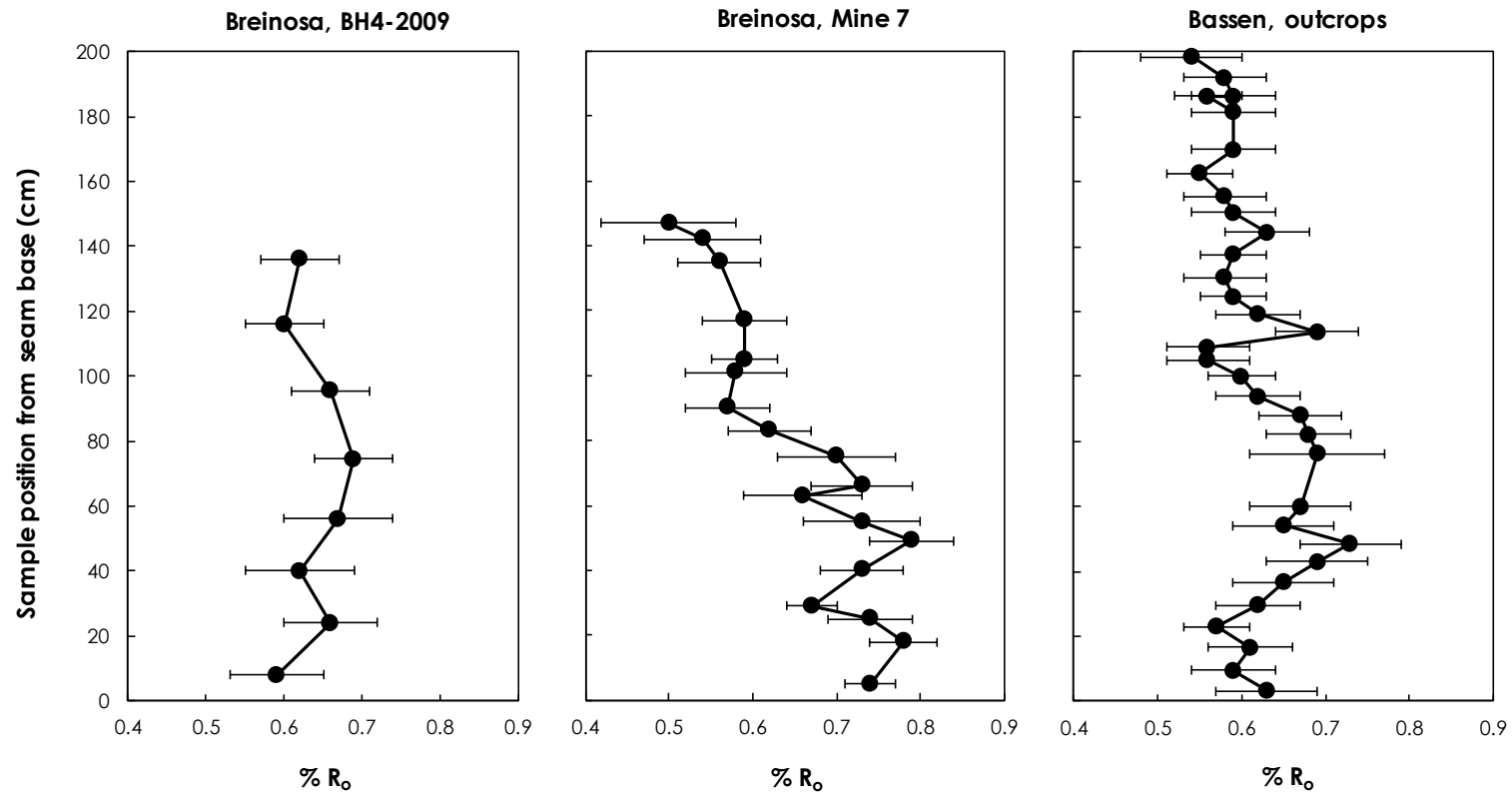


Figure 4.2. Comparing VR profiles within the Longyear seam across Adventdalen. Note: large variations in VR within single seams which generally decrease from base to top of seam in Mine 7 and Bassen. Error bars represent standard deviation of VR measurements (STDEV range 0.03 – 0.08 % R_o)

On examination of the VR histograms of the Bassen samples (Figure 4.3), it was observed that samples with relatively lower VR values, displayed broader histograms which are accompanied by a reduction in the number of higher reflectance measurements, compared to samples having higher VR values. In addition, rather than a single main peak, measurements tend to display a multi-modal distribution (e.g. Sample Ba1 at 198.5 cm above seam base; Figure 4.3). The broad and multi-modal distribution is attributed to the variations in hydrogen enrichment between vitrinite particles, which is consistent with the findings of Wilkins *et al.* (1992) who noted a relatively large intra- and inter-particle variation in the fluorescence of desmocollinites in a marine influenced Greta coal from Sydney Basin.

4.2.2. Lunckefjellet

The Lunckefjellet sub-region is vitrinite dominated with low inertinite and liptinites (Table 5.1), which is similar to observations of the Adventdalen samples. The vitrinites also exhibit fluorescence under blue light excitation (Figure 5.18). Greatest range of VR values (0.58 - 0.76% R_o) is observed in the northernmost sampling locality (BH6A-2007) which appears to decrease down-dip to BH10-2007 (0.58 - 0.71% R_o), BH10-2009 (0.61 - 0.75% R_o) and BH15-2011 (0.55 - 0.70% R_o) contrary to expectations (Figure 4.4). In addition, the Longyear coals show a general decrease in VR values from base to top of seam (Figure 4.4), which is similar to observations in Adventdalen. On examination of the VR histograms, a rather broad range of measurements were observed, with some samples displaying bi-modal distribution (e.g. Sample L10 at 200 cm above seam base at BH15-2001 locality; Figure 4.5).

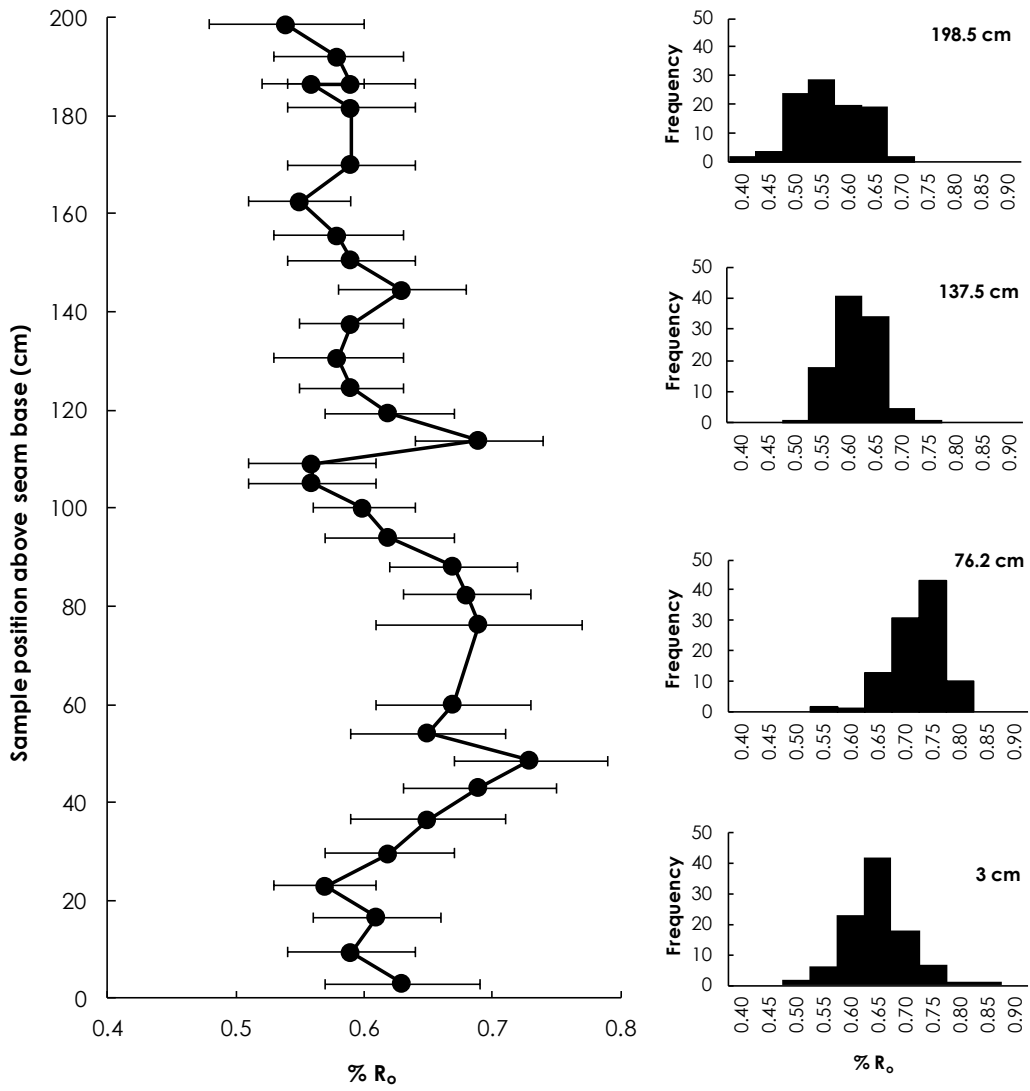


Figure 4.3. VR variation within the Longyear seam in Bassen. Note: Samples with lower VR values tend to display multi-modal distribution, with less number of higher reflectance measurements. Error bars represent standard deviation of VR measurements (STDEV range 0.04 – 0.08 % R_o)

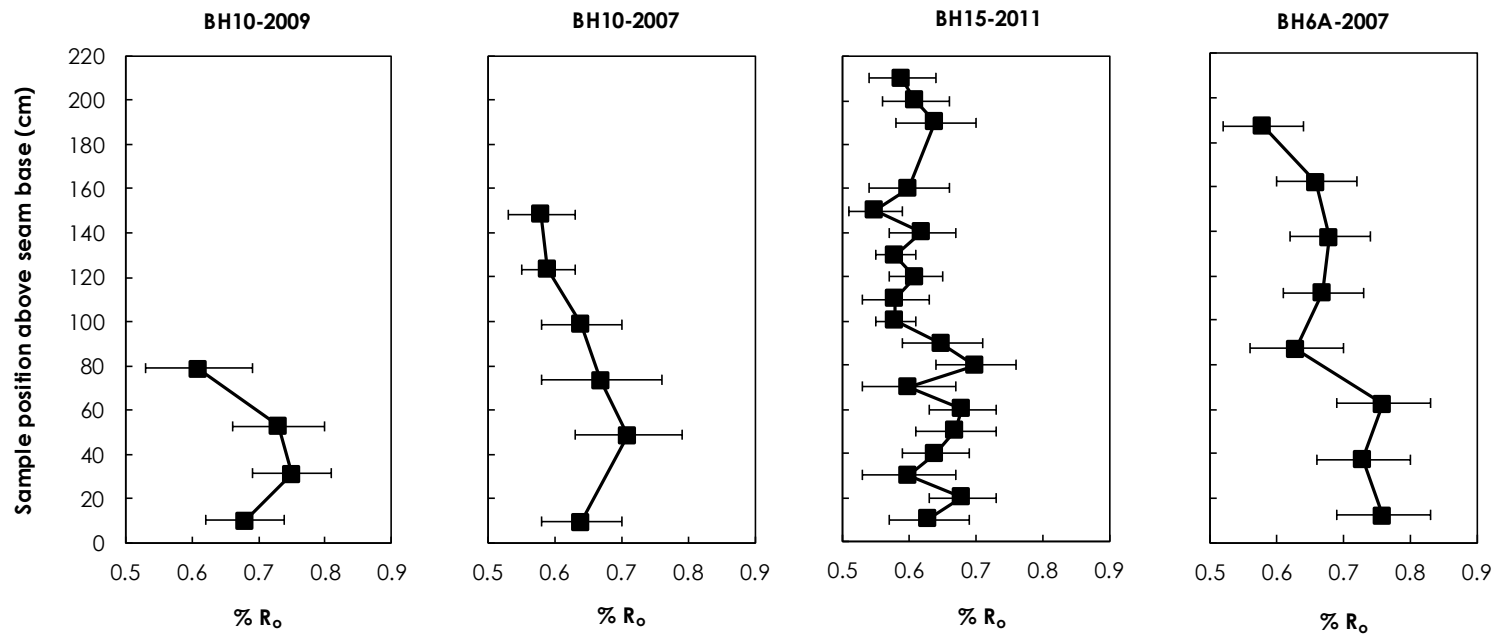


Figure 4.4. Comparing VR profiles within the Longyear seam across Lunckefjellet. Note: the large variations in VR within single seams and general decrease from base to top of seam. Error bars represent standard deviation of VR measurements (STDEV range 0.03 – 0.09 % R_o)

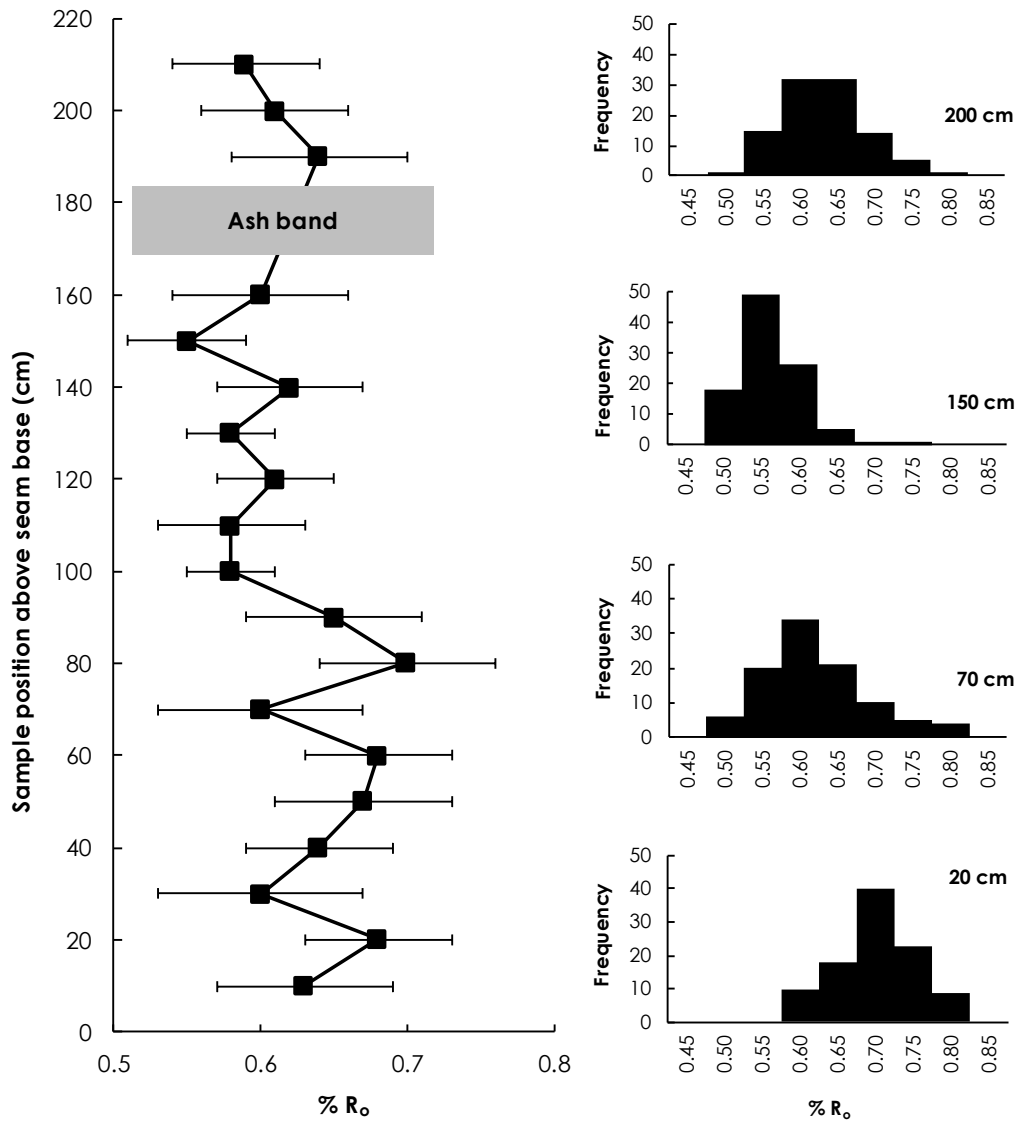


Figure 4.5. VR variation within the Longyear seam at Lunckefjellet BH15-2011 locality. Note: Measurements are generally lower in the upper seam. Broad and bimodal histograms are also observed. Error bars represent standard deviation of VR measurements (STDEV range 0.03 – 0.07 % R_o)

4.2.3. Colesdalen

Although the Sputnik coals in Colesdalen have higher inertinite contents compared to the Longyear coals in Adventdalen and Lunckefjellet, they are nonetheless vitrinite dominated (Table 5.1). These coals show elevated VR values compared to the Longyear coals, but also display a wide range of VR values (0.65 – 0.80% R_o) (Figure 4.6). The relatively higher VR values observed in the Sputnik coals are consistent with their closer proximity to basin center, even though their high inertinite content may be having some effects on VR as vitrinites next to inertinites have higher reflectance compared to vitrinites farther away from inertinites (Taylor *et al.*, 1998). The vitrinites exhibit varying fluorescence intensities (Figure 4.1.3), which is reflected in the broad VR histograms (Figure 4.6). Also, samples with lower VR (e.g. Sample C6 at 80.5 cm above seam base) tend towards a bi-modal distribution, while those with higher VR (e.g. Sample C8 at 34.5 cm above seam base) display a clear uni-modal distribution.

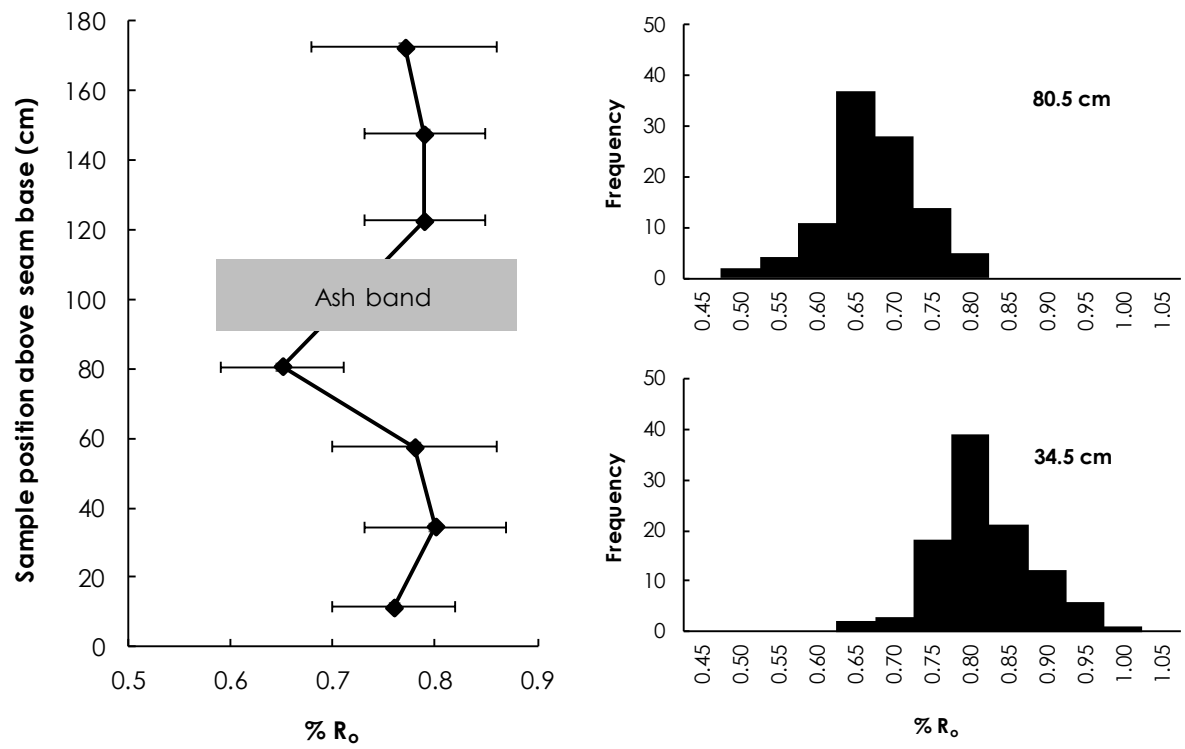


Figure 4.6. Left: VR profile in the Sputnik seam in Colesdalen. Error bars represent standard deviation of VR measurements (STDEV range between 0.06 – 0.09 % R_o). VR histogram of sample C8 at 34.50 cm from seam base in Colesdalen area (Synndalen BH3-2008 locality). Note: the broad distribution of measurements indicates the presence of both normal and perhydrous vitrinites

4.2.4. Summary

The VR measurements from the Adventdalen, Lunckefjellet and Colesdalen sub-regions show large variations (up to $\sim 0.3\%$ R_o) within seams, and importantly replicate the documented VR gaps (Orheim *et al.*, 2007). Also, numerous small and large scale variations, comprising rapid VR drops and rise have been observed, and are prominent within the Longyear coals in Bassen, Mine 7, Lunckefjellet BH15-2011 and Lunckefjellet BH6A-2007 localities (Figures 4.2 and 4.4). In addition, VR measurements generally decrease from base to the top of the Longyear seam. The high degree of similarity in VR distributions, particularly between the Adventdalen and Lunckefjellet samples implies similar control(s) on the relatively large VR variations in the coals under study. Because these seams are ≤ 2.1 m thick, these variations are unlikely a product of differing thermal histories. Fluorescence variation within and between vitrinite particles in the coals under study have been observed (Figures 4.1, 5.2, 5.11, 5.18 and 5.19), and it is reflected by the bi-modal histograms and the generally broad range of VR measurements that have been seen (Figures 4.3, 4.5 and 4.6). These observations are consistent with the relatively large intra- and inter-particle variation in the fluorescence of desmocollinites in a marine influenced Greta coal from Sydney Basin (Wilkins *et al.*, 1992), which has been earlier noted. Considering vitrinite fluorescence indicates hydrogen enrichment/oil potential (e.g. Lo, 1993; Diessel and Gammidge, 1998 and references within), variations in hydrogen enrichment within and between vitrinites may be responsible for the observed VR variations in these coals. Consequently, measured VR may not indicate the true maturities of the coals under study. The suitability of VR as a measure of maturity in these coals will therefore be further examined by comparing VR data with alternative measures of maturity including biomarkers and Rock-Eval analysis.

4.3. Geochemical Assessment of Maturity

The variability in VR measurements leads to uncertainties about the real thermal maturities of the Firkanten Fm. coals at the different areas under study. Consequently, further investigation is done by assessing the alkanes and biomarker maturity parameters of the Soxhlet extracted bitumen. This section firstly examines the distribution of *n*-alkanes, isoprenoids and biomarkers present.

4.3.1. Alkane and Biomarker Distribution

The TIC shows that *n*-alkanes typically ranging from nC_{13}/nC_{14} to nC_{34}/nC_{35} and maximizing at around nC_{22-25} (Figure 4.7), which are indicative of terrestrial plant waxes. However, it is noted that the absence of *n*-alkanes below nC_{13} may be partly due to losses during solvent evaporation after extraction (Peters, 1986). The *n*-alkanes show odd over even predominance consistent with lacustrine/terrestrial source (Peters and Moldowan, 1993; Peters *et al.*, 2005).

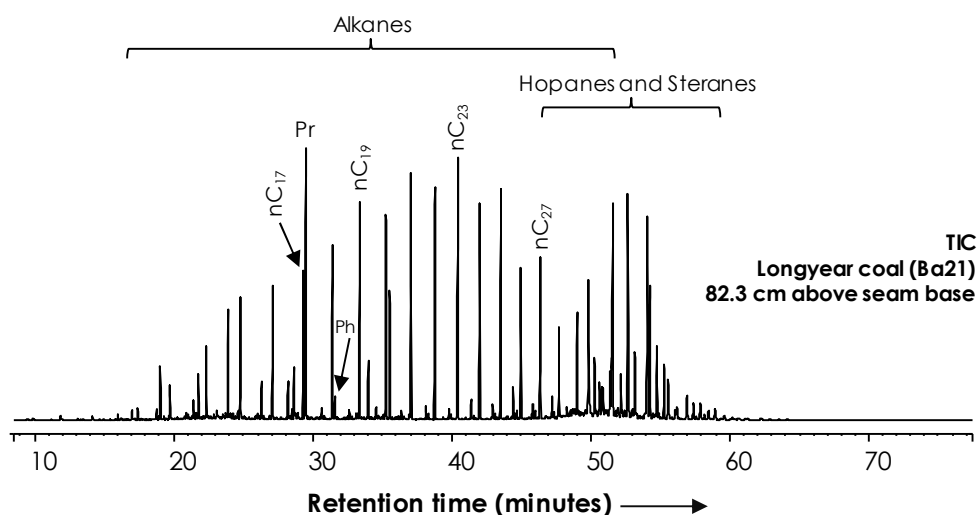


Figure 4.7. Representative TIC of the aliphatics in Soxhlet extracts (Sample Ba21, Longyear coal 82.3 cm from seam base in Bassen). Note: *n*-alkanes show odd over even predominance, and maximizing around nC_{23} indicative of lacustrine/terrestrial source. High hopane abundance is also indicative terrestrial source (Peters *et al.*, 2005).

Pristane (Pr) dominance over phytane (Ph) as observed in the aliphatic fractions of the extracts (Figure 4.7; Table 4.1) is typical of crude oils from coal (Peters *et al.*, 2005). It is generally recommended that Pr/Ph ratios >3.0 should be interpreted as oxic to suboxic depositional conditions with terrigenous plant input, but ratios between 0.8 - 3.0 should not be used as an environmental indicator without other supporting data (Peters *et al.*, 2005). In all 37 samples analysed by GC-MS, Pr/Ph ratio range between 1.6 – 26.5, and values appear to generally decrease from the stratigraphically oldest coal (i.e. Svea), towards the younger coals (i.e. Askeladden, Svarteper and Verkny) (Table 4.1). For example; at the Lunckefjellet BH15-2011 locality, Pr/Ph ratio range between 4.3 – 11.4 within the Longyear seam, and between 1.6 – 2.6 within the Svarteper seam. Also, at the Colesdalen BH3-2008 locality, the older Sputnik coal shows Pr/Ph values between 3.5 – 6.4, while the younger Verkny coal shows value of 2.5. The observed decrease in Pr/Ph values from the older to younger coals is due to vertical variations in depositional environment, i.e. increasing marine organic matter (less oxidising) deposition (Peters and Moldowan, 1993) from the stratigraphically older to younger Firkanten Fm. coals, which is consistent with previous reports (e.g. Orheim *et al.*, 2007).

Pr/ nC_{17} and Ph/ nC_{18} values are generally higher in the north-eastern/eastern basin margins (Bassen and Lunckefjellet) relative to samples down-dip of margins (Breinosa) and near basin centre (Colesdalen). Considering only the Longyear and Sputnik coals for example, maximum Pr/ nC_{17} values of 379.2, 488.7, 14.0 and 3.2 were observed in Bassen, Lunckefjellet, Breinosa and Colesdalen respectively (Table 4.1). Similarly, maximum Ph/ nC_{18} values for the Longyear and Sputnik coals are 35.0, 59.6, 1.9 and 0.6 at these areas respectively. The observed variation is possibly due to thermal maturity (Tissot *et al.*, 1971), although these ratios are affected by organic matter input (Alexander *et al.*, 1981) and secondary

processes such as biodegradation (Peters *et al.*, 2005). Variations in these ratios between areas are further discussed in subsequent sections.

High hopane abundance (Figure 4.7) is consistent with previous reports on oil-prone Svalbard coals (>100 µg/g TOC as per Marshall *et al.*, 2015a); this is indicative of high bacterial degradation (George *et al.*, 1994) and characteristic of terrestrially sourced bitumen (Peters *et al.*, 2005). The abundance of Ts (C₂₇ 18a(H)-trisorhopane II) relative to Tm (17a(H)-trisorhopane) is anomalously low in the coals examined (Figure 4.8; Table 4.2); similar observations have been reported in oil-prone coals from around the world including Australia and New Zealand (e.g. Curry *et al.*, 1994), and north-western Taiwan (Shen and Huang, 2007). According to Peters *et al.*, (2005), the ratio of Ts/Tm is influenced by thermal maturity, lithology and oxicity of depositional environment; this is further examined in subsequent sections.

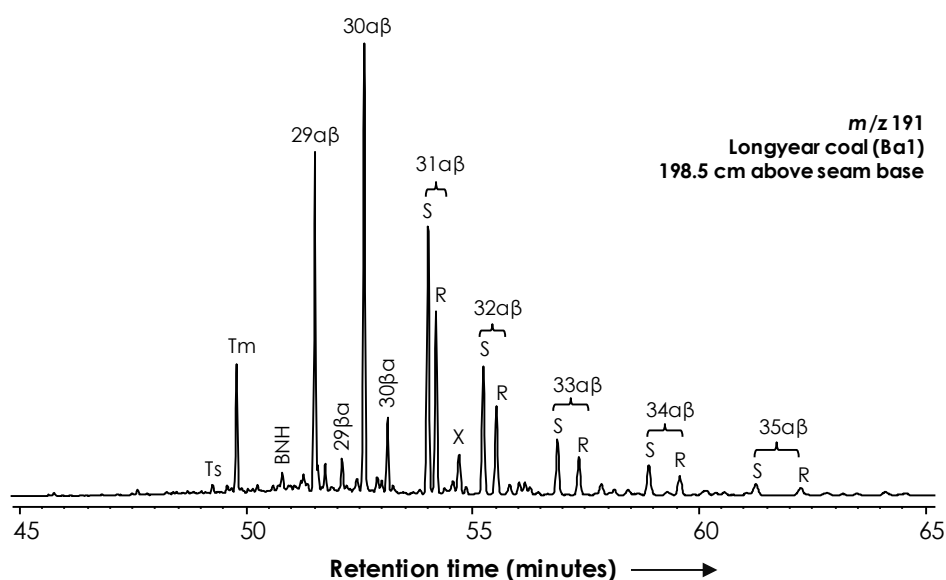


Figure 4.8. Representative *m/z* 191 mass chromatogram of aliphatics in Soxhlet extracts (sample Ba1; a Longyear coal 198.5 cm from seam base in Bassen). Ts and Tm = C₂₇ 18a(H)-trisorhopane II and 17a(H)-trisorhopane. 29aβ and 30aβ = C₂₉ and C₃₀ 17a(H),21β(H)-hopanes. 29βa and 30βa = C₂₉ and C₃₀ 17β(H),21a(H)-moretanes. 31aβ to 35aβ = C₃₁ to C₃₅ 17a(H),21β(H)-homohopanes. B = Bisnorhopane

Sample ID	Area	Location and sample Type	Seam	Sample position above seam base (cm)	VR (R _o)	Pr/Ph	Pr/nC17	Ph/nC ₁₈	CPI(1)	OEP(1)
S1	Svea Nord	Mine section	Svea	Bulk	0.78	7.1	0.9	0.1	1.1	ND
Br43	Breinosa	Mine section	Longyear	Bulk	0.65	13.4	4.5	0.2	1.1	ND
L1	Lunckefjellet	BH15-2011	Svarteper	80	0.53	1.6	20.4	4.0	1.0	0.9
L3	Lunckefjellet	BH15-2011	Svarteper	60	0.56	2.3	73.9	12.8	1.1	1.0
L5	Lunckefjellet	BH15-2011	Svarteper	40	0.50	2.2	ND	ND	1.1	1.0
L8	Lunckefjellet	BH15-2011	Svarteper	10	0.56	2.6	15.7	3.4	1.1	1.0
L9	Lunckefjellet	BH15-2011	Longyear	210	0.59	4.3	124.9	5.5	1.4	1.1
L11	Lunckefjellet	BH15-2011	Longyear	190	0.64	6.4	13.3	1.3	1.3	1.2
L12	Lunckefjellet	BH15-2011	Longyear	160	0.60	6.7	206.0	21.0	1.4	1.2
L14	Lunckefjellet	BH15-2011	Longyear	140	0.62	8.1	488.7	40.7	1.5	1.2
L16	Lunckefjellet	BH15-2011	Longyear	120	0.61	7.0	182.8	26.1	1.4	1.0
L18	Lunckefjellet	BH15-2011	Longyear	100	0.58	7.5	331.0	59.6	1.4	1.0
L20	Lunckefjellet	BH15-2011	Longyear	80	0.70	11.4	3.8	0.2	1.3	1.2
L22	Lunckefjellet	BH15-2011	Longyear	60	0.68	10.5	6.7	0.4	1.3	1.2
L25	Lunckefjellet	BH15-2011	Longyear	30	0.60	8.6	95.6	5.6	1.4	1.2
L27	Lunckefjellet	BH15-2011	Longyear	10	0.63	7.8	45.7	3.0	1.4	1.2
Br1	Breinosa	BH4-2009	Askeladden	46.5	0.61	2.3	5.9	2.5	1.1	0.9
Br8	Breinosa	BH4-2009	Svarteper	11.5	0.55	1.9	9.4	6.4	1.2	1.0
Br12	Breinosa	BH4-2009	Longyear	95.5	0.66	6.2	14.0	1.9	1.2	1.1
Br16	Breinosa	BH4-2009	Longyear	24.0	0.66	6.4	10.5	1.3	1.2	1.1
Br21	Breinosa	BH5-2009	Svea	124.5	0.76	26.5	75.5	1.9	1.4	ND
Br22	Breinosa	BH5-2009	Svea	99.5	0.79	3.5	2.7	0.7	1.5	ND
Br23	Breinosa	BH5-2009	Svea	49.5	0.78	6.3	17.3	2.0	1.5	ND
Br24	Breinosa	BH5-2009	Svea	7.5	0.78	3.5	22.5	3.8	1.4	ND
C1	Colesdalen	BH3-2008	Verkny	16.0	0.62	2.5	2.2	0.4	1.1	1.0
C2	Colesdalen	BH3-2008	Sputnik	172.5	0.77	6.4	2.6	0.3	1.1	1.0
C3	Colesdalen	BH3-2008	Sputnik	147.5	0.79	6.1	2.4	0.2	1.1	1.0
C4	Colesdalen	BH3-2008	Sputnik	122.5	0.79	3.5	1.3	0.3	1.1	1.0
C5	Colesdalen	BH3-2008	Sputnik	101.0	0.63	4.5	2.7	0.5	1.1	1.0
C6	Colesdalen	BH3-2008	Sputnik	80.5	0.65	4.2	3.2	0.6	1.1	1.0
C7	Colesdalen	BH3-2008	Sputnik	57.5	0.78	5.4	1.3	0.2	1.1	1.0
C8	Colesdalen	BH3-2008	Sputnik	34.5	0.80	6.1	1.3	0.2	1.2	1.1
C9	Colesdalen	BH3-2008	Sputnik	11.5	0.76	5.4	1.5	0.2	1.1	1.0
Ba1	Bassen	Outcrop	Longyear	198.5	0.54	11.2	27.3	1.6	1.5	1.3
Ba11	Bassen	Outcrop	Longyear	137.5	0.59	8.6	379.2	35.0	1.2	1.0
Ba21	Bassen	Outcrop	Longyear	82.3	0.68	14.3	2.4	0.1	1.4	1.3
Ba32	Bassen	Outcrop	Longyear	3.0	0.63	13.8	7.7	0.4	1.4	1.2

Table 4.1. VR (% R_o) and alkane parameters used to assess the source and maturity of the Firkanten Fm. coals under study. Note: higher isoprenoid /n-alkane values in the upper sections of the Longyear and Sputnik seams compared to the lower sections; see Chapter 6 for further discussions on this variation. CPI = Carbon Preference Index; OEP = Odd-to-Even Predominance. Peak areas data for Pr/Ph and Isoprenoid/n-alkane ratios were measured using m/z 71 chromatogram.

Oleanane, a source and age-related biomarker highly specific of flowering land plants (angiosperms) of Cretaceous or younger age (Peters *et al.*, 2005) is notably absent in all areas under study (Figure 4.8). Although some Cretaceous/Tertiary lacustrine rocks/coal formed in freshwater swamps lack oleanane despite abundant angiosperm input (Murray *et al.*, 1994), the general absence of angiosperm biomarkers within the coals under study is surprising as the fossil evidence indicates that they formed a significant component of the CTB flora (Marshall, 2013). With high hopane abundance, indicative of high bacterial activity, a possible explanation is that angiosperms are depleted as they are significantly more susceptible to biodegradation relative to gymnosperms (Faix *et al.*, 1985); consequently, both the fossil and biomarker records are enriched in gymnosperm (Marshall, 2013). With high hopane abundance, indicative of high bacterial activity, a possible explanation is that angiosperms are depleted because they are significantly more susceptible to biodegradation relative to gymnosperms (Faix *et al.*, 1985); consequently, both the fossil and biomarker records are enriched in gymnosperm (Marshall, 2013). The abundance of C₃₅ relative to C₃₄ homohopane in the samples (Table 4.2) is consistent with crude oils from coal source (Peters *et al.*, 2005). It is noted that peak "X" in Figure 4.8 is not gammacerane; assessment was done using the *m/z* 412 molecular ion as per the recommendation of Seifert and Moldowan (1986), which showed a very small *m/z* 412 molecular ion, whereas the other C₃₀ compounds showed (relatively) very large *m/z* 412 molecular ion. Also, peak X has a large *m/z* 426 molecular ion, alongside the C₃₁ S and R; hence, it is a C₃₁ compound.

The sterane fractions are C₂₉ sterane and diasterane dominated (Figure 4.9), which is indicative of a terrestrial source (Philp, 1994). It is noted that the peak

areas of C₂₇ and C₂₈ steranes could not be determined due to their very low concentrations and co-elution.

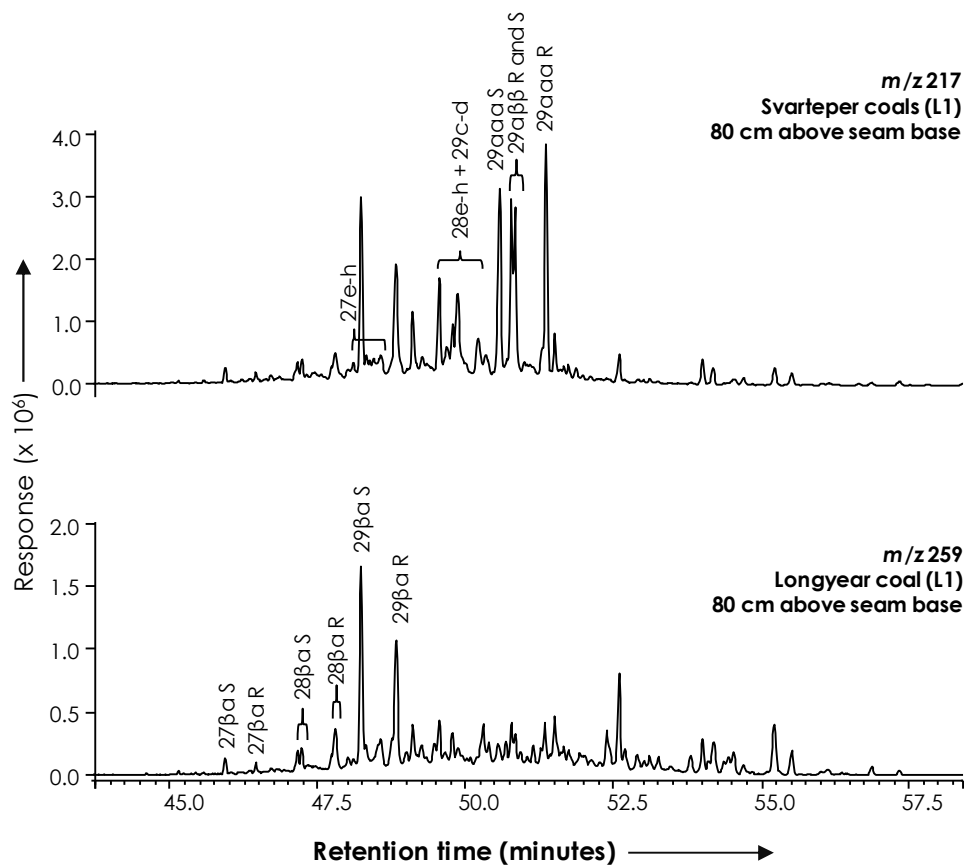


Figure 4.9. Representative *m/z* 217 and *m/z* 259 mass chromatograms of aliphatic fraction in Soxhlet extract (Sample L1; Svarteper coal 80 cm from seam base in Lunckefjellet). 27e-h = C₂₇ aaa (20S and 20R) and aββ (20R and 20S) steranes. 28e-h = C₂₈ aaa (20S and 20R) and aββ (20R and 20S) steranes. 29c-d = C₂₉ aβ 20S and 20R diasteranes. 29aaa S and R = C₂₉ aaa 20S and 20R steranes. 29aββ R and S = C₂₉ aββ 20R and 20S steranes. 27–29 βa S and R = C₂₇–C₂₉ 13β(H),17a(H)-diasteranes 20S and 20R

Sample ID	Area	Location and Sample Type	Seam	Sample position above seam base (cm)	VR (%R _c)	Hopanes						Steranes and Diasteranes					Aromatics	
						Ts/Tm	C30 βa/αβ	C31 S/(S+R)	C32 S/(S+R)	C29/C30 αβ	C35/C34 αβ S	C29 aaa	C29 αββ	C29 αββ/(aaa+αββ)	C29 βa	C29 βa/(aaa+αββ)	MPI-1	MPI-1 calculated VR (R _c)
S6	Svea Nord	Mine section	Svea	Bulk	0.78	ND	0.07	0.64	0.62	0.75	0.31	0.54	-	0.46	-	-	0.60	0.76
Br43	Breinosa	Mine 7 section	Longyear	Bulk	0.65	ND	0.10	0.64	0.63	0.75	0.41	0.56	-	0.49	-	-	0.63	0.78
L1	Lunckefjellet	BH15-2011	Svarteper	80	0.53	0.06	0.16	0.60	0.59	0.62	0.47	0.50	0.48	0.38	0.58	0.43	0.44	0.66
L3	Lunckefjellet	BH15-2011	Svarteper	60	0.56	0.07	0.13	0.60	0.59	0.59	0.46	0.52	0.47	0.44	0.57	0.48	0.45	0.67
L5	Lunckefjellet	BH15-2011	Svarteper	40	0.50	0.07	0.11	0.60	0.59	0.61	0.32	0.50	0.47	0.48	0.57	0.46	0.04	0.43
L8	Lunckefjellet	BH15-2011	Svarteper	10	0.56	0.08	0.13	0.60	0.58	0.59	0.31	0.50	0.47	0.44	0.58	0.43	0.44	0.67
L9	Lunckefjellet	BH15-2011	Longyear	210	0.59	0.02	0.26	0.60	0.60	0.74	0.34	0.51	0.48	0.36	0.56	0.18	0.25	0.55
L11	Lunckefjellet	BH15-2011	Longyear	190	0.64	0.03	0.22	0.60	0.59	0.72	0.36	0.49	0.47	0.39	0.59	0.24	0.71	0.83
L12	Lunckefjellet	BH15-2011	Longyear	160	0.60	0.02	0.21	0.60	0.59	0.69	0.32	0.49	0.47	0.37	0.56	0.18	0.32	0.59
L14	Lunckefjellet	BH15-2011	Longyear	140	0.62	0.02	0.23	0.60	0.59	0.72	0.35	0.49	0.49	0.36	0.55	0.16	0.38	0.63
L16	Lunckefjellet	BH15-2011	Longyear	120	0.61	0.02	0.28	0.60	0.58	0.76	0.27	0.49	0.53	0.34	0.52	0.15	0.22	0.53
L18	Lunckefjellet	BH15-2011	Longyear	100	0.58	0.03	0.27	0.60	0.59	0.75	0.32	0.50	0.51	0.35	0.53	0.15	0.38	0.63
L20	Lunckefjellet	BH15-2011	Longyear	80	0.70	0.01	0.31	0.60	0.60	0.72	0.28	0.46	0.48	0.32	0.53	0.12	0.51	0.71
L22	Lunckefjellet	BH15-2011	Longyear	60	0.68	0.02	0.32	0.60	0.59	0.67	0.25	0.48	0.48	0.32	0.53	0.14	0.42	0.65
L25	Lunckefjellet	BH15-2011	Longyear	30	0.60	0.02	0.26	0.60	0.59	0.74	0.30	0.52	0.47	0.39	0.51	0.18	0.34	0.60
L27	Lunckefjellet	BH15-2011	Longyear	10	0.63	0.02	0.26	0.60	0.60	0.76	0.27	0.51	0.50	0.35	0.55	0.17	0.34	0.60
Br1	Breinosa	BH4-2009	Askeladden	46.5	0.61	0.22	0.10	0.60	0.58	0.36	0.34	0.54	0.47	0.49	0.59	0.38	0.55	0.73
Br8	Breinosa	BH4-2009	Svarteper	11.5	0.55	0.17	0.10	0.60	0.58	0.40	0.03	0.51	0.47	0.48	0.55	0.33	0.36	0.62
Br12	Breinosa	BH4-2009	Longyear	95.5	0.66	0.09	0.10	0.60	0.61	0.44	0.29	0.51	0.52	0.48	0.55	0.22	0.57	0.74
Br16	Breinosa	BH4-2009	Longyear	24.0	0.66	0.11	0.12	0.60	0.59	0.46	0.26	0.53	0.52	0.45	0.54	0.28	0.56	0.73
Br21	Breinosa	BH5-2009	Svea	7.5	0.78	ND	0.09	0.59	0.59	0.63	0.23	0.51	ND	0.51	ND	ND	0.51	0.71
Br22	Breinosa	BH5-2009	Svea	49.5	0.78	ND	0.11	0.60	0.60	0.59	0.14	0.54	ND	0.50	ND	ND	0.51	0.70
Br23	Breinosa	BH5-2009	Svea	99.5	0.79	ND	0.09	0.62	0.62	0.56	ND	0.47	ND	0.53	ND	ND	0.49	0.69
Br24	Breinosa	BH5-2009	Svea	124.5	0.76	ND	0.10	0.59	0.59	0.47	0.19	0.45	ND	0.55	ND	ND	0.47	0.68
C1	Colesdalen	BH3-2008	Verkny	16.0	0.62	0.16	0.16	0.60	0.58	0.42	0.40	0.50	0.50	0.43	0.53	0.31	0.56	0.74
C2	Colesdalen	BH3-2008	Sputnik	172.5	0.77	0.11	0.13	0.60	0.58	0.42	0.37	0.47	0.53	0.45	0.55	0.19	0.65	0.79
C3	Colesdalen	BH3-2008	Sputnik	147.5	0.79	0.09	0.11	0.60	0.59	0.43	0.24	0.49	0.50	0.48	0.56	0.19	0.66	0.80
C4	Colesdalen	BH3-2008	Sputnik	122.5	0.79	0.11	0.11	0.60	0.45	0.42	0.48	0.53	0.50	0.46	0.54	0.24	0.74	0.84
C5	Colesdalen	BH3-2008	Sputnik	101.0	0.63	0.29	0.11	0.60	0.58	0.49	0.38	0.53	0.49	0.48	0.53	0.47	0.65	0.79
C6	Colesdalen	BH3-2008	Sputnik	80.5	0.65	0.16	0.10	0.60	0.58	0.45	0.42	0.51	0.48	0.49	0.56	0.32	0.77	0.86
C7	Colesdalen	BH3-2008	Sputnik	57.5	0.78	0.09	0.10	0.60	0.58	0.47	0.23	0.51	0.51	0.47	0.52	0.22	0.73	0.84
C8	Colesdalen	BH3-2008	Sputnik	34.5	0.80	0.09	0.10	0.60	0.58	0.45	0.29	0.55	0.51	0.46	0.56	0.18	0.73	0.84
C9	Colesdalen	BH3-2008	Sputnik	11.5	0.76	0.12	0.11	0.60	0.58	0.40	0.28	0.52	0.55	0.47	0.52	0.21	0.62	0.77
Ba1	Bassen	Outcrop	Longyear	198.5	0.54	0.03	0.23	0.61	0.59	0.04	0.18	0.51	0.52	0.34	0.57	0.16	0.54	0.73
Ba11	Bassen	Outcrop	Longyear	137.5	0.59	0.02	0.24	0.60	0.59	0.93	0.19	0.49	0.55	0.34	0.57	0.12	1.33	1.20
Ba21	Bassen	Outcrop	Longyear	82.3	0.68	0.01	0.30	0.60	0.59	0.76	0.19	0.45	0.46	0.32	0.55	0.12	0.34	0.61
Ba32	Bassen	Outcrop	Longyear	3.0	0.63	0.02	0.27	0.61	0.60	0.72	0.22	0.50	0.48	0.34	0.53	0.13	0.53	0.72

Table 4.2. VR (% R_c), hopane, sterane and aromatic biomarker parameters used to assess the source and maturity of the Firkanten Fm. coals under study. MPI-1 and R_c after Radke and Welte (1983). ND = not determined

4.3.2. Maturity Assessment Using Terpanes

1) $22S/(22S + 22R)$ Homohopanes

The C₃₁ or C₃₂ homohopanes are typically used to calculate the $22S/(22S + 22R)$ maturity ratio, which rises from 0 to ~0.6 during maturation, and reach equilibrium between 0.57 - 0.62 (Seifert and Moldowan, 1980). The C₃₁ to C₃₂ $22S/(22S + 22R)$ ratio for all samples examined range from 0.58 to 0.62 (Table 4.2), with no vertical variation within seams (Figure 4.11). This disputes vertical maturity variations within and between the Firkanten Fm. coals as suggested by VR measurements, as well as indicate equilibrium maturity has been reached.

2) Moretanes/Hopanes

Very high hopane abundances relative to their moretane counterparts (Figure 4.8) indicates maturity (Peters *et al.*, 2005). The ratio of $\beta\alpha$ moretanes to their corresponding $\alpha\beta$ hopanes decreases with thermal maturity from ~0.80 in immature bitumens, to <0.15 in mature source rocks/oils, to a minimum of 0.05. Values for the C₃₀ moretane/hopane ratios for the studied coals are at or approaching equilibrium (0.07 – 0.32) (Table 4.2), with no vertical variation within seams (Figure 4.11). However, two sets of values were observed between areas; the higher values ranging between 0.21 – 0.32 were seen at basin margins (Bassen and Lunckefjellet), while lower values (0.10 and 0.13) were observed in samples down-dip of basin margins (Breinosa) and basin center (Colesdalen). This observation is likely due to maturity variations.

3) $Ts/(Ts + Tm)$

The $Ts/(Ts + Tm)$ ratio increases with maturity as Tm is less stable than Ts during catagenesis (Seifert and Moldowan, 1978). Whilst values of this ratio showed no

vertical variation within seams (Figure 4.11), thereby suggesting similar maturity levels, it is anomalously low (0.01 – 0.29; Table 4.2) for the level of maturity attained by the Firkanten Fm. sediments. Also, lower values (0.01 – 0.08) were observed at basin margins (Bassen and Lunckefjellet), whereas higher values (between 0.09 – 0.29) were observed down-dip of basin margin (Breinosa) and basin centre (Colesdalen). According to Peters *et al.*, (2005), the relative importance of lithology and oxicity of depositional environment in controlling this ratio remains unclear, although some results show substantial effects. This ratio is unusually low in oils from carbonate source rocks compared with oils from shales (e.g. Rullkötter *et al.*, 1985; Price *et al.*, 1987), which suggests that the formation of Ts is dependent on the presence of clay minerals. However, Shen and Huang (2007) reported that clays/minerals showed no influence on the transformation of Tm to Ts in extracted bitumen from coals, coaly shales and shales in north-western Taiwan. In terms of depositional environment, the Ts/(Ts + Tm) ratio is observed to increase at lower Eh (more anoxic) and decreases at higher pH in a series of Lower Toarcian marine shales from south-western Germany (Peters *et al.*, 2005). Very low Ts/Tm ratios (<0.05) were measured within the marine influenced Greta coal seam in the Sydney basin, which shows true VR of at least 0.75% R_o (George *et al.*, 1994). Thus, the generally low abundance of Ts relative to Tm observed in this study is possibly due to a high pH associated with marine input, while the increase in values from the eastern basin margin to basin centre is consistent with increasing anoxicity as water levels become deeper towards basin center.

4.3.3. Maturity Assessment Using Steranes and Diasteranes

1) 20S/(20S + 20R) Isomerisation

In the C₂₉ sterane, 20S/(20S + 20R) ratio rises from 0 to ~0.50 with increasing thermal maturity, and attains equilibrium between 0.52 - 0.55 (Seifert and Moldowan, 1986). In the coals under study, values for this ratio range between 0.45 – 0.56, and thus indicates the coals are close to or at equilibrium maturity (Table 4.2), with no vertical variation within seams (Figure 4.11). As with the moretane/hopane ratio, values are generally higher towards basin centre in Colesdalen and thus indicate lateral maturity variations.

2) $\alpha\beta\beta/(\alpha\beta\beta + aaa)$ Isomerisation

Isomerisation in the C₂₉ 20S and 20R regular steranes causes increase in $\alpha\beta\beta/(\alpha\beta\beta + aaa)$ from near zero to ~0.70, and reaches equilibrium around 0.67 – 0.71 with increasing maturity (Seifert and Moldowan, 1986). Whilst no vertical maturity variation was observed within seams (Figure 4.11), there are however two notable observations regarding the $\alpha\beta\beta/(\alpha\beta\beta + aaa)$ values. Firstly, they range between 0.32 – 0.55 for all samples (Table 4.2), thereby suggesting the coals are not as mature as other parameters indicated. Secondly, values are generally lower within the Longyear seam in the eastern margins; for example, the Longyear seam in Lunckefjellet BH15-2011 shows values between 0.32 – 0.39, while the Svarteper coals, which are ~12 meters above the Longyear coals, show values between 0.38 – 0.48. These observations are explained as follows:

- The relatively low values for the $\alpha\beta\beta/(\alpha\beta\beta + aaa)$ ratios in the Firkanten Fm. coals in general is possibly because it is slower to reach equilibrium compared to the 20S/(20S + 20R) ratio (Peters *et al.*, 2005). Also, the $\alpha\beta\beta/(\alpha\beta\beta + aaa)$ ratio for Tertiary oils is generally not at equilibrium (unlike

in older oils) as a result of insufficient time for complete sterane isomerisation in Tertiary rocks, even though the generated oils are thermally mature (Grantham, 1986).

- The much lower values of the $\alpha\beta\beta/(\alpha\beta\beta + \text{aaa})$ ratio observed within the Longyear seam are possibly due to biodegradation considering the lowest *n*-alkane abundance is observed within these coals (Table 4.1). Peters *et al.* (2005) stated that the microbial alteration and removal of the regular steranes from petroleum occurs after complete removal of C₁₅ - C₂₀ isoprenoids; however, Ahmed *et al.* (1999) reported unusual sequence of hydrocarbon biodegradation in Permian Moura coals of Bowen Basin of Australia. Perhaps this is the case with the coals under investigation. Degradation/alteration in the CTB coals is assessed in detail in Chapter 6.

3) 20S/(20S + 20R) 13 β , 17 α (H) - Diasteranes

The 20S/(20S + 20R) ratio for C₂₇ - C₂₉ diasteranes increases with thermal maturity and reaches equilibrium at ~0.60 (Mackenzie *et al.*, 1980). Values for the coals under investigation range between 0.51 – 0.59 (Table 4.2), indicating the coals are close to or have reached equilibrium maturity with no vertical variation within seams (Figure 4.11).

4.3.4. Maturity Assessment Using Alkanes

1) Isoprenoid/*n*-alkane ratios

Pr/*n*C₁₇ and Ph/*n*C₁₈ decrease with thermal maturity as more *n*-alkanes are generated from kerogen by cracking (Tissot *et al.*, 1971), although these ratios are affected by organic matter input (Alexander *et al.*, 1981) and secondary

processes such as biodegradation (Peters *et al.*, 2005). Representative TIC from the four main areas under investigation (Figure 4.10) shows that samples from the eastern basin margin have low *n*-alkane abundance relative to samples down-dip and closer to basin centre, while isoprenoids remained persistent (Figure 4.10).

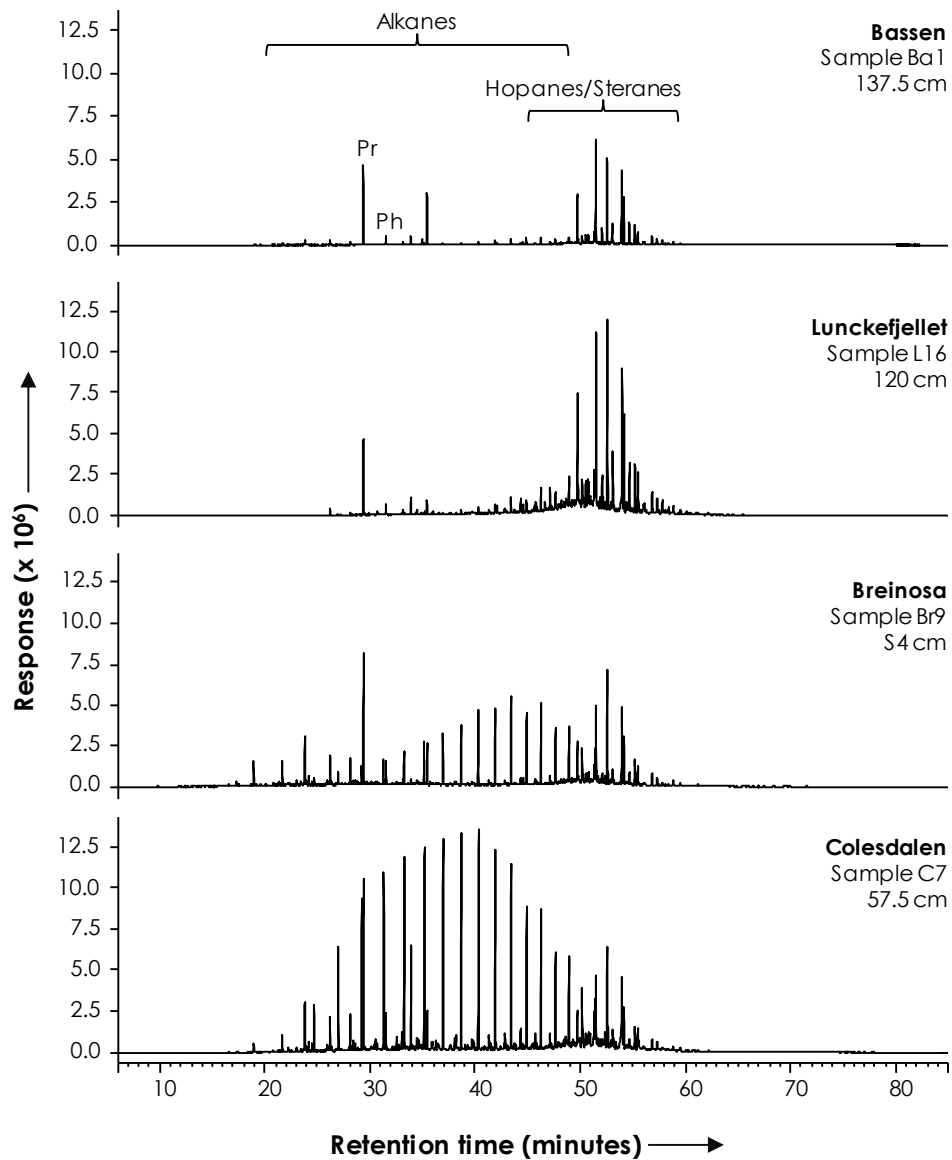


Figure 4.10. Representative TIC of aliphatic hydrocarbons fraction of Soxhlet extracts from the Longyear and Sputnik coals in main areas under investigation. Note: the lower abundance of *n*-alkanes in the eastern margin of the basin (Bassen and Lunckefjellet) compared to Breinosa (down dip of basin margin) and Colesdalen (basin center) possibly due to biodegradation.

The Pr/nC₁₇ and Ph/nC₁₈ ratios show huge variations within seams and between locations with highest values occurring within the marginal Longyear seam (Table 4.1). For example; the Longyear coals at the Lunckefjellet BH15-2011 locality shows Pr/nC₁₇ values between 3.8 – 488.7, and Ph/nC₁₈ values between 0.2 – 59.6. Thus, these ratios are believed to be significantly influenced by biodegradation and to a much lesser degree, maturity, and therefore cannot be used to infer thermal maturity in the CTB

2) Carbon Preference Index (CPI) and Odd-to-Even Predominance (OEP)

The relative abundance of odd versus even carbon numbered *n*-alkanes can give a crude estimate of thermal maturity; these measurements include the Carbon Preference Index (CPI) and Odd-to-Even Predominance (OEP). CPI(1) and OEP(1) are defined by Peters *et al.* (2005) and applied in this study as:

$$\text{CPI(1)} = \frac{2(\text{C23} + \text{C25} + \text{C27} + \text{C29})}{\text{C22} + 2(\text{C24} + \text{C26} + \text{C28}) + \text{C3}} \quad (4.1)$$

$$\text{OEP(1)} = \frac{\text{C21} + 6\text{C23} + \text{C25}}{(4 * \text{C22}) + (4 * \text{C24})} \quad (4.2)$$

CPI values for extracts of Types II and III organic matter decrease with increasing maturity down to about 1.5 – 1.0 in the mature stage (Taylor *et al.*, 1998). Similarly, OEP values of around 1.0 suggest that an oil or rock extract is thermally mature, while values significantly above or below 1.0 indicate low thermal maturity (Peters *et al.*, 2005). In the Firkanten Fm. coals, the *n*-alkanes show little odd over even predominance with CPI(1) ranging between 1.0 – 1.5, and OEP(1) values ranging between 0.9 – 1.3 in all 37 samples analysed (Table 4.1), with no significant

variation within seams (Figure 4.11). However, it is noted that the marginal Longyear coals generally show higher values possibly due to biodegradation.

4.3.5. Maturity Assessment Using Aromatics

The Methylphenanthrene Index (MPI) has considerable potential for resolving practical problems in maturation assignments of oils and sediments (Boreham *et al.*, 1988); this ratio is calculated from the intensities of the 4 methylphenanthrene (MP) isomers seen in the *m/z* 192 mass chromatogram and the intensity of phenanthrene (P) in the *m/z* 178 mass chromatogram. The Methylphenanthrene Index (MPI-I) is defined (Radke and Welte; 1983 and references within) as:

$$\text{MPI} - 1 = \frac{1.5 * (2\text{MP} + 3\text{MP})}{\text{P} + 1\text{MP} + 9\text{MP}} \quad (4.3)$$

In equation 4.3 above, P is the abundance of phenanthrene, while 2MP, 3MP, 1MP and 9MP are the abundances of 2-, 3-, 1- and 9-methylphenanthrenes respectively. The progressive change with maturation of the distribution of phenanthrene and the four methylphenanthrene isomers used to define MPI-1 has been explained in terms of the different reactivities of the ring carbons (Radke *et al.*, 1982a; b). In mature samples the dominance of the methyl isomers in the 1- and 9- positions is attributed to the greater reactivity of these sites to methylation reactions. As maturation progresses, there is a systematic increase in the relative abundance of 2- and 3-methylphenanthrene due to rearrangement reactions to these more thermodynamically stable isomers. With increasing maturity, MPI-1 increases to the end of the oil window, and then decreases; the working relationship between calculated vitrinite reflectance (R_c) and MPI-I when mean VR range between >0.65 to <1.35% R_o (e.g. Radke and Welte, 1983; Radke, 1988) as in the CTB coals is:

$$R_c = (0.6 * MPI - 1) + 0.4 \quad (4.4)$$

It is noted that R_c values in this study are expressed as % R_o since they are estimates of VR measurements under oil. The R_c data for the investigated samples (Table 4.2) do not show trends of decreasing maturity towards seam top (Figure 4.11) in contrast to measured VR under oil, and for the purpose of clarity and consistency, further discussions will be focused on the Longyear and Sputnik coals. R_c values between 0.73 – 0.74% R_o were observed for the Longyear coals in Breinosa BH4-2009 sampling locality; this is similar to reported R_c values from Mine 7 (0.67 – 0.73% R_o , Marshall et al., 2015b) which is also in the Breinosa area. The Longyear coals in Bassen and Lunckefjellet show wide ranges of R_c values (0.61 – 1.20% and 0.53 – 0.83% R_o respectively), which is surprising. The R_c values for the Colesdalen samples are between 0.77 – 0.86% R_o , which is somewhat consistent with their nearness to basin center. Comparison of measured VR vs R_c values for the Longyear and Sputnik samples show that mean R_c for the Longyear/Sputnik coals in Bassen (0.73% R_o), Breinosa (0.74% R_o) and Colesdalen (0.82% R_o) are higher than the mean measured VR (0.61, 0.66 and 0.75% R_o respectively) in these areas. However, for the Longyear samples in Lunckefjellet; mean R_c (0.63% R_o) is the same value as the mean measured VR (0.63% R_o) (Table 4.2). The fact that the minimum R_c values are substantially higher than the minimum measured VR at all locations (minimum R_c vs minimum measured VR = 0.61 vs 0.54% R_o in Bassen, 0.67 vs 0.50% R_o in Mine 7, 0.73 vs 0.59% R_o in BH4-2009, 0.77 vs 0.65% R_o in Colesdalen) besides Lunckefjellet (0.53 vs 0.55% R_o) is an indication that measured VR do not represent the true maturity of these coals. A possible explanation for R_c being lower than measured VR in Lunckefjellet is the effect of the degree of impregnation by migrated bitumen (Peters et al., 2005).

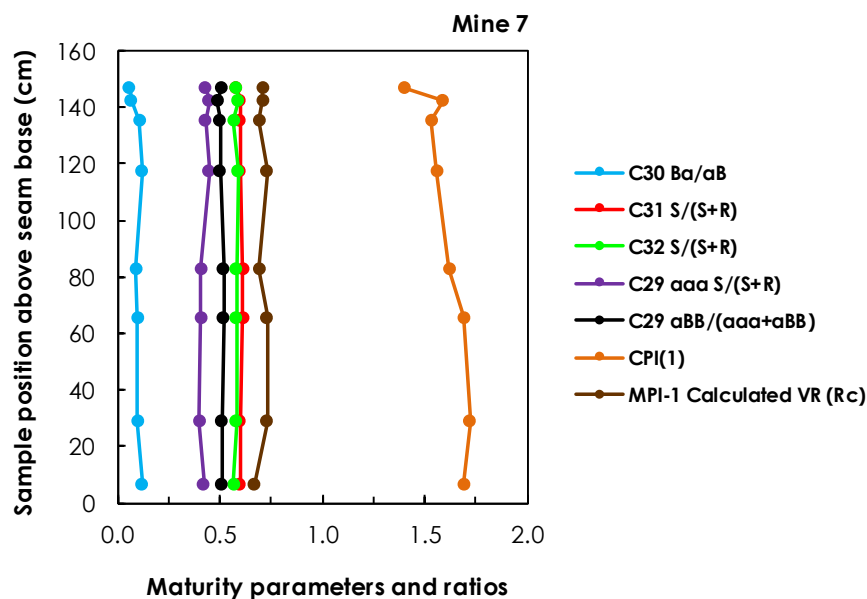
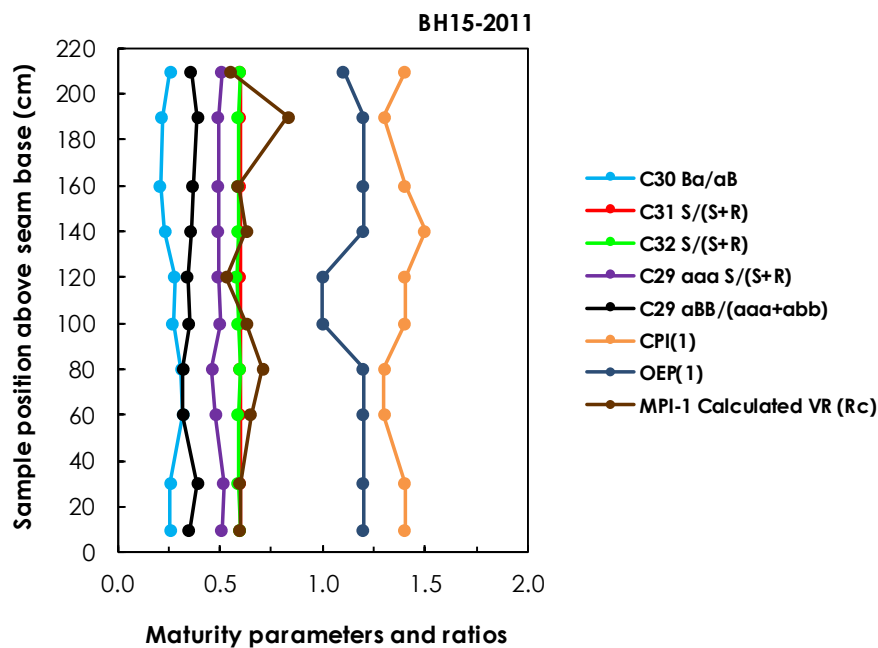


Figure 4.11. Aliphatic and aromatic maturity assessments of the Longyear coal in Lunckefjellet BH15-2011 locality (top) and Mine 7 (bottom). Note: The hopane and sterane ratios show no change from base to top of seam and are close to, or have reached equilibrium. The aromatic maturity parameter (MPI-1 calculated VR of Radke and Welte, 1983) also shows no decrease from base to top of seam as observed in the measured VR trend. The *n*-alkane ratios - CPI(1) and OEP(1) indicate equilibrium maturity (~1) although may have been influenced by biodegradation. Results indicate that maturity is approximately 0.70% R_o or greater in these coals. Mine 7 data are as per Marshall *et al.* (2015b).

The low R_c values observed in Lunckefjellet, and the wide range of R_c values observed for the Bassen and Lunckefjellet samples is further investigated by examining the distribution of phenanthrene and 1-, 2-, 3- and 9-methylphenanthrenes. Samples from basin margins (Bassen and Lunckefjellet) show low abundance of phenanthrene relative to methylphenanthrenes, whereas samples down-dip of basin margin (Breinosa) and at basin center (Colesdalen) show greater abundance of phenanthrene compared to methylphenanthrenes (Figure 4.12).

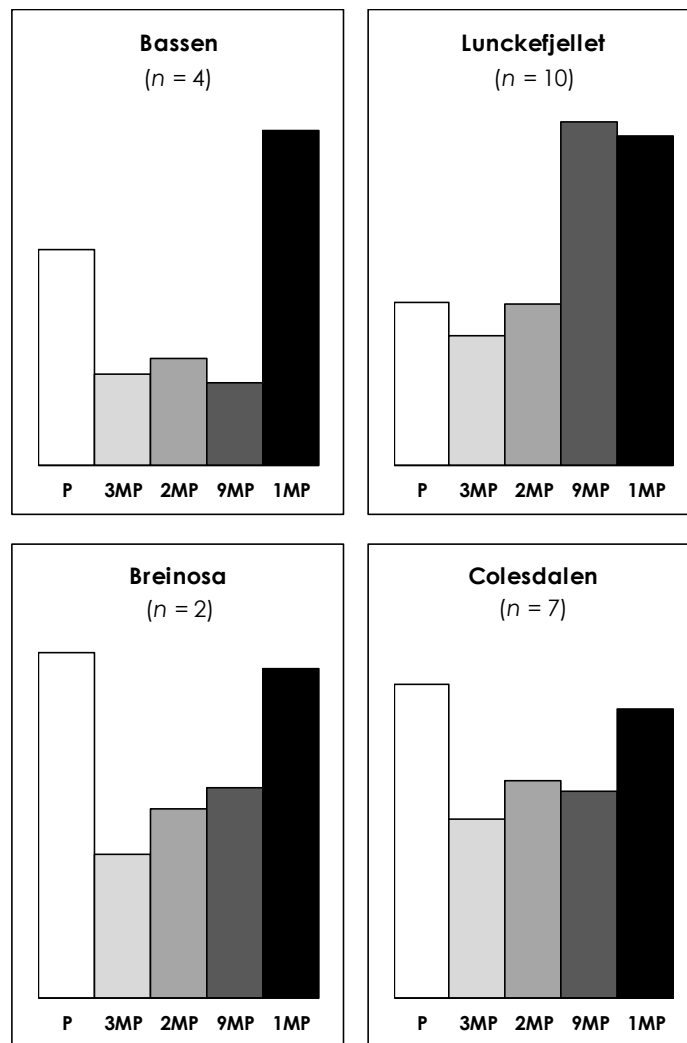


Figure 4.12. Comparing the mean relative abundance of phenanthrene and 1-, 2-, 3- and 9 - methylphenanthrenes in the Longyear and Sputnik coals.

It has been noted that the MPI-1 parameter is based on the premise that with increasing maturity, 1MP and 9MP are re-arranged into the more stable 2MP and 3MP isomers (e.g. Radke *et al.*, 1982a; b); however, there is a high relative abundance of 1MP and 9MP in Lunckefjellet, but in other three areas, 9MP is relatively low in abundance (Figure 4.12). The observed variation in the relative abundances of phenanthrene and methylphenanthrene, which appear to have significantly influenced the MPI-1 predicted maturity values in the Bassen and Lunckefjellet samples is believed to result from:

- It may be suggested that adsorbed bitumen reduces the rate of cross-linking and condensation of aromatic framework, i.e. delayed/suppressed aromatic formation by high aliphatic contents (Diessel, 1992; Petersen and Vosgerau, 1999).

The above reference implies that the Lunckefjellet samples in particular, are possibly experiencing delays in the re-arrangement of 9MP to 2MP and/or 3MP and thus may be more oil-prone. Also, coals from other areas may be experiencing similar delays in the formation of aromatic hydrocarbons with increasing maturity.

4.3.5.1. How Reliable are the MPI-1 Estimated Maturity Values?

Because of variations in the relative abundance of phenanthrene and methylphenanthrene isomers, this section examines the reliability of the MPI-1 estimated VR values for further application in this study. Kvalheim *et al.* (1987) used multivariate analysis methods to examine the distribution of P and MP isomers of 15 coals in the reflectance range 0.5 - 1.3% R_o and concluded that increasing maturity correlates only with the distribution of methylphenanthrene isomers, and not with the abundance of phenanthrene, thereby suggesting

that MPI-1 inferred maturity values are somewhat unreliable. These workers reduced the deviation between calculated and measured VR compared with MPI-1 and proposed a maturity indicator termed the Methylphenanthrene Distribution Factor (MPDF) as follows:

$$\mathbf{MPDF} = \frac{\mathbf{2MP+3MP}}{\mathbf{2MP+3MP+1MP+9}} \quad (4.5)$$

The predictive relationship between MPDF and VR is:

$$\mathbf{Rc1} = (\mathbf{MPDF * 2.2424}) - \mathbf{0.166} \quad (4.6)$$

For clarity, the MPDF predicted VR values are denoted as R_{C1} (expressed as % R_o because it estimates VR measurements under oil.), while those of MPI-1 are denoted by R_c . The Bassen and Lunckefjellet samples show relatively wide and unrealistic ranges of values (0.37 – 1.02 and 0.15 – 0.73% R_o respectively) compared to the Breinosa (0.66 – 0.71% R_o) and Colesdalen (0.71 – 0.96% R_o) samples (Table 4.3). Notably, the R_{C1} for most of the Lunckefjellet coals show estimated thermal maturities that are lower than the maturities shown by both the measured VR under oil, and the R_c values, which are unlikely as aliphatic biomarkers maturity parameters indicate that the coals are within the main oil window. If the abundances of 2MP and 3MP relative to 1MP and 9MP are expected to increase with increasing maturity (e.g. Radke and Welte, 1983), then the relatively large variations in R_{C1} values observed for the Bassen and Lunckefjellet samples are possibly related to the delayed re-arrangements of these isomers by aliphatic enrichment (e.g. Diessel, 1992).

Sample ID	Area	Locality and sample type	Seam	Sample position above seam base (cm)	MPI-1	MPI-1 estimated VR (R_C)	MPDF	MPDF estimated VR (R_{C1})
L9	Lunckefjellet	BH15-2011	Longyear	210	0.25	0.55	0.15	0.17
L11	Lunckefjellet	BH15-2011	Longyear	190	0.71	0.69	0.40	0.73
L12	Lunckefjellet	BH15-2011	Longyear	160	0.32	0.59	0.19	0.26
L14	Lunckefjellet	BH15-2011	Longyear	140	0.38	0.63	0.22	0.33
L16	Lunckefjellet	BH15-2011	Longyear	120	0.22	0.53	0.14	0.15
L18	Lunckefjellet	BH15-2011	Longyear	100	0.38	0.63	0.22	0.33
L20	Lunckefjellet	BH15-2011	Longyear	80	0.51	0.71	0.31	0.53
L22	Lunckefjellet	BH15-2011	Longyear	60	0.42	0.65	0.25	0.39
L25	Lunckefjellet	BH15-2011	Longyear	30	0.34	0.60	0.20	0.28
L27	Lunckefjellet	BH15-2011	Longyear	10	0.34	0.60	0.20	0.28
Br12	Breirosa	BH4-2009	Longyear	95.5	0.57	0.74	0.39	0.71
Br16	Breirosa	BH4-2009	Longyear	24.0	0.56	0.73	0.37	0.66
C2	Colesdalen	BH3-2008	Sputnik	172.5	0.65	0.79	0.44	0.82
C3	Colesdalen	BH3-2008	Sputnik	147.5	0.66	0.80	0.41	0.75
C4	Colesdalen	BH3-2008	Sputnik	122.5	0.74	0.84	0.44	0.82
C6	Colesdalen	BH3-2008	Sputnik	80.5	0.77	0.86	0.45	0.84
C7	Colesdalen	BH3-2008	Sputnik	57.5	0.73	0.94	0.50	0.96
C8	Colesdalen	BH3-2008	Sputnik	34.5	0.73	0.84	0.44	0.82
C9	Colesdalen	BH3-2008	Sputnik	11.5	0.62	0.76	0.39	0.71
Ba1	Bassen	Outcrop	Longyear	198.5	0.57	0.73	0.33	0.57
Ba11	Bassen	Outcrop	Longyear	137.5	0.73	1.20	0.53	1.02
Ba21	Bassen	Outcrop	Longyear	82.3	0.34	0.61	0.24	0.37
Ba32	Bassen	Outcrop	Longyear	3.0	0.53	0.72	0.42	0.78

Table 4.3. Comparing MPI-1 and MPDF estimated maturities in the four main areas of the CTB under investigation. Note: R_C values are more representative than the R_{C1} values. *MPI-1 is after Radke and Welte (1983). MPDF is after Kvalheim et al. (1987).*

Boreham *et al.* (1988) used samples containing only terrestrial organic matter with varying hydrogen contents (Types II, III and IV Kerogens) to evaluate the calibrations of MPI-1 and MPDF against VR, and observed that MPDF display a much lower correlation coefficient to VR than MPI-1. These authors concluded that MPI-1 is a universal indicator of maturation level in terrestrial sediments and oils and can be used to calculate equivalent VR values. Other authors including Taylor *et al.* (1998) also support the use of MPI-1 calculated VR by stating that values (R_c) correlate well with microscopically measured VR. From evidence, R_c values are more representative of the maturity of the CTB coals compared to the R_{c1} values, which supports the idea that phenanthrene abundance is maturity related. Consequently, the MPI-1 values are applied as a guide to estimating the true maturities of the CTB coals.

4.3.6. Summary

Aliphatic biomarker maturity parameters for all seams under study are at or approaching equilibrium; this indicates maturity of around 0.70% R_o and higher. The *n*-alkanes show little odd over even predominance, with CPI(1) and OEP(1) values of ~ 1.0 suggesting samples are close to thermal maturity. Notably, aliphatic biomarker maturity parameters showed no vertical change within coal seams (Figures 4.11), and thus dispute maturity gaps as suggested by VR measurements. Whilst no vertical variation in maturity was observed within and between seams, slight lateral variations do however occur; samples from the eastern margin of the basin (Bassen and Lunckefjellet) are less mature than samples down-dip of the eastern basin margin (Breinosa), and nearer to basin center (Colesdalen). Results generally indicate the Svea, Longyear, Svarteper and Askeladden, Verkny and Sputnik seams have comparable maturities and thermal histories. Significantly, the VR gap seen both within the

Longyear seam and between the Svea and Longyear seams is not reproduced geochemically. Therefore, measured VR values of the upper Firkanten Fm. coal seams (i.e. Longyear, Svarteper, Askeladden, Verkny and Sputnik) do not represent their true maturity and are suppressed.

4.4. Maturity and Oil Potential of the Longyear and Sputnik Coals Using Rock-Eval Analysis

T_{max} like many maturity parameters is highly dependent upon source material (Peters, 1986 and references within), and it provides a good maturation index in types II and III kerogens (Tissot *et al.*, 1987). The threshold of the oil zone is approximately in the T_{max} range 430 - 435 °C for types II and III kerogens, but the threshold of the gas zone is somewhat different; it is in the T_{max} ranges of 450 - 455 °C and 465 - 470 °C for types II and III kerogens respectively. T_{max} values range between 425 - 437, 431 - 439, 433 - 447 and 440 - 445 °C respectively for the Longyear coals in Bassen, Lunckefjellet and Breinosa, and the Sputnik coals in Colesdalen. Average T_{max} values are 430, 434, 441 and 443 °C respectively at these locations (Tables 5.4 and 5.5), and thus indicate that maturity increases from Bassen, through Lunckefjellet and Breinosa to Colesdalen. The T_{max} values also indicate that bulk of the samples are in the oil window (Tissot *et al.*, 1987), and within the "effective oil window" for oil-prone Cenozoic coals (Petersen, 2006).

A plot of T_{max} vs HI (indicative of source rock potential) displays a generally positive correlation (Figure 4.13), which increases from Bassen through Lunckefjellet to Breinosa and Colesdalen. The HI_{max} concept is the increase in HI at the start of oil generation up to a maximum prior to the onset of oil expulsion (Sykes, 2001; Petersen, 2002; Sykes and Snowdon, 2002; Petersen,

2005). In Figure 4.13, the HI of the coals appears to peak between T_{max} range of 430 – 435 °C, which is similar to the HI_{max} concept. This increase in HI is postulated to result from the structural reorganisation of the coal matrix during diagenesis and catagenesis (Killops *et al.*, 1998), and possibly includes incorporation of water-derived hydrogen (Lewan 1997; Schenk and Horsfield, 1998). According to Sykes and Snowdon (2002), this process has been linked to solid-state aromatisation reactions, and results in the formation of new, higher energy bonds and an increase in potentially hydrocarbon generating units within the coal.

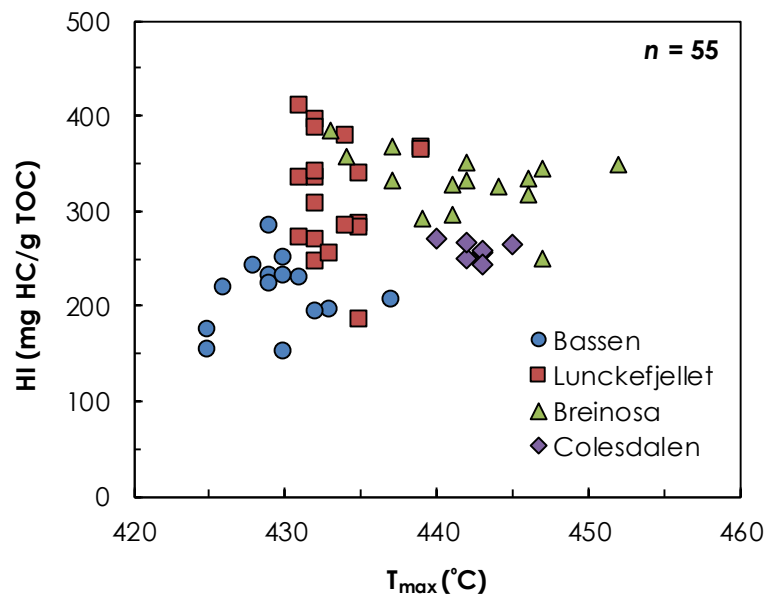


Figure 4.13. T_{max} vs HI of the Longyear and Sputnik coals shows a general positive correlation which increases from Bassen, through Lunckefjellet to Breinosa and Coledalen.

The Correlation between T_{max} and VR (after Teichmüller and Durand, 1983) is presented in Tables 4.4 and 4.5; the Longyear samples in Bassen, Lunckefjellet, Breinosa and Coledalen show mean T_{max} predicted VR values of 0.57, 0.66, 0.81 and 0.83% R_o respectively. Evidence from biomarker maturity assessments

suggest the Longyear and Sputnik coals from all areas under study have at least reached the main oil window ($\geq 0.70\%$ R_o); thus the low T_{max} predicted VR values for Bassen (0.57% R_o) and Lunckefjellet (0.66% R_o) is surprising. In a study of New Zealand Eocene coals, Newman *et al.* (1997) observed that T_{max} was lower in perhydrous coals than in the other coals (orthohydrous) with the same burial and thermal histories. Similarly, the T_{max} values of Canadian Cretaceous high HI coals have been noted to be anomalously low (Snowdon, 1995). Sykes and Snowdon (2002) also observed T_{max} suppression in Cretaceous to Cenozoic coals from New Zealand. Therefore, it appears that the T_{max} of the CTB coals, particularly those from the eastern basin margin, may be suppressed. It is however noted that weathering within the Bassen field samples, may have contributed to their low T_{max} predicted VR values.

Scatter plots of VR vs HI show strong negative correlations for all four areas under study (Figure 4.14).

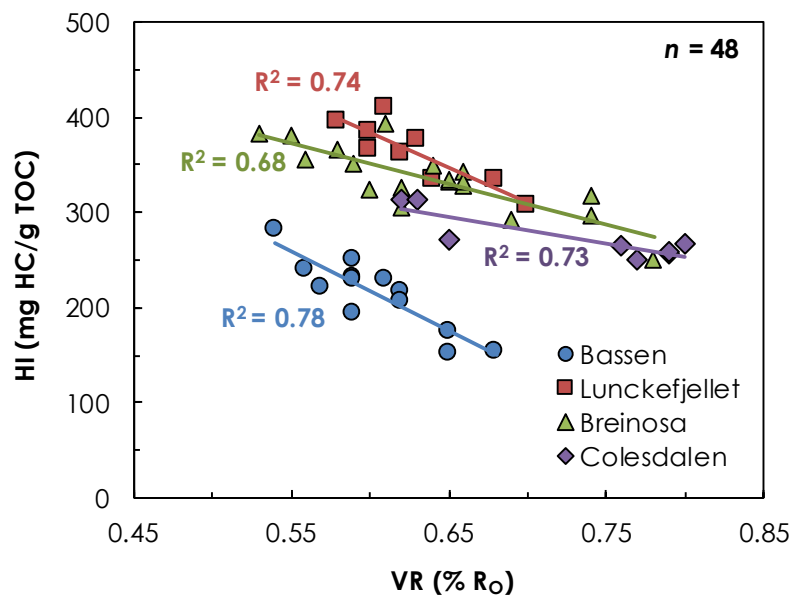


Figure 4.14. VR vs HI of the Longyear and Sputnik coals. Note: Strong negative correlation indicates VR suppression.

Whilst HI is expected to decrease with increasing VR given that hydrocarbon generation should result in a decrease in HI, it has been noted that HI increases up to a maximum at $T_{max} \sim 430 - 440 \text{ }^\circ\text{C}$, and $VR \sim 0.65 - 0.80\% R_o$ (Sykes and Snowdon, 2002) prior to expulsion. Therefore, the relationship in Figure 4.14 is not due to any maturity-induced chemical change in the coals, but is due to suppression of VR by hydrogen enrichment. However, the different gradients and positions of the R^2 lines is complicated by other factors; these are likely to be positional, and weathering effects in the case of the Bassen field samples.

To further assess VR suppression, the trends of Soxhlet extracts and VR from base to top of the Longyear coals in Bassen and Mine 7 are examined (Figure 4.15); sections with higher Soxhlet extracts displayed lowest VR values. Therefore, bitumen must have a suppressing effect on VR across the CTB. This implies that samples with the lowest oil potential will provide a better indication of the degree of maturation.

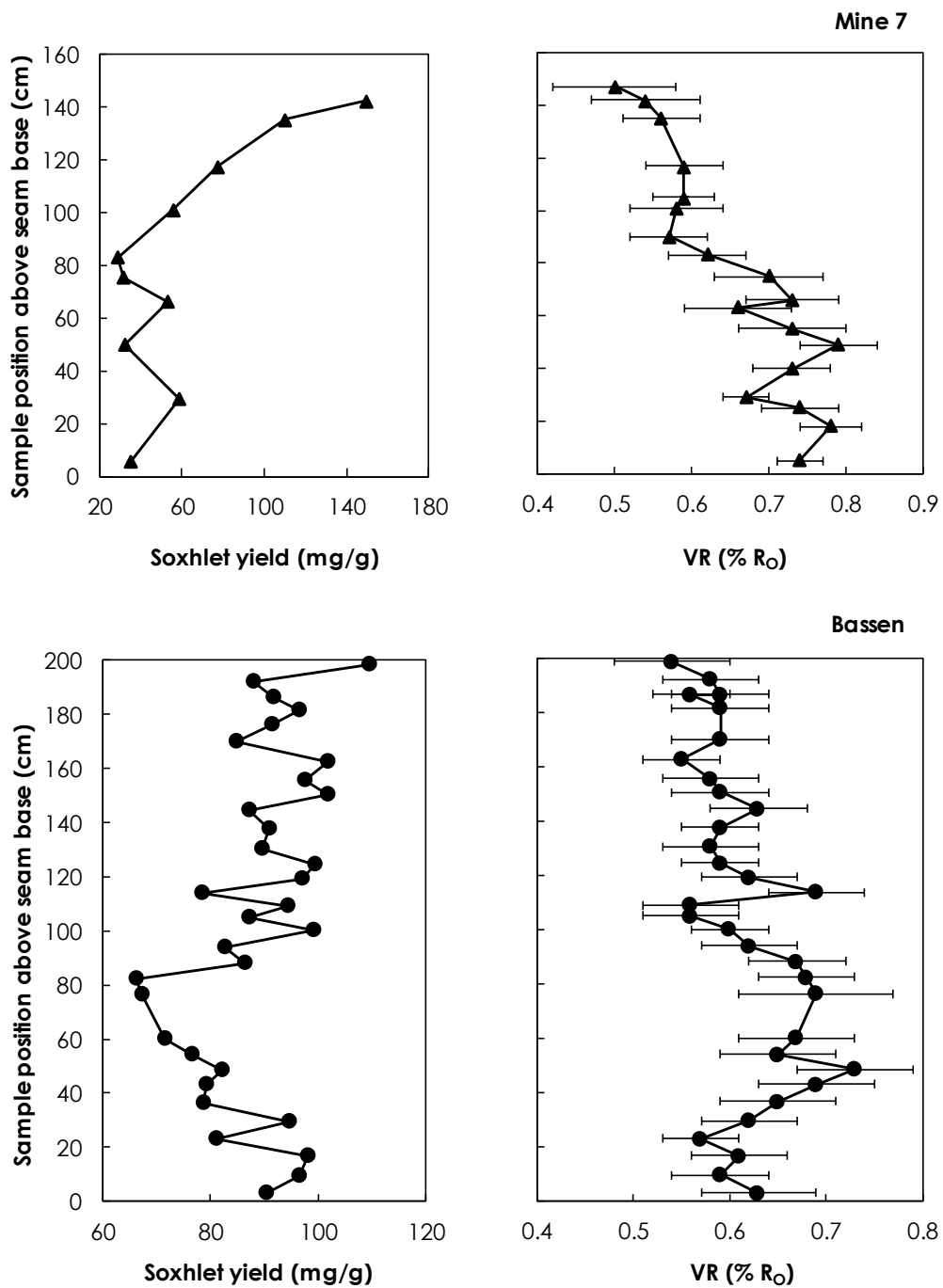


Figure 4.15. Comparing trends of Soxhlet yield (dry whole coal basis) with VR from base to top of the Longyear seam in Mine 7 and Bassen. Note: coals with greatest oil potential display lowest VR which indicates VR suppression by bitumen impregnation. Error bars represent standard deviation of VR measurements.

4.5. Assessing VR Suppression Effect Using ^{13}C NMR

Direct measurement of aromaticity such as ^{13}C NMR (of which VR is an indirect measurement) has been shown to be a useful tool in the derivation of maturity in coals (Stephens *et al.*, 1985; Carr and Williamson, 1990). Marshall *et al.* (2015b) used ^{13}C NMR to show that the aromaticity (%) differ greatly between the Longyear and Svea seams (50 % vs 70 % respectively), and using the calibration of Carr and Williamson (1990), these values yield equivalent VR values of 0.50 and 0.78% R_o for the Longyear and Svea seam respectively (Figure 8 of Marshall *et al.*, 2015b). The maturity of 0.50% R_o indicates that the Longyear sample has at least reached the early oil window. The Svea on the other hand, which is not oil prone, exhibits an aromaticity consistent with measured maturity. Consequently, the observed VR gap between the Svea and Longyear seams must be caused by significant amounts of additional aliphatic material within the Longyear seam.

4.6. The True Maturity of the CTB Coals Under Study

The VR variation observed by Orheim *et al.* (2007) at a bulk scale has been replicated with the Longyear seam in particular appearing to show a rapid VR decrease towards seam top. However, this variability does not appear to be replicated by other measures of maturity, particularly the aliphatic biomarkers maturity parameters assessments. In addition, these parameters suggest that the coals have a thermal maturity of at least 0.7% R_o indicating that they have reached maturities consistent with the main oil window (0.7 – 1.0% R_o). Marshall *et al.* (2015b) reported that the Longyear coal contains around 30 % extra aliphatic material compared to the Svea coal. Provided adequate maturity, a liquid hydrocarbon potential leads to hydrocarbon generation and migration as well as the subsequent bitumen enrichment observed throughout the

sampled areas with Rock-Eval HI values ranging from 250 - 400 mg HC/g TOC. This is consistent with observed oil expulsion from the Longyear coals (Orheim *et al.*, 2007) as well as oil potential assessments and hydrocarbon yields of Marshall *et al.*, 2015a (HI of 300 – 400 mg HC/g TOC; Soxhlet solvent extract plus hydrous pyrolysis yield of 300 – 400 mg HC/g TOC). The effect upon VR is clear which shows a negative relationship the higher the oil potential, the more suppressed VR values become (Figures 4.14 and 4.15). This vitrinite suppression effect by the enrichment of the Askeladden, Svarteper and Longyear, Verkny and Sputnik seams in aliphatic rich bitumen compared to the “non oil-prone” Svea seam is therefore considered the primary cause of VR gaps observed by Orheim *et al.* (2007). Consequently, earlier Carboniferous, Jurassic and Cretaceous coals in the basin with observed coal rank inversion and VR gaps (Paech and Koch, 2001) may benefit from further examination of this effect.

In Section 4.3, the aromatic maturity parameter (MPI-1) was used to estimate mean VR values of 0.82, 0.62, 0.74 and 0.83% R_o in Bassen, Lunckefjellet, Breinosa and Colesdalen respectively, while in Section 4.4, the T_{max} to VR correlation (Teichmüller and Durand, 1983) estimated VR values of 0.57, 0.65, 0.81 and 0.83% R_o for these four areas respectively. However, there are indications that T_{max} values are suppressed, and the formation of aromatics with increasing maturity may be delayed/suppressed (Section 4.3.5) within the CTB coals. Consequently, the true maturities of the CTB coals are further assessed. Marshall *et al.* (2015b) reported that the most accurate measured VR values for the Longyear seam tend to occur at the seam base which led to conclusions that thermal maturities (VR) are 0.68, 0.76, 0.78 and 0.80% R_o in Bassen, Lunckefjellet, Breinosa and Colesdalen respectively. The reliability of adopting these measured VR values for the CTB is assessed by using the Lo

(1993) model for correcting the suppression of VR in hydrogen rich kerogens to obtain the “true vitrinite reflectance” (R_T). The Lo (1993) VR correction model incorporates HI; although it is recommended to use the original HI (H_{I0}) when applying this model, it was thought that using the HI is not a problem since the HI is a measure of the amount of hydrogen that is “currently” suppressing the VR that is “currently” measured. Also, the inferred T_{max} suppression in these coals results in unreliable H_{I0} prediction from existing mathematical relationships for Type III kerogen (e.g. Banerjee *et al.*, 1998). On applying the Lo (1993) model on the CTB coals, mean R_T values of 0.68, 0.78, 0.80 and 0.88% R_o were estimated at Bassen, Lunckefjellet, Breinosa and Colesdalen respectively (Figure 4.16; Tables 4.4 and 4.5). The Svea coal from Svea Nord showed 0.87% R_o , which is similar to values of the Sputnik coals in Colesdalen. Comparing R_T values and the measured VR values from the lower parts of the coal seams as adopted by Marshall *et al.* (2015b) shows that in Bassen, Lunckefjellet and Breinosa, both sets of values are generally similar. However, in Colesdalen area, the difference is significantly greater (0.08% R_o). Reason being that the Colesdalen coals show significant VR variations (Figure 4.6), and contain abundant perhydrous vitrinites with varying fluorescence intensities (Figure 4.1), which is reflected in the broad VR histograms (Figure 4.6), the relatively high HI values (~240 – 310 mg HC/g TOC; Table 5.5) and the high amounts of Soxhlet extracts (up to 143 mg/g; Table 5.7) from these coals. Therefore, it will be erroneous to adopt the measured VR values from any section of the Sputnik seam in Colesdalen as suggested by Marshall *et al.* (2015b), and the basin center in general. It is advised that VR measurements from the seam base in the north-eastern and eastern parts of the basin should be used with caution. Thus, the Lo (1993) corrected VR values are considered most accurate, and they reflect the degree of thermal maturity of these coals.

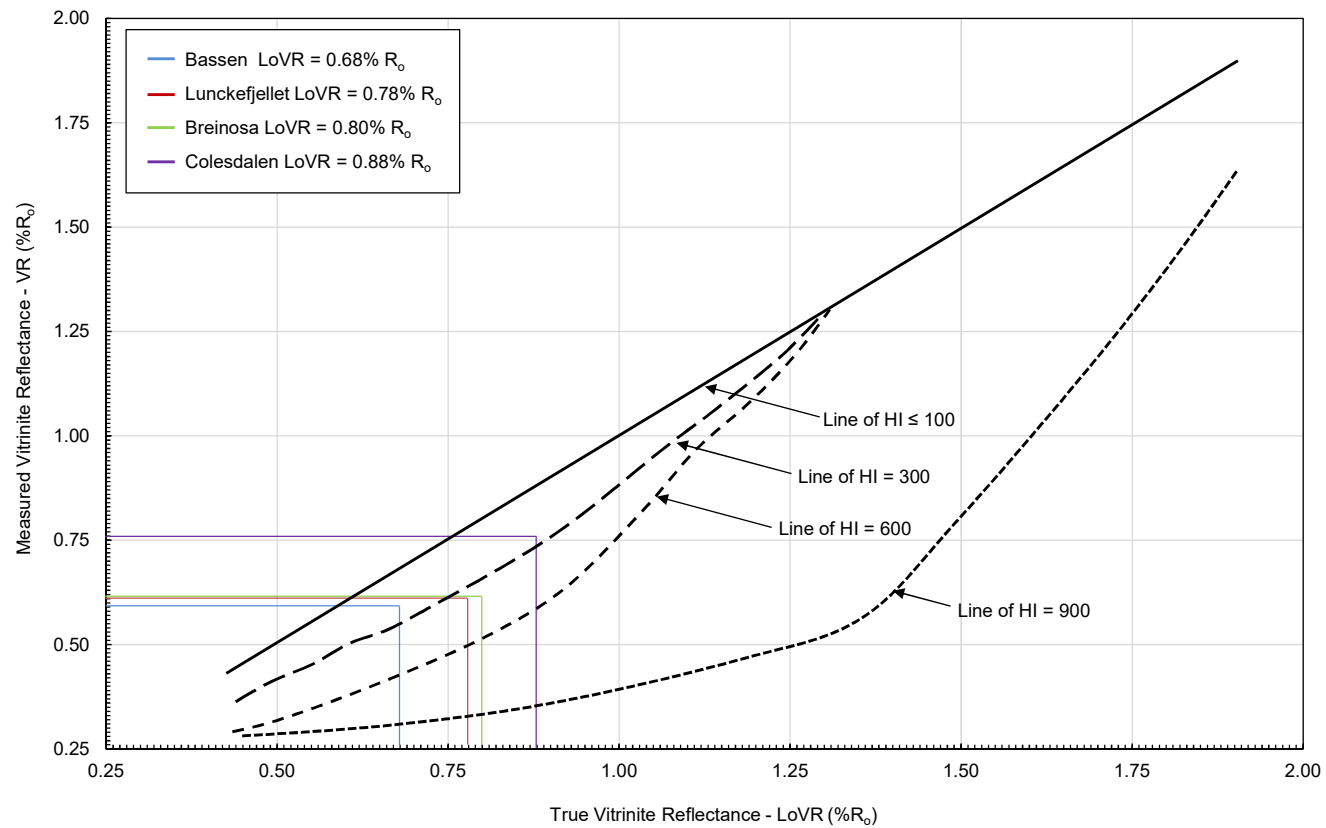


Figure 4.16. Model for correcting the suppression of VR (modified from Lo, 1993). Note: the estimated true VR (R_T) of the Longyear seam in Bassen, Lunckefjellet, Breinosa and the Sputnik seam in Colesdalen are 0.68, 0.78, 0.80 and 0.88% R_0 respectively. Standard deviation of Lo (1993) corrected VR are 0.02, 0.04, 0.05 and 0.05% R_0 respectively in all four areas.

Sample ID	Area	Location and sample type	Seam	Drill depth (m)	Sample position above seam base (cm)	VR measured (% Ro)	T _{max} (°C)	T _{max} predicted VR ^a	MPI-1 predicted VR (R _c)	Lo (1993) corrected VR (R _i)
Br1	Breinosa	BH4-2009	Askeladden	298.4	46.5	0.61	447	0.93	0.73	0.81
Br8	Breinosa	BH4-2009	Svarteper	301.2	11.5	0.55	437	0.73	0.62	0.74
Br9	Breinosa	BH4-2009	Unknown	313.8	24.0	0.66	442	0.83	ND	0.82
Br11	Breinosa	BH4-2009	Longyear	314.7	116.0	0.6	444	0.87	ND	0.76
Br12	Breinosa	BH4-2009	Longyear	314.9	95.5	0.66	447	0.93	0.74	0.84
Br13	Breinosa	BH4-2009	Longyear	315.2	74.5	0.69	439	0.77	ND	0.81
Br16	Breinosa	BH4-2009	Longyear	315.7	24.0	0.66	442	0.83	0.73	0.83
Br17	Breinosa	BH4-2009	Longyear	315.8	8.0	0.59	442	0.83	ND	0.78
Br20	Breinosa	BH5-2009	Svarteper	-	93.5	0.65	437	0.73	ND	0.80
Br22	Breinosa	BH5-2009	Svea	-	50.0	0.78	447	0.93	ND	0.85
Br26	Breinosa	Mine 7 section	Longyear	-	142.5	0.53	433	0.64	ND	0.72
Br27	Breinosa	Mine 7 section	Longyear	-	135.5	0.56	434	0.66	ND	0.76
Br28	Breinosa	Mine 7 section	Longyear	-	117.5	0.58	437	0.73	ND	0.75
Br32	Breinosa	Mine 7 section	Longyear	-	83.0	0.62	441	0.81	ND	0.78
Br34	Breinosa	Mine 7 section	Longyear	-	66.0	0.65	446	0.91	ND	0.82
Br39	Breinosa	Mine 7 section	Longyear	-	29.0	0.74	446	0.91	ND	0.90
Br42	Breinosa	Mine 7 section	Longyear	-	5.0	0.74	441	0.81	ND	0.88
Ba1	Bassen	Outcrop section	Longyear	-	198.5	0.54	429	0.56	0.73	0.66
Ba3	Bassen	Outcrop section	Longyear	-	186.5	0.59	429	0.56	ND	0.68
Ba6	Bassen	Outcrop section	Longyear	-	170.0	0.59	430	0.58	ND	0.70
Ba9	Bassen	Outcrop section	Longyear	-	150.5	0.59	431	0.60	ND	0.67
Ba11	Bassen	Outcrop section	Longyear	-	137.5	0.59	433	0.64	ND	0.65
Ba14	Bassen	Outcrop section	Longyear	-	119.3	0.62	426	0.50	ND	0.70
Ba16	Bassen	Outcrop section	Longyear	-	109.0	0.56	428	0.54	ND	0.65
Ba19	Bassen	Outcrop section	Longyear	-	94.0	0.62	437	0.73	ND	0.71
Ba21	Bassen	Outcrop section	Longyear	-	82.3	0.68	425	0.48	0.61	0.73
Ba24	Bassen	Outcrop section	Longyear	-	54.0	0.65	425	0.48	ND	0.70
Ba27	Bassen	Outcrop section	Longyear	-	36.5	0.65	430	0.58	ND	0.69
Ba29	Bassen	Outcrop section	Longyear	-	23.0	0.57	429	0.56	ND	0.66
Ba30	Bassen	Outcrop section	Longyear	-	16.5	0.61	430	0.58	ND	0.69
Ba32	Bassen	Outcrop section	Longyear	-	3.0	0.63	432	0.62	0.72	0.69

Table 4.4. Comparing data from various measures of thermal maturity for the CTB coals in the Bassen and Breinosa areas. ^a after Teichmüller and Durand (1983). MPI-1 is after Radke and Welte (1983). ND = not determined.

Sample ID	Area	Location and sample type	Seam	Drill depth (m)	Sample position above seam base (cm)	VR measured (% R _o)	T _{max} (°C)	T _{max} predicted VR ^a	MPI-1 predicted VR (R _o)	Lo (1993) corrected VR (R _i)
L1	Lunckefjellet	BH15-2011	Svarteper	246.00	80.0	0.53	437	0.73	0.66	0.81
L3	Lunckefjellet	BH15-2011	Svarteper	246.20	60.0	0.56	434	ND	0.67	0.70
L4	Lunckefjellet	BH15-2011	Svarteper	246.30	50.0	0.57	435	0.68	ND	0.77
L5	Lunckefjellet	BH15-2011	Svarteper	246.40	40.0	0.50	439	ND	0.57	0.68
L7	Lunckefjellet	BH15-2011	Svarteper	246.60	20.0	0.53	431	ND	ND	0.71
L8	Lunckefjellet	BH15-2011	Svarteper	246.70	10.0	0.56	436	0.71	0.67	0.73
L9	Lunckefjellet	BH15-2011	Longyear	258.30	210.0	0.59	432	0.62	0.55	0.70
L11	Lunckefjellet	BH15-2011	Longyear	258.50	190.0	0.64	431	0.60	0.69	0.77
L12	Lunckefjellet	BH15-2011	Longyear	258.80	160.0	0.60	439	0.77	0.59	0.79
L14	Lunckefjellet	BH15-2011	Longyear	259.00	140.0	0.62	439	0.77	0.63	0.79
L16	Lunckefjellet	BH15-2011	Longyear	259.20	120.0	0.61	431	0.60	0.53	0.81
L18	Lunckefjellet	BH15-2011	Longyear	259.40	100.0	0.58	432	0.62	0.63	0.78
L20	Lunckefjellet	BH15-2011	Longyear	259.60	80.0	0.70	432	0.62	0.71	0.83
L22	Lunckefjellet	BH15-2011	Longyear	259.80	60.0	0.68	432	0.62	0.65	0.84
L24	Lunckefjellet	BH15-2011	Longyear	260.00	40.0	0.64	431	0.60	ND	0.80
L25	Lunckefjellet	BH15-2011	Longyear	260.10	30.0	0.60	432	0.62	0.60	0.80
L27	Lunckefjellet	BH15-2011	Longyear	260.30	10.0	0.63	434	0.66	0.60	0.81
L32	Lunckefjellet	BH10-2009	Svarteper	55.14	10.5	0.53	436	0.71	ND	0.71
L33	Lunckefjellet	BH10-2009	Longyear	69.71	79.0	0.61	435	0.68	ND	0.78
L36	Lunckefjellet	BH10-2009	Longyear	70.40	10.5	0.68	435	0.68	ND	ND
L38	Lunckefjellet	BH10-2007	Svarteper	237.03	20.5	0.59	435	0.68	ND	0.77
L39	Lunckefjellet	BH10-2007	Longyear	247.06	148.5	0.58	432	0.62	ND	0.76
L41	Lunckefjellet	BH10-2007	Longyear	247.56	98.5	0.64	435	0.68	ND	0.78
L44	Lunckefjellet	BH10-2007	Longyear	248.45	9.5	0.64	434	0.66	ND	0.78
L45	Lunckefjellet	BH6A-2007	Svarteper	210.36	110.5	0.59	434	0.66	ND	0.76
L48	Lunckefjellet	BH6A-2007	Longyear	223.03	187.5	0.58	432	0.62	ND	0.69
L51	Lunckefjellet	BH6A-2007	Longyear	223.78	112.5	0.67	433	0.64	ND	0.80
L54	Lunckefjellet	BH6A-2007	Longyear	224.53	37.5	0.73	435	0.68	ND	0.79
S4	Svea Nord	Mine section	Svea	-	81.5	0.78	442	0.83	ND	0.84
S5	Svea Nord	Mine section	Svea	-	7.0	0.77	444	0.87	ND	0.90
C1	Colesdalen	BH3-2008	Verkny	258.18	16.0	0.62	437	0.73	0.74	0.77
C2	Colesdalen	BH3-2008	Sputnik	274.13	172.5	0.77	442	0.83	0.79	0.88
C3	Colesdalen	BH3-2008	Sputnik	274.38	147.5	0.79	443	0.85	0.80	0.90
C4	Colesdalen	BH3-2008	Sputnik	274.63	122.5	0.79	443	0.85	0.84	0.90
C6	Colesdalen	BH3-2008	Sputnik	275.05	80.5	0.65	440	0.79	0.56	0.77
C7	Colesdalen	BH3-2008	Sputnik	275.28	57.5	0.78	443	0.85	0.94	0.89
C8	Colesdalen	BH3-2008	Sputnik	275.51	34.5	0.80	442	0.83	0.84	0.93
C9	Colesdalen	BH3-2008	Sputnik	275.74	11.5	0.76	445	0.89	0.76	0.89

Table 4.5. Comparing data from various measures of thermal maturity for the CTB coals in the Lunckefjellet, Svea Nord and Colesdalen areas. ^a after Teichmuller and Durand (1983). MPI-1 is after Radke and Welte (1983). ND = not determined.

4.7. Thermal Regime and Implications for Overburden Models

Previous models measuring coalification gradients in the Tertiary strata from the Adventdalen sub-region range between 0.17 - 0.3 % Ro/km (Paech and Koch, 2001); however due to the VR suppression effect, it is likely that VR values lie somewhat higher than previously thought. With estimated VR values of 0.68, 0.78, 0.80 and 0.88% Ro in Bassen, Lunckefjellet, Breinosa and Colesdalen, the maximum overburden and thermal regime at peak burial was calculated using the empirical palaeo-temperature equation of Barker and Pawlewicz (1994) given as:

$$\mathbf{Max\ T(^{\circ}C) = \frac{Ln(Ro) + 1.68}{0.0124}} \quad (4.7)$$

VR values indicate estimated peak temperatures of 104 °C at Bassen, 116 °C at Lunckefjellet, 118 °C at Breinosa and 125 °C in the Colesdalen area. It is noted that peak temperatures of 100, 110, 111 and 116 °C in these areas respectively have been reported (Marshall *et al.*, 2015b). The difference in values is because this study utilised the Lo (1993) corrected VR values, whereas Marshall *et al.* (2015b) used measured VR values of samples from the lower parts of the seam as they appeared least affected by suppression. VR values indicate the coals nearer to basin center seem to have been exposed to the highest temperatures and vice versa. Controls on VR include the depth of burial and geothermal gradient. Considering Fourier's law:

$$\mathbf{Q = k * dT/dz} \quad (4.8)$$

Where Q is the heat flow, k is the thermal conductivity, and dT/dz is the geothermal gradient. The above relationship shows that geothermal gradients are inversely related to thermal conductivity, and bearing in

mind that thermal conductivity is influenced by lithology (e.g. Robertson, 1988), porosity, grain size and shape, fluid content, temperature and pressure (e.g. Cronoble, 1969).

Given the generally poor thermal conductivity of sediments immediately after burial (e.g. Sharp and Domenico, 1976), the central parts of the CTB with thicker accumulations of sediments, would have lower geothermal gradients than basin margins during the Tertiary. The tendency of geothermal gradient to increase with decreasing thickness of sedimentary strata has been reported by Majorowicz and Jessop (1981). Higher geothermal gradient at basin margins associated with the distribution of palaeogeothermal heat flow during sediment deposition has also been inferred by these workers. According to Rybach (1984), heat flows and geothermal gradients are inversely proportional to depth of basement. Thus, during the Tertiary, the CTB margins may have experienced the highest geothermal gradient; however, as the maturities are highest in the central parts of the basin, this appears to have been the area with the deepest burial and/or geothermal gradient.

Considering normal continental geothermal gradients (25 °C/km) and assuming no other heat sources (Corcoran and Clayton, 1999), the estimated peak temperatures would reflect maximum burial depths of 4.2, 4.6, 4.7 and 5.0 km respectively in Bassen, Lunckefjellet, Breinosa and Colesdalen areas. As approximately 1.0 km of overlying strata still remain in Adventdalen (Thronsen, 1982), this would equate to a total missing overburden of between 3.2 – 3.6 km in this sub-region, which is much greater than other estimates from the CTB (Paech and Koch, 2001). It has been noted that the island of Spitsbergen was exposed to volcanic activities (Section 4.1), therefore continental heat

flows/geothermal gradients are unlikely. However, there was no access to a petroleum system modelling software in this study, and thus the exact geothermal gradient could not be determined. Still focussing on the Adventdalen sub-region, VR values of 0.43% R_o for the upper Tertiary coals from the Aspelintoppen Fm. in Nordenskioldfjellet (~15 km west of Breinosa, Figure 2.12) has been reported (Thronsdén, 1982). Assuming this is correct, and the VR of the stratigraphically lower Firkanten Fm. coals in Breinosa is 0.80% R_o , then the VR gradient will be 0.37 R_o /km. Using equation 4.7 of Barker and Pawlewicz (1994) indicates a geothermal gradient of around 55 °C/km, which is higher than previous estimates (50 °C/km in Marshall *et al.*, 2015b; 40 °C/km in Braathén *et al.*, 2012), and maximum burial depths of 1.9 km in Bassen, 2.1 km in Lunckefjellet, 2.2 km in Breinosa and 2.3 km in Colesdalen. As approximately 1.0 km of overlying strata remains in Adventdalen (Thronsdén, 1982), the missing overburden would be between 0.9 - 1.2 km; this is slightly higher than estimates by Marshall *et al.* (2015b) (1.0 km), but much lower than the estimates by Paech and Koch (2001) (1.7 km). In more central areas of the basin such as Colesdalen, considering the present day highest peak in the area (Nathorstfjellet; Figure 2.12) is ~0.9 km as per the Norwegian Polar Institute – NPI (2015), missing overburden estimates would be around 1.4 km. Also, the present day highest peak in Lunckefjellet is around 1.0 km (NPI, 2015); this implies missing overburden estimates of around 1.1 km in this area. Thus, accounting for VR suppression has greatly reduced the current estimated 3 km of eroded overburden (Manum and Thronsdén, 1978). It is noted that the prediction of temperature using VR data assumes that pressure has no control on the VR values in geological basins. This is inconsistent with work of Uguna *et al.* (2012; 2015), which shows that pressure also affects VR. However, the volcanic history of Spitsbergen (Jamtveit *et al.*, 2006 and references within) means that temperature may have been relatively

high during burial, and given that the coals under study have only been buried to a maximum depth of around 2.3 km, pressure would not have been relatively high. Thus, temperature will be the main control on VR in the CTB.

Previous studies (Major and Nagy, 1972, Manum and Thronsen, 1978, Thronsen, 1982, Paech and Koch, 2001) reported relatively high geothermal gradient in the CTB during burial. This is not surprising as the basin was formed during a period of both local and regional tectonic activity (e.g. Hjelle, 1993). The presence of a dolerite sill in the Bjørndalen area (Pers. Comm. Trygvason Eliassen, 2014 cited in Marshall *et al.*, 2015b), the numerous volcanic bentonites within the Tertiary strata and several basaltic Quaternary-age volcanoes in north-western Spitsbergen (Treiman, 2012) indicate volcanism played an important role in shaping the thermal history of the basin. Elevated heat flows may also explain the relatively low levels of compaction observed in the Tertiary strata when compared to their apparent maturity. Within a regional context, the Northern Barents, including Svalbard (regarded as an uplifted north-western edge of the Barents Shelf; Harland *et al.*, 1997), was subjected to less burial and subsequent uplift and erosion than previously thought (Manum and Thronsen, 1978, Thronsen, 1982, Paech and Koch, 2001). This fits with lower estimates of erosion and sediment load to the Southern Barents during the late Cenozoic (Rasmussen and Fjeldskaar, 1996).

4.8. Summary and Conclusions

VR suppression by bitumen impregnation and/or hydrogen enrichment is well documented in oil source rocks, and often leads to incorrect maturity estimates and unreliable source rock evaluation. Also, T_{max} suppression in oil source rocks has also been reported. Consequently; this chapter compares vitrinite

reflectance measurements with alternative measurements of maturity including aliphatic and aromatic biomarker parameters, Rock-Eval and aromaticity to assess the true maturity of the CTB coals. The following conclusions are drawn;

- Inferred VR gaps within the Firkanten Fm. coals are due to suppression of VR by bitumen impregnation and hydrogen enrichment of vitrinites; evidences include a general decrease in VR values towards the top of the Longyear seam, which correlates with increasing Soxhlet yields in the same direction. Also, plots of VR vs HI show strong negative correlations (R^2 up to 0.78). Other indicators of VR suppression include wide ranges of VR values within seams (between 0.5 – 0.79% R_o) that are ≤ 2.1 m thick, and wide ranges of VR measurements with bi-modal histograms observed in many samples. In addition, values from biomarkers maturity assessments do not decrease towards the top of the seams (unlike the VR trend) and indicates the CTB coals are generally in the maturity range of around 0.7% R_o or higher. The VR of coals from the eastern coalfield (Bassen, Lunckefjellet and Breinosa) appear to be more suppressed than those from the western coalfield (Colesdalen), and in all four areas investigated, greatest suppression was observed in Lunckefjellet. T_{max} appear suppressed, and the re-arrangements of methylphenanthrene isomers with increasing maturity also appear delayed/suppressed. Using the Lo (1993) model for correcting VR suppression, the Adventdalen sub-region shows maturities ranging between 0.68% R_o at the basin margin (Bassen), to 0.80% R_o down-dip (Breinosa). At Lunckefjellet VR values are around 0.78% R_o , while the more centrally located Colesdalen show values of 0.88% R_o .

- Estimated true VR values of the investigated samples indicate peak temperatures of around 104 °C at Bassen, 116 °C at Lunckefjellet, 118 °C at Breinosa and 125 °C in the Colesdalen area.
- Coalification gradients in Adventdalen equate to $\sim 0.37 R_o/km$. A geothermal gradient of approximately 55 °C/km is estimated with peak burial depths of 1.9 – 2.2 km in the Adventdalen area, which indicates overall overburden erosion estimates are in the range of 0.9 – 1.2 km in this area. In Lunckefjellet, peak burial depth is around 2.1 km which implies missing overburden of 1.1 km. In more central areas of the basin such as Colesdalen, peak burial depths are considerably higher at around 2.3 km, with missing overburden estimate of 1.4 km. There are differences in peak burial depths/missing overburden estimates between this study and Marshall *et al.* (2015b); this is because this study utilised the Lo (1993) corrected VR values, whereas Marshall *et al.* (2015b) utilised measured VR values of the samples at or near seam base, as they appear least affected by suppression. The approach by Marshall *et al.* (2015b) is erroneous because measured VR values around seam base are nonetheless suppressed. For example, at Colesdalen, Marshall *et al.* (2015) adopted the measured VR (i.e. average of 100 VR measurements per sample) of 0.80% R_o from the coal at 34.5 cm above seam base; however, this coal is Sample C8 of this study, which shows evidences of VR suppression including a broad range of VR values (0.65 – 1.0% R_o) and abundant perhydrous vitrinites with varying fluorescence. Also, sample C8 displays relatively high S1 and HI values (19 mg/g and 267 mg HC/g TOC respectively) and Soxhlet extracts of 73.1 mg/g daf, which indicates oil-proneness.

- The results indicate that burial and subsequent uplift and erosion were perhaps lower than previously thought, leading to reduced sediment load from Svalbard to the Barents Shelf in the Late Tertiary.

OIL SOURCE ROCK AND RETORTING POTENTIAL OF THE CENTRAL TERTIARY BASIN COALS, SPITSBERGEN

5.1. Introduction

The petroleum potential of Tertiary coals from Mine 7 and Svea Nord Mine in the CTB (Figure 3.1) was investigated by Marshall *et al.* (2015a); the study concluded that majority of the coal seams may hold substantial liquid hydrocarbon potential. Marshall *et al.* (2015a) postulated that greatest oil potential is favoured by conditions including: marine influence (>0.5 % S), high bacterial degradation (>100 µg/g TOC hopanes), stable hydrology and fen (rheotrophic) conditions. The role of marine influence on the formation of oil prone coals cannot be overemphasised and it is well documented (e.g. Diessel, 1992; Taylor *et al.*, 1998; Wilkins and George, 2002). Marine influence not only supplies sulphur (e.g. Petersen, 2005; 2006; Sykes and Snowdon, 2002; Wilkins and George, 2002; Chou, 2012), which promotes hydrogen enrichment and consequently oil potential (Petersen, 2005 and references within), but it is also linked to bacteria degradation (Taylor *et al.*, 1998), stable hydrology and fen conditions during peat deposition in Spitsbergen (Marshall, 2013). Wilkins and George (2002) noted that variable marine influence throughout the deposition of coal measures resulted in pronounced variation in petroleum potential in the New Zealand Taranaki Basin. Considering the CTB coals are deposited in a paralic setting (Orheim *et al.*, 2007; Marshall, 2013; Marshall *et al.*, 2015a), and bearing in mind that the conditions favouring petroleum potential in the basin (Marshall *et al.*, 2015a) are somewhat related to marine influence upon the coals (albeit these conditions would show considerably different degrees of variability); petroleum potential would consequently vary between areas of the CTB. This constitutes a main aspect of assessing the source rock potential of the CTB coals.

In Chapter 4, the true maturities of the CTB coals were estimated as 0.68, 0.78, 0.8 and 0.88% R_o in Bassen, Lunckefjellet, Breinosa and Colesdalen respectively. Considering the threshold of the main oil window lies between 0.7 to 1.0% R_o , the maturity variation from basin margins to center will invariably influence the volume of oil generated and/or expelled from coals in these 4 main areas of the basin. This will help in oil potential assessments and thus forms another main part of assessing the source rock potential of these coals within this chapter.

Pyrolysis of coal generally seeks to increase the liquid hydrocarbon yield whereas processes such as carbonization is usually practised for the production of coke with minimum yield of tar and other hydrocarbon by-products (Taylor *et al.*, 1998). Retorting technologies have been applied to expel liquid hydrocarbons from oil shales in the last 100 years (e.g. Dinneen, 1976, Lewan *et al.*, 1979). In Chapter 1, it was noted that retorting techniques have been used to expel liquid hydrocarbons from Svalbard coals in the Kings Bay region (yield of 180 – 214 mg/g; Hoel, 1925) and from Tertiary coals in Breinosa (yield of 175 – 195 mg/g; Wang, 2011); this led to the inference that the CTB coals may hold significant retorting potential. Considerable research has been carried out to investigate the factors governing the transformation of coal into coke; during the transformation, the coal melts at approximately 350 - 380 °C, devolatilizes while undergoing some swelling, and solidifies again at approximately 450 - 515 °C into a porous plastic mass which shrinks and sets into a semi-coke (Taylor *et al.*, 1998). Therefore, the adopted nitrogen pyrolysis technique in this study (Section 3.2.2.3) with maximum temperatures of 520 °C will not only generate and expel liquid hydrocarbons, but also produce a usable semi-coke which is an added advantage. Another advantage of the retorting process is the reduction of sulphur contents in the coke relative to the feedstock by 30 – 50 %

through the thermal decomposition conversion of pyrite (FeS_2) to pyrrhotite ($\text{Fe}_{(1-x)}\text{S}$ where $x = 0$ to 0.17) (Lambert *et al.*, 1998). This means areas previously considered uneconomic due to their sulphur content ($>2\%$) would become economic, thereby increasing existing resource estimates. Additionally, the retorting process would lead to improved oil quality by cracking of bitumen (Peters *et al.*, 2005; Killops and Killops, 2005) and thus resulting in generally lighter oils. Orheim (1982) estimated that the coal within the CTB represented a maximum resource of 3,300 Mt, of which 600 Mt was recoverable. Assuming crude oil density of 847 kg/m^3 at 35.6° API , $1 \text{ Kg} = 7.43\text{E-}03 \text{ bbl}$. Thus, with an average retorting yield of 175 mg/g coal, the resource size could be as much as 4,290 Mbbl hydrocarbons in place, with 780 Mbbl hydrocarbons accessible by mining. In-situ retorting methods would access the considerably larger deposits estimated by Orheim (1982), which if used alongside coal gasification technology could yield significant quantities of liquid and gaseous hydrocarbons. However, the economics of this process depends on a number of factors including but not limited to the distribution of oil prone materials and oil quality.

Therefore, this chapter will firstly investigate the oil source rock potential of the Tertiary coals of the CTB from organic petrography and geochemistry points of view to assess possible variation in petroleum potential. Also, focussing on the findings of Marshall *et al.* (2015a), the controls on petroleum potential in the basin will be further examined. Additionally, the oil potential and source(s) of oil-proneness between the Carboniferous and Tertiary coals in Spitsbergen are compared. The retorting potential of the coals will be subsequently assessed to see if documented retorting yields (Wang, 2011) can be replicated in other areas of the basin. Evaluation of the source rock and retorting potential of the

coals will provide invaluable data that will help in delineating optimum hydrocarbon resource areas in the basin.

5.1.1. Samples and Methodology

Samples investigated in this chapter are from the 4 main sampled areas from the present-day eastern basin margin to center; these include Bassen, Lunckefjellet, Breinosa and Colesdalen. Sampling and sample distribution are detailed in Section 3.1.1. Main analytical methods utilised include organic petrography, Rock-Eval 6, GC-MS, Py-GCMS and retorting. Maceral analysis was used to assess the distribution of oil-prone macerals as well as assess palaeoenvironment relative to oil potential. Oil potential and kerogen quality were assessed via Rock-Eval 6 analysis and Py-GCMS. Retorting was simulated using nitrogen pyrolysis and oil quality was assessed via fractionation into aliphatic, aromatic and NSO compounds, followed by GC-MS analysis of hydrocarbon fractions. All adopted methods and techniques are as described in Chapter 3.

5.2 Oil-Prone Coals – Characterisation and Occurrence in the CTB

Early characterisation of oil prone coals was being based on petrology and maceral composition; however, the complete reliance on maceral composition for the classification of coals as oil prone has proven to be unreliable, which has led to the use of other laboratory techniques such as Rock-Eval analysis (e.g. Peters, 1986; Snowdon, 1995; Newman *et al.*, 1997; Petersen 2002, 2006; Sykes and Snowdon, 2002; Petersen *et al.*, 2009; Sykes *et al.*, 2014; Marshal *et al.*, 2015a). This section will assess the types and distribution of macerals present in relation to oil potential of the Firkanten Fm. coals as well as utilise Rock-Eval parameters to examine the kerogen types.

5.2.1. Coal Maceral Analysis

Increased oil yields have been shown to be associated with the transition of the Longyear seam from a more ombrotrophic (precipitation fed) peatland to a more rheotrophic (groundwater fed) system (Marshall *et al.*, 2015a). The hydrological conditions and redox conditions of a peatland can be represented using coal maceral analysis (Stach, 1982; Casareo *et al.*, 1996; Taylor *et al.*, 1998); therefore, oil potential can be inferred from coal maceral analysis.

5.2.1.1. Peatland Environment and Oil Potential - the Longyear and Sputnik Seams

The Longyear coals from Bassen, Lunckefjellet BH15-2011, Breinosa BH4-2009, and Breinosa Mine 7, and the Sputnik coals from Colesdalen BH3-2008 were selected for palaeoenvironmental interpretation relative to oil potential, which was achieved via maceral analysis. Mean vitrinite contents are 90.8, 86.8, 93.1, 77.5 and 79.6 vol % on mineral matter free (mmf) basis respectively at these locations (Table 5.1.A and 5.1.B). Although there are no previous reports on Bassen, measured values are similar to existing reports on the Adventdalen area (77.2 vol %, Ćmiel and Fabiańska, 2003) to which the Bassen sampling locality belongs (Figure 3.1). Values from the Colesdalen coals could not be compared as there are limited or no existing maceral work on the area.

Detrovitrinites are a sub-maceral group of vitrinites, and represents fine degraded organic matter; they indicate wetter conditions (Diessel and Gammidge, 1998), they are oil-prone (Boreham and Powell, 1993), and have been linked to the oil-proneness of CTB coals (e.g. Marshall *et al.*, 2015a; b). Mean detrovitrinite contents are 23.5, 26.5, 33.6, 21.9 and 15.5 vol % mmf in the Bassen, Lunckefjellet, Breinosa BH4-2009, Mine 7 and Colesdalen samples

respectively. (Table 5.1.A and 5.1.B), and they correlate with greater Soxhlet yields (Figure 5.1).

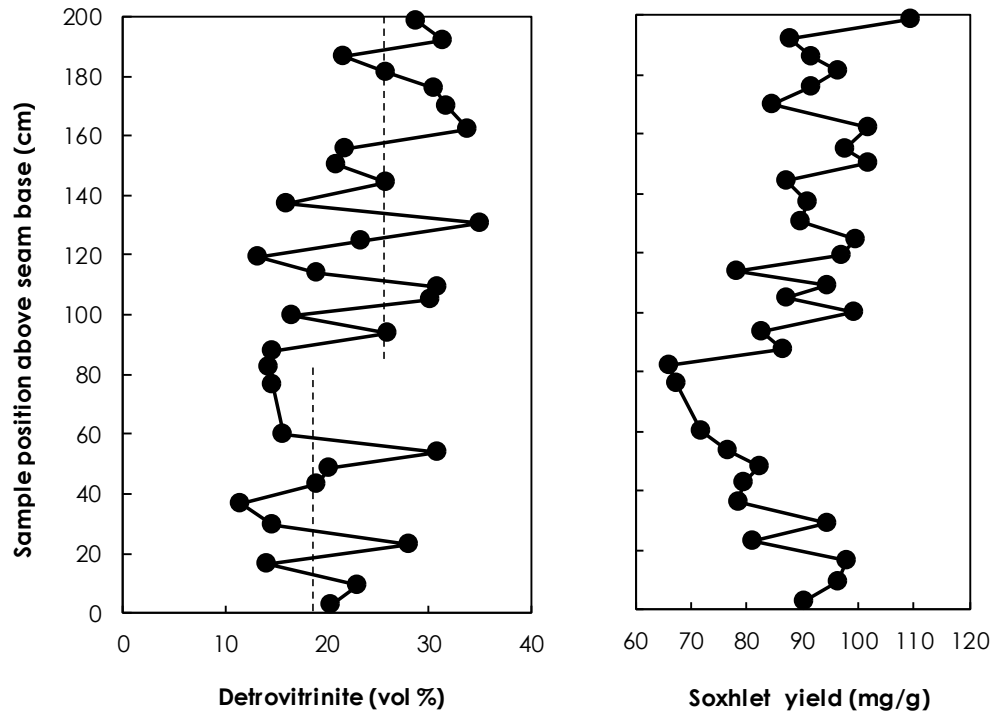


Figure 5.1. Comparing trends of detrovitrinite and Soxhlet yield in the Longyear seam at Bassen. Note: Broken black lines represent mean contents of detrovitrinites in the upper and lower sections of the seam. Higher mean detrovitrinite content increased from 18.6 in the lower seam to 25.4 vol % in upper seam and correlates with increased oil potential from lower to upper seam. This indicates detrovitrinites have significantly contributed to oil-proneness.

The inertinite distribution (Table 5.1.A and 5.1.B) shows the Colesdalen coals are most enriched in inertinites, with average values of 18.6 vol % mmf, compared to the Bassen (5.2 vol % mmf), Lunckefjellet (8.2 vol % mmf) and Breinosa BH4-2009 samples (4.4 vol % mmf), although the Mine 7 samples are also relatively rich in inertinites (14.9 vol % mmf). Inertinite contents for the Bassen, Lunckefjellet and Breinosa BH4-2009 are comparable to documented values (10.3 vol % by Ćmiel and Fabiańska, 2003; and 7.0 vol % by Orheim *et al.*, 2007). The inertinite abundance for the Colesdalen samples could not be compared to existing

reports; however, values indicate that the Colesdalen coals may have been exposed to higher oxidation, dessication or wildfires (Taylor *et al.*, 1998; Scott *et al.*, 2000; Scott, 2000) which may limit their oil potential.

Liptinites are hydrogen rich and precursors of oil and gas (e.g. Boreham and Powell, 1993), and values of 4.1, 4.7, 2.4, 7.7 and 1.9 vol % mmf were measured in Bassen, Lunckefjellet, Breinosa BH4-2009, Mine 7 and Colesdalen respectively. These values are comparable to previous reports (6.6 vol % by Ćmiel and Fabiańska, 2003; 2.4 vol % by Orheim *et al.*, 2007).

The contents and distribution of oil-prone macerals, as well as the general observations during maceral analysis therefore suggest that:

- Oil potential of the CTB coals is particularly due to their enrichment in perhydrous detrovitrinites (Figures 4.1, 5.2, 5.11, 5.17, 5.18 and 5.19).
- Other vitrinitic macerals including but not limited to collotelinite and corpogelinite, in addition to liptinites (Figures 4.1 and 5.17) seem to have contributed to the oil-prone nature of these coals.
- The eastern CTB coals may be more oil-prone than coals from the western parts of the basin.

Macerals	Bassen outcrops						Lunckefjellet BH15-2011					
	No. of samples	Mean (vol %)	Minimum (vol %)	Maximum (vol %)	Median (vol %)	STDEV (vol %)	No. of samples	Mean (vol %)	Minimum (vol %)	Maximum (vol %)	Median (vol %)	STDEV (vol %)
Vitrinite	32	87.4	69.6	95.8	87.4	6.0	19	82.5	59.6	94.8	85.6	9.3
Telinite	32	0.8	0.0	4.4	0.4	1.2	19	0.8	0.0	2.4	0.4	0.8
Collotelinite	32	61.5	40.5	78.0	61.8	8.7	19	54.1	17.2	83.2	53.2	16.4
Collodetrinite	32	20.0	10.0	31.8	19.9	6.5	19	23.6	4.4	42.4	27.6	11.1
Vitrodetrinite	32	2.7	0.4	6.8	2.4	1.6	19	1.7	0.0	7.6	0.2	2.5
Corpogelinite	32	2.5	0.0	7.0	2.0	1.9	19	2.3	0.0	8.8	0.8	3.1
Inertinite	32	4.9	1.4	18.8	4.0	3.3	19	7.9	0.8	31.6	6.0	7.4
Fusinite	32	0.7	0.0	6.8	0.4	1.4	19	1.7	0.0	16.0	0.4	3.7
Semifusinite	32	1.3	0.0	8.4	0.8	1.6	19	3.5	0.0	12.8	2.4	3.7
Funginite	32	1.6	0.4	4.0	1.6	0.9	19	1.9	0.0	5.6	1.2	1.8
Macrinite	32	0.1	0.0	1.6	0.0	0.3	19	0.0	0.0	0.4	0.0	0.1
Micrinite	32	0.2	0.0	1.2	0.0	0.3	19	0.1	0.0	0.4	0.0	0.2
Inertodetrinite	32	0.9	0.0	3.6	0.8	0.8	19	0.7	0.0	2.6	0.0	0.9
Liptinite	32	3.9	0.8	13.2	3.4	2.4	19	9.6	2.8	31.2	8.0	6.6
Sporinite	32	0.7	0.0	2.0	0.8	0.6	19	1.3	0.0	4.4	0.8	1.4
Cutinite	32	0.8	0.0	3.6	0.6	0.8	19	1.3	0.0	3.6	1.2	1.0
Resinite	32	1.3	0.0	7.6	0.8	1.4	19	1.2	0.0	2.4	1.2	0.8
Liptodetrinite	32	1.3	0.0	4.0	1.0	1.0	19	0.7	0.0	2.8	0.4	0.9
Mineral matter	32	3.8	0.0	12.8	3.4	3.2	19	5.0	0.8	29.6	2.4	7.3
GI	32	56.0	4.1	222.0	47.2	49.3	19	42.9	2.1	220.0	18.6	54.7
TPI	32	3.1	1.2	6.1	2.9	1.3	19	4.2	1.1	19.7	1.9	5.2

Table 5.1.A. Maceral distribution of the Longyear coals in Bassen and Lunckefjellet BH15-2011 localities. Data on whole coal basis.

$GI = (Vitrinite + Macrinite) / (Semifusinite + Fusinite + Inertodetrinite)$

$TPI = (Telinite + Collotelinite + Semifusinite + Fusinite) / (Detrovitrinite + Macrinite + Inertodetrinite)$

Macerals	Breinosa BH4-2009						Breinosa Mine 7						Colesdalen BH3-2008					
	No. of samples	Mean	Min	Max	Med	STDEV	No. of samples	Mean	Min	Max	Med	STDEV	No. of samples	Mean	Min	Max	Med	STDEV
Vitrinite	5	78.5	60.8	90.8	77.6	12.0	32	74.5	49.2	86.0	75.6	7.9	7	73.4	53.2	84.2	75.0	10.2
Telinite	5	0.5	0.0	1.6	0.0	0.7	32	ND	ND	ND	ND	ND	7	0.5	0.0	1.2	0.4	0.5
Collotelinite	5	49.5	27.2	68.8	50.4	18.0	32	53.6	19.2	79.6	54.0	14.1	7	58.4	42.4	75.6	57.6	9.7
Collodetrinite	5	24.8	12.4	46.0	21.6	12.6	32	20.9	1.2	49.2	19.4	11.2	7	11.7	7.4	17.6	10.8	3.5
Vitrodetrinite	5	2.9	1.6	4.4	2.8	1.0	32	ND	ND	ND	ND	ND	7	2.5	0.8	6.8	2.4	2.1
Corpogelinite	5	0.8	0.0	2.0	0.8	0.8	32	ND	ND	ND	ND	ND	7	0.3	0.0	1.0	0.0	0.4
Inertinite	5	3.8	1.2	8.0	3.6	2.8	32	14.4	6.0	46.8	12.5	8.2	7	17.2	11.6	26.8	16.4	5.3
Fusinite	5	0.1	0.0	0.4	0.0	0.2	32	3.7	0.0	15.6	2.0	4.4	7	1.9	0.6	5.6	1.2	1.7
Semifusinite	5	1.8	0.0	5.6	1.2	2.2	32	6.2	0.4	44.0	4.2	7.5	7	12.9	7.2	22.4	12.8	5.4
Funginite	5	0.3	0.0	1.2	0.0	0.5	32	2.4	0.0	4.8	2.4	1.2	7	0.1	0.0	0.4	0.0	0.2
Macrinite	5	0.0	0.0	0.0	0.0	0.0	32	0.0	0.0	0.0	0.0	0.0	7	0.1	0.0	0.2	0.0	0.1
Micrinite	5	0.5	0.0	1.6	0.4	0.7	32	0.0	0.0	0.0	0.0	0.0	7	0.0	0.0	0.0	0.0	0.0
Inertodetrinite	5	1.2	0.0	2.0	1.2	0.7	32	2.1	0.0	5.2	1.8	1.5	7	2.3	1.4	3.4	1.8	0.9
Liptinite	5	2.1	0.8	4.4	1.2	1.5	32	7.3	2.4	16.4	6.4	3.8	7	1.7	0.6	3.0	1.8	1.0
Sporinite	5	0.2	0.0	0.4	0.4	0.2	32	4.3	0.0	13.6	3.6	3.4	7	0.6	0.0	1.6	0.6	0.5
Cutinite	5	0.5	0.0	2.0	0.0	0.9	32	2.5	0.4	7.0	2.0	1.6	7	0.3	0.0	0.8	0.4	0.3
Resinite	5	1.0	0.4	1.6	0.8	0.6	32	0.5	0.0	2.8	0.0	0.8	7	0.5	0.0	1.0	0.4	0.4
Liptodetrinite	5	0.4	0.0	0.8	0.4	0.4	32	0.1	0.0	0.8	0.0	0.2	7	0.3	0.0	0.6	0.2	0.2
Mineral matter	5	15.6	3.2	37.2	12.8	13.0	32	3.8	0.4	10.0	3.2	2.5	7	7.6	1.4	34.4	3.0	11.9
GI	5	40.3	9.8	73.7	38.8	23.9	32	10.4	1.1	71.7	7.5	12.1	7	4.6	2.6	7.3	4.6	1.5
TPI	5	2.2	0.6	4.3	2.1	1.4	32	5.2	0.4	39.2	3.1	7.2	7	4.8	3.4	8.6	4.0	1.9

Table 5.1.B. Maceral distribution of the Longyear coals from the Breinosa BH4-2009 and Mine 7 localities, and the Sputnik coals from Colesdalen BH3-2008 locality. Data are in vol % on whole coal basis.

ND = not determined. Min, Max, Med = Minimum, Maximum, Median

GI = (Vitrinite + Macrinite)/(Semifusinite + Fusinite + Inertodetrinite)

TPI = (Telinite + Collotelinite + Semifusinite + Fusinite)/(Detrovitrinite + Macrinite + Inertodetrinite)

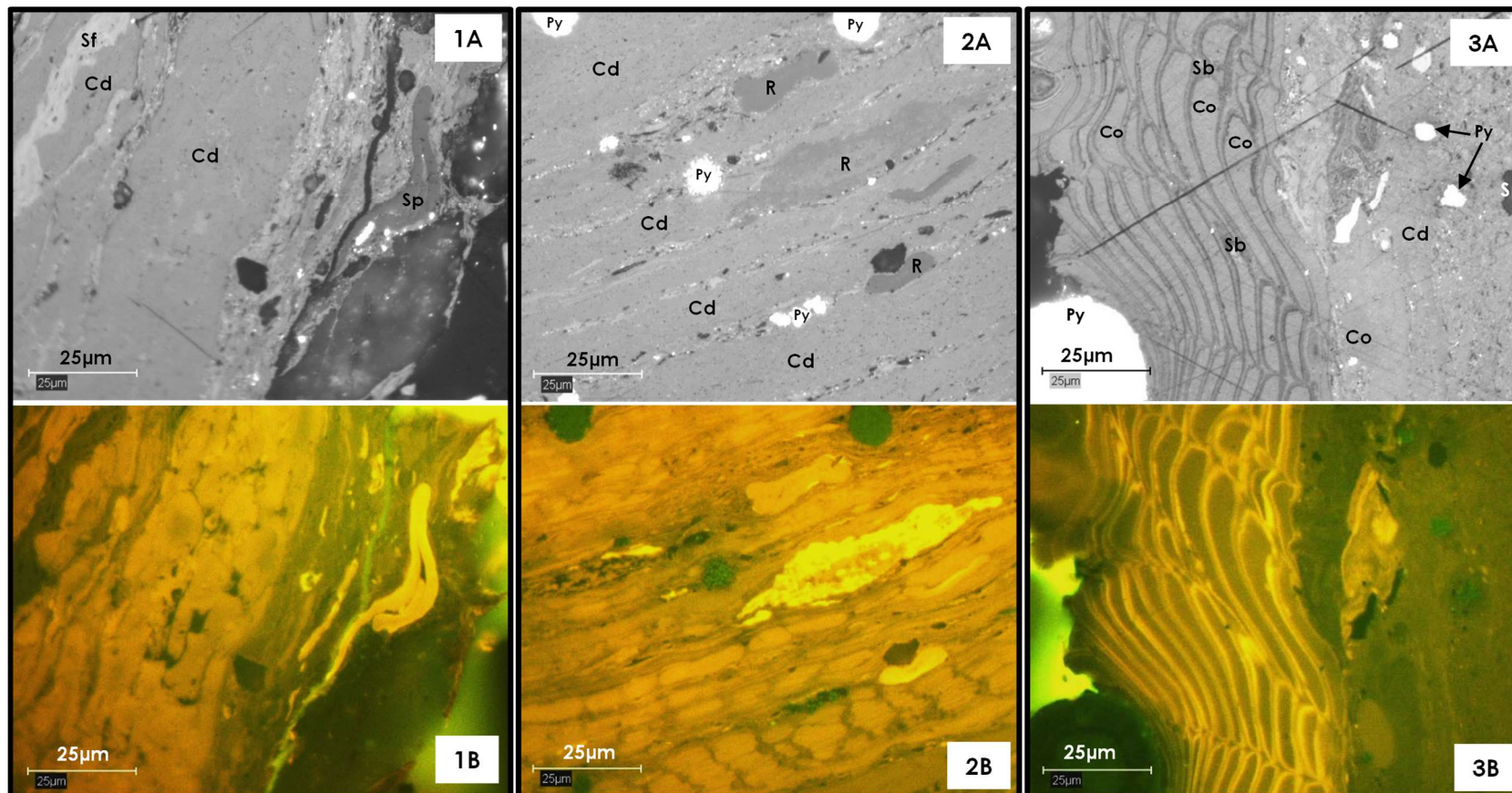


Figure 5.2. Photomicrographs of coals from Breinosa BH4-2009 locality. 1 and 2) Sample Br1, the top 19 cm coal from Askeladden seam. 3) Sample Br16, a Longyear coal 24 cm above seam base. A) Normal light. B) Blue light. Note: enrichment in fluorescing collodetrinite (Cd). Liptinites in addition to other fluorescing vitrinites including but not limited to corpogelinite (Co) appear to have contributed to the oil-prone nature of these coals. In 3, suberinite (Sb) cell walls are typically in-filled with Co. R = resinite, Sf = semifusinite, Sp = sporinite, Py = pyrite.

The Tissue Preservation Index (TPI) is a coal maceral parameter which provides information about the degree of preservation of source materials; higher values indicate higher tree density/oxidation while lower values are associated with greater microbial decomposition. TPI is developed by Diessel (1986) and defined as:

$$\mathbf{TPI} = \frac{\mathbf{Telinite+Collotelinite+Semifusinite+Fusinit}}{\mathbf{Detrovitrinite+Macrinite+Inertodetrinit}} \quad (5.1)$$

The Gelification Index (GI) shows the ratio of macerals formed in wetter conditions (vitrinites) and macerals associated with oxidation/desiccation/wild fires (inertinites) and it is defined as:

$$\mathbf{GI} = \frac{\mathbf{Vitrinite+Macrini}}{\mathbf{Semifusinite+Fusinite+Inertodetrinit}} \quad (5.2)$$

TPI and GI have been deemed unreliable for interpreting peat forming environments (Scott and Glasspool, 2007) for reasons examined below. With regards to TPI, it was argued that many of the macerals used for its calculation may have been blown or washed into the peat-forming environment (Scott *et al.*, 2000; Scott, 2000). From a GI point of view, Scott and Glasspool (2007) while working on modern charcoal assemblages, showed that the proportions of semifusinite, fusinite and inertodetrinite are controlled by a range of factors including fire type, temperature and transport, and concluded that GI may not tell much about the nature of peat forming systems. However; Marshall *et al* (2015a) used TPI versus GI plot to infer that in the CTB, the Svea coals (due to their generally high TPI and low- intermediate GI) formed in a raised-bog environment, whereas the younger coals (Longyear, Svarteper and Askeladden) show generally low TPI and high GI values indicating they formed in a wetter

environment with high levels of decay (i.e. “fen-like” condition). The TPI vs GI analysis of Marshall *et al.* (2015a) agrees with the geochemical assessments in their study as the Longyear, Svarteper and Askeladden coals show significantly greater oil potential compared to the Svea coals (Table 5.2). Also, estimated retorting yields are in the range of 170 - 190 mg/g for the Longyear, Svarteper and Askeladden coals, while 24 mg/g is estimated for the Svea coals (Marshall *et al.*, 2015a). Therefore, TPI and GI analysis is considered reliable for the CTB coals and thus applied in this study.

Seam	HI (mg HC/g TOC)			Accelerated solvent extraction (mg/g)			TOC (%)		
	No. of samples	Mean	STDEV	No. of samples	Mean	STDEV	No. of samples	Mean	STDEV
Svea	5	215	25.6	5	35.8	23.4	5	81.9	0.8
Longyear	7	340	30.6	20	47.5	20.3	20	81	1.7
Svarteper	3	283	11.3	6	78.5	25	6	76.2	3.2
Askeladden	2	266	48.1	4	74.3	9.1	4	76	2.2

Table 5.2. Geochemical data from Marshall *et al.* (2015a) which compares oil potential between the Svea, Longyear, Svarteper and Askeladden coals. Note: The Svea coals display lowest oil potential despite having the highest TOC content.

The TPI vs GI plot of the Longyear and Sputnik coals under study (Figure 5.3) is believed to indicate how oil potential would vary between the four main areas under study. The eastern CTB coals (Bassen, Lunckefjellet, and Breinosa), due to their generally low TPI and high GI values, would show greatest oil potential. Conversely, coals from the western parts of the basin in Colesdalen would show lowest oil potential by virtue of their relatively lower GI even though they show low TPI values. This observation is consistent with greater VR suppression observed within the eastern CTB coals (Chapter 4), although this may also be maturity related.

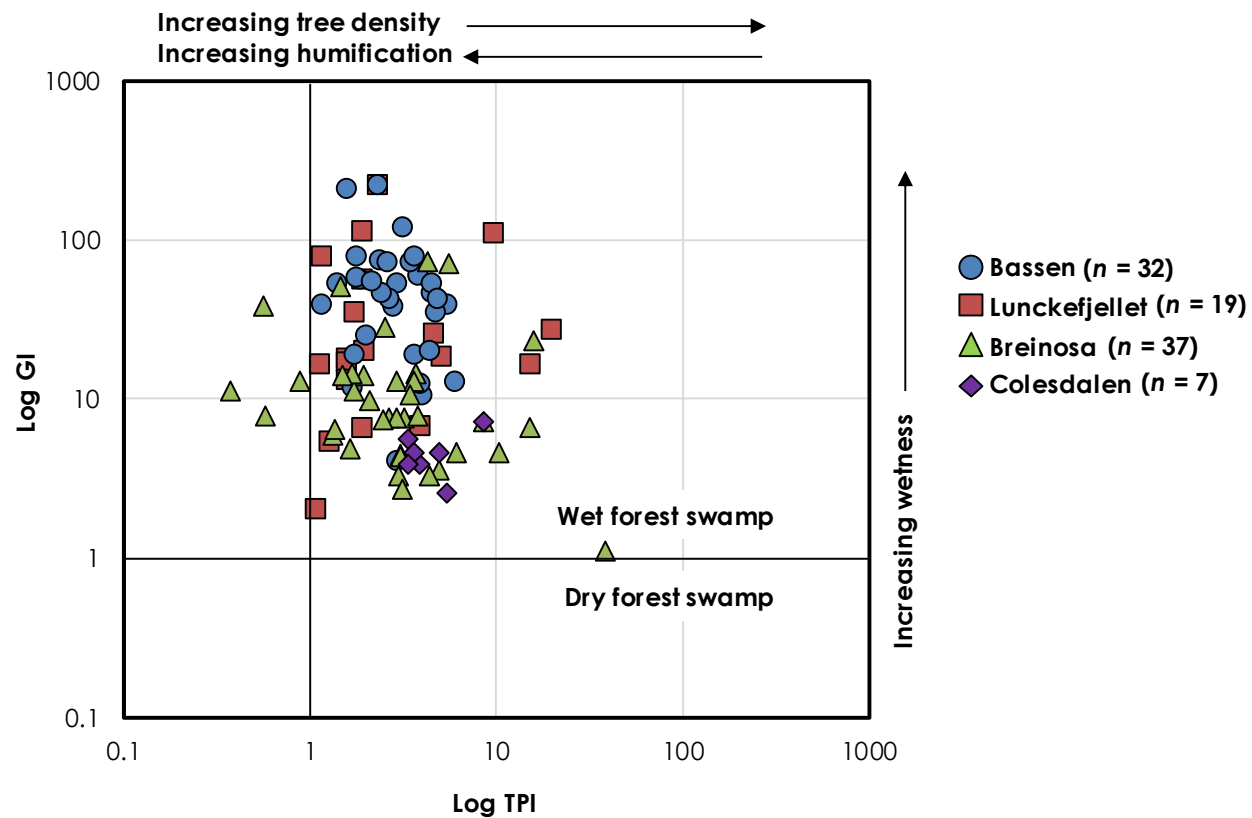


Figure 5.3. Coal facies plot of the Longyear coals from Bassen, Lunckefjellet and Breinosa, and the Sputnik coals from Colesdalen (after Casareo *et al.*, 1996). Note: The Lunckefjellet coals show relatively low TPI and high GI values which suggest greatest oil potential. (Bassen = outcrop samples, Lunckefjellet = BH15-2011, Breinosa = BH4-2009 + Mine 7 samples, Colesdalen = Synndalen BH3-2008 samples)

5.2.1.2. Peatland Environment and Oil Potential - Longyear vs Svarteper Seam

As the upper Longyear coals experienced similar hydrological conditions to the Svarteper coals (Marshall, 2013), one might expect both seams to display similar range of oil potential. The Lunckefjellet BH15-2011 samples present a good opportunity for this analysis, and for the purpose of clarity, the adopted approach involves sub-dividing the coals as follows:

- The Svarteper seam
- The Upper Longyear seam (100 – 220 cm from seam base)
- The Lower Longyear seam (0 – 90 cm from seam base)

Table 5.3 shows the maceral distribution of the Svarteper, the Upper Longyear, and Lower Longyear coals respectively in Lunckefjellet BH15-2011. The Svarteper coals show vitrinite contents of 83.6 vol % mmf, while the upper and lower Longyear coals show 87.4 and 86.6 vol % mmf respectively (Table 5.3)

The inertinite content is much lower within the Svarteper seam which contains 4.4 vol % mmf, compared to 8.3 and 8.2 vol % mmf in the Upper and Lower Longyear seam respectively. This is a clear indication of greater oxidation/desiccation/wild fire (Diessel and Gammidge, 1998 and references therein) within the Longyear peatland.

In terms of the oil prone macerals, liptinites are highest within the Svarteper coals (12 vol % mmf) compared to the Upper and Lower Longyear coals showing values of 4.3 and 5.2 vol % mmf respectively. Also, detrovitrinites are highest within the Svarteper coals (31.0 vol % mmf), with slightly lower value in the Upper Longyear (29.2 vol % mmf) and much lower value within the Lower Longyear coals (23.6 vol % mmf).

TPI and GI are also assessed. TPI values decrease from the Lower Longyear (6.2) to the Upper Longyear (2.4) and the Svarteper coals (3.1), which indicates greater microbial decomposition (e.g. Diessel and Gammidge, 1998) within the Upper Longyear and Svarteper peatlands, and thus leading to higher detrovitrinite content and likely greater oil potential. GI values decrease from the lower Longyear (52.9) to the Upper Longyear (33.9) but are highest for the Svarteper coals (61), which indicate wetter conditions within the Svarteper peatland. Whilst the higher GI values observed in the Lower Longyear, compared to the Upper Longyear may suggest wetter conditions within the Lower Longyear peatland (e.g. Casareo *et al.*, 1996), the bigger and more closely spaced (relatively) inertinite peaks in the Lower Longyear (Figure 5.4) suggest that relatively drier spells (e.g. Taylor *et al.*, 1998) may have occurred more frequently during the depositing of the Lower Longyear peatland. Thus, the Longyear peatland can be described to have changed from “raised-bog” conditions in the lower peatland, to “fen-like” conditions in the upper peatland, while the Svarteper peatland experienced predominantly “fen” conditions. This is consistent with reports by Marshall *et al.* (2015a), and implies that groundwater supply was generally more stable within the Svarteper peatland leading to predominantly wetter conditions and possibly greater oil potential. Comparing the trends of TPI and Soxhlet yield from base to top of the Longyear seam at Lunckefjellet BH15-2011 locality shows that lower TPI values correlate with greater Soxhlet yields within the upper Longyear seam (Figure 5.5). This clearly displays the positive link between oil-potential and fen condition within the Upper Longyear and younger peatlands in the CTB. The influence of groundwater is further examined in Chapter 6.

Macerals	Svarteper coals, Lunckefjellet BH15-2011						Upper Longyear (100 - 210 cm) Lunckefjellet BH15-2011						Lower Longyear (0 - 90 cm) Lunckefjellet BH15-2011					
	No. of samples	Mean	Min	Max	Med	STDEV	No. of samples	Mean	Min	Max	Med	STDEV	No. of samples	Mean	Min	Max	Med	STDEV
Vitrinite	8	65.4	48.0	74.8	65.6	8.3	10	83.8	73.2	94.8	85.5	7.4	9	81.1	59.6	90.8	86.0	11.4
Telinite	8	ND	ND	ND	ND	ND	10	1.2	0.2	2.4	1.2	0.9	9	0.3	0.0	0.8	0.4	0.3
Collotelinite	8	40.0	10.0	61.2	43.2	18.8	10	51.2	36.2	70.0	50.8	9.7	9	57.3	17.2	83.2	58.4	21.9
Collodetrinite	8	25.4	6.8	58.0	13.0	20.7	10	26.5	12.0	34.4	30.2	8.7	9	20.4	4.4	42.4	24.4	13.1
Vitrodetrinite	8	ND	ND	ND	ND	ND	10	1.7	0.0	6.4	0.2	2.3	9	1.8	0.0	7.6	0.0	2.9
Corpogelinite	8	ND	ND	ND	ND	ND	10	3.2	0.0	8.8	1.5	3.6	9	1.3	0.0	6.4	0.0	2.2
Inertinite	8	3.6	0.8	6.0	4.0	2.1	10	8.0	2.4	15.2	8.1	4.5	9	7.9	0.8	31.6	3.6	10.0
Fusinite	8	0.5	0.0	1.6	0.2	0.6	10	1.1	0.0	4.8	0.4	1.5	9	2.4	0.0	16.0	0.4	5.2
Semifusinite	8	1.2	0.0	2.4	1.0	0.9	10	3.0	0.0	10.2	2.2	3.2	9	4.0	0.0	12.8	2.8	4.4
Funginite	8	1.5	0.4	3.2	1.2	1.0	10	2.7	0.8	5.6	2.2	1.8	9	1.0	0.0	4.0	0.4	1.4
Macrinite	8	0.0	0.0	0.0	0.0	0.0	10	0.0	0.0	0.4	0.0	0.1	9	0.0	0.0	0.0	0.0	0.0
Micrinite	8	0.0	0.0	0.0	0.0	0.0	10	0.1	0.0	0.4	0.0	0.2	9	0.1	0.0	0.4	0.0	0.2
Inertodetrinite	8	0.4	0.0	1.6	0.0	0.7	10	1.0	0.0	2.6	0.8	1.1	9	0.4	0.0	1.6	0.0	0.7
Liptinite	8	9.4	4.8	17.2	8.6	3.9	10	8.2	2.8	22.3	6.8	5.6	9	11.0	7.2	31.2	8.8	7.6
Sporinite	8	4.5	2.8	6.8	3.8	1.7	10	1.3	0.0	4.4	0.8	1.4	9	1.3	0.0	4.4	0.8	1.5
Cutinite	8	4.7	0.0	10.8	4.6	3.9	10	1.0	0.0	2.4	0.9	0.7	9	1.7	0.0	3.6	1.6	1.1
Resinite	8	0.0	0.0	0.0	0.0	0.0	10	1.2	0.0	2.4	1.6	0.9	9	1.2	0.4	2.4	0.8	0.8
Liptodetrinite	8	0.3	0.0	0.8	0.2	0.3	10	0.7	0.0	2.0	0.6	0.7	9	0.8	0.0	2.8	0.0	1.1
Mineral matter	8	21.7	10.8	43.6	20.0	10.5	10	4.1	0.8	19.5	1.8	5.7	9	6.0	0.8	29.6	2.4	9.0
GI	8	61.0	17.6	170.0	27.1	57.0	10	33.9	5.5	115.3	18.4	35.4	9	52.9	2.1	220.0	20.4	71.4
TPI	8	3.1	0.2	8.4	3.5	2.7	10	2.4	1.1	5.1	1.7	1.5	9	6.2	1.1	19.7	2.0	7.0

Table 5.3. Comparing the maceral distribution of the Svarteper coals, the Upper Longyear (100 – 210 cm from seam base) coals and the Lower Longyear coals (0 – 90 cm above seam base) in Lunckefjellet BH15-2011 locality. Data are in vol % on whole coal basis. Min, Max, Med = Minimum, Maximum and Median respectively. ND = not determined

$GI = (Vitrinite + Macrinite) / (Semifusinite + Fusinite + Inertodetrinite)$

$TPI = (Telinite + Collotelinite + Semifusinite + Fusinite) / (Detrovitrinite + Macrinite + Inertodetrinite)$

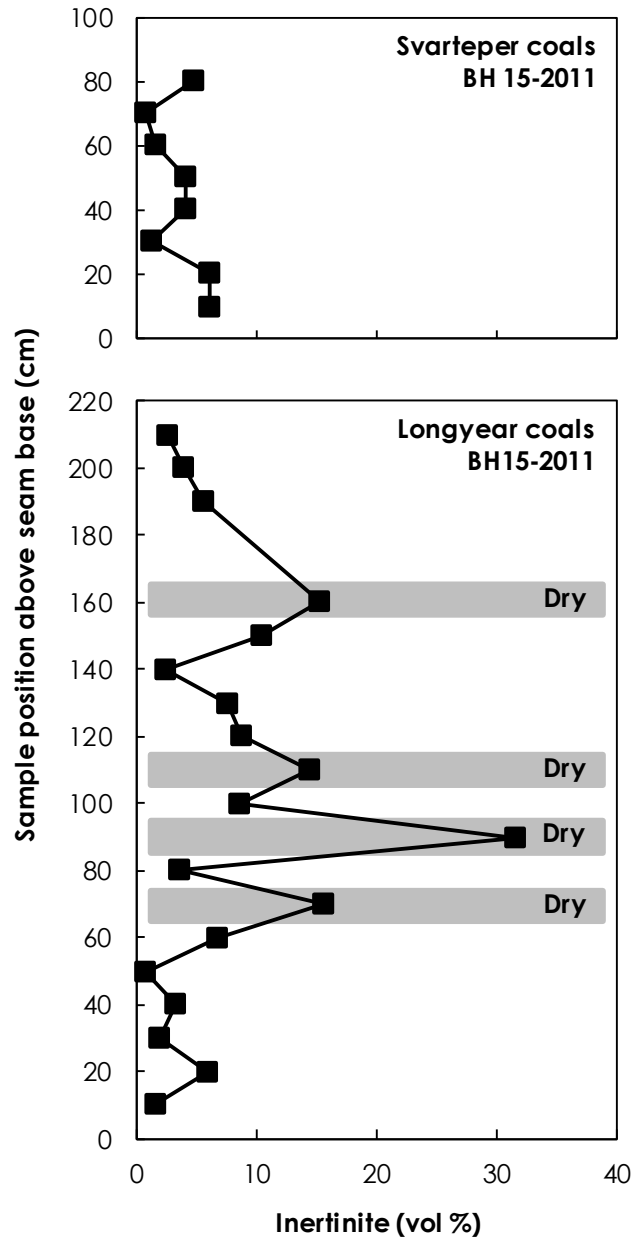


Figure 5.4. The inertinite profile of the Svarteper and Longyear seams at Lunckefjellet BH15-2011 locality. Note: The Longyear seam shows higher inertinite contents with peaks indicative of much drier periods and/or fire frequency during peat deposition.

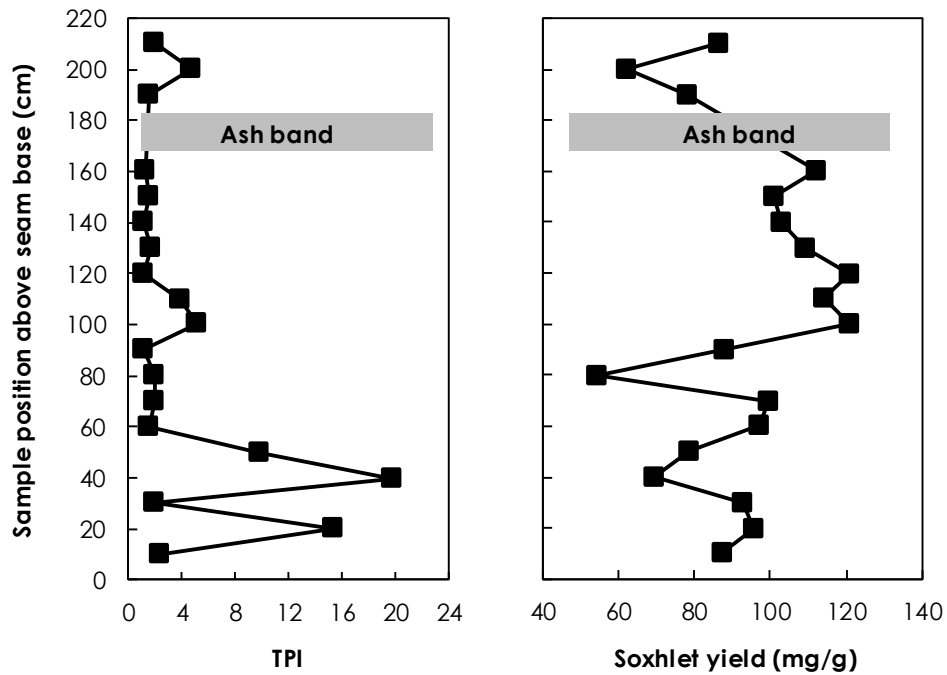


Figure 5.5. Comparing TPI and Soxhlet yield (dwc) from base to top of the Longyear seam in Lunckefjellet BH15-2011 locality. Note: Lower TPI in upper seam correlates with greater oil potential.

5.2.2. Rock-Eval 6 Analysis - Kerogen Typing and Source Rock Potential

A method for indicating kerogen type is the van Krevelen plot (Oxygen Index - OI vs Hydrogen Index - HI). HI and OI are Rock-Eval pyrolysis parameters defined as follows (Peters, 1986 and references within);

$HI = (S2 * 100) / TOC$ – expressed in mg HC/g TOC, and TOC is the total organic matter. $OI = (S3 * 100) / TOC$ – expressed as mg CO₂/g TOC.

Additional notes on these parameters is detailed in Section 3.2.2.2.

The van Krevelen plot shows that all the Breinosa, Colesdalen and bulk of the Lunckefjellet samples are enriched in Type II kerogen, while a few Lunckefjellet samples, and all the Bassen samples contain a mixture of Types II and III kerogens, with the Bassen samples plotting closest to the Type III line (Figure 5.6). HI values are higher than expected for typical type III kerogen and indicates enrichment in

paraffinic hydrocarbons (Killops *et al.*, 1998) possibly due to the presence of long-chain aliphatics in the coal structure (e.g. Petersen and Nytoft, 2006; Petersen *et al.*, 2009). According to Petersen (2005); HI values <150 mg HC/g TOC are mainly gas prone, while values >150 mg HC/g TOC is indicative of oil potential for coals; hence the Askeladden, Svarteper, Longyear, Verkny and Sputnik coal seams may have significant oil potential (Figure 5.6; Tables 5.4 and 5.5). Comparing coal seams, HI values appears to be in the order of Askeladden>Svarteper>Longyear>Svea in the eastern CTB, and Verkny>Sputnik in the western CTB, which indicates oil potential increases from the stratigraphically older to younger Firkanten Fm. coals.

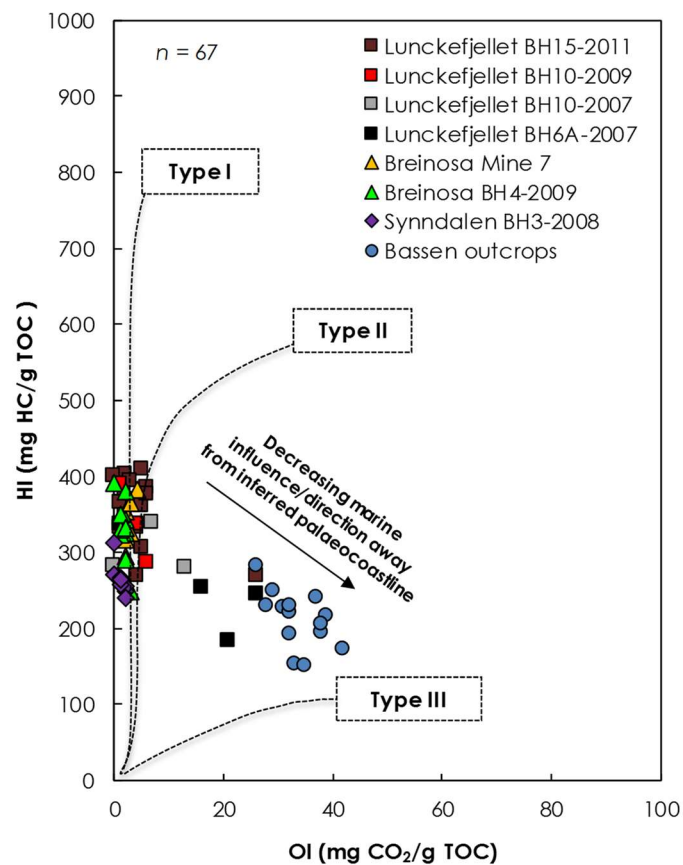


Figure 5.6. van Krevelen plot of 67 coals from the Askeladden, Svarteper, Longyear, Verkny and Sputnik seams from the four main areas under investigation. Note: HI >150 mg HC/g TOC is indicative of oil potential (Petersen, 2005). Trend of decreasing HI and increasing OI is towards the eastern/north-eastern basin margin and away from the inferred palaeocoastline of Marshall (2013). Colesdalen represented by Synndalen BH3-2008.

The total organic carbon (TOC) contents are high (44.5 – 89.8 %), and the S2 contents (i.e. the amount of hydrocarbons produced from the cracking of heavy hydrocarbons and from the thermal breakdown of kerogen) are also high (109 – 368 mg/g) (Tables 5.4 and 5.5). A graph of TOC vs S2 (Figure 5.7) shows that 32 samples (i.e. all the Bassen samples, bulk of the Colesdalen samples and a few of the Lunckefjellet and Breinosa samples) plot between the HI lines of 150 - 300 mg HC/g TOC, while 35 samples (i.e. most of the Lunckefjellet and Breinosa samples) plot between the HI lines of 300 - 600 mg HC/g TOC, which indicates excellent potential for oil generation.

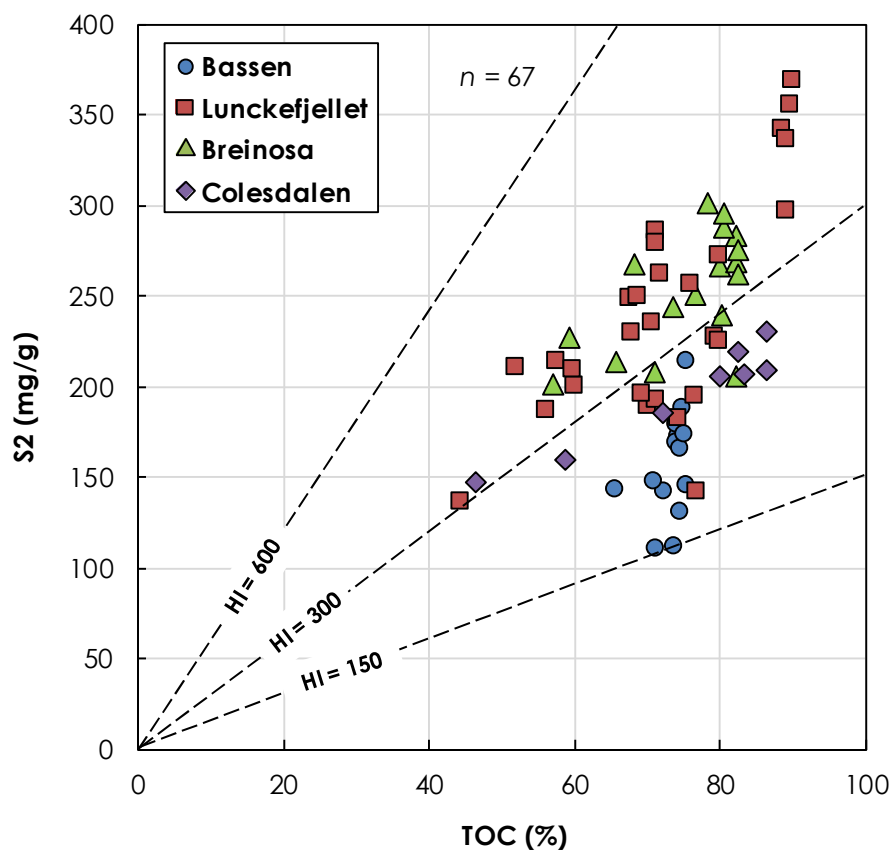


Figure 5.7. TOC vs S2 plot of 67 coals from the Askeladden, Svarteper, Longyear, Verkny and Sputnik seams from the four main areas under investigation.

Sample ID	Area	Location and sample type	Seam	Drill depth (m)	Sample position above seam base (cm)	S1 (mg/g)	S2 (mg/g)	S3 (mg/g)	TOC (%)	T _{max} (°C)	HI	OI	BI	QI	PI
Br1	Breinosa	BH4-2009	Askeladden	298.4	46.5	17.8	267.5	0.1	68.1	447	393	0	26.1	418.9	0.06
Br8	Breinosa	BH4-2009	Svarteper	301.2	11.5	15.8	226.1	0.9	59.3	437	381	2	26.6	407.9	0.07
Br9	Breinosa	BH4-2009	Unknown	313.8	24	11.3	250.3	1.6	76.6	442	327	2	14.8	341.5	0.04
Br11	Breinosa	BH4-2009	Longyear	314.7	116	13.3	212.5	0.6	65.7	444	324	1	20.2	343.7	0.06
Br12	Breinosa	BH4-2009	Longyear	314.9	95.5	19.9	282.3	1.8	82.2	447	343	2	24.2	367.6	0.07
Br13	Breinosa	BH4-2009	Longyear	315.2	75.5	15.6	207.6	1.4	71	439	292	2	22.0	314.4	0.07
Br16	Breinosa	BH4-2009	Longyear	315.7	24	13.1	243.3	0.8	73.5	442	331	1	17.8	348.8	0.05
Br17	Breinosa	BH4-2009	Longyear	315.8	8	10.8	200.3	0.5	57.1	442	351	1	18.9	369.7	0.05
Br20	Breinosa	BH5-2009	Svarteper	-	93.5	25.8	265.5	1.7	80	437	332	2	32.3	364.1	0.09
Br22	Breinosa	BH5-2009	Svea	-	50	10.6	204.7	2.5	82	447	250	3	12.9	262.6	0.05
Br26	Breinosa	Mine 7 section	Longyear	-	142.5	16.8	300.1	3.5	78.2	433	383	4	21.5	405.2	0.05
Br27	Breinosa	Mine 7 section	Longyear	-	135.5	15.9	287.3	2.1	80.5	434	356	2	19.8	376.6	0.05
Br28	Breinosa	Mine 7 section	Longyear	-	117.5	17	295.3	2.6	80.5	437	366	3	21.1	388.0	0.05
Br32	Breinosa	Mine 7 section	Longyear	-	83	15.8	268	2.5	82	441	326	3	19.3	346.1	0.06
Br34	Breinosa	Mine 7 section	Longyear	-	66	13.1	275	1.8	82.5	446	334	2	15.9	349.2	0.05
Br39	Breinosa	Mine 7 section	Longyear	-	29	10.7	261.5	2.1	82.5	446	317	2	13.0	329.9	0.04
Br42	Breinosa	Mine 7 section	Longyear	-	7	12.1	238.3	2.3	80.1	441	296	2	15.1	312.6	0.05
Ba1	Bassen	Outcrop section	Longyear	-	198.5	11	212.6	19.4	75.4	429	282	26	14.6	296.6	0.05
Ba3	Bassen	Outcrop section	Longyear	-	186.5	7.9	171.3	21	74.2	429	231	28	10.6	241.5	0.04
Ba6	Bassen	Outcrop section	Longyear	-	170	8.6	186.7	22	74.8	430	250	29	11.5	261.1	0.04
Ba9	Bassen	Outcrop section	Longyear	-	150.5	6	168.5	23.1	73.9	431	228	31	8.1	236.1	0.03
Ba11	Bassen	Outcrop section	Longyear	-	137.5	5	140.6	27.6	72.4	433	194	38	6.9	201.1	0.03
Ba14	Bassen	Outcrop section	Longyear	-	119.3	5.1	141.9	25.3	65.5	426	217	39	7.8	224.4	0.03
Ba16	Bassen	Outcrop section	Longyear	-	109	7.7	178	27.3	74	428	240	37	10.4	250.9	0.04
Ba19	Bassen	Outcrop section	Longyear	-	94	5.7	146.4	27.2	71	437	206	38	8.0	214.2	0.04
Ba21	Bassen	Outcrop section	Longyear	-	82.3	3.9	109.1	23.3	71.3	425	153	33	5.5	158.5	0.03
Ba24	Bassen	Outcrop section	Longyear	-	54	5.8	129.6	31.3	74.7	425	174	42	7.8	181.3	0.04
Ba27	Bassen	Outcrop section	Longyear	-	36.5	5.6	110.8	26	73.6	430	151	35	7.6	158.2	0.05
Ba29	Bassen	Outcrop section	Longyear	-	23	7	165.1	24	74.6	429	221	32	9.4	230.7	0.04
Ba30	Bassen	Outcrop section	Longyear	-	16.5	8.7	172.2	24.3	75	430	230	32	11.6	241.2	0.05
Ba32	Bassen	Outcrop section	Longyear	-	3	7.5	144.9	24.4	75.3	432	192	32	10.0	202.4	0.05

Table 5.4. Rock-Eval data of the Bassen and Breinosa areas in the Adventdalen sub-region of the CTB

HI (Hydrogen Index) in mg HC/g TOC. OI (Oxygen Index) in mg CO₂/g TOC, values of zero suggests measurements are perhaps too low to be determined. BI (Bitumen Index) = (S1*100)/TOC in mg HC/g TOC (Killops et al. 1998). QI (Quality Index) = [(S1+S2)*100]/TOC in mg HC/g TOC (Pepper and Corvi, 1995a). PI (Production Index) = S1/(S1+S2)

Sample ID	Area	Location and sample type	Seam	Drill depth (m)	Sample position above seam base (cm)	S1 (mg/g)	S2 (mg/g)	S3 (mg/g)	TOC (%)	T _{max} (°C)	HI	OI	BI	QI	PI
L1	Lunckefjellet	BH15-2011	Svarteper	246	80	12.4	212.9	0.9	57.6	437	370	2	21.5	391.1	0.06
L3	Lunckefjellet	BH15-2011	Svarteper	246.2	60	13.5	200	0.8	60.1	434	333	1	22.5	355.2	0.06
L4	Lunckefjellet	BH15-2011	Svarteper	246.3	50	12.4	209.1	0.9	51.9	435	403	2	23.9	426.8	0.06
L5	Lunckefjellet	BH15-2011	Svarteper	246.4	40	9.9	284.7	0.3	71.1	439	400	0	13.9	414.3	0.03
L7	Lunckefjellet	BH15-2011	Svarteper	246.6	20	12.5	248.2	0.5	67.7	431	367	1	18.5	385.1	0.05
L8	Lunckefjellet	BH15-2011	Svarteper	246.7	10	11.8	185.7	1.3	56.2	436	330	2	21.0	351.4	0.06
L9	Lunckefjellet	BH15-2011	Longyear	258.3	210	6.5	188.5	18.3	70	432	269	26	9.3	278.6	0.03
L11	Lunckefjellet	BH15-2011	Longyear	258.5	190	8.2	192	3.1	71.2	431	270	4	11.5	281.2	0.04
L12	Lunckefjellet	BH15-2011	Longyear	258.8	160	11.2	261.7	2.6	71.7	439	365	4	15.6	380.6	0.04
L14	Lunckefjellet	BH15-2011	Longyear	259	140	8.2	249.2	3.2	68.8	439	362	5	11.9	374.1	0.03
L16	Lunckefjellet	BH15-2011	Longyear	259.2	120	16.6	368.4	4.7	89.8	431	410	5	18.5	428.7	0.04
L18	Lunckefjellet	BH15-2011	Longyear	259.4	100	14.3	354.5	3	89.7	432	395	3	15.9	411.1	0.04
L20	Lunckefjellet	BH15-2011	Longyear	259.6	80	4.6	136	2	44.5	432	306	5	10.3	316.0	0.03
L22	Lunckefjellet	BH15-2011	Longyear	259.8	60	9.2	296.3	2.9	89.1	432	333	3	10.3	342.9	0.03
L24	Lunckefjellet	BH15-2011	Longyear	260	40	5.4	234.8	3	70.6	431	333	4	7.6	340.2	0.02
L25	Lunckefjellet	BH15-2011	Longyear	260.1	30	10.1	340.7	5.3	88.5	432	385	6	11.4	396.4	0.03
L27	Lunckefjellet	BH15-2011	Longyear	260.3	10	9.7	335.7	5.2	89.1	434	377	6	10.9	387.7	0.03
L32	Lunckefjellet	BH10-2009	Svarteper	55.14	10.5	20.5	277.8	0.9	71.2	436	390	1	28.8	419.0	0.07
L33	Lunckefjellet	BH10-2009	Longyear	69.71	79	13.2	228.3	2.8	67.8	435	337	4	19.5	356.2	0.05
L36	Lunckefjellet	BH10-2009	Longyear	70.4	10.5	13.2	226.9	4.5	79.4	435	286	6	16.6	302.4	0.05
L38	Lunckefjellet	BH10-2007	Svarteper	237.03	20.5	17.8	208.5	1	59.8	435	348	2	29.8	378.4	0.08
L39	Lunckefjellet	BH10-2007	Longyear	247.06	148.5	15.6	271.8	5.6	79.9	432	340	7	19.5	359.7	0.05
L41	Lunckefjellet	BH10-2007	Longyear	247.56	98.5	13.7	224.6	10.3	80	435	281	13	17.1	297.9	0.06
L44	Lunckefjellet	BH10-2007	Longyear	248.45	9.5	12.4	195	0.1	69.2	434	282	0	17.9	299.7	0.06
L45	Lunckefjellet	BH6A-2007	Svarteper	210.36	4.8	22.4	256.1	0.9	76	434	337	1	29.5	366.4	0.08
L48	Lunckefjellet	BH6A-2007	Longyear	223.03	1	8.7	182	19.1	74.4	432	245	26	11.7	256.3	0.05
L51	Lunckefjellet	BH6A-2007	Longyear	223.78	0.5	9	194.1	12	76.5	433	254	16	11.8	265.5	0.04
L54	Lunckefjellet	BH6A-2007	Longyear	224.53	0.9	6.5	141.1	16.1	76.7	435	184	21	8.5	192.4	0.04
S1	Svea Nord	Svea Nord	Svea	-	183	25.7	174	1.7	81.4	443	214	2	31.6	245.3	0.13
S2	Svea Nord	Svea Nord	Svea	-	127	6.4	143	1.6	81.2	448	176	2	7.9	184.0	0.04
S3	Svea Nord	Svea Nord	Svea	-	83	7.5	153.5	1.8	82	447	185	2	9.1	196.3	0.05
S4	Svea Nord	Svea Nord	Svea	-	81.5	8.3	128.6	2.6	82.5	442	155	3	10.1	165.9	0.06
S5	Svea Nord	Svea Nord	Svea	-	7	15	256	5.5	82	444	311	7	18.3	330.5	0.06
C1	Colesdalen	BH3-2008	Verkny	258.18	16	9.7	146.3	0	46.5	437	314	0	20.9	335.5	0.06
C2	Colesdalen	BH3-2008	Sputnik	274.13	172.5	15	206.8	2	83.1	442	249	2	18.1	266.9	0.07
C3	Colesdalen	BH3-2008	Sputnik	274.38	147.5	13.2	204.9	1.4	80	443	256	2	16.5	272.6	0.06
C4	Colesdalen	BH3-2008	Sputnik	274.63	122.5	12.4	185.4	0.8	72	443	258	1	17.2	274.7	0.06
C6	Colesdalen	BH3-2008	Sputnik	275.05	80.5	12.8	159.2	0.1	58.7	440	271	0	21.8	293.0	0.07
C7	Colesdalen	BH3-2008	Sputnik	275.28	57.5	18.4	208.4	1.6	86.2	443	242	2	21.3	263.1	0.08
C8	Colesdalen	BH3-2008	Sputnik	275.51	34.5	19	230.3	1.2	86.3	442	267	1	22.0	288.9	0.08
C9	Colesdalen	BH3-2008	Sputnik	275.74	11.5	15.7	218.2	1.1	82.3	445	265	1	19.1	284.2	0.07

Table 5.5. Rock-Eval data of the Lunckefjellet, Svea Nord and Colesdalen areas of the CTB

HI (Hydrogen Index) in mg HC/g TOC. OI (Oxygen Index) in mg CO₂/g TOC, values of zero suggests measurements are perhaps too low to be determined. BI (Bitumen Index) = (S1*100)/TOC in mg HC/g TOC (Killops et al. 1998). QI (Quality Index) = [(S1+S2)*100]/TOC in mg HC/g TOC (Pepper and Corvi, 1995a). PI (Production Index) = S1/(S1+S2)

The S1 (i.e. the quantity of already generated hydrocarbons) range between 3.9 – 25.8 mg/g in all samples (Tables 5.4 and 5.5); mean S1 values are 6.8, 11.8, 15.0 and 14.5 mg/g for the Bassen, Lunckefjellet, Breinosa and Colesdalen samples respectively, and reflects the maturity trend across these four localities (i.e. increasing maturity from Bassen, through Lunckefjellet and Breinosa to Colesdalen) as inferred in Chapter 4.

The coals under investigation show a trend of decreasing HI and increasing OI in the north-eastern direction of the CTB (Figure 5.6); this trend is consistent with the direction towards the eastern basin margin. Hydrogen enrichment is related to the activity of sulphate-reducing bacteria, and is commonly associated with increased contents of sulphur (Petersen, 2005 and references within); hence decreasing HI away from palaeocoast is as a result of decreasing marine sulphur deposition. In terms of increasing OI towards basin margins, it is believed to be associated with increasing shallowness of water in the peatland. Increasing water shallowness will lead to increasing oxicity which favours aerobic degradation (Peters and Moldowan, 1993); consequently, OI increases towards basin margin. The alkane source/depositional parameters were examined to further assess increasing OI towards basin margins. Pristane/phytane ratio generally increases from marine to terrestrial deposition (Peter and Moldowan, 1993) and it is recommended that Pr/Ph ratios >3.0 be interpreted as oxic to suboxic depositional conditions with terrigenous plant input (Peters *et al.*, 2005). Also, Pr/Ph values of 3.0 and higher are common in coals (Tissot and Welte, 1984). George *et al.* (1994) while working on the marine influenced Greta coals seam in Sydney basin, attributed Pr/Ph values of 4.6 – 5.3 to varying contributions from marine and terrestrially derived organic matter, and values of 7.2 – 9.0 were associated with oxic environments in peat swamps. Within the Longyear and Sputnik coals, Pr/Ph

ratio generally increase towards the eastern basin margins from 5.2 in Colesdalen, to 12.0 in Bassen (Figure 5.8). This suggests that the deposition of the Longyear and Sputnik coals varied in oxicity which increases from Colesdalen (basin center) towards the north-eastern basin margin (Bassen) as deposition became increasingly terrestrial. It is however noted that weathering of the coals may have played a part in increasing OI and will be examined in Chapter 6.

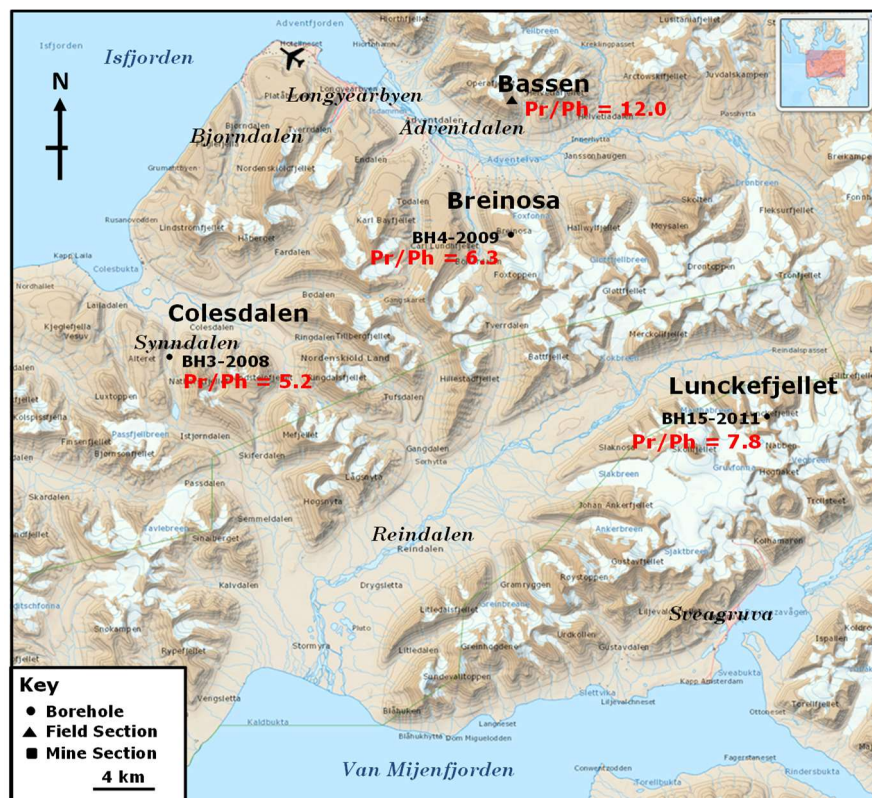


Figure 5.8. Map showing variation in the mean Pr/Ph values across the CTB. Note: values increase from basin center (Colesdalen) towards the eastern and north-eastern basin margin indicating increasing terrestrial deposition.

5.2.2.1. Multiple S₂ Peaks and T_{max} Shift

Multiple and complex minor S₂ peaks with slightly different T_{max} values were observed in the Rock-Eval 6 pyrolysis graphic (Figures 5.9.A, 5.9.B and 5.9.C). It is well documented that T_{max} is affected by the type of organic matter because of variation in the thermal energy required to break the different types of bonds

present (e.g. Peters, 1986; Peters *et al.*, 2005). Given that this study is dealing with perhydrous coals, such complex S2 peaks probably reflects a source rock with more than one hydrocarbon generating kerogen, and in the samples analysed in this study, the kerogens/macerals are liptinitic and vitrinitic as shown by the van Krevelen plot (Figure 5.6) and microscope examination (Figures 4.1, 5.2, 5.17 and 5.18). Type II kerogens (liptinites) are more labile (i.e. more oil-prone) than Type III kerogens (vitrinites). This can be clearly observed in Py-GCMS pyrograms in general as those of Type II kerogens contain *n*-alkane/*n*-alkene distribution centred on carbon numbers below C₂₀, whereas those of Type III are richer in *n*-alkanes and *n*-alkenes in the C₂₀ - C₃₀ range (e.g. Taylor *et al.*, 1998). Thus, where organic matter is enriched with a mixed Type II and III, hydrocarbons from each source would be released at slightly different stages (with Type II materials released first), leading to multiple S2 peaks as observed in this study. It is however noted that for a mixed Type II and III to show multiple S2 peaks, both kerogen types would probably have to be present in similar proportions and/or bear similar levels of hydrocarbon potential. In source rocks containing kerogens of one dominant-type with a minor secondary kerogen, then the S2 peak may contain a 'shoulder' depending on the relative concentrations of the primary and minor kerogens. This is also observed in some of the coals under study (Figure 5.8.D). Peters (1986) gave guidelines for evaluating petroleum source rocks using Rock-Eval pyrolysis, and stated the following:

When bimodal peaks are well resolved, Rock-Eval assigns T_{max} to the largest S2 peak. If two peaks are not well resolved (as in this study), T_{max} is assigned to the first (heavy-ends) peak; it is shifted by up to 5 °C for each peak in the direction of the other. Thus, the T_{max} of the lower temperature peak might be raised 5 °C whereas that of the higher temperature peak could be reduced by up to 5 °C.

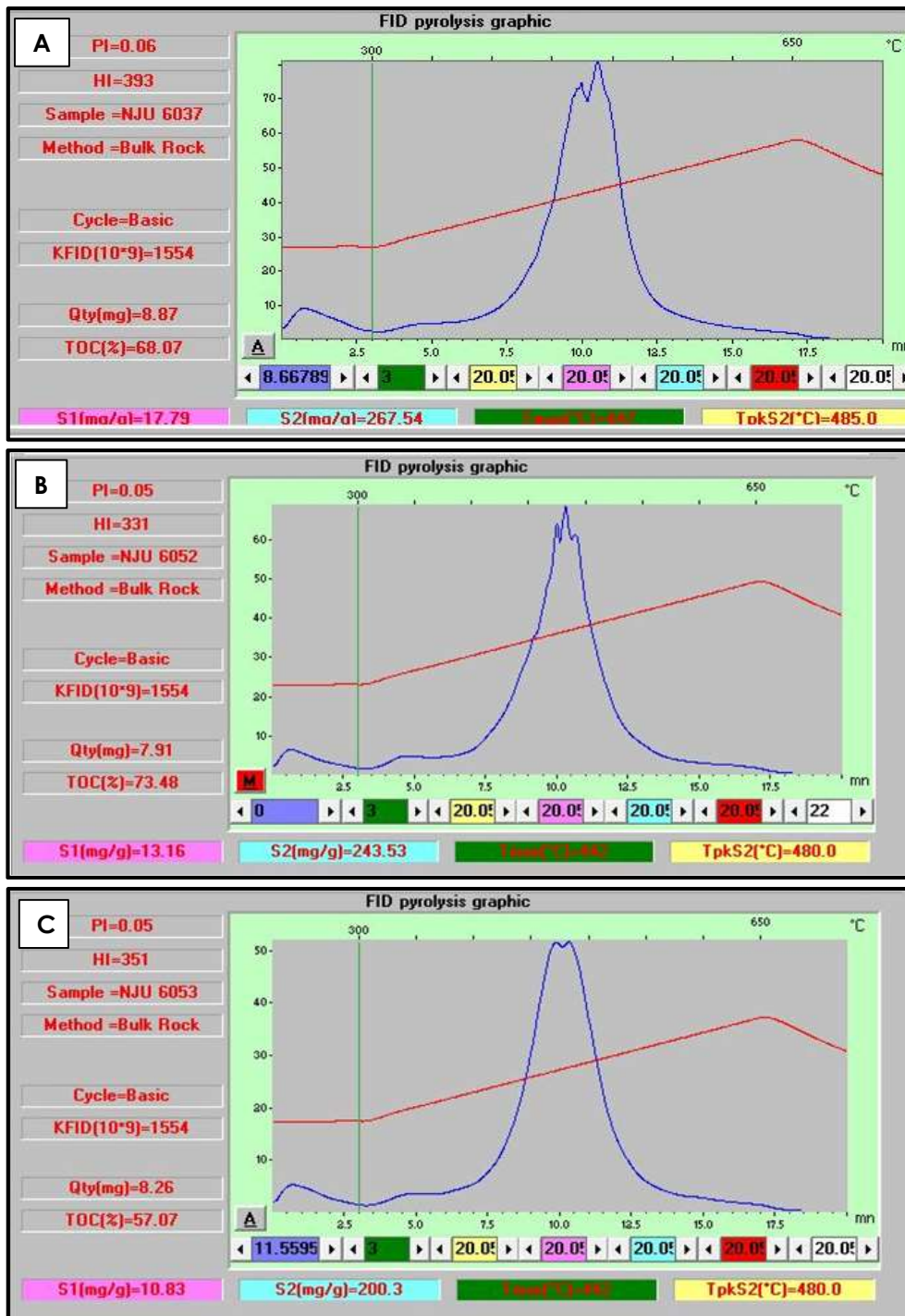


Figure 5.9.A-C. Rock-Eval 6 pyrograms showing multiple S2 peaks indicative of mixed liptinitic and vitrinitic hydrocarbon sources in coals from Breinosa BH4-2009. A) Sample Br1 - Top 19 cm of Askeladden seam, B) Sample Br16 – 24 cm from Longyear seam base, C) Sample Br17 - 8 cm from Longyear seam base.

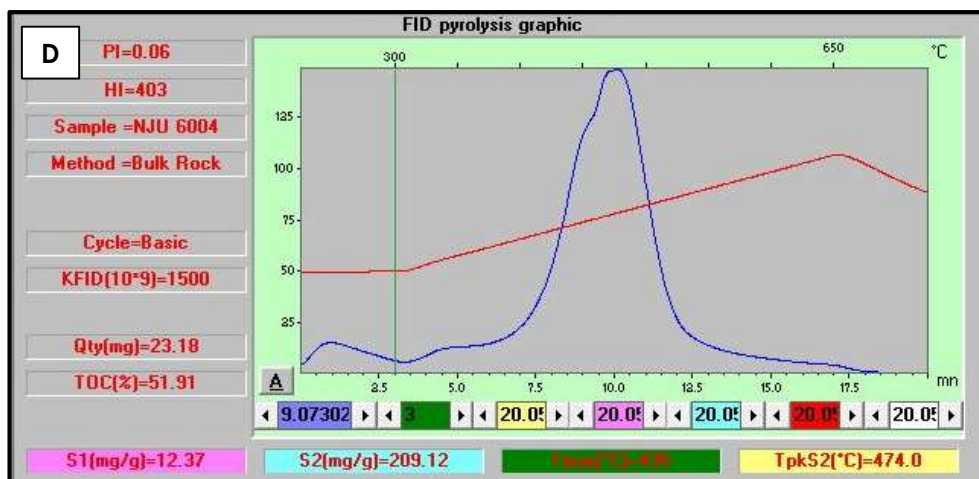


Figure 5.9.D. Rock-Eval 6 pyrogram of Sample L4, a Svarteper coal 50 cm from seam base at BH15-2011 locality. Note: shoulder to the left of the S2 peak suggests low relative proportions of a second (i.e. minor) kerogen

Although Peters (1986) mainly focused on the Rock-Eval 2 instrument, whereas this study utilised a Rock-Eval 6 instrument which is more advanced, the discussions in Peters (1986) are generally applicable to other Rock-Eval instruments and the guidelines are believed to be applicable in this study. Examination of the Rock-Eval 6 pyrograms shows that the true T_{max} values are less than the recorded peak temperature of S2 (T_{pkS2}) by 38 – 39 °C (Figure 5.9. A, B and C). There is often a problem in Rock-Eval in that the T_{max} as recorded by the instrument is higher than the temperature of the sample. Although an attempt has been made to rectify this problem in Rock-Eval 6 by relocating the oven thermocouple to the crucible (i.e. sample container) immediately below the sample (as against the oven wall in Rock-Eval 2 for example), the measured temperature is still not the real sample temperature (albeit measured and real sample temperature are now close) (Lafargue *et al.*, 1998). This temperature difference is associated with the decrease of kinetic parameters due to the fast heating rates of Rock-Eval pyrolysis which results from the delay of heat transfer from the inert gas stream to the sample (Schenk and Dieckmann, 2004). Consequently, the T_{max} values are adjusted by Rock-Eval to obtain the real T_{max} . This is clearly seen in Figures 5.9,

where the T_{max} appears to be shifted towards lower temperatures (i.e. backwards), and resolved around the first point where the temperature programme (red line) intersects the hydrocarbon traces (blue line). Thus, for samples shown in Figures 5.9.A, B, C and D, recorded T_{pkS2} are 485, 480, 480, 474 °C respectively, whereas the true T_{max} are 447, 442, 442 and 435 °C respectively.

5.2.3. Assessing Source Rock Quality using Py-GCMS

According to Horsfield (1989), the products of temperature-programmed analytical pyrolysis from a given kerogen, share fundamental compositional features with petroleum generated from the same kerogen during natural catagenesis. Thus, the source quality of kerogens with unknown or unproven petroleum-generating potential can be inferred with some confidence, using simple parameters that are easily determinable using Py-GCMS. The main resolved classes and selected components used to determine petroleum type and source rock organic facies from open Py-GCMS of 13 fresh coal samples are shown in Figure 5.10, while the parameters obtained using these main resolved classes and selected components are shown in Table 5.6 (i.e. calculated percentages of the main resolved classes and selected components used to determine petroleum type and source rock organic facies. The tri-plot of the total resolved pyrolysates in the C_1 - C_5 range, C_6 - C_{14} *n*-alkanes plus *n*-alkenes, and C_{15+} *n*-alkanes plus *n*-alkenes shows that the studied coals will produce some high-wax, mixed paraffinic-naphthenic-aromatic (P-N-A) oil, in addition to condensate and gas (Figure 5.11.A). Also, the tri-plot of the aromatic moieties (phenols and aromatic hydrocarbons), *n*-alkyl moieties (alkenes plus alkanes) and unknowns (all other major resolved peaks summed together) shows that the studied coals will produce aromatic and mixed P-N-A petroleum products (Figure 5.11.B).

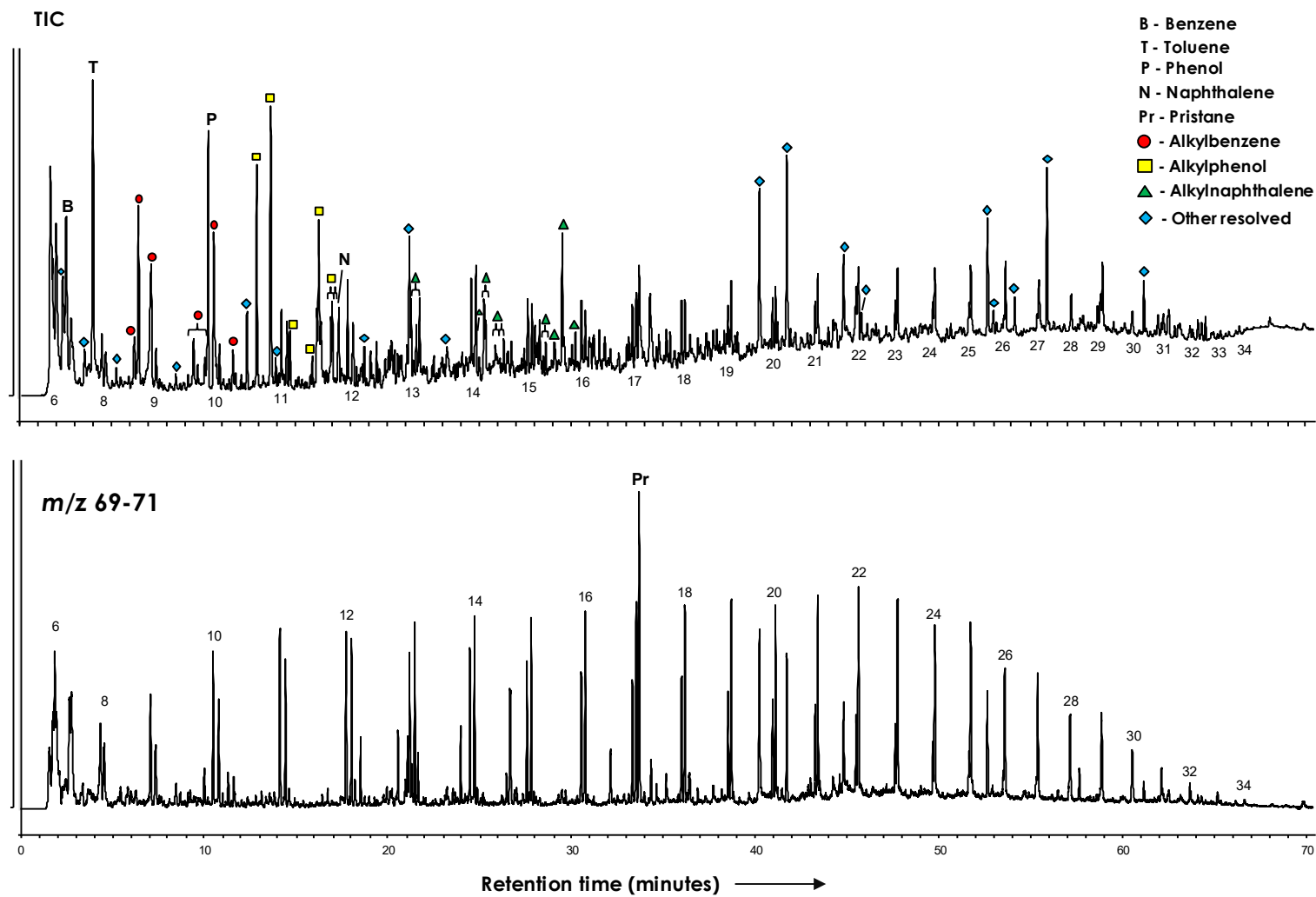


Figure 5.10. Representative TIC and m/z 69-71 from the Py-GCMS analysis of investigated coals (sample Ba1) showing selected components used to determine petroleum type and source rock organic facies. Numbers indicate the number of carbon atoms in the n-alkane/n-alkene doublets.

Sample ID	Locality	Seam	Chain length distribution normalisation (%)			C ₅ + gross composition normalisation (%)		
			C ₁ -C ₅ total resolved	C ₆ -C ₁₄ n-alkanes + n-alkenes	C ₁₅ + n-alkanes + n-alkenes	Aromatic moieties	N-alkyl moieties	Other resolved
Ba1	Bassen	Longyear	57.6	13.8	28.6	38.5	11.3	50.2
Ba11	Bassen	Longyear	57.4	14.3	28.4	33.4	10.0	56.7
Ba21	Bassen	Longyear	72.7	9.8	17.5	55.6	7.8	36.6
Ba32	Bassen	Longyear	58.4	12.0	29.5	43.7	11.0	45.3
L9	BH15-2011	Longyear	59.8	14	26.2	36.8	10.2	53.0
L14	BH15-2011	Longyear	42.0	17.3	40.7	43.1	13.7	43.2
L20	BH15-2011	Longyear	65.8	12.2	22.0	57.4	8.4	34.2
L27	BH15-2011	Longyear	63.2	12.8	24.0	41.2	11.1	47.7
Br12	BH4-2009	Longyear	57.0	14.7	28.3	46.1	11.5	42.5
Br16	BH4-2009	Longyear	71.1	11.0	17.9	44.9	10.7	44.4
C3	BH3-2008	Sputnik	57.4	15.5	27.2	48.3	5.4	46.2
C6	BH3-2008	Sputnik	66.3	10.5	23.2	45.9	8.0	46.1
C9	BH3-2008	Sputnik	57.4	15	27.6	46.2	10.6	43.3

Table 5.6. Calculated percentages of the main resolved classes and parameters used to determine petroleum type and source rock organic facies from open Py-GCMS

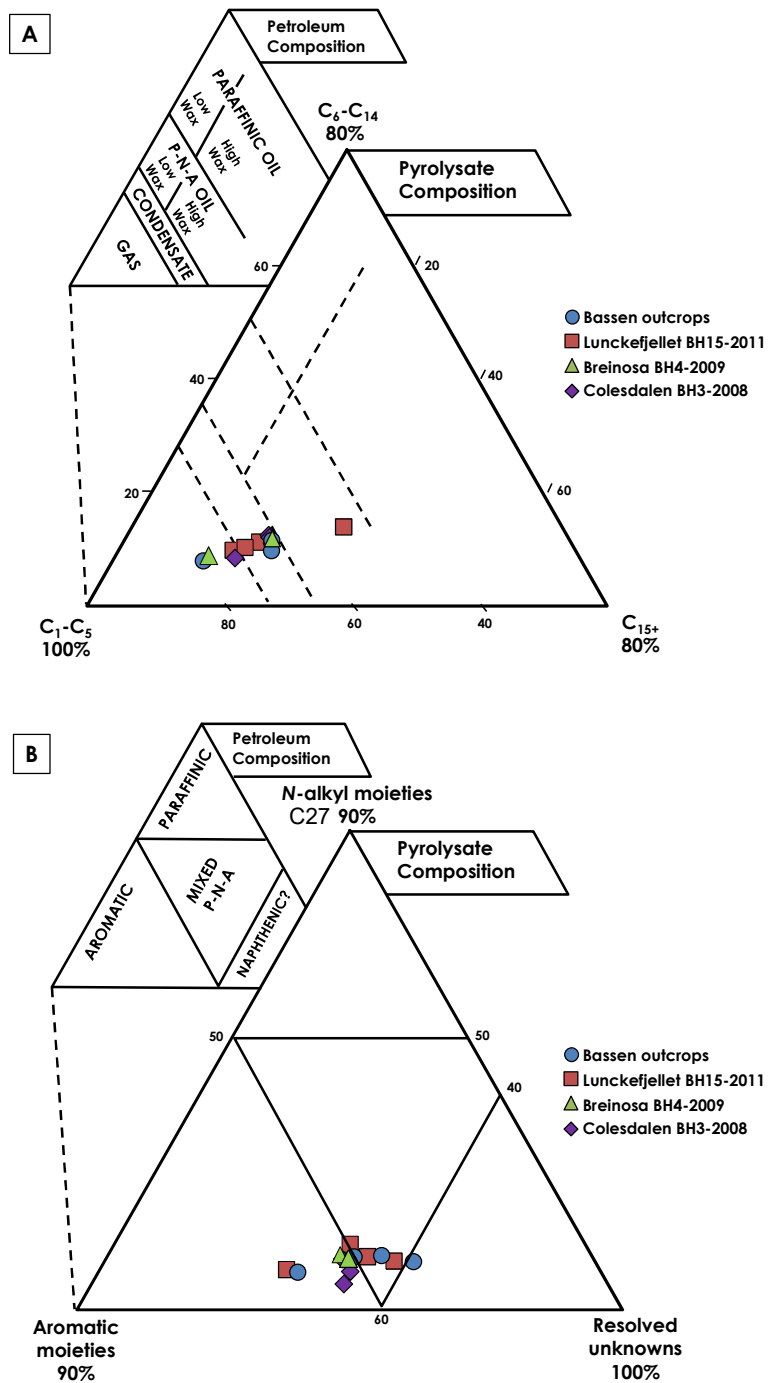


Figure 5.11. (A) Composition of kerogen pyrolysates according to the chain length distribution of total resolved $C_1 - C_5$, C_6-C_{14} *n*-alkanes plus *n*-alkenes and C_{15+} *n*-alkanes plus *n*-alkenes. (B) Composition of kerogen pyrolysates of C_5+ fraction according to the proportion of *n*-alkyl moieties, aromatic moieties and resolved unknowns. Inferred petroleum compositions are shown in the background (After Horsfield, 1989).

5.3. Oil Present in the CTB Coals under Study

Soxhlet yield is a measure of the amount of free bitumen plus already generated oil present in a source rock. This was measured in the coals under investigation via Soxhlet solvent extraction technique as described in Section 3.2.2.1. In the Longyear coals, greatest bulk yields were measured at Lunckefjellet with all four areas averaging 100 mg on dry whole coal basis (dwc), while lowest bulk yields were measured at Breinosa BH4-2009 (65 mg/g dwc) and Mine 7 (63 mg/g dwc) (Table 5.7). Bulk yield of 89 mg/g dwc was measured in Bassen, while the Sputnik seam in the Colesdalen area show bulk yield of 76 mg/g dwc. On dry ash free basis (daf), bulk yields at Lunckefjellet, Bassen, Breinosa BH4-2009 and Colesdalen are 108, 90, 78 and 82 mg/g respectively indicating the Breinosa BH4-2009 sampling locality is not very representative due to their high ash contents. Soxhlet yields generally suggest that coals from the eastern/north eastern basin margins (i.e. Bassen and Lunckefjellet) may be the most oil-prone, and that oil-proneness decreases from these areas through Breinosa, to the western parts of the basin in Colesdalen. Although this Soxhlet yield trend is somewhat consistent with the results of maceral analysis (Section 5.2.1), It is however noted that maturity variations across these four localities may be influencing Soxhlet yields and will be further examined in subsequent sections.

With regards to the stratigraphically younger coals, greatest (bulk) Soxhlet yield on dwc basis within the Svarteper seam were measured at Lunckefjellet with an average of 89 mg across all four locations. In Breinosa, bulk yields from the Askeladden and Svarteper seams are 97 and 52 mg/g dwc respectively. At Colesdalen, the Verkny coal showed bulk yield of 80 mg/g dwc.

Area	Location and sample type	Seam	No. of Samples	Soxhlet yield (mg/g dwc)					Mean Soxhlet yield (mg/g daf)
				Mean	Minimum	Maximum	Median	STDEV	
Bassen	Outcrop section	Longyear	32	88.7	66.2	109.6	90.0	10.3	90.2
Breirosa	BH4-2009	Askeladden	2	97.3	66.0	128.5	97.3	44.2	117.0
Breirosa	BH4-2009	Svarteper	5	52.0	36.0	79.3	50.2	16.0	81.7
Breirosa	BH4-2009	Longyear	5	65.1	50.3	79.2	69.6	12.0	78.2
Breirosa	Mine 7 section	Longyear	10	63.2	28.8	150.0	54.5	39.5	-
Lunckefjellet	BH15-2011	Svarteper	8	89.8	69.3	112.1	90.2	13.9	110.9
Lunckefjellet	BH15-2011	Longyear	19	93.2	54.5	120.8	95.7	18.8	100.7
Lunckefjellet	BH10-2009	Svarteper	4	79.3	48.0	133.2	68.1	39.8	111.5
Lunckefjellet	BH10-2009	Longyear	4	109.1	93.4	126.4	108.4	13.8	116.9
Lunckefjellet	B10-2007	Svarteper	2	92.1	83.6	100.6	92.1	12.0	116.1
Lunckefjellet	B10-2007	Longyear	6	105.6	74.8	153.0	100.7	29.4	111.7
Lunckefjellet	BH6A-2007	Svarteper	3	95.5	56.4	126.7	103.3	35.8	114.4
Lunckefjellet	BH6A-2007	Longyear	8	97.4	63.9	147.0	96.1	27.2	100.7
Colesdalen	BH3-3008	Verkny	1	80.2	80.2	80.2	80.2	-	115.9
Colesdalen	BH3-3008	Sputnik	7	75.8	42.3	143.2	69.4	35.5	82.4

Table 5.7. Soxhlet yields of the Firkanten Formation coals under study. Greatest yield is measured in the Longyear coals in Lunckefjellet. Samples with >50 % ash content are excluded (0.1 mg/g = 1 wt %). (dwc = dry whole coal, daf = dry ash free).

Significantly higher bulk values were observed on daf basis with the Svarteper seam in Lunckefjellet averaging 108 mg across all four sampling localities. In Breinosa, the Askeladden and Svarteper seams showed bulk values of 117 and 82 mg/g daf respectively, while the Verkny coal in Colesdalen showed bulk value of 116 mg/g daf. Results indicate oil potential increases from the stratigraphically older to younger seams which is consistent with HI results (Tables 5.4 and 5.5). Oil potential of the Askeladden, Svarteper and Verkny coal seams is notably limited by their generally higher ash content relative to that of the Longyear and Sputnik seams.

5.4. Marine Sulphur and Oil Potential of the CTB Coals under Study

According to Chou (2012), the total sulphur content in coals is most commonly between the ranges of 0.5 - 5.0 % but may vary considerably. The sulphur content in peat is closely related to its depositional environment; in general, peats accumulating in a freshwater environment will have lower sulphur content than peats accumulating under the influence of seawater mainly due to the availability of seawater sulphate (e.g. Chou, 2012). In a study of the marine influence on the coaly source rocks of the Eocene Mangahewa Formation in the Taranaki Basin, Sykes *et al.* (2014) stated that all total S values > 0.5 % indicate some degree of marine influence; these workers classed S values of 0.5 –1.5 % and >1.5 % as slightly and strongly marine influenced respectively. Hence, coal sulphur content should reflect the amount of marine input into the peatland in a paralic depositional environment such as the CTB.

Table 5.8 shows the sulphur distribution of 84 Firkanten Fm. coals under investigation. Sulphur contents range from 0.38 – 17.7 %, which indicates seawater influence. As per the classification by Sykes *et al.* (2014), the Longyear coals in

Bassen are slightly marine influenced (0.5 – 1.5 % S), while the Longyear coals from Lunckefjellet range from non-marine to strongly marine influenced (0.4 – 8.2 % S). The Longyear coals from Breinosa BH4-2009, and the Sputnik coals from Colesdalen all belong to the strongly marine influenced class (1.9 – 7.0 and 1.4 – 12.0 % S respectively). The Askeladden, Svarteper and Verkny coals belong to the strongly marine influenced class with sulphur contents (8.1 – 8.3, 3.4 – 8.2 and 17.7 % S respectively) generally greater than the Longyear and Sputnik coals, which is consistent with previous reports of increasing marine influence from the stratigraphically older to younger Firkanten Fm. coals (e.g. Orheim *et al.*, 2007).

Area	Location and sample type	Seam	No. of Samples	Mean (ppm)	Min (ppm)	Max (ppm)	Med (ppm)	STDEV (ppm)
Bassen	Outcrops	Longyear	13	8399	5356	15088	6901	3368
Breinosa	BH4-2009	Askeladden	2	82200	80900	83500	82200	1800
Breinosa	BH4-2009	Svarteper	5	88000	46300	104700	70800	46546
Breinosa	BH4-2009	Longyear	8	50400	19100	70400	64100	23400
Lunckefjellet	BH15-2011	Svarteper	8	59261	40286	82281	57819	13119
Lunckefjellet	BH15-2011	Longyear	19	13180	4145	36002	8903	8914
Lunckefjellet	BH10-2009	Svarteper	3	46699	34104	58904	47090	12405
Lunckefjellet	BH10-2009	Longyear	8	5875	3822	10481	5103	2247
Lunckefjellet	BH6A-2007	Svarteper	5	61918	40014	73586	68799	14569
Lunckefjellet	BH6A-2007	Longyear	4	28120	10598	68855	16514	27558
Colesdalen	BH3-2008	Verkny	1	177000	177000	177000	177000	177000
Colesdalen	BH3-2008	Sputnik	8	35753	13895	120493	19402	36665

Table 5.8. Sulphur data of the Firkanten Formation coals under study. (10,000 ppm = 1 wt %).

Increasing marine influence from the older to younger Firkanten Fm. coals was notably observed in the petrographic character of the 19 uppermost centimetres of the Askeladden seam at Breinosa BH4-2009 (i.e. Sample Br1) as fragments of fluorescing (perhydrous) vitrinites were embedded within non-fluorescing (orthohydrous) vitrinite groundmass (Figure 5.12.1). According to Taylor *et al.* (1998), most workable coal seams are autochthonous. However, minor re-

arrangements of peat take place repeatedly within an essentially autochthonous peat deposit during times of flooding, and coals which form this way are termed "hypautochthonous". These coals are commonly characterised by a finely detrital texture, higher mineral matter content than truly autochthonous coals and pronounced microlayering. Thus, the high ash and sulphur contents of sample Br1 (16.5 and 8.4 % respectively) and the Askeladden seam in general, and the microlayering (Figure 5.12.1 and 5.12.2) does reflect a hypautochthonous depositional environment.

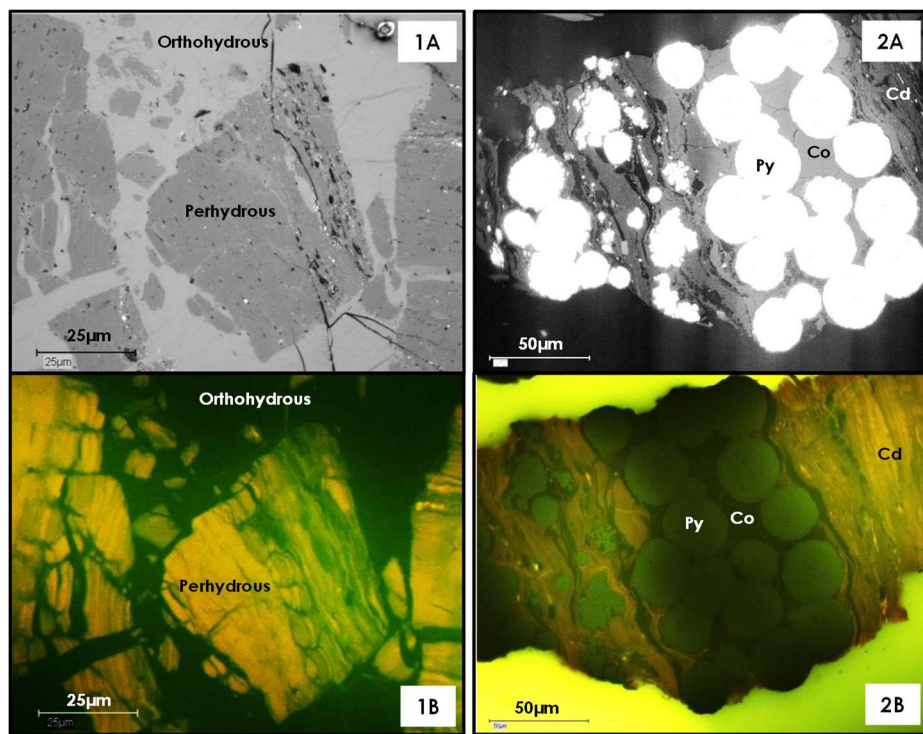


Figure 5.12. Photomicrographs of sample Br1 - the top 19 cm coal from Askeladden seam in Breinosa BH4-2009. A) White light, B) Blue light. 1) Perhydrous (fluorescing) vitrinites embedded in orthohydrous (non-fluorescing) vitrinite groundmass. 2) Pyrite framboids (up to 35 µm in diameter) indicates relatively high marine influence upon peatland. Note: microlayering is indicative of hypautochthonous deposition. (Cd – collodetrinite, Co – collotelinite, Py - pyrite).

Pyrite framboids of up to 35 µm in diameter were also observed in sample Br1 (Figure 5.12.2), which indicates oxygen-poor depositional conditions (Raiswell and

Berner, 1985; Wignall *et al.*, 2005) associated with relatively high marine influence on the peatland. Pyrite framboids are also indicative of abundant H₂S (Bulter and Rickard, 2000), which allows organosulphur compound formation (Sandison, 2001) leading to the high oil potential of this sample (Soxhlet yield = 153.8 mg/g daf, S1 = 17.8 mg/g, HI = 393 mg HC/g TOC), and the CTB coals in general.

5.4.1. The Longyear Peatland - Oil Potential, Sea Level Drop/Rise and Peatland Transition

Within the Longyear seam, there is a general trend of a decrease followed by an increase in sulphur contents towards the top of the seam. At Bassen for example, sulfur contents decrease from ~1.0 % at seam base, to a minimum of ~0.5 % between 94 - 109 cm above seam base, and then increase to ~1.5 % at seam top (Figure 5.13). This is interpreted as sea level drop, followed by sea level rise.

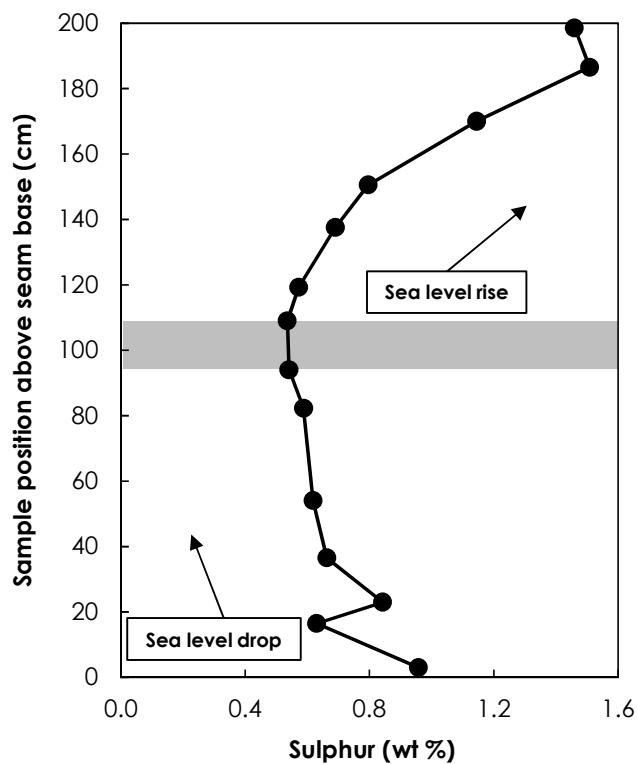


Figure 5.13. The sulphur trend from the base to top of the Longyear seam in Bassen. Note: the observed trend reflects sea level drop, followed by sea level rise.

The effect of sea level drop and rise on the oil potential of the Longyear seam is clear; at Bassen for example, it was observed that sulphur and Soxhlet yield display similar trend from base to seam top (Figure 5.14). This observation is consistent with previous work on the positive impact of marine sulphur content on perhydrous (oil-prone) coal formation (e.g. Diessel and Gammidge, 1998; George *et al.*, 1994; Wilkins and George, 2002; Sykes and Snowdon, 2002; Sykes *et al.*, 2004b; 2014; Marshal *et al.*, 2015a). Rock-Eval S1 represents the amount of thermo-vaporized free hydrocarbons present in source rocks, while HI is the S2 contents (i.e. the amount of hydrocarbons produced from the cracking of heavy hydrocarbons and from the thermal breakdown of kerogen in source rocks) normalised to TOC contents (e.g. Lafargue *et al.*, 1998 and references within). When the trends from base to top of seam for Soxhlet yield, S1 and HI were compared to sulphur; all measurements display similar trend (Figure 5.14). A multiple regression analysis for the Bassen samples (not shown) at 95 % confidence level using sulphur as the dependent variable, and Soxhlet yield, S1 and HI as independent variables displays a strong coefficient of multiple correlation (Multiple R = 0.70) and a moderate coefficient of determination ($R^2 = 0.50$). This confirms sulphur control on oil potential.

Oil potential is greatest within the upper Longyear relative to the lower Longyear seam due to the transition from raised-bog (ombrotrophic) conditions in the lower Longyear peatland, to fen-like (minerotrophic) conditions in the upper Longyear peatland (Marshall *et al.*, 2015a). The transition zone, which marks increasing oil potential towards the top of the seam, is associated with increased groundwater supply, brought about by sea level rise and consequent marine sulphate deposition. The compositional data of the CTB coals shows the transition zone varies between areas in the CTB relative to the levels of marine influence, but

generally occurs around 60 – 120 cm above seam base. The transition zone is observed in the vertical profiles of sulphur contents, Soxhlet yield, S1 and HI of the Longyear seam at Bassen (Figure 5.14) and other areas under study (Figure 5.15). Notably, the Sputnik coal seam in BH3-2008 locality, which represents the western coalfield of the CTB in Spitsbergen, displays similar transition; hence it is likely a Longyear seam equivalent.

It is noted that the S1 yields are more than 10 times less than the Soxhlet yield on average for all samples. This is not surprising as although S1 is an independent measure of the amount of bitumen in a sample; it does not correspond directly to solvent extracted bitumen because of procedural differences (Peters, 1986). S1 represents organic compounds from C₁ to about C₃₂ (Tarafa *et al*, 1983) and is based primarily on separation by distillation temperature (up to about 400 °C) and the FID response factor of each compound (Peters, 1986). Soxhlet extract represents the weight percentage of organic compounds removed by an organic solvent; this percentage varies with solvent polarity, extraction method, sample size, and extraction time (Peters, 1986). Additionally, compounds below about C₁₅ are mostly lost during evaporation of the solvent in extraction. Thus, in Soxhlet extraction, the solvent removes bitumen plus oil, whereas S1 measures volatile oil.

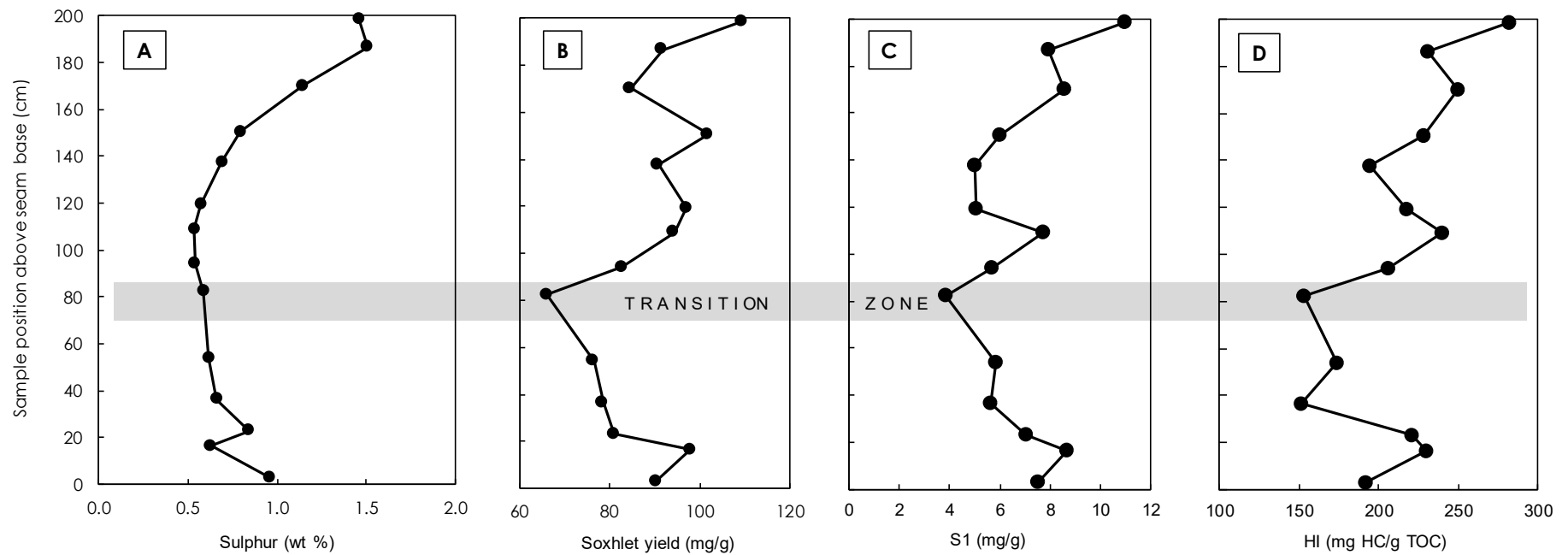


Figure 5.14. Comparing the profiles of A) Sulphur contents, B) Soxhlet yield (dwc), C) Rock-Eval S1, D) Rock-Eval HI, from base to top of the Longyear seam at Bassen
 Note: similar trend with prominent fen transition displayed by all measurements/parameters indicates marine control (drop/rise in sea level) on oil potential

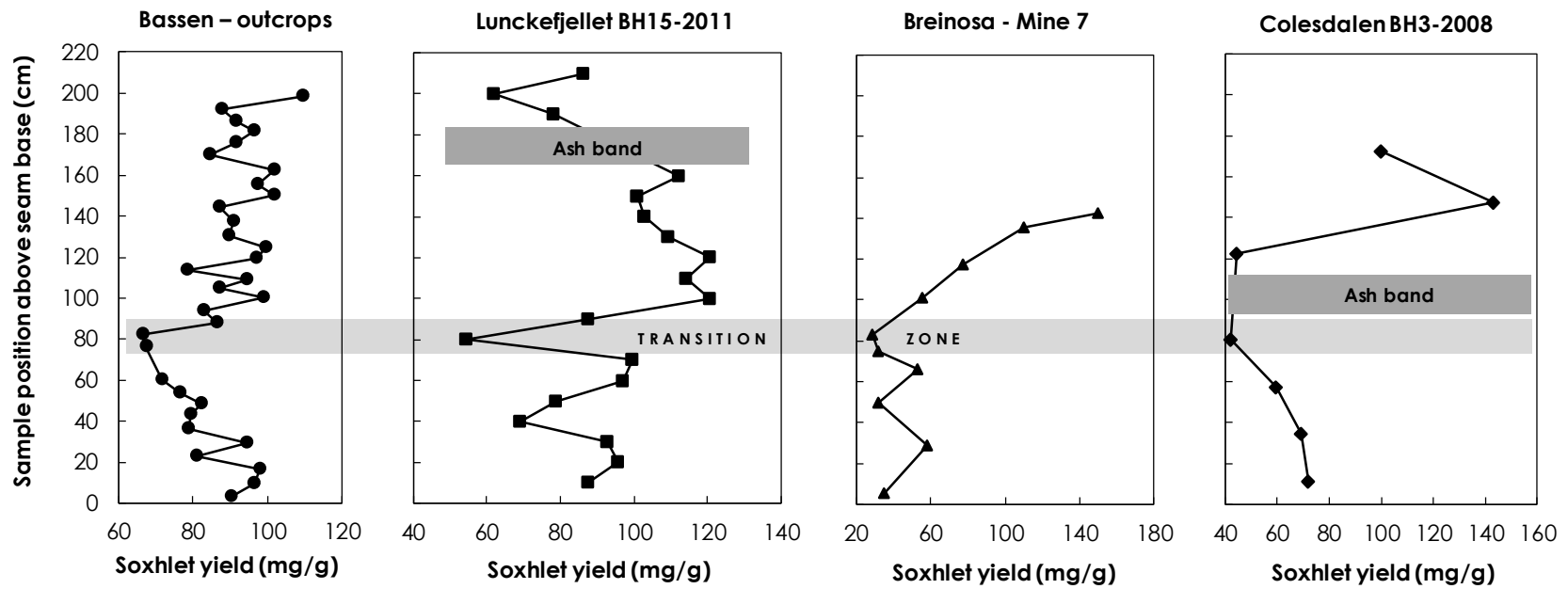


Figure 5.15. Comparing the profiles of Soxhlet yield from base to top of the Longyear seam in Bassen, Lunckefjellet and Mine 7, and the Sputnik seam in Colesdalen (dry whole coal basis) Note: Increase in Soxhlet yield in upper seams due to transition from raised-bog in lower seam, to fen-like conditions in upper seam.

5.4.2. Organosulphur Compound Formation in the CTB

Sandison (2001) proposed the following mechanism for the formation of organosulphur compounds (OSC):

- Plant lipids are preserved in coal forming environments during deposition and early diagenesis.
- The presence of saline sulphur rich waters prevents the normal biodegradation of hydrogen rich compounds (anaerobes at expense of aerobes).
- Sulphate reducing bacteria produce H₂S in anaerobic conditions, to levels which exceed the iron supply, allowing the formation of OSC.
- The reaction of H₂S with organic matter occurs preferentially with functionalised molecules (Sinninghe Damsté and de Leeuw, 1990), preserving both carbon skeleton and functionality. These functionalised molecules are often higher plant biomarkers (oleananes, tricyclic diterpanes and *n*-alkanes) and bacterial biomarkers (hopanes).

In the CTB, the upper Firkanten Fm. coals (Longyear/Sputnik and younger coals) would display the requirement of pH regulation and sulphur supply derived from saline/brackish waters due to their significant marine influence; this is consistent with many oil-prone coals such as in the Taranaki Basin, Gippsland Basin and Beaufort-Mackenzie Basin (Sandison, 2001; Sandison *et al.*, 2002).

The high hopane concentrations within the free phase (Soxhlet extracts) of the CTB coals (Section 4.3.1) (Marshall *et al.*, 2015a) is an evidence of significant OSC formation. Evidence for significant OSC formation also includes good preservation of higher plant biomarkers, which would otherwise be lost (Sandison, 2001); however, oleanane (a higher plant triterpenoid) is notably absent in the coals

under study (Section 4.3.1). This is possibly due to quick decay before marine influence (Sandison, 2001) as angiosperms show relatively high susceptibility to biodegradation (Faix *et al.*, 2009). Thus the absence of oleanane and angiosperms from the CTB coals in general (Marshall, 2013) may indicate OSC formation was limited, perhaps insignificantly, as the coals nonetheless display high oil potential.

According to Sykes *et al.* (2014), inundation of brackish water into early diagenetic peat forming environment will enhance the bio-resistance of higher plant and other lipids through sulphurisation. Thus, OSC formation during early diagenesis, aided by the excess sulphur from marine deposition, provides a method of binding and protecting the hydrogen rich materials produced by bacteria action within less reactive humic material (Hao and Chen, 1992) during subsequent diagenesis and coalification. This preservation effect explains the hydrocarbon enrichment of the upper Firkanten Fm. coals and a plausible mechanism for the formation of perhydrous vitrinites responsible for much of the oil potential of these coals.

5.5. Thresholds for Oil Generation and Expulsion from the CTB Coals

Sykes and Snowdon (2002) stated that the relationships between some key Rock-Eval parameters (e.g. Bitumen Index and Hydrogen Index) for coals differ from corresponding relationships for marine and lacustrine kerogens because of the unique maturation characteristics of higher plant-derived kerogen. Consequently, these workers developed maturation pathways for a set of 591 New Zealand Late Cretaceous-Cenozoic humic coals ranging in rank from peat to bituminous by cross plotting Rock-Eval parameters against the Rank (Sr) scale of Suggate (2000) and T_{max} . All parameters plotted well within the New Zealand Coal Band (NZ-CB)

and allowed improved identification of the thresholds for oil generation and expulsion. Evidence in this study (Chapter 4) and in previous work (Marshall *et al.*, 2015b) show that the VR of the CTB coals are suppressed. The T_{max} of the coals also appear suppressed (Section 4.4), but to a lesser degree compared to VR suppression. Thus, the maturation pathways of Sykes and Snowdon (2002) may be useful in estimating the threshold for oil generation and expulsion from the CTB coals. This was assessed in this section using 56 coals from the Bassen, Lunckefjellet, Breinosa and Colesdalen areas. Assessment was done via cross plots of Rock-Eval parameters including Bitumen Index – BI, Quality Index – QI and T_{max} . BI is $(S1*100)/TOC$ in mg HC/g TOC (Killops *et al.*, 1998), while QI is $[(S1+S2)*100]/TOC$ in mg HC/g TOC (Pepper and Corvi, 1995a). All other Rock-Eval parameters utilised are as defined in Section 3.2.2.2.

The T_{max} vs BI of the CTB coals plot well within the NZ-CB, and show maturity increases from the north-eastern basin margin (Bassen), towards the basin center in Colesdalen (Figure 5.16); this trend is consistent with the NE-SW structural trend and southerly tilting of the CTB (e.g. Harland *et al.*, 1997). The upturn in coal band indicates the onset of oil generation at $T_{max} \sim 420 - 430$ °C, while the peak in coal band at $T_{max} \sim 445 - 455$ °C indicates a change from increasing to decreasing hydrocarbon saturation of the coal pore structure and probably marks the onset of primary gas generation and the efficient expulsion of oil (Sykes and Snowdon, 2002). On the T_{max} vs BI graph, all coals plot between the onset of oil generation and the onset of gas generation, with the Bassen coals just beyond the onset of oil generation, the Lunckefjellet coals are well within the oil generation window while the Breinosa and Colesdalen coals are closest to gas generation.

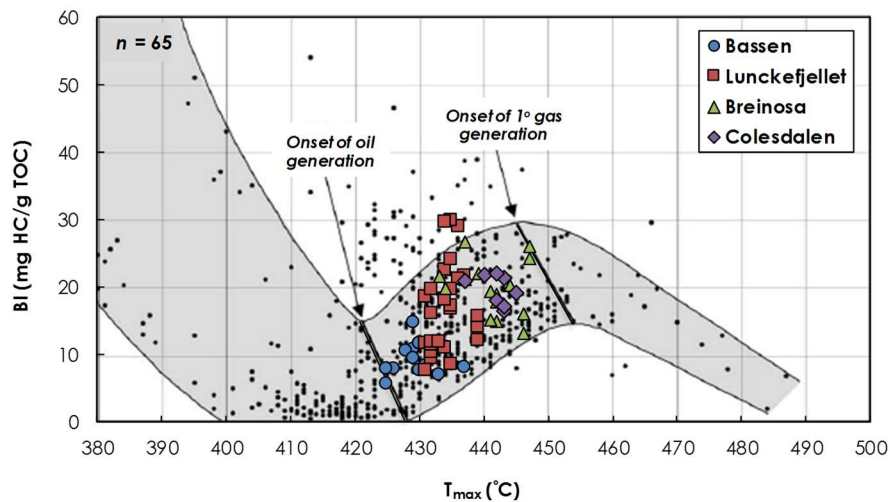


Figure 5.16. T_{max} vs BI and the inferred threshold for oil and gas generation for the CTB coals under study (Adapted from Sykes and Snowdon, 2002). Note: Coloured plots = 65 coals from the Askeladden, Svarteper, Longyear, Verkny and Sputnik seams. Grey band = New Zealand Coal Band. Black dots = New Zealand Late Cretaceous – Cenozoic humic coals of peat to bituminous rank

As observed in the T_{max} vs BI plot, the plot of T_{max} vs QI (Figure 5.17) also display the maturity trend of the CTB coals and appears to peak in the same region as the NZ-CB. The downturn in coal band at T_{max} ~430 – 440 °C coincides with the beginning of the decrease in atomic H/C; this is consistent with a pulse of paraffin expulsion (Killops *et al.*, 1998), and generally marks the onset of oil expulsion (Sykes and Snowdon, 2002) (Figure 5.17). The T_{max} vs QI plot shows the Bassen coals are yet to expel oil, the Lunckefjellet coals are within the range of oil expulsion, while the Breinosa and Colesdalen coals are already expelling oil. In Figure 5.17, samples plotting on the upper part, and above the coal band, are more perhydrous than samples in the lower part of the band. The top of the coal band peaks at lower maturity (T_{max} ~430 °C) compared to the base of the band (T_{max} ~440 °C) (Figure 5.17), which implies that the more perhydrous coals (and supposedly the more marine influenced coals *ceteris paribus*) would commence generation and expulsion at lower thermal maturities compared to coals in the lower part of the coal band (Sykes and Snowdon, 2002) due to their greater initial

Hydrogen Index (HI^0) (Pepper and Corvi, 1995b). The estimated unsuppressed VR of the Breinosa and Colesdalen coals are 0.80 and 0.88% R_o respectively (Chapter 4); however, the Breinosa coals generally plot above the Colesdalen coals within the oil expulsion window (Figure 5.17) because the Breinosa coals, having HI (between 292 – 393 mg HC/g TOC) greater than the Colesdalen coals (HI between 242 – 314 mg HC/g TOC) (Tables 5.4 and 5.5), probably also have greater HI^0 . The fact that both sets of samples from Breinosa and Colesdalen appear to have already generated similar amounts of hydrocarbons (Tables 5.4 and 5.5; Figure 5.16) also supports the idea that the more perhydrous Breinosa coals probably commenced generation and expulsion before the less perhydrous Colesdalen coals.

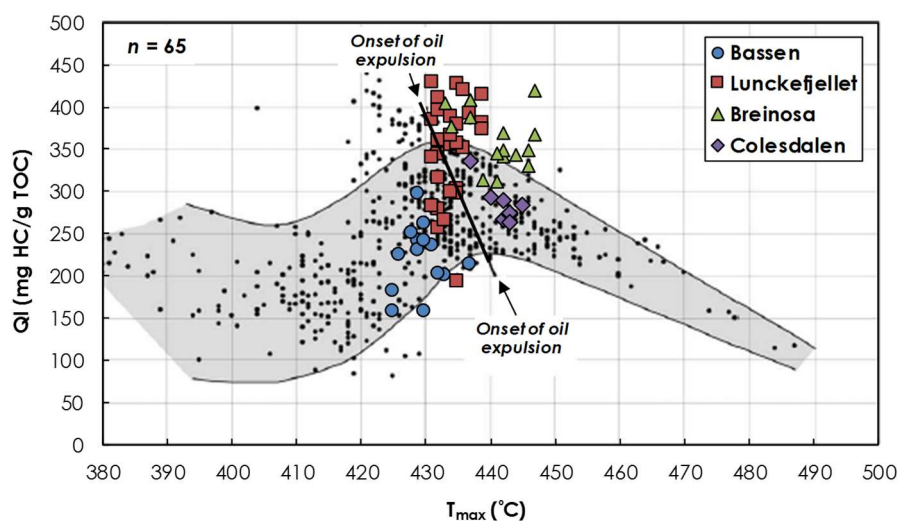


Figure 5.17. T_{max} vs QI and the inferred threshold for oil expulsion from the CTB coals under study (Adapted from Sykes and Snowdon, 2002). Note: Coloured plots = 65 coals from the Askeladden, Svarteper, Longyear, Verkny and Sputnik seams. Grey band = New Zealand Coal Band. Black dots = New Zealand Late Cretaceous - Cenozoic humic coals of peat to low Volatile bituminous rank

Micrinites are fine granular macerals belonging to the inertinite group and are thought to be a remnant of oil generation from lipid materials (Taylor *et al.*, 1998). Although the occurrence of micrinite is generally lower in Permian and other post-

Carboniferous coals (ICCP, 1998), they have been observed in the CTB coals under investigation (Figures 5.18 and 5.19). Exsudatinitite is a secondary maceral like micrinite, which is generated during coalification at the beginning of the bituminization process when petroleum-like substances begin to form from lipid materials in liptinites and perhydrous vitrinites (Taylor *et al.*, 1998), and they have been observed in the CTB coals under study (Figure 5.19). Oil expulsion from cracks on perhydrous vitrinite was also noted during optical examination (Figures 5.19 and 5.20). These microscopic evidences support oil generation and expulsion from the coals under study.

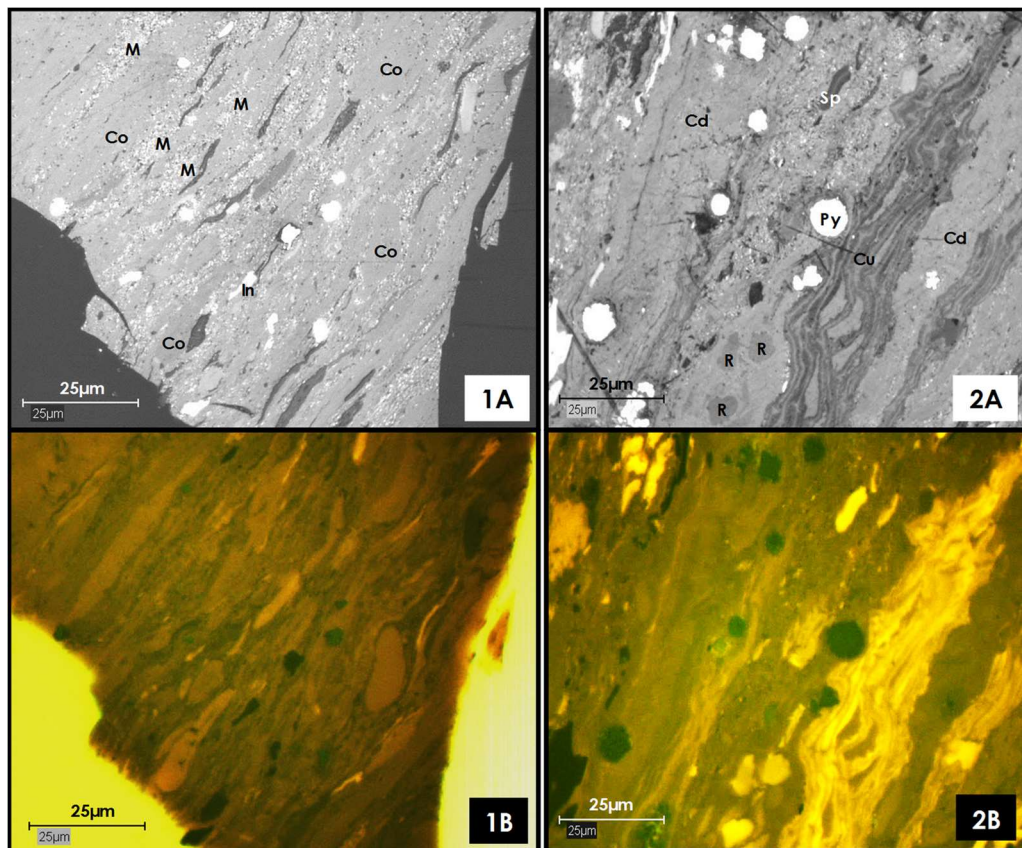


Figure 5.18. Photomicrographs from coals in Breinosa BH4-2009. A) White light, B) Blue light. 1) Agregates of micrinite (M) grains (fine granular white macerals) in sample Br1. 2) Liptinitic macerals in a collodetrinite + liptodetrinite groundmass in sample Br16. Note: the fluorescing nature of the vitrinitic macerals e.g. coropogelinite (Co) in (1), which suggest that while detrovitrinites are responsible for much of the oil potential of these coals, other vitrinitic macerals and some liptinites have contributed significantly; this supports a mixed type II and III source. The presence of framboidal pyrite is indicative of anoxicity and abundant H₂S which allows OSC formation and greater oil potential. Cu – cutinite, Cd – collodetrinite, Sp – sporinite, R – resinite, Py – pyrite, In – inertodetrinite, Lpd - liptodetrinite

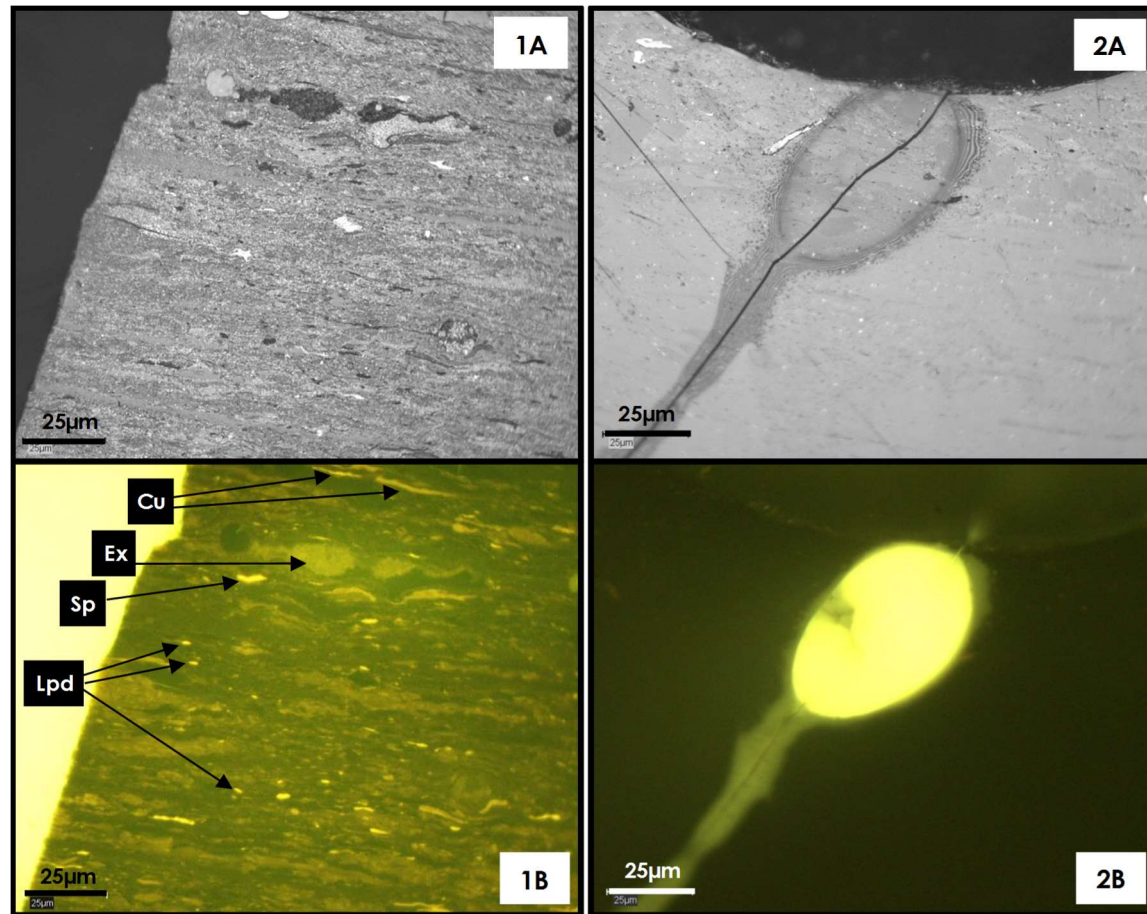


Figure 5.19. Photomicrographs from Longyear coals in Lunckefjellet BH6A-2007 locality. A) White light, B) Blue light). 1) Micrinite (fine granular white macerals) in perhydrous vitrinite groundmass in Sample L48. 2) Oil expulsion from crack on a perhydrous vitrinite in sample L51. Note: abundant liptinites in addition to perhydrous vitrinite macerals in (1) which supports a mixed Types II and III source. Cu – cutinite, Ex – exsudatinites, Sp – Sporinite, Lpd - liptodetrinite

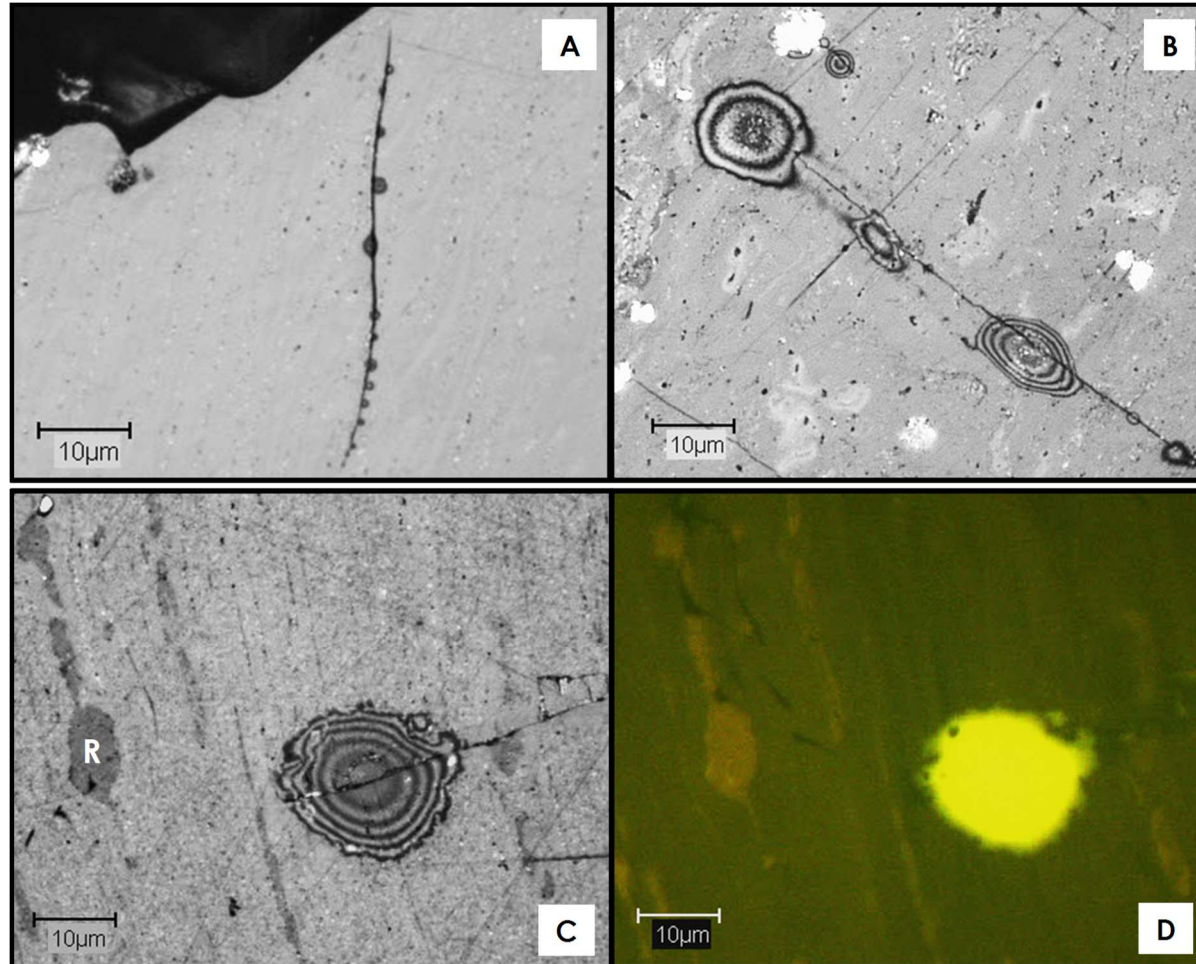


Figure 5.20. Oil expulsion with Newton's rings from cracks on perhydrous vitrinites in coals from Breinosa BH4-2009 locality. A and B) Sample Br1, C) Sample Br16, D) Blue light picture of (C). R – resinite.

The high proportions of detrovitrinites + liptodetrinites groundmass in these coals (e.g. Figures 4.1, 5.2, 5.18 and 5.19) may not only favour oil-proneness, but also favour primary migration of oil in the coals, thereby enhancing their expulsion efficiency (Stout, 1994). The positive relationship between marine influence and the oil potential of the CTB coals is clear (Section 5.4); consequently, the relatively low Soxhlet yield measured in the Longyear coals in Breinosa, and the Sputnik coals in Colesdalen (Table 5.7) despite their greatest marine influence (Table 5.8) is further examined below. A comparison between HI, Soxhlet yield and S1 in the Longyear and Sputnik coals at Bassen and Colesdalen respectively, shows that the Bassen samples display bulk HI, Soxhlet yield and S1 of 212 mg HC/g TOC, 88.7 and 6.7 mg/g respectively, while the Colesdalen samples display bulk HI, Soxhlet yield and S1 values of 268 mg HC/g TOC, 75.8 and 15.2 mg/g respectively (Tables 5.4, 5.5 and 5.7) (i.e., the Colesdalen coals with greater sulphur, S1 and HI show lower Soxhlet yields compared to the Bassen coals). With regards to the relative values of S1 and Soxhlet yield in these two areas, there is an argument that S1 represents free oil + gas, whereas only liquids (oil) are accounted for in Soxhlet extracts. Thus, greater S1 and lower Soxhlet yield in Colesdalen relative to Bassen is possibly because the Colesdalen coals originally contained greater abundance of light hydrocarbons which were lost during Soxhlet extraction but accounted for in S1. The HI variation relative to Soxhlet yield at these two areas is also examined; according to reports (e.g. Isaksen *et al.*, 1998; Petersen *et al.*, 2009), measured HI is not always a good indicator of the oil potential of humic coal because:

- Enhanced hydrogen content will only increase the capacity to generate oil if the hydrogen is incorporated as long aliphatic chains.
- Part of the HI can be attributed to hydrogen in compounds with less than 10 carbon atoms which represent a potential for generation of gas and light liquid hydrocarbons.

Perhaps these reasons are partly responsible for the lower Soxhlet yield in Colesdalen. The $C_{21}-C_{33}/C_8-C_{20}$ ratio from Py-GC was used to assess the chain length distribution of *n*-alkanes + *n*-alkenes, which shows similar distribution at all locations with mean values of 0.54, 0.58, 0.55 and 0.59 at Bassen, Lunckefjellet, Breinosa and Colesdalen respectively (Table 5.9; Figure 5.21). This indicates the lower Soxhlet yield in Breinosa and Colesdalen is not due to relatively greater concentrations of light aliphatic hydrocarbons.

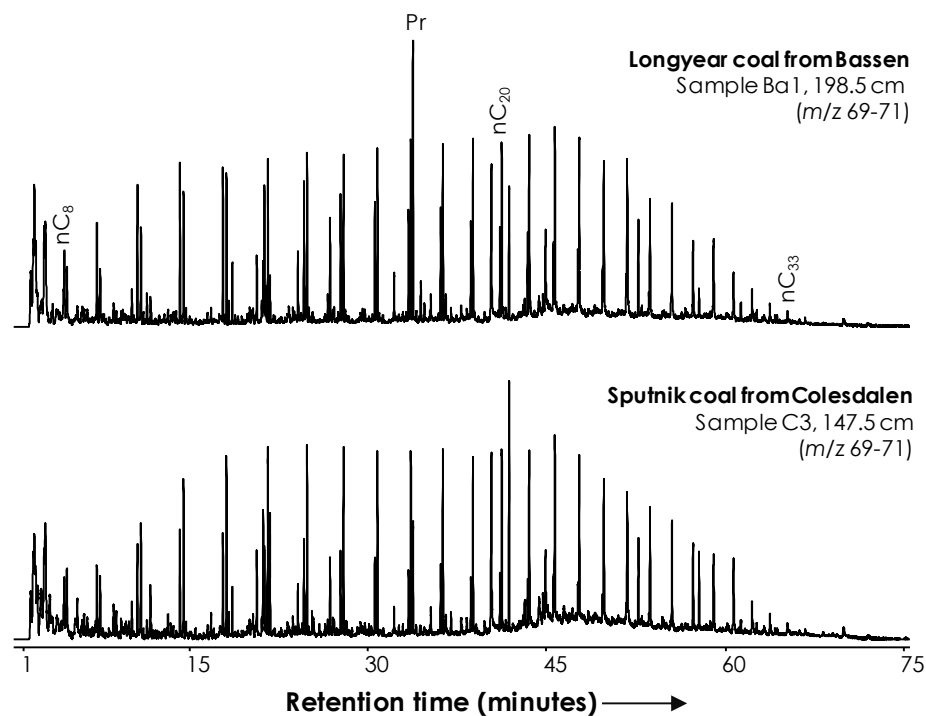


Figure 5.21. Comparing the Py-GCMS aliphatic traces of coals from the eastern and western coalfields of the CTB. Top: Sample Ba1 - A Longyear coal at Bassen 198.5 cm from seam base. Bottom: Sample C3 - A Sputnik coal at Colesdalen 147.5 cm from seam base.

Further assessments involved comparing the trends of HI, S1 and Soxhlet yield from base to seam top; all three parameters appear similar in Bassen, whereas in Colesdalen, S1 and Soxhlet show similar but different trend to HI (Figure 5.22).

Sample ID	Area	Location and sample type	Seam	Age	Drill depth (m)	Height above seam base (cm)	C ₂₁ -C ₃₃ /C ₈ -C ₂₀ (alkane + alkene)	VR (% R _o)	Mean estimated VR (% R _o) based on Lo (1993) Correction
Ba1	Bassen	Outcrop	Longyear	Paleocene	-	198.5	0.50	0.54	0.68
Ba11	Bassen	Outcrop	Longyear	Paleocene	-	137.5	0.58	0.59	0.68
Ba21	Bassen	Outcrop	Longyear	Paleocene	-	32.3	0.44	0.68	0.68
Ba32	Bassen	Outcrop	Longyear	Paleocene	-	3.0	0.65	0.63	0.68
Br12	Breirosa	BH4-2009	Longyear	Paleocene	314.9	95.5	0.54	0.66	0.80
Br16	Breirosa	BH4-2009	Longyear	Paleocene	315.7	24.0	0.55	0.66	0.80
L9	Lunckefjellet	BH15-2011	Longyear	Paleocene	258.3	210.0	0.63	0.59	0.78
L14	Lunckefjellet	BH15-2011	Longyear	Paleocene	259.0	140.0	0.62	0.62	0.78
L20	Lunckefjellet	BH15-2011	Longyear	Paleocene	259.6	80.0	0.44	0.70	0.78
L27	Lunckefjellet	BH15-2011	Longyear	Paleocene	260.3	10.0	0.63	0.63	0.78
C3	Colesdalen	BH3-2008	Longyear	Paleocene	274.4	147.5	0.51	0.79	0.88
C6	Colesdalen	BH3-2008	Longyear	Paleocene	275.1	80.5	0.69	0.65	0.88
C9	Colesdalen	BH3-2008	Longyear	Paleocene	275.7	11.5	0.55	0.76	0.88
P1	Pyramiden	Outcrop	-	L. Carboniferous	-	-	0.56	0.85	0.98

Table 5.9. Comparing the *n*-alkanes + *n*-alkenes chain length distributions and VR of coals from the main areas under investigation

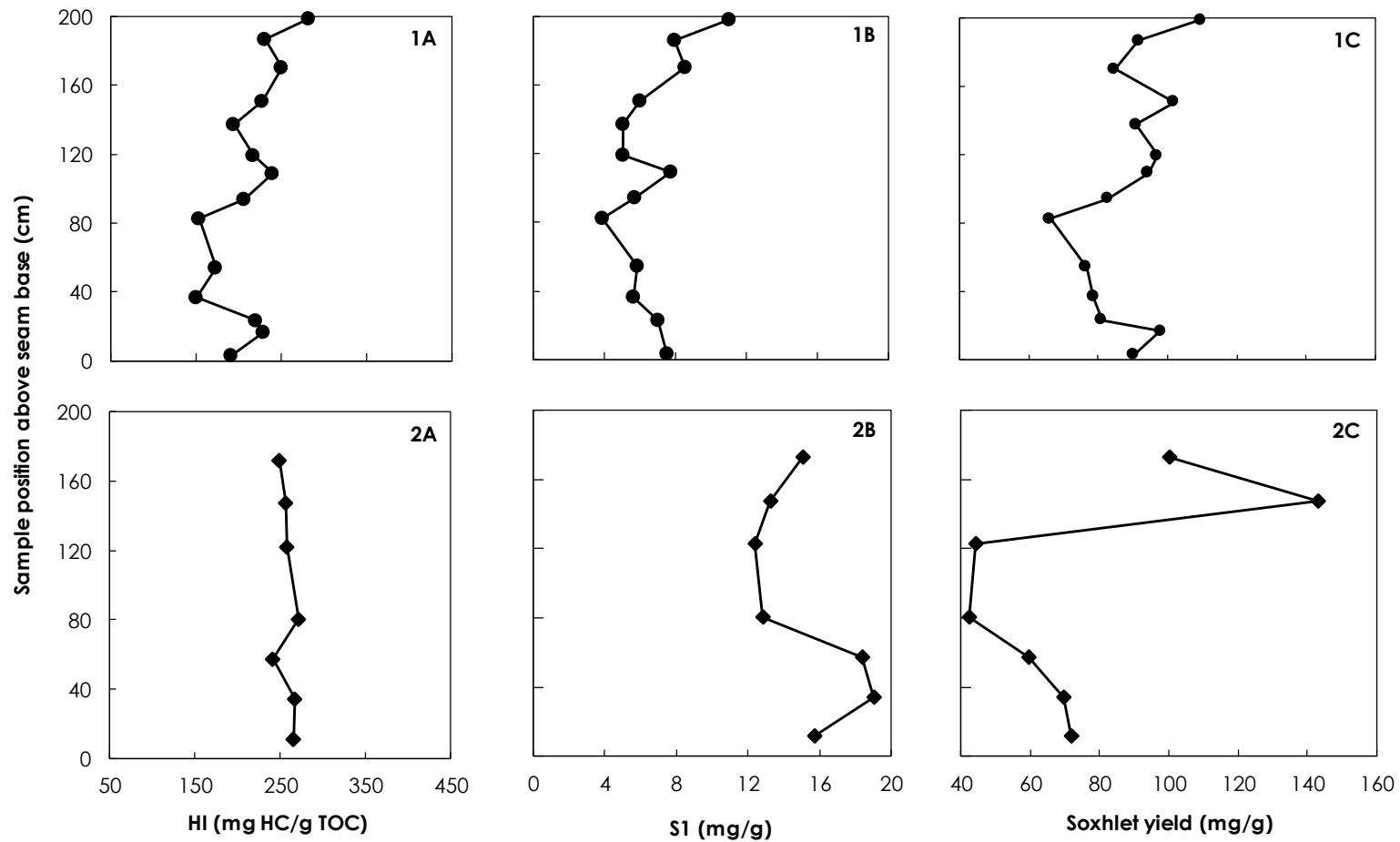


Figure 5.22. Comparing HI, S1 and Soxhlet yield in the Longyear seam in Bassen (top), and the Sputnik seam in Colesdalen (bottom). Note: Bassen show similar up-seam trends, but dissimilar trends observed between HI and S1/Soxhlet yield in Colesdalen. Estimated unsuppressed VR are 0.68 and 0.88% R_o in Bassen and Colesdalen respectively (Chapter 4).

Scatter plots (not shown) of HI vs S1, and HI vs Soxhlet yield showed moderate correlations for the Bassen (north-east basin margin) samples ($R^2 = 0.66$ and 0.61 respectively). Correlations are poorer in the Lunckefjellet (eastern basin margin) samples ($R^2 = 0.58$ and 0.47 for HI vs S1 and HI vs. Soxhlet yield respectively), while samples down-dip of basin margins (Breinosa) and around basin center (Colesdalen) showed no correlation for either HI vs S1, or HI vs Soxhlet yield ($R^2 \leq 0.02$). Below $0.70\% R_o$, generated bitumen has neither been converted into oil nor expelled from the coal, and remains in the coal porosity (mainly micro-, and nano-porosity), or absorbed within the coal structure and gives a better indication of primary hydrocarbon potential (e.g. Carr and Williamson, 1990); this explains the better correlation observed at Bassen where estimated unsuppressed VR is $0.68\% R_o$. Above $0.70\% R_o$, oil generation from bitumen becomes intense, and the coal pore structure becomes saturated leading to oil expulsion from perhydrous coals. Consequently, there is a poorer correlation in Lunckefjellet (Unsuppressed VR = $0.78\% R_o$), and no correlation in Breinosa (Unsuppressed VR = $0.80\% R_o$) and Colesdalen (Unsuppressed VR = $0.88\% R_o$). It is therefore concluded that the low Soxhlet yield measured in Breinosa and Colesdalen is likely due to expulsion.

Jones *et al.* (1986) stated that maceral composition is one of the two most important characteristics of coals that determine aromaticity (the other being maturity). Therefore, as the aromaticity of coals generally increase from liptinites to vitrinites to inertinites (Zilm *et al.*, 1981; Pugmire *et al.*, 1982; Davis *et al.*, 1985; Axelson and Parkash, 1986; Carr and Williamson, 1990), the relatively low Soxhlet yield in the Colesdalen area may be related to their much higher inertinite contents as inferred from coal maceral analysis (Section 5.2.1).

The main findings from this section are summarised as follows:

- The cross-plots of T_{\max} against BI and QI provide empirical insights of the natural maturation process from the eastern/north-eastern CTB margins to center, including the maturity thresholds for oil generation and expulsion.
- The Bassen samples are yet to generate significant amounts of oil, the Lunckefjellet samples are at peak oil generation/onset of oil expulsion, while the Breinosa and Colesdalen coals are already expelling oil.
- The Lunckefjellet coals give the best indication of oil expulsion threshold, and as such, will provide a more realistic indication of the petroleum generative potential and the maturity at which oil expulsion occurs in the CTB.
- Coals with greater marine influence, and are consequently more perhydrous, will commence oil generation/expulsion earlier than the less perhydrous coals.
- The lower Soxhlet yield at Breinosa and Colesdalen is due to losses associated with expulsion. However, the higher inertinite content in Colesdalen may be a slight limiting factor on the oil potential of coals in this area.

Oil expulsion is further discussed in Section 5.6.3, while controls on oil potential variation in the CTB are examined in detail in Chapter 6.

5.6. Lower Carboniferous vs Tertiary Coals in Spitsbergen – Petrography, Maturity, Oil Generation and Expulsion

It has been noted in Section 1.1 that there are two main types of oil-prone coals in Svalbard; the Lower Carboniferous and the Tertiary coals. Abdullah *et al.* (1988) investigated the Lower Carboniferous coals in Central Spitsbergen (Figure 1.1), and consequently identified two groups on the basis of depositional environment;

- a) The algal cannel coals from the Birger Johnsonfjellet Mb. inferred to be deposited under lacustrine conditions in highly eutrophic, freshwater lakes.
- b) Coals from the Hoelbreen Member are richer in vitrinite, sporinite and inertinite, suggesting deposition as peat-swamps or flood plain deposits.

This section involves a petrographic and geochemical assessment of a L. Carboniferous coal from Pyramiden (Figures 1.1 and 5.23), which is ~50 km north of Longyearbyen in Central Spitsbergen, to allow comparison with the two groups of L. Carboniferous coals identified by Abdullah *et al.* (1988), and thus leading to depositional environment assessment of the Pyramiden coal. Determination of depositional environment will lead to comparison of oil potential and sources of oil-proneness between the Lower Carboniferous and Tertiary samples.

5.6.1. Petrographic Description and Maceral Distribution

Maceral analysis shows the L. Carboniferous coal contains 46.6, 30.9 and 22.5 vol % mmf respectively of vitrinite, inertinite and liptinite group macerals (Table 5.10); this is similar to the maceral distribution of coals from the Hoelbreen Member (Figure 5.23) as reported by Abdullah *et al.* (1988). The absence of alginite in this coal suggests it belongs to the vitrinite-rich, as opposed to the alginite-rich coals of the L. Carboniferous. The vitrinite content of the Pyramiden coal (46.6 vol % mmf) is much lower than those of the Tertiary coals (mean values between 79.6 – 93.1 vol % mmf; Tables 5.1 and 5.3) and are dominated by very weakly fluorescing

to non-fluorescing collotelinite and collodetrinite (Figure 5.24). The Tertiary coals on the other hand, bear abundant strongly (relatively) fluorescing vitrinite group macerals, including collodetrinite and corpogelinite (Figures 4.1, 5.2, 5.12 and 5.18). The liptinite content of the L. Carboniferous coal is much higher (22.5 vol % mmf) compared to the Tertiary coals (mean values between 1.9 – 12.0 vol % mmf; Tables 5.1 and 5.3), and are dominated by sporinite (10.5 vol % mmf) with abundant megaspores (Figures 5.25 and 5.26), which is typical of Palaeozoic coals but rarely found in Mesozoic and Cenozoic coals (Taylor *et al.*, 1998). The inertinite contents of the L. Carboniferous coal (30.9 vol % mmf) is higher than the values seen in the Tertiary coals (mean values between 4.4 – 18.6 vol % mmf), and it is dominated by semifusinite, with significant amounts of fusinite, micrinite and inertodetrinite (Table 5.10). The relatively high micrinite contents of the Pyramiden coal is consistent with reports that micrinite is generally higher in the Carboniferous compared to Permian and younger coals (ICCP, 1998).

Macerals	Vol %
Vitrinite	41.0
Collotelinite	16.4
Collodetrinite	16.0
Vitrodetrinite	7.6
Corpogelinite	1.0
Inertinite	27.2
Fusinite	6.6
Semifusinite	10.4
Micrinite	3.8
Macrinite	0.2
Inertodetrinite	6.2
Liptinite	19.8
Sporinite	9.2
Cutinite	4.2
Resinite	5.4
Liptodetrinite	1.0
Mineral matter	12.0

Table 5.10. Maceral composition of the Lower Carboniferous coal sample from Pyramiden

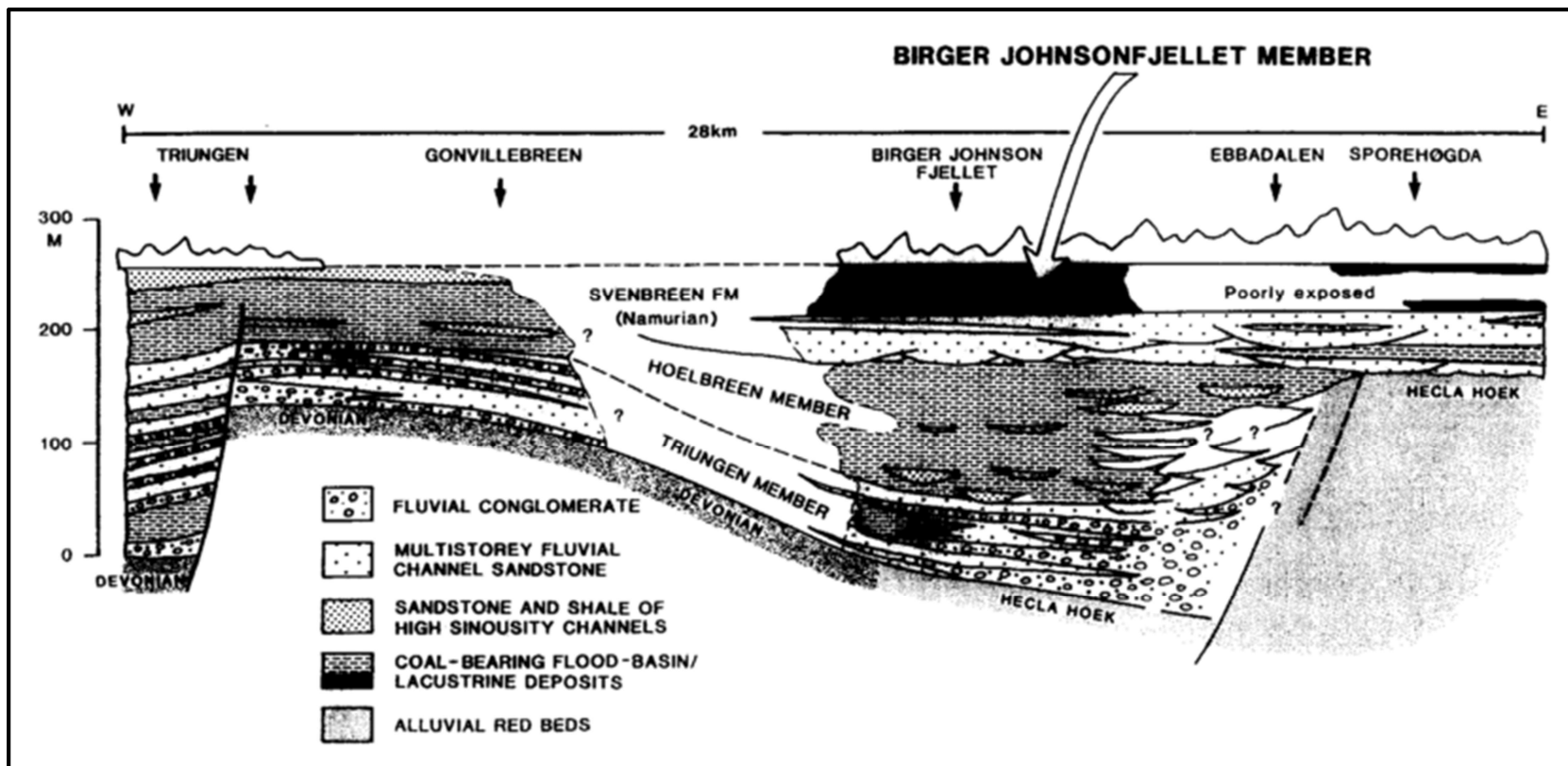


Figure 5.23. An east-west cross section through the Lower-Middle Carboniferous of Central Spitsbergen (Modified from Abdullah *et al.*, 1987)

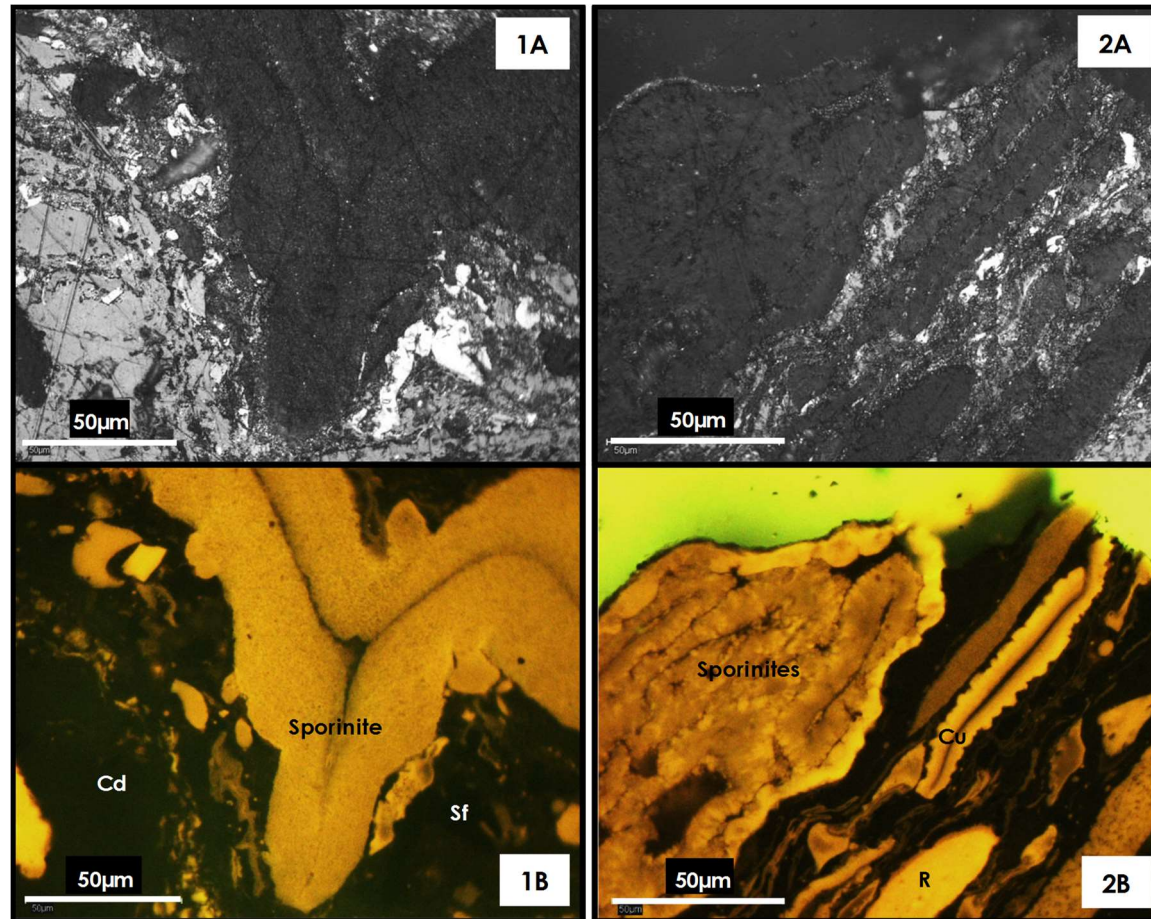


Figure 5.25. Photomicrographs of oil-prone Lower Carboniferous coal from Pyramiden, Spitsbergen. A) White light, B) Blue light. Note: Weakly fluorescing vitrinite macerals and abundant liptinites indicating oil-proneness is due to liptinites group macerals. Detrital nature of coal will enhance oil migration and expulsion efficiency. Cd – collodetrinite, Sf – semifusinite, R – resinite, Cu – cutinite

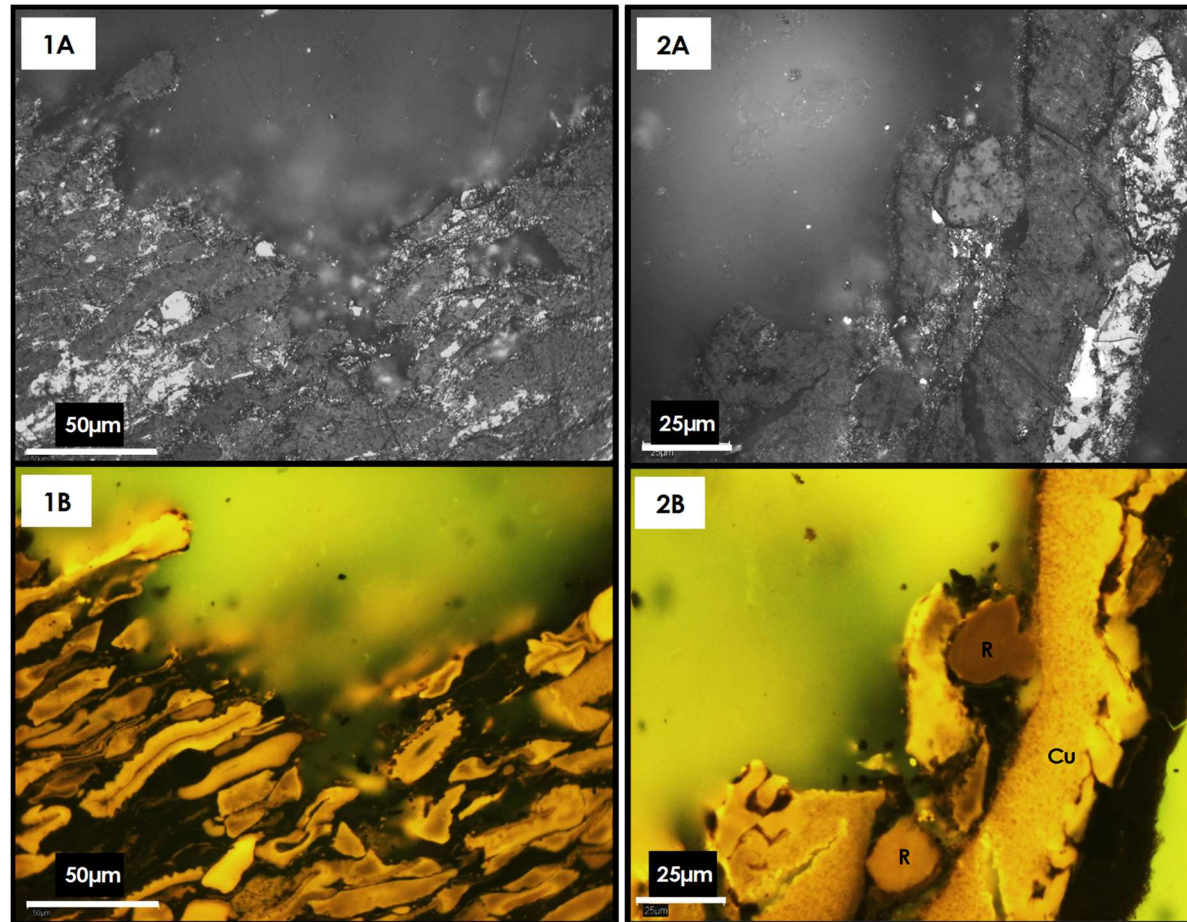


Figure 5.26. Photomicrographs of oil-prone Lower Carboniferous coal from Pyramiden, Spitsbergen. A) White light, B) Blue light. Note: Abundant liptinitic macerals (with sporinites dominating) indicates oil-proneness is due to liptinitic group macerals. Micrinites infilling voids in spores and in between macerals are indicative of oil generation. Detrital nature of coal enhances oil migration and expulsion efficiency. R – resinite, Cu - cutinite

The Lower Carboniferous humic coals in Central Spitsbergen are postulated to have been deposited as peat-swamps or flood plain deposits (Abdullah *et al.*, 1988). Thompson *et al.* (1985) suggested that re-working coastal plain peats to form drift deposits along coastal margins was a mechanism of liptinites enrichment. These references probably explain why the Carboniferous coals shows high concentration of liptinites and detritus, as a high concentration of detritus reflects a hypautochthonous depositional environment (Taylor *et al.*, 1998). Micrinite infills partially open cell lumens of spores in the Pyramiden coal; these fine granular macerals together with other detrital macerals and mineral matter, form a detrital groundmass for the majority of the particles (Figures 5.25 and 5.26). This feature bears a striking resemblance to Lower Carboniferous coals belonging to the Hoelbreen Member (Figures 6 and 7 of Abdullah *et al.*, 1988), and thus confirms the Pyramiden sample is of the Hoelbreen Member.

5.6.2. Coal Maturity

The T_{max} for the Pyramiden coal (440 °C; Table 5.11) is comparable to reported values from the Hoelbreen Member (438 – 444 °C, Abdullah *et al.*, 1988); however, the measured VR of the Pyramiden coal (0.85% R_o) is significantly lower than reported values from the Hoelbreen Member (0.94 – 0.95% R_o , Abdullah *et al.*, 1987). VR Suppression arising from the high liptinite content may arise due to bitumen-expulsion from liptinite into the vitrinite structure; thus, measured VR may be suppressed by bitumen enrichment as indicated by the fluorescing nature of the vitrinites (albeit a weak fluorescence) and the rather broad range of VR measurements, with somewhat bi-modal histogram (Figure 5.27). Applying the mean VR value (0.85% R_o) in the Lo (1993) method for correcting suppressed VR (Figure 4.16) gives a true VR of around 0.98% R_o ; this is slightly higher than values

reported by Abdullah *et al.* (1987) possibly because these workers did not account for VR suppression.

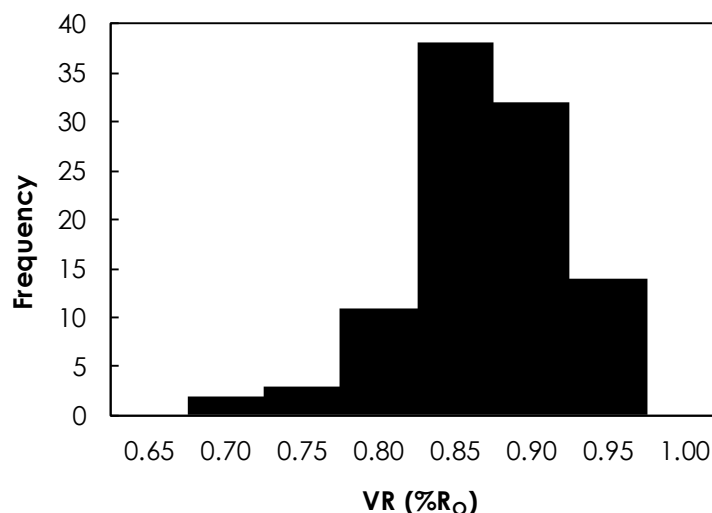


Figure 5.27. VR histogram of the Lower Carboniferous coal from Pyramiden. STDEV = 0.05. Note: the wide spread of measurements suggests the vitrinites bear varying degrees of bitumen impregnation which suggest VR suppression.

5.6.3. Oil Generation and Expulsion

Rock-Eval data of the Pyramiden coal (Table 5.11) suggest a relatively higher oil potential compared to the Hoelbreen Member coals reported in Abdullah *et al.* (1987), but show similar range of values as the Tertiary coals (Tables 5.4 and 5.5). Although the Soxhlet yield of the Pyramiden coal could not be compared to those of the L. Carboniferous coals in Abdullah *et al.* (1988), the relatively low Soxhlet yield of this coal (58 mg/g) is unexpected.

It has been suggested that HI is not always indicative of oil potential as enhanced hydrogen content will only increase the capacity to generate oil if the hydrogen is incorporated as long aliphatic chains (Petersen *et al.*, 2009 and references within). Also, alginite, cutinite, and suberinite, contain a higher proportion of aliphatic moieties in their structure compared to other liptinites such as sporinite

and resinite and are, therefore, more oil-prone (e.g. Isaksen *et al.*, 1998; Wilkins and George, 2002). Given that sporinite and resinite are the most abundant macerals of the liptinite group in the Pyramiden coal (Table 5.10); the low Soxhlet oil yield may perhaps be due to lower proportions of long-chain aliphatics. However, the Hoelbreen Member coals reportedly display a high relative abundance of long chain aliphatics (Abdullah *et al.*, 1987). The $C_{21}-C_{33}/C_8-C_{20}$ ratio from Py-GC for *n*-alkanes + *n*-alkenes chain length distribution shows value of 0.56 for the Pyramiden coal (Table 5.9, Figure 5.27); this is similar to mean values for the Tertiary coals in Bassen (0.54), Lunckefjellet (0.58), Breinosa (0.55) and Colesdalen (0.59) (Table 5.9). Thus the relatively low Soxhlet yield for the Pyramiden coal is not due to lower concentrations of long-chain aliphatics.

The occurrence of micrinite in these coals is an indication of oil generation (e.g. Taylor *et al.*, 1998). At the onset of expulsion, the contribution of initial bitumen should decrease (Killops *et al.*, 1998). Also, the original HI may have been significantly higher given that as coalification progresses in coals, HI increases up to a maximum (HI_{max}) prior to the onset of expulsion (i.e. $\sim 0.70\% R_o$), and then decreases (Durand and Paratte, 1983; Sykes and Snowdon, 2002; Petersen, 2005). Considering the Pyramiden coal is well within the main oil window ($VR \sim 0.98\% R_o$); therefore, the relatively low Soxhlet yield is likely due to losses associated with expulsion, and possibly weathering (albeit to a much lesser extent) as this is not a fresh sample. Further discussion on weathering is covered in Chapter 6 under controls on oil potential.

Measurements (dwc basis)	L. Carboniferous - Pyramiden	CTB
S1 (mg/g)	14.1	12.0
S2 (mg/g)	248.3	220.4
TOC (%)	71.1	73.4
T _{max} (°C)	440.0	436.1
HI (mg HC/g TOC)	350.0	300.5
OI (mg CO+CO ₂ /g TOC)	0.0	10.1
Soxhlet yield (mg/g)	5.8	105.6

Table 5.11. Comparing geochemical data between the L. Carboniferous and Tertiary coals in Spitsbergen. Note: Data shown for the Tertiary coals is the mean values from 68 samples from the Askeladden, Svarteper, Longyear, Verkny and Sputnik seams. OI of zero suggest values are perhaps too low to be measured.

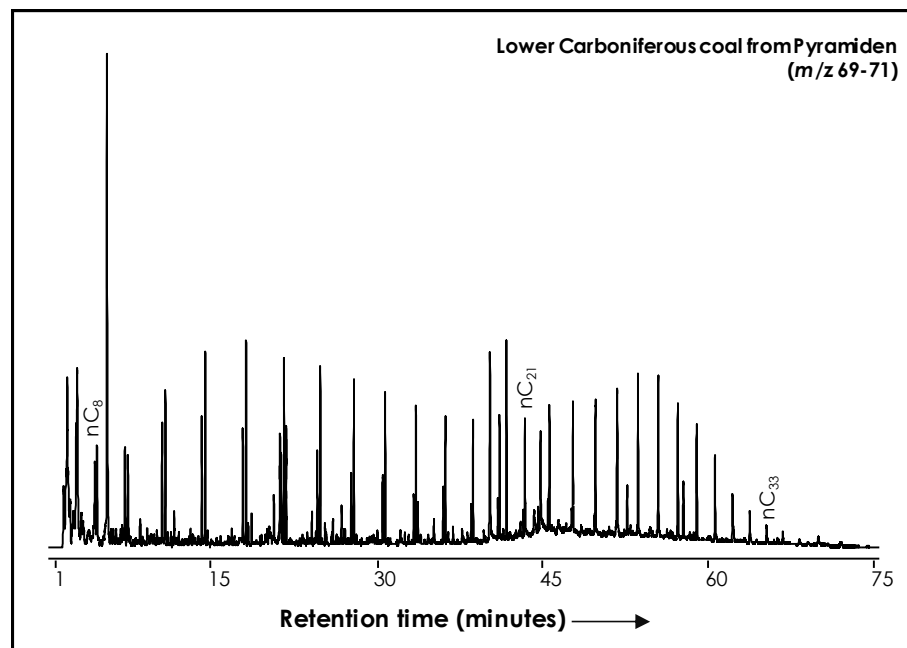


Figure 5.28. *m/z* 69-71 from the Py-GCMS analysis of the Lower Carboniferous coal from Pyramiden. Note: Ratio $C_{21}-C_{33}/C_8-C_{20} = 0.56$

It is believed that the true control on hydrocarbon release from coal is expulsion rather than generation, and the main reason for poor expulsion in coals is the adsorption of oil on the organic macromolecule (e.g. Killops *et al.*, 1998; Wilkins and George, 2002), which may be overcome if;

- Coal seams are thin and interbedded with clastic sediments, preferably with higher permeabilities, and or
- If the coals are very hydrogen-rich and generate large quantities of oil

The expulsion threshold provides a link between generation and expulsion, and suggests that coals from Breinosa, Colesdalen (Figure 5.17) and Pyramiden (Figure 5.29) are already expelling oil.

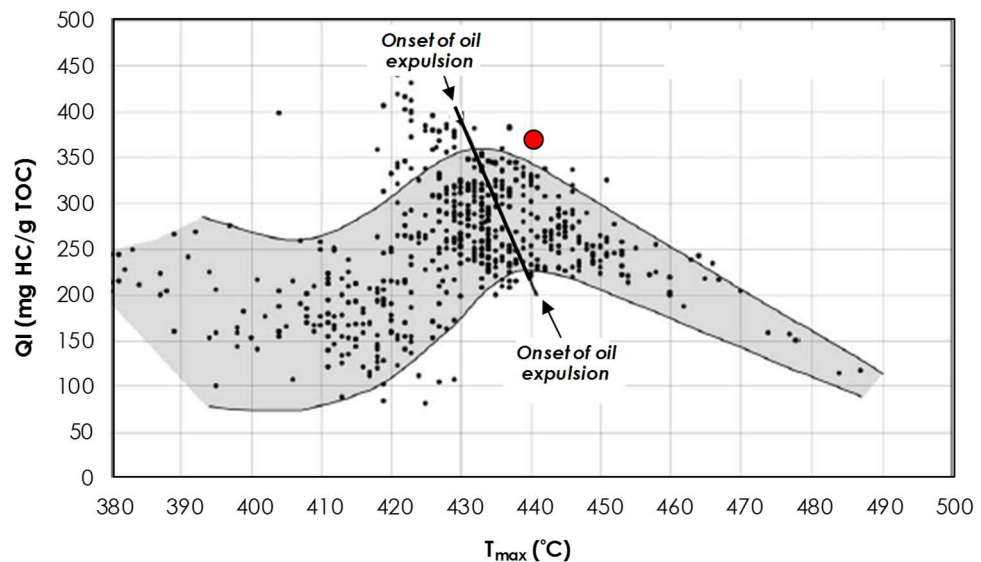


Figure 5.29. T_{max} vs QI plot of the Pyramiden coal (red plot) (Modified from Sykes and Snowdon, 2002). Note: Pyramiden coal is beyond the threshold for oil expulsion. Black dots = New Zealand Late Cretaceous - Cenozoic humic coals of peat to low Volatile bituminous rank

Based upon palaeotemperature, Wilkins and George (2002) summarised a rule of thumb on whether oil or gas will be produced; according to this rule, if generation occurs between 120 and 150 °C, oil may be a product, but above 150 °C cracking becomes dominant and gas is the likely result. It is borne in mind that for perhydrous coals, calculations of palaeotemperature are most likely to be subject to error if modelling is carried out against VR (i.e. due to suppression); however, in

Chapter 4, peak burial temperature of up to 125 °C is estimated for the Tertiary coals in Colesdalen after correcting for VR suppression. This supports the idea that oil expulsion is likely to have occurred in that area of the CTB. With regards to the Lower Carboniferous coals which belong to the Hoelbreen Member, considering they are more thermally mature than the Tertiary coals, peak burial temperature would probably be in excess of 125 °C, which parallels the palaeotemperature rule of thumb and supports loss of oil through expulsion. The high detrital contents of the Tertiary and Lower Carboniferous coals in Spitsbergen would aid primary migration of oil, and enhance expulsion efficiency (Stout, 1994).

The main findings in this section is summarised as follows:

- The Lower Carboniferous and Tertiary coals are all within the main oil window, and the oil window maturity of the L. Carboniferous coal suggests that it has not been buried that much deeper than the Tertiary coals, or the Central Tertiary basin had a higher temperature gradient.
- Both the Carboniferous and Tertiary coals are oil-prone, and display similar range of oil potential.
- The oil-proneness of the L. Carboniferous coal is due to enrichment in liptinites, with sporinites being the main contributors, whereas in the Tertiary coals, the oil is mainly sourced from perhydrous vitrinites.
- The L. Carboniferous coal may have lost significant amounts of oil through expulsion; this is believed to be the case with the Tertiary coals in Breinosa and Colesdalen.

5.7. Retorting Potential of the CTB Coals

5.7.1. Retorting Estimates

44 coals were selected to examine the retorting potential of the CTB coals under study. Samples were selected to;

- Reflect the four main maturity levels (i.e. from Bassen, Lunckefjellet, Breinosa and Colesdalen).
- Reflect the vertical variation in sulphur contents from base to top of seam because of the marine influence on oil potential.
- Reflect the general increase in marine influence (and consequently oil potential) from the stratigraphically older to younger Firkanten Formation coals. Hence, samples were selected from all five oil-prone seams (Askeladden, Svarteper, Verkny, Longyear and Sputnik).

This section firstly examines the bulk retorting yield estimates from all areas under study, and compares yield estimates between and within coal seams. The quality of retorting oil and efficiency of adopted retorting technique are also assessed leading to the hydrocarbon resource estimate of the CTB coals.

5.7.1.1. Retorting Yields in Various Areas

On a dwc basis, the maximum yield from all areas range from 90 mg/g in Bassen, to 240 mg/g in Lunckefjellet (Table 5.12), and importantly replicates documented retorting yields from Svalbard coals (Hoel, 1925; Wang, 2011). The highest average bulk yield of 160 mg/g dwc was measured in Lunckefjellet (Figure 5.30). At Breinosa and Colesdalen, average bulk yields of 140 and 100 mg/g dwc were respectively measured. Lowest average bulk yield (80 mg/g dwc) was measured in Bassen. Residual coke ranges between 600 – 750 mg/g of starting material

across all areas. Retorting yields increased considerably on daf basis with average bulk values of 170, 165, 120 and 80 mg/g respectively measured in Lunckefjellet, Breinosa, Colesdalen and Bassen.

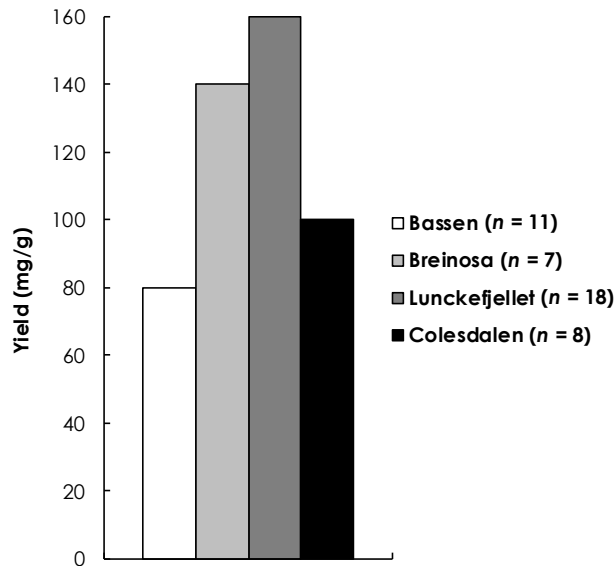


Figure 5.30. Mean bulk retorting yields from all areas of the CTB under study. Note: standard deviation of 15, 44, 53 and 36 mg/g dwc at Bassen, Breinosa, Lunckefjellet and Colesdalen respectively

5.7.1.2. Comparing Retorting Yields between the Askeladden, Svarteper, Longyear, Verkny and Sputnik Seams in Various Areas

In Breinosa BH4-2009, the top 20 cm section from Askeladden seam, the basal 23 cm section from Svarteper seam and 5 sections (averaging 18.5 cm) from the Longyear seam were retorted. The Askeladden coal displayed highest retorting yield of 190 mg/g dwc. The Svarteper coal produced 120 mg/g dwc while bulk yield of 130 mg/g dwc was obtained from the Longyear seam (Table 5.12).

The Lunckefjellet coals were sampled from four borehole locations; 1 sample per borehole location was selected for retorting from the Svarteper seam while for the

Longyear seam, 11 samples were selected from BH15-2011 location and 1 sample each from the other three borehole locations. Bulk yield estimates of 180 mg/g and 150 mg/g dwc were measured respectively for the Svarteper and Longyear seams (Table 5.12).

In Colesdalen, 1 sample from the Verkny seam which may be the Svarteper seam equivalent, and 7 samples from the Sputnik seam which is possibly the Longyear seam equivalent were retorted. Bulk yields of 100 mg/g dwc were obtained from each coal seam (Table 5.12).

In Bassen, only the Longyear coals have been sampled, hence comparisons between seams could not be made; retorting yields averaged 80 mg/g dwc for 11 samples (Table 5.12).

5.7.1.3. Comparing Retorting Yields within the Longyear and Sputnik Seams in Various Areas

Within the Longyear seam, the Lunckefjellet coals with the highest bulk yields, generally display a widest range of 90 – 240 mg/g dwc (Table 5.12 and Figure 5.31). At Colesdalen and Breinosa, yields range between 70 – 160 and 60 – 130 mg/g dwc respectively. In Bassen, where the lowest bulk yield was measured, the lowest range was also observed (60 – 90 mg/g dwc). The retorting yield from base to top of seam generally display similar trend of greater potential within the upper Longyear seam (Figure 5.31) as observed in the Soxhlet yields in Figure 5.15. However, variations such as observed in Colesdalen where Soxhlet yield is greater than retorting yield within the upper seam, is an indication that significant amounts of liquid hydrocarbon potential of the coals are not realised under current method.

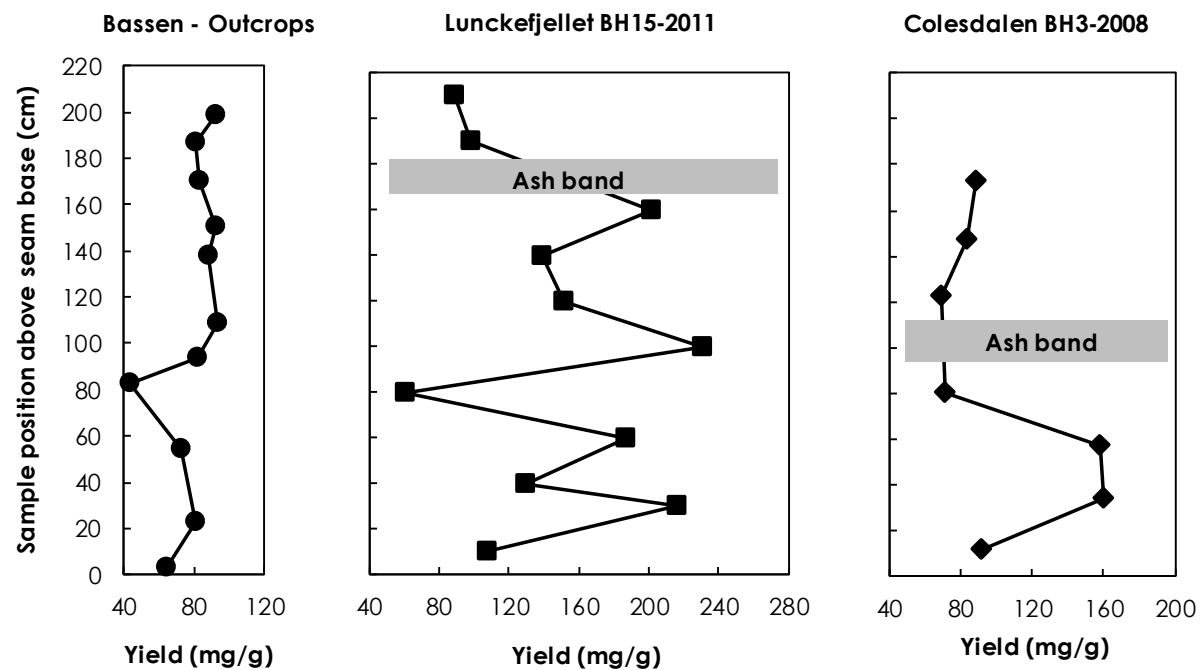


Figure 5.31. Comparing the retorting yields from base to top of seam for the Longyear coals in Bassen and Lunckefjellet BH15-2011, and Sputnik coals in Colesdalen BH3-2008. Measurements are on dwc basis. Note: transition to greater liquid hydrocarbon potential in upper seam is not clearly displayed particularly in Colesdalen; this suggest significant liquid hydrocarbon potential is not realised with current method

Sample ID	Area	Location and sample type	Seam	Drill depth (m)	Height above seam base (cm)	Retorting yield (mg/g dwc)	Retorting yield (mg/g daf)	Rock-Eval S1+S2 (mg/g dwc)
Ba1	Bassen	Outcrop	Longyear	-	198.5	92.4	93.7	223.6
Ba3	Bassen	Outcrop	Longyear	-	186.5	80.8	81.9	179.2
Ba6	Bassen	Outcrop	Longyear	-	170.0	82.5	83.7	195.2
Ba9	Bassen	Outcrop	Longyear	-	150.5	92.6	93.8	174.4
Ba11	Bassen	Outcrop	Longyear	-	137.5	87.8	90.3	145.6
Ba16	Bassen	Outcrop	Longyear	-	109.0	93.3	95.3	185.7
Ba19	Bassen	Outcrop	Longyear	-	94.0	82.0	82.9	152.1
Ba21	Bassen	Outcrop	Longyear	-	82.3	43.2	45.6	113.0
Ba24	Bassen	Outcrop	Longyear	-	54.0	72.0	72.9	135.4
Ba29	Bassen	Outcrop	Longyear	-	23.0	80.4	82.1	172.1
Ba32	Bassen	Outcrop	Longyear	-	3.0	64.0	65.0	152.4
Br1	Breinosa	BH4-2009	Askeladden	298.4	46.5	188.7	225.8	285.3
Br8	Breinosa	BH4-2009	Svarteper	301.2	11.5	122.7	163.4	241.8
Br11	Breinosa	BH4-2009	Longyear	314.7	116.0	130.2	162.4	225.9
Br12	Breinosa	BH4-2009	Longyear	314.9	95.5	182.0	197.4	302.1
Br13	Breinosa	BH4-2009	Longyear	315.2	74.5	92.9	111.2	223.1
Br16	Breinosa	BH4-2009	Longyear	315.7	24.0	163.7	185.3	256.4
Br17	Breinosa	BH4-2009	Longyear	315.8	8.0	75.3	106.9	211.1
L7	Lunckefjellet	BH15-2011	Svarteper	246.6	20.0	161.3	182.5	260.7
L9	Lunckefjellet	BH15-2011	Longyear	258.3	210.0	88.4	92.2	194.9
L11	Lunckefjellet	BH15-2011	Longyear	258.5	190.0	98.3	111.2	200.2
L12	Lunckefjellet	BH15-2011	Longyear	258.8	160.0	202.0	215.7	272.9
L14	Lunckefjellet	BH15-2011	Longyear	259.0	140.0	139.4	140.7	257.3
L16	Lunckefjellet	BH15-2011	Longyear	259.2	120.0	151.0	155.2	385.0
L18	Lunckefjellet	BH15-2011	Longyear	259.4	100.0	230.3	236.2	368.8
L20	Lunckefjellet	BH15-2011	Longyear	259.6	80.0	60.3	90.4	140.6
L22	Lunckefjellet	BH15-2011	Longyear	259.8	60.0	186.7	190.2	305.5
L24	Lunckefjellet	BH15-2011	Longyear	260.0	40.0	129.4	157.2	240.2
L25	Lunckefjellet	BH15-2011	Longyear	260.1	30.0	216.3	222.6	350.8
L27	Lunckefjellet	BH15-2011	Longyear	260.3	10.0	107.8	110.3	345.4
L32	Lunckefjellet	BH10-2009	Svarteper	55.1	10.5	175.9	202.0	298.3
L36	Lunckefjellet	BH10-2009	Longyear	70.4	10.5	138.5	145.6	240.1
L38	Lunckefjellet	BH10-2007	Svarteper	237.0	20.5	140.4	181.3	226.2
L39	Lunckefjellet	BH10-2007	Longyear	247.1	148.5	187.7	195.3	287.4
L45	Lunckefjellet	BH6A-2007	Svarteper	210.4	110.5	237.2	255.8	278.5
L52	Lunckefjellet	BH6A-2007	Longyear	224.0	87.5	149.3	153.6	-
C1	Colesdalen	BH3-2008	Verkny	258.2	16.0	99.3	143.6	156.0
C2	Colesdalen	BH3-2008	Sputnik	274.1	172.5	88.4	92.0	221.9
C3	Colesdalen	BH3-2008	Sputnik	274.4	147.5	83.4	90.0	218.2
C4	Colesdalen	BH3-2008	Sputnik	274.6	122.5	69.2	83.0	197.8
C6	Colesdalen	BH3-2008	Sputnik	275.1	80.5	71.6	94.6	172.1
C7	Colesdalen	BH3-2008	Sputnik	275.3	57.5	157.8	160.8	226.8
C8	Colesdalen	BH3-2008	Sputnik	275.5	34.5	160.2	168.8	249.3
C9	Colesdalen	BH3-2008	Sputnik	275.7	11.5	92.1	96.9	233.9

Table 5.12. Comparing the Retorting yields and Rock-Eval S1+S2 contents of 44 CTB coals under study. (dwc = dry whole coal, daf = dry ash free)

In summary, the Lunckefjellet coals display the greatest retorting potential relative to all other areas of the CTB investigated, while retorting potential between seams appear to be in the order of Askeladden>Svarteper>Longyear which is generally consistent with Soxhlet yield, HI and sulphur content and the distribution of oil-prone macerals, although more samples from the Askeladden seam covering various locations needs to be assessed to confirm this. Residual coke ranges between 60 – 75 % of starting material in all locations.

5.7.2. How Effective is the Adopted Retorting Technique?

Retorting of coal is aimed at expelling the free hydrocarbons present, as well as generating hydrocarbons through thermal cracking of non-volatile organic matter, and thus theoretically represents the maximum hydrocarbon potential. Rock-Eval data supports oil generation in coals and allow a quantitative estimation of hydrocarbon generation either in nature or during pyrolysis (Teichmüller and Durand, 1983). It has been noted that Rock-Eval S1 represents the amount of thermo-vaporized free hydrocarbons present in source rocks, while the Rock-Eval S2 represents the amount of hydrocarbons produced from the cracking of heavy hydrocarbons and from the thermal breakdown of kerogen in source rocks (e.g. Lafargue *et al.*, 1998); therefore, maximum hydrocarbon potential of the Firkanten Fm. coals can be represented as:

$$\text{Retorting yield} = \text{S1} + \text{S2} \quad (5.3)$$

A scatter plot of Retorting yields vs. S1+S2 (Figure 5.32) shows a moderate coefficient of determination ($R^2 = 0.65$); thus the effectiveness of the adopted retorting method was assessed using the above relationship. At Lunckefjellet BH15-2011 for example, Rock-Eval showed much greater yield compared to retorting (Figure 5.32). For all 44 coals investigated, bulk values of 130 and 220 mg/g dwt were respectively measured for retorting yield and Rock-Eval S1+S2 (Table 5.12). One might argue that this difference in yields partly resulted from the fact that the adopted retorting technique mainly measures liquid hydrocarbons whereas Rock-Eval accounts for both gaseous and liquid hydrocarbons; however, hydrocarbons released by pyrolysis in general are mostly liquid hydrocarbons (oil) up to maturity levels of about 1.5 % R_o ($T_{max} \sim 475$ °C) irrespective of the petrographic composition (Teichmüller and Durand, 1983), whereas maximum

T_{max} measured in the coals under study is 452 °C. During retorting of the CTB coals, blockage of sweep gas flow due to coal swelling often occurred; meaning some hydrocarbon products were not swept out of the reactor and did not arrive at the cold trap (Figure 3.6) for collection.

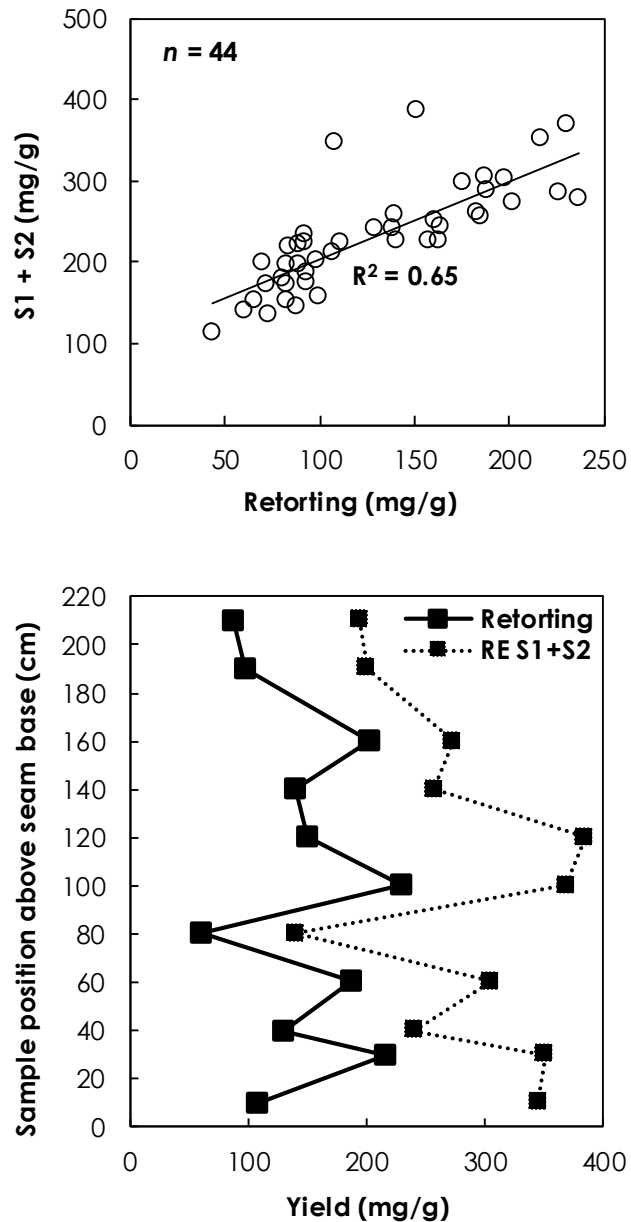


Figure 5.32. Retorting yields vs Rock-Eval S1+S2 contents for the coals under study. Top: Scatter plot of retorting yield vs Rock-Eval S1+S2 for Askeladden, Svarteper, Longyear, Verkny and Sputnik coals. Bottom: Comparing profiles of retorting yields and Rock-Eval S1+S2 of the Longyear seam from base to top of seam at Lunckefjellet BH15-2011 locality.

Coal swelling has been linked to increasing H/C ratio (Xie *et al.*, 2015) and perhydrous (oil-prone) vitrinites (Taylor, *et al.*, 1998) believed to be responsible for much of the oil-prone nature of the CTB coals. A comparison of Soxhlet yield and Free Swelling Index (FSI) shows similar trend (Figure 5.33), which means that samples with the greatest oil potential, shows the highest FSI and will be most affected by coal swelling and sweep gas blockage during retorting. This explains the relatively low retorting yields observed in the coals from the upper Longyear seam (Figures 5.28) despite their greater oil potential compared to samples from the lower parts of the seam (Sections 5.3.2 and 5.3.3), although the variations between coal swelling and sweep gas blockage relative to retorting yields is also influenced by coal ash content amongst other factors. Therefore, the significant difference in hydrocarbon contents measured between the Rock-Eval S1+S2 and retorting yields (bulk value ~90 mg/g dwc) is a clear indication that significant amount of liquid hydrocarbon potential of these coals is not achieved by current method.

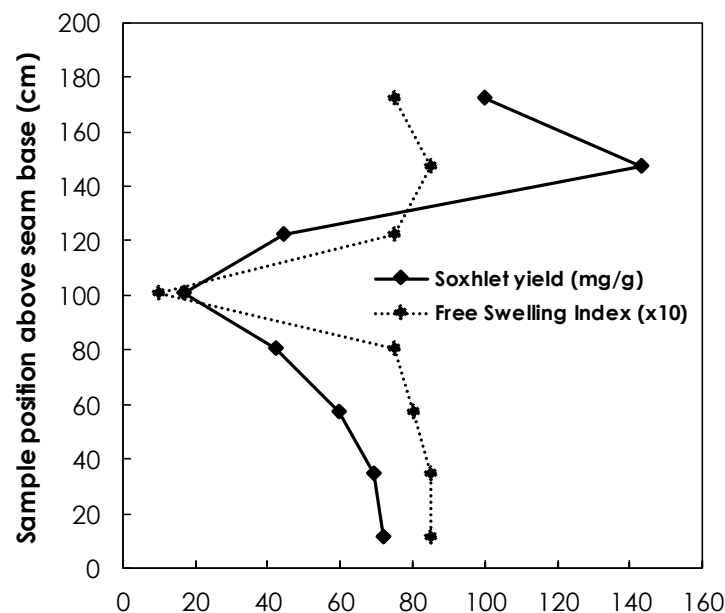


Figure 5.33. Soxhlet yield vs Free Swelling Index of the Sputnik coals under study (BH3-2008 locality). Note: FSI data provided by Store Norske Spitsbergen AS.

5.7.3. Qualitative Assessment of Retort Oils from the Firkanten Fm. Coals

The quality of the retorting oils from the Firkanten Fm. coals were assessed by fractionating the oils into aliphatic and aromatic hydrocarbons, and polar compounds (NSO), and then compared with the composition of 636 crude oils from around the world; this shows the retort oils are well within the range of global crude oils (Figure 5.34). The Lunckefjellet samples contain the highest amounts of aliphatic hydrocarbons in their retorting product (between 12.2 – 18.9 %), while the Breinosa and Colesdalen samples contain between 9.5 – 9.7 and 5.3 – 9.8 % aliphatics respectively (Table 5.13). Aromatic hydrocarbons contents are of similar amounts in all three locations (between 21.4 – 27.7, 21.7 – 27.3 and 19.57 – 28.1 % in Lunckefjellet, Breinosa and Colesdalen respectively). It is noted that the retorting oils from the Bassen samples were not fractionated as yields were much lower than the standard amounts (50 mg) required for the fractionation set-up. The higher aliphatic contents of retort oil seen in the Lunckefjellet samples, compared to the Breinosa and Colesdalen samples is further examined by comparing the aliphatic and aromatic compositions of the Soxhlet extracts at these locations. In Lunckefjellet, aliphatic hydrocarbon contents range between 4.5 – 12.8 % in the Soxhlet extracts, while values between 10.6 – 12.8 and 6.4 – 13.4 % were measured at Breinosa and Colesdalen respectively (Table 5.13). Aromatic hydrocarbons constitute between 16.8 – 27.5, 19.5 – 22.0 and 18.3 – 26.8 % respectively at all three locations. The reverse trend observed in the amounts of aliphatic hydrocarbons (in the retort oil and Soxhlet extracts) between the Lunckefjellet samples and the Breinosa/Colesdalen samples is believed to be due to maturity variation. Petroleum evolve toward greater thermodynamic stability during maturation (e.g. Peters and Moldowan, 1993); the Lunckefjellet samples, due to their marginal setting, contained more aliphatic hydrocarbons within their retorting product because they are less mature, and thus less thermally stable.

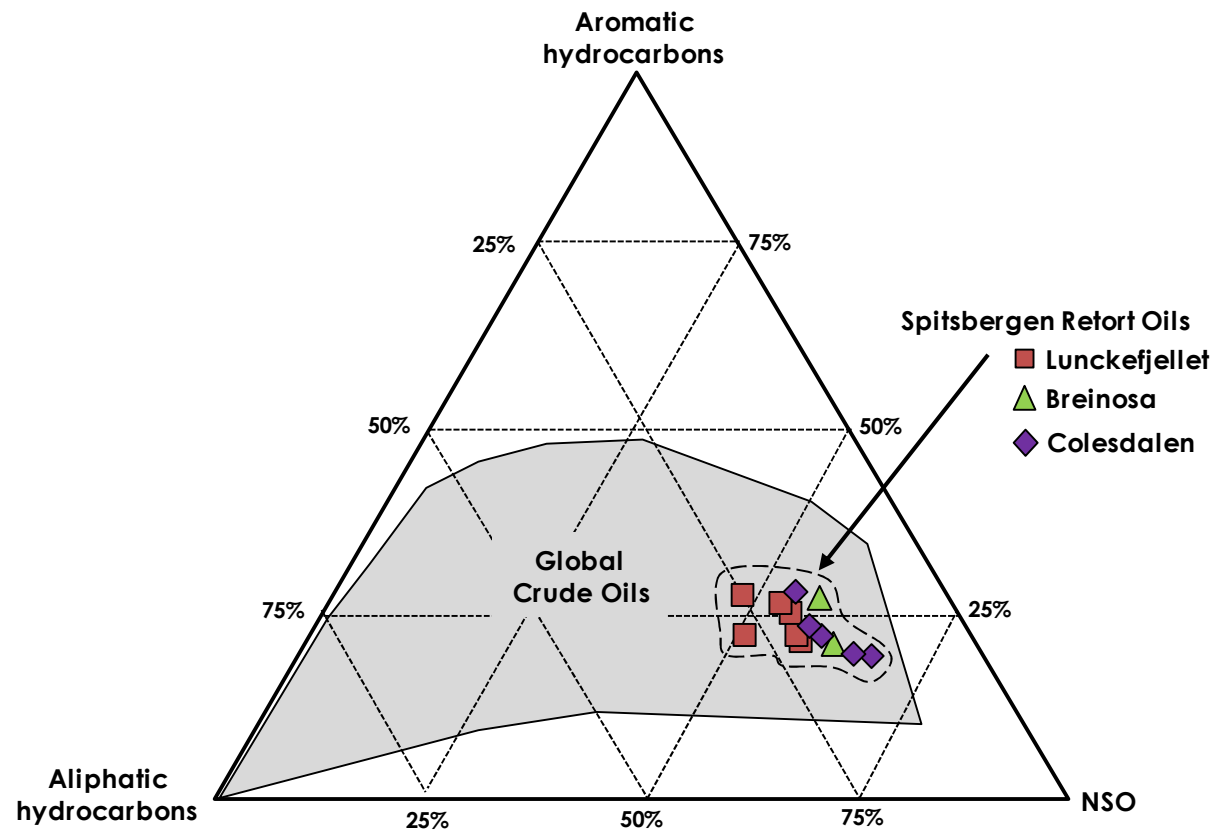


Figure 5.34. Spitsbergen retort oils vs global crude oils (modified from Lundegard and Knott, 2001). Note: Oils from retorting are within the range of global crude oils. Bassen retort yields are not assessed as yields were lower than the required 50 mg for fractionation.

Sample ID	Area	Location and sample type	Seam	Drill depth (m)	Sample position above seam base (cm)	Soxhlet extracts			Retorting		
						Aliphatic hydrocarbons (wt %)	Aromatic hydrocarbons (wt %)	Polar compounds (wt %)	Aliphatic hydrocarbons (wt %)	Aromatic hydrocarbons (wt %)	Polar compounds (wt %)
L12	Lunckefjellet	BH15-2011	Longyear	258.8	160	4.5	19.6	ND	14.8	27.7	49.0
L14	Lunckefjellet	BH15-2011	Longyear	259	140	10.4	22.9	ND	13.9	21.4	59.1
L16	Lunckefjellet	BH15-2011	Longyear	259.2	120	8.5	27.5	58.8	12.2	25.3	56.0
L21	Lunckefjellet	BH15-2011	Longyear	259.7	70	7.5	19.2	ND	12.4	22.3	58.0
L22	Lunckefjellet	BH15-2011	Longyear	259.8	60	9.3	16.8	ND	18.9	26.7	54.0
L25	Lunckefjellet	BH15-2011	Longyear	260.1	30	11.4	19.1	60.6	16.0	22.2	52.0
Br12	Breinosa	BH4-2009	Longyear	314.94	95.5	12.8	22.0	ND	9.7	27.3	58.3
Br16	Breinosa	BH4-2009	Longyear	315.65	24	10.6	19.5	ND	9.5	21.1	63.0
C2	Colesdalen	BH3-2008	Sputnik	274.13	172.5	6.4	18.3	53.2	6.9	19.5	68.3
C4	Colesdalen	BH3-2008	Sputnik	274.63	122.5	10.2	23.4	ND	7.1	19.9	66.0
C6	Colesdalen	BH3-2008	Sputnik	275.05	80.5	13.4	26.8	ND	9.8	28.1	55.0
C7	Colesdalen	BH3-2008	Sputnik	275.28	57.5	11.5	22.7	ND	5.3	22.2	61.0
C8	Colesdalen	BH3-2008	Sputnik	275.51	34.5	9.0	20.2	ND	8.7	23.6	59.0

Table 5.13. Aliphatic, aromatic and polar contents of Soxhlet extracts and oils from retorting. *ND* = not determined.

Consequently, the Lunckefjellet samples are more susceptible to cracking during retorting. On the other hand, the Breinosa samples which are down-dip of the eastern basin margin, and Colesdalen samples occurring in the basin center, contained less aliphatic material within their retorting product because they are more mature, more thermally stable, and comparatively less susceptible to cracking.

Improved oil quality by cracking during retorting is one of the advantages of retorting technique (Peters *et al*, 2005). Alkenes do not normally occur in crude oils but can occur as a result of laboratory pyrolysis (Peters and Moldowan, 1993). When the GC-MS TIC of retort oil and Soxhlet extracts were compared, the retort oil showed very high abundance of *n*-alkanes and *n*-alkenes doublets (Figure 5.35); this is a clear indication of hydrocarbon cracking and improved oil quality.

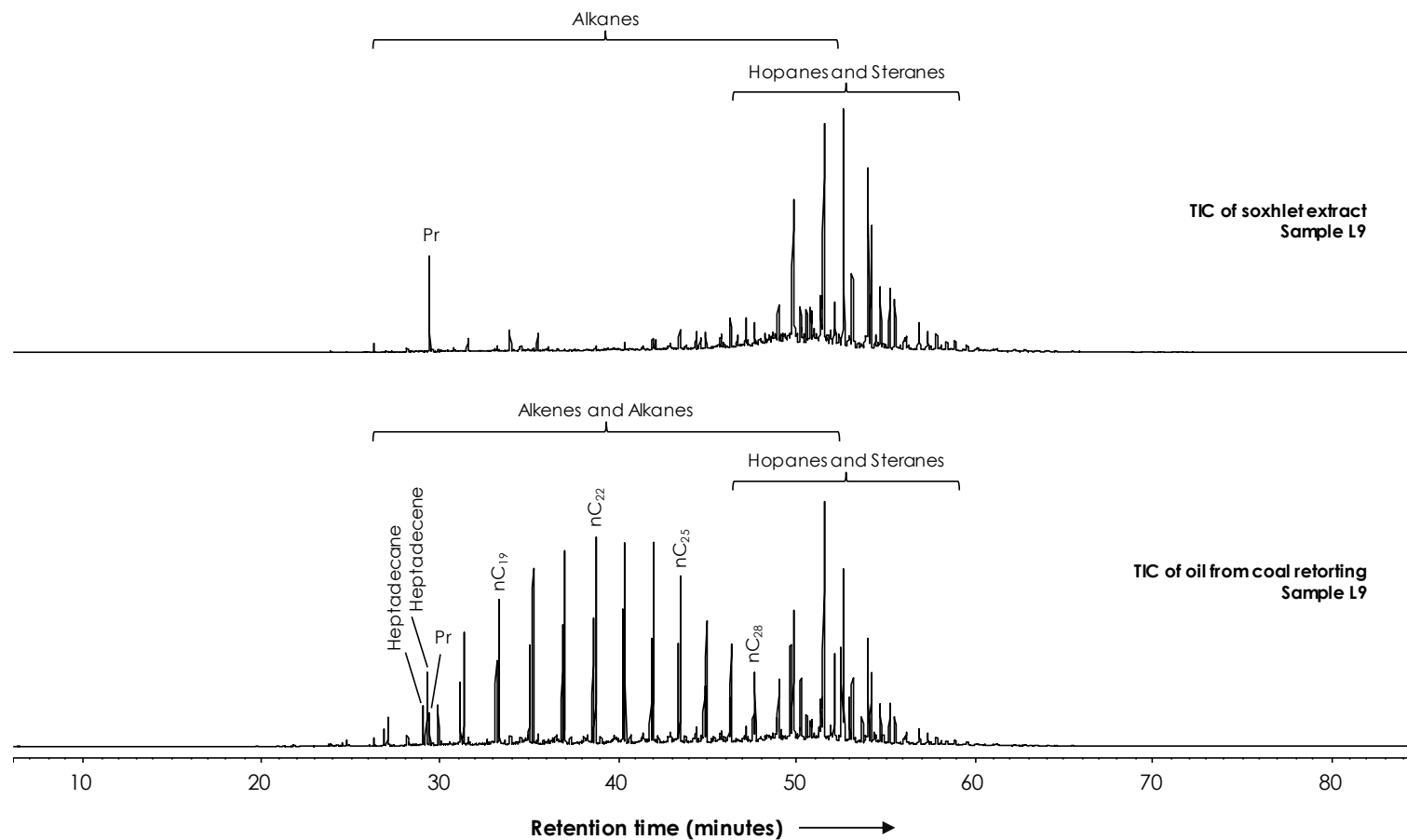


Figure 5.35. Comparing representative TIC of aliphatic hydrocarbons between Soxhlet extracts and retort oil. Sample L9 (the top 10 cm of the Longyear coal in Lunckefjellet BH15-2011 locality). Note: very high abundance of *n*-alkenes + *n*-alkanes doublets from retorting.

5.7.4. Resource Estimate

Unless otherwise stated, coal resource estimates quoted in this section are as per Pers. Comm., M. Jochmann, Store Norske Spitsbergen Kulkompani AS, 20th April, 2015. For oil estimates, assuming a density of 847 kg/m³ (35.6° API) for crude oil, 1 kg will be equivalent to 7.43E-03 bbl (OC, 2015). Coal and hydrocarbon resource estimates are presented in Table 5.14. The Longyear coal resource at Lunckefjellet is estimated at 13 Mt of which 8.4 Mt is recoverable; the new mine is scheduled to commence production when the Svea Nord coal deposits becomes depleted. If retorting yield of 150 mg/g and Rock-Eval S1+S2 contents of 280 mg/g (Table 5.12) represented the lower and upper limits of hydrocarbon potential of the Longyear coals in Lunckefjellet, maximum hydrocarbon resource in place would range between 14.5 – 27.0 Mbbl, with 9.4 – 17.5 Mbbl recoverable by mining Table 5.14.

Similarly, at Bassen where coal resource estimate for the Longyear seam is 15.4 Mt with 14.9 Mt recoverable, if retorting yield of 80 mg/g and Rock-Eval S1+S2 yield of 170 mg/g represented the lower and upper limits of hydrocarbon potential Table 5.12, maximum hydrocarbon resource would range between 9.2 and 19.5 Mbbl, of which 8.9 – 18.8 Mbbl is recoverable Table 5.14.

At Colesdalen, coal resource estimates, albeit a very rough one, is 53 Mt, with 52 Mt recoverable for the investigated Sputnik seam believed to be a Longyear seam equivalent. With retorting estimates of 100 mg/g and Rock-Eval S1+S2 yield of 150 mg/g Table 5.12, maximum hydrocarbon resource would range between 39.4 and 59.1 Mbbl with 38.6 – 58 Mbbl recoverable Table 5.14.

From a basin-wide point of view, Orheim (1982) estimated that the CTB bears maximum coal resource of 3,300 Mt of which 600 Mt was recoverable. Therefore,

if bulk retorting yield of 130 mg/g and bulk Rock-Eval S1+S2 yield of 220 mg/g represented the lower and upper limits of hydrocarbon potential of the CTB coals in general, maximum hydrocarbon resource would range between 3,188 – 5,394 Mbbbl in place with 580 – 981 Mbbbl recoverable by mining Table 5.14. In-situ retorting methods would access the considerably larger deposits estimated by Orheim (1982), which if used alongside coal gasification technology could yield significant quantities of liquid and gaseous hydrocarbons. It is noted that hydrocarbon resource estimates for the CTB as a whole unit is based on coal resource estimates from over 30 years ago (Orheim, 1982) and includes the relatively less oil-prone Svea seam; thus the true estimates may be considerably closer to, and possibly less than the lower range.

Resource description	Resource estimates			
	Bassen	Lunckefjellet	Colesdalen	Basin-wide
Total Coal Resource (TCR) in Mt	15.4	13.0	53.0	3300.0
Coal Resource Recoverable by Mining (CRRM) in Mt	14.9	8.4	52.0	600.0
Retorting yield (RY) in kg/tonne	80.0	150.0	100.0	130.0
Rock Eval S1+S2 (RE) in Kg/tonne	170.0	280.0	150.0	220.0
Lower Limit of Maximum Hydrocarbon Resource in Mbbbl = $TCR*RY*C$	9.2	14.5	39.4	3187.5
Upper Limit of Maximum Hydrocarbon Resource in Mbbbl = $TCR*RE*C$	19.5	27.0	59.1	5394.2
Lower Limit of Hydrocarbon Resource Recoverable by Mining in Mbbbl = $CRRM*RY*C$	8.9	9.4	38.6	579.5
Upper Limit of Hydrocarbon Resource Recoverable by Mining in Mbbbl = $CRRM*RE*C$	18.8	17.5	58.0	980.8

Table 5.14. Coal and liquid hydrocarbon resource estimate of the CTB coals. Estimates for Bassen and Lunckefjellet are for the Longyear coal, while the Colesdalen estimates are for the Sputnik coal.

Note: C = 7.43E-03 in bbl (i.e. assuming crude oil density of 847 kg/m³ at 35.6° API, 1 Kg = 7.43E-03 bbl) (OC, 2015)

5.8. Summary and Conclusions

This chapter evaluates the source rock and retorting potential of the CTB coals and assesses the variation in hydrocarbon potential within and between coal seams in four major areas. The oil-potential and sources of oil-proneness between the L. Carboniferous and Tertiary coals in Spitsbergen are also examined. Organic petrography was used for coal maceral analysis and palaeoenvironmental interpretation relative to oil potential. Rock-Eval analysis and Py-GCMS were utilised to evaluate the kerogen types and further assess oil potential. Variation in sulphur content relative to oil potential in areas of the CTB was also assessed. Retorting was simulated using nitrogen pyrolysis technique leading to resource estimate of the CTB coals. The conclusions are:

- Coal maceral analysis suggests that the oil potential of the Firkanten Fm. coals is mainly due to perhydrous detrovitrinites; however, other vitrinitic macerals including but not limited to collotelinite, in addition to liptinites, seem to have significantly contributed. In the L. Carboniferous coals, oil is sourced from the liptinite group macerals (alginite and sporinite). Maceral analysis also indicates the eastern CTB coals may be more oil-prone than coals from the western parts of the basin, and oil-proneness between seams is in the order of Askeladden>Svarteper>Longyear.
- Rock-Eval analysis indicates the Tertiary and L. Carboniferous coals are enriched in Type II and a mixture of Types II/III kerogens, with HI values in the range of 150 - 410 mg HC/g TOC. Between locations, HI decreases in the direction away from the inferred palaeocoastline. Between the Tertiary coal seams, HI values appear to be in the order of Askeladden>Svarteper>Longyear>Svea indicating oil potential increases

from the stratigraphically older to younger Firkanten Fm. coals which is consistent with results of maceral analysis. The coals show high TOC values between 44.5 – 89.8 %, and high S₂ contents of between 109 – 368 mg/g, which indicate excellent oil generation potential.

- The Longyear coals at Bassen are slightly marine influenced coals (0.5 – 1.5 % S), the Lunckefjellet coals range from non-marine to strongly marine influenced (0.4 – 8.2 %), while the Longyear in Breinosa and the Sputnik coal in Colesdalen are strongly marine influenced (1.9 – 7.0 and 1.4 – 12.0 % S respectively). The Askeladden, Svarteper and Verkny coals are all strongly marine influenced and generally contain higher sulphur contents (8.1 – 8.3, 3.4 – 8.2 and 17.7 % S respectively) compared to the Longyear and Sputnik coals. This trend is consistent with the distribution of HI values.
- The upper Longyear seam show greater oil potential compared to the lower Longyear seam. This is consistent with greater sulphur deposition associated with sea level rise, which resulted in a transition from raised-bog (ombrotrophic) conditions in the lower Longyear, to predominantly “fen-like” (minerotrophic) conditions in the upper Longyear. Sulphur, Soxhlet yield, S₁ and HI all show similar trends from base to top of the Longyear seam with a prominent raised-bog to fen transition, although the strength of correlation between these parameters/measurements at various locations do vary considerably. Notably, the Sputnik coal seam in Colesdalen, representing the western coalfield of the CTB displays similar transition observed in Bassen, Breinosa and Lunckefjellet; consequently, it may be a Longyear seam equivalent.

- The mean S1 contents of the investigated coals are 6.8, 11.8, 15.0 and 14.5 mg/g for the Bassen, Lunckefjellet, Breinosa and Colesdalen samples respectively, and reflects increasing maturity from Bassen, through Lunckefjellet to Breinosa and Colesdalen. Analysis shows that the Bassen coals are yet to generate significant volumes of oil, the Lunckefjellet coals are at peak oil generation/onset of oil expulsion, while the Breinosa and Colesdalen samples are already expelling oil. All samples nonetheless have low PI values (<0.10), which would normally suggest that significant expulsion have not occurred. Because the Lunckefjellet coals are at peak generation/onset of expulsion, they will give the best indication of the maturity at which oil expulsion occurs in the CTB.
- The Soxhlet yields from the marginal samples (Bassen and Lunckefjellet) are significantly higher than in samples down-dip of basin margins (Breinosa) and in basin center (Colesdalen) despite a general increase in marine influence towards basin center. This soxhlet yield trend is inconsistent with the Rock-Eval S1 trend, and thus the lower Soxhlet yields for the Breinosa and Colesdalen samples is believed to be mainly due to losses associated with expulsion.
- Retorting yields on dry whole coal basis (dwc) from all investigated coals show maximum yield in areas range between 90 mg/g in Bassen, to 240 mg/g in Lunckefjellet; this importantly replicates documented retorting yields from the CTB (Wang, 2011). Highest bulk estimate (from all coal seams) is 160 mg/g dwc in Lunckefjellet. At Breinosa and Colesdalen, yields of 140 and 100 mg/g dwc were respectively measured, while lowest yield (80 mg/g dwc) was measured at Bassen. Residual semi-coke ranges

between 60 – 75 % of starting material in all areas. Between seams, retorting yield is in the order of Askeladden>Svarteper>Longyear coals, which is consistent with the results of maceral analysis, HI and sulphur distribution. Retorting yields are notably limited by swelling of the coals within the reactor vessel leading to blockage of sweep gas flow. It has been noted that one of the advantages of the retorting technique is the reduction of sulphur contents in the semi-coke relative to the feedstock through the thermal decomposition conversion of pyrite to pyrrhotite. However, measuring the sulfur contents of the semi-coke was not achieved. This is because the semi-coke is in a sand mixture (i.e. coal was pre-mixed with sand to avoid sweep gas blockage), which could not be properly separated and there was no access to a suitable elemental analysis technique during this period of work.

- With a maximum coal resource of 3,300 Mt of which 600 Mt is recoverable in the CTB (Orheim, 1982), maximum hydrocarbon resource via retorting would range between 3,188 – 5,394 Mbbl in place, with 580 – 981 Mbbl recoverable by mining. In-situ retorting methods would access the considerably larger deposits, which if used alongside coal gasification technology, could yield significant quantities of liquid and gaseous hydrocarbons.

CONTROLS ON THE OIL POTENTIAL OF PERHYDROUS COALS IN CENTRAL TERTIARY BASIN, SPITSBERGEN

6.1. Introduction

Very low abundance of *n*-paraffins has been observed in the Firkanten Fm. coals, particularly within the upper Longyear seam in Bassen and Lunckefjellet (Table 4.1; Figure 4.10); this could be related to biodegradation and/or low thermal maturity (Peters and Moldowan, 1993). However, because the samples under study are mature as shown in Chapter 4, biodegradation is more likely to have caused *n*-alkane depletion. Biodegradation appears to show a positive relationship with oil potential; for example, at Lunckefjellet BH15-2011 locality where very low abundance of *n*-paraffin was measured (Table 4.1), a relatively high oil potential was also observed. Therefore, further assessment of biodegradation will help understand whether it influences the basin-wide variation in oil potential, and will also allow an assessment of its extent.

Organo-sulphur compound (OSC) formation is favoured when sulphur deposition exceeds Iron supply (Sinninghe Damsté and de Leeuw, 1990); thus the relative contents of Fe and S may reflect the basin-wide variation in oil potential, and consequently represent a key parameter for oil potential assessment in the CTB, and will be assessed in this Chapter. Whilst the Bassen outcrop samples show significant oil potential, this chapter will attempt to provide answers as to whether weathering, biodegradation and/or the relative contents and distribution of Fe and S does play a significant role in limiting their oil potential.

Large *et al.* (2011) modelled the effect of sea salt sulphate deposition at low, medium and high latitudes, which lead Marshall (2013) to predict that the

optimum proximity for coal and petroleum resources to inferred palaeocoastline in the CTB would be within 2 – 4 km. However, the prediction by Marshall (2013) was based on samples from only 2 localities (Mine 7 and Lunckefjellet BH15-2011) and as such, further works involving a geographically wider sample spread is required. As this study involves samples from 10 different localities in 4 main areas across the CTB (Figure 3.1), it presents a good opportunity to assess possible variations in petroleum potential, and in the process, provide information that will help in estimating optimum resource proximity to palaeocoastline. This constitutes a major aspect of this chapter.

Ash is one of the main coal quality issues affecting the CTB coals, particularly those from the Askeladden, Svarteper and Verkny seams. Although these seams may be more oil prone than the Longyear and Sputnik seams as shown in Chapter 5, their ash content may be a factor on their oil potential and needs to be assessed.

6.1.1. Sample Distribution and Methodology

Main analytical methods adopted in this chapter include biodegradation assessment, coal ash contents, and the contents and distribution of some major elements including Al, Ca, Fe, K, Mg, Mn, Na, P, S and Ti. All locations referred to in this chapter are shown in Figure 3.1.

6.2. Biodegradation

6.2.1. Organic Geochemical Assessment

Biodegradation results in depletion of *n*-paraffins prior to significant alteration of any other compound class, including the acyclic isoprenoids; pristane (Pr) and

phytane (Ph) (Peters *et al.*, 2005). Within the Longyear and Sputnik seams, the Pr/nC₁₇ and Ph/nC₁₈ ratios show significant variations as values are higher within the upper seam (>80 cm); this difference is much greater at basin margins (Bassen and Lunckefjellet), and decreases towards basin center (Breinosa and Colesdalen) (Table 6.1). George *et al.* (1994) reported lower *n*-alkane abundance within the more marine influenced, and more oil-prone top section of the Greta seam in the Sydney basin; these workers concluded that bacterial reworking of peat, lead to the removal of long chain *n*-alkane precursors, and consequently lower amounts of *n*-alkanes, together with the addition of bacteria derived lipids such as hopane precursors. Similarly, Pr/nC₁₇, Ph/nC₁₈ and Rock-Eval S1 all show positive relationships and increase towards the top of the more marine influenced Longyear seam in Mine 7 (Figure 6.1). The lower *n*-alkane abundance observed in the more oil-prone samples in Mine 7 is consistent with observations in the Longyear seam in Lunckefjellet (Figure 6.2).

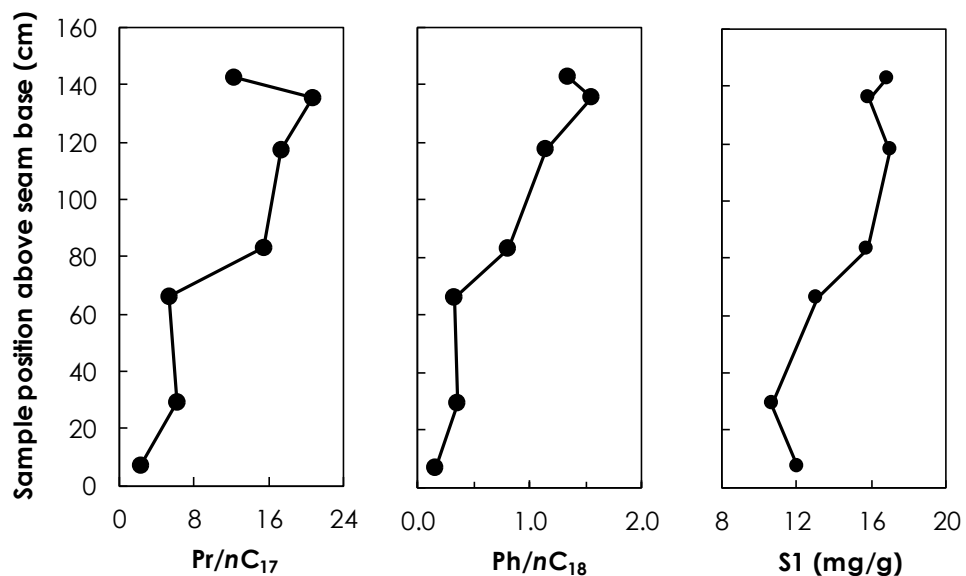


Figure 6.1. Comparing the profiles of Isoprenoid/*n*-alkane ratios and Rock-Eval S1 from bottom to top of the Longyear seam in Mine 7. Note: Increasing oil potential towards the upper part of the seam correlate with increasing isoprenoid/*n*-alkane values. S1 data is from Marshall *et al.* (2015a), while Isoprenoid/*n*-alkane data is from Marshal *et al.* (2015b).

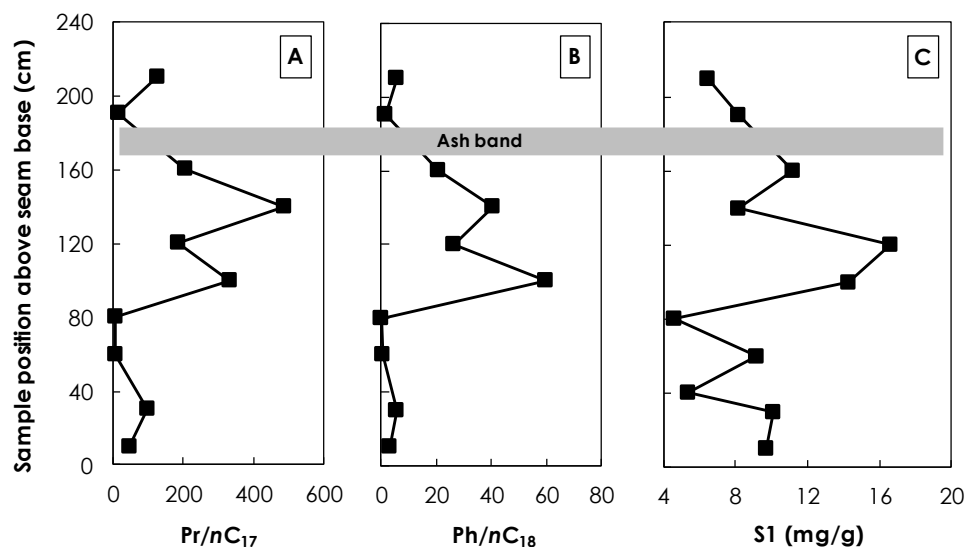


Figure 6.2. Comparing the profiles of Isoprenoid/*n*-alkane ratios and Rock-Eval S1 from bottom to top of the Longyear seam in Lunckefjellet BH15-2011 locality. Note: greater oil potential in the upper seam correlate with greater *n*-alkane depletion.

The Pr/*n*C₁₇ ratios are generally highest at the eastern basin margin (Bassen = 104, Lunckefjellet = 150), and decreases towards basin centre from Breinosa (12) to Colesdalen (2). Similarly, Ph/*n*C₁₈ values are higher at the eastern basin margin (Bassen = 9.3, Lunckefjellet = 16.4), and decreases towards basin center from Breinosa (1.6) to Colesdalen (0.3) (Table 6.1). This trend is replicated by all but the 22S/(22S + 22R) homohopane biomarker maturity ratios (Table 4.2; Section 4.3.2), and is consistent with the direction towards increasing depth of burial (Chapter 4); it is therefore believed to be mainly due to biodegradation, and to a lesser degree, maturity variation.

Area	Pr/Ph	Pr/ <i>n</i> C ₁₇			Ph/ <i>n</i> C ₁₈		
	Bulk	Bulk	0 – 80 cm	> 80cm	Bulk	0 – 80 cm	>80 cm
Bassen	12.0	104.2	5.1	203.3	9.3	0.3	18.3
Lunckefjellet	7.8	149.9	38	224.4	16.4	2.3	25.7
Breinosa	6.3	12.3	10.5	14.0	1.6	1.3	1.9
Colesdalen	5.2	2.1	1.8	2.3	0.3	0.3	0.3

Table 6.1. Summary of bulk *n*-alkane and isoprenoid ratios of the Longyear and Sputnik coals under study. Note: lower *n*-alkane abundance within the upper parts of the seams and at basin margins (Bassen and Lunckefjellet). Lunckefjellet = BH15-2011, Bassen = outcrops, Breinosa = BH4-2009, Colesdalen = BH3-2008. Detailed distribution is shown in Table 4.1.

Biodegradation was further investigated by examination of a biodegraded oil seep from the western coalfield (basin center) of the CTB in Spitsbergen, and compared to bitumen extracts from coals in the area. A prominent UCM (unresolved complex mixture) indicative of heavy biodegradation (Peters *et al.*, 2005) was observed in the seep (Figure 6.3.). The m/z 217 from the seep showed higher C_{29} diasteranes relatively to the C_{29} regular steranes (Figure 6.4) and thus indicates biodegradation as diasteranes are more bio-resistant than regular steranes (Peters *et al.*, 2005). Biodegradation depletion susceptibility appear to be in the order of $C_{29} > C_{28} > C_{27}$, with the C_{29} aaa (20S and 20R) appearing more depleted than C_{29} a $\beta\beta$ (20R and 20S); this is contrary to the general biodegradation susceptibility order ($C_{27} - C_{30}$ aaa 20R > other isomeric forms of $C_{27} > C_{28} > C_{29} > C_{30}$) where partial biodegradation of steranes have occurred (Peters *et al.*, 2005).

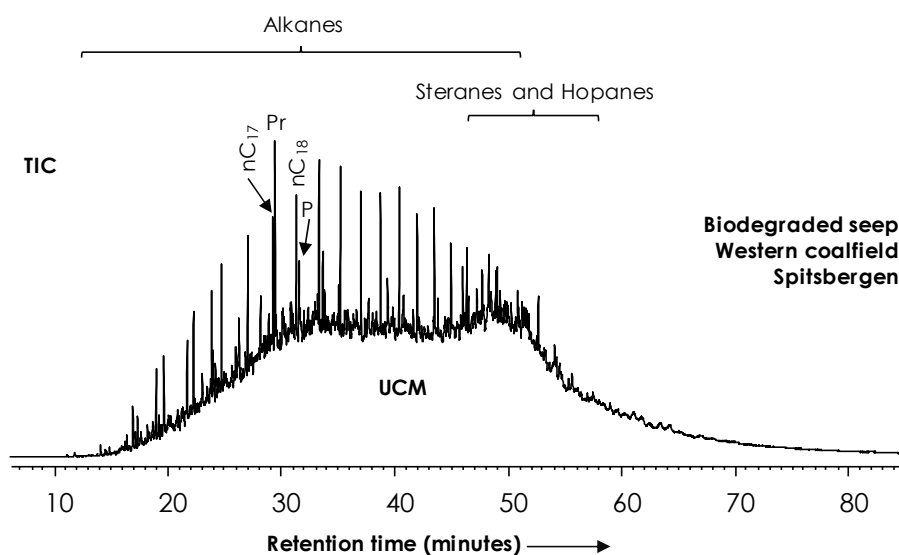


Figure 6.3. TIC of severely biodegraded oil seep from the western coalfield of the CTB.

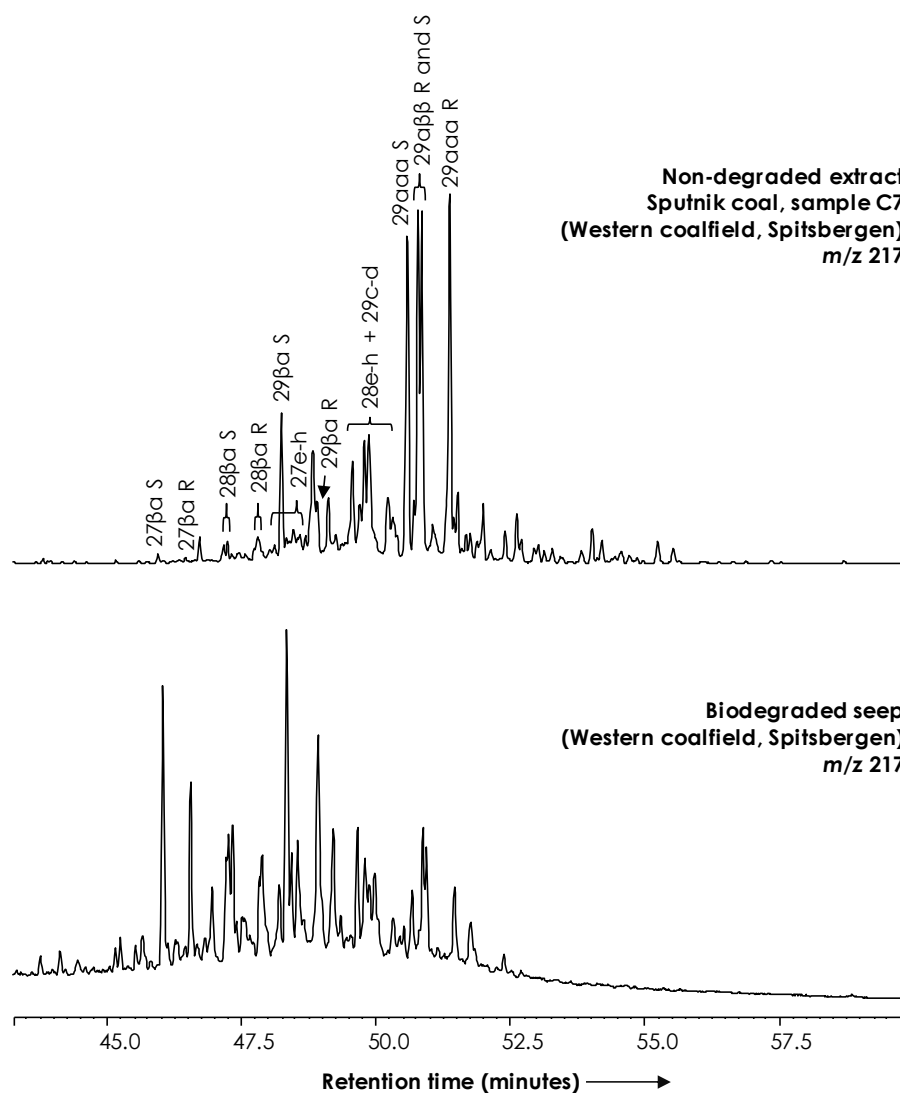


Figure 6.4. Top - m/z 217 of non-degraded Soxhlet extract from a Sputnik coal (sample C7). Bottom - m/z 217 of the severely biodegraded oil seep shown in Fig. 6.3. Note: Biodegradation susceptibility seem to be in order of $C_{29} > C_{28} > C_{27}$ with C_{29} aaa depleting faster than C_{29} $\alpha\beta\beta$ isomers which is unusual. 27e-h = C_{27} aaa (20S and 20R) and $\alpha\beta\beta$ (20R and 20S) steranes. 29βa S and R = C_{29} βa 20S and 20R diasteranes. 28e-h = C_{28} aaa (20S and 20R) and $\alpha\beta\beta$ (20R and 20S) steranes. 29c-d = C_{29} $\alpha\beta$ 20S and 20R diasteranes. 29aaa S and R = C_{29} aaa 20S and 20R steranes. 29 $\alpha\beta\beta$ R and S = C_{29} $\alpha\beta\beta$ 20R and 20S steranes.

The extent of biodegradation within the marginal samples of the CTB is further assessed. In Lunckefjellet, the sterane traces shows the abundance of the C_{29} $\alpha\beta\beta$ (20R and 20S) relative to C_{29} aaa (20S and 20R) is low in the Longyear coals, but high in the Svarteper coals which are 12 meters above (Figure 6.3); this is therefore

due to biodegradation and/or depositional environment, and not maturity induced. In Bassen, similarly low abundance of C_{29} $\alpha\beta$ relative to C_{29} aaa isomers was also observed in the Longyear coals; thus this geochemical character may be sub-regional and encompassing the eastern margin of the CTB basin.

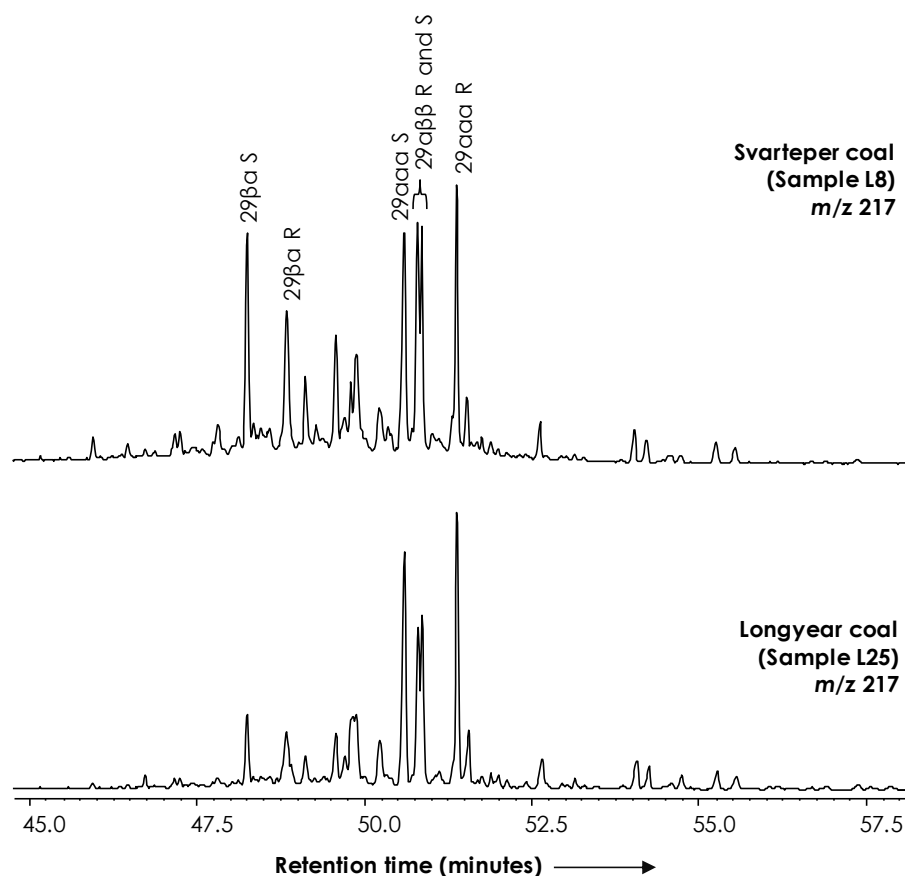


Figure 6.5. Comparing sterane distribution in the Soxhlet extracts from a Svarteper and a Longyear coal in Lunckefjellet BH15-2011 locality. Note: the higher abundance of C_{29} $\alpha\beta\beta$ relative to C_{29} aaa isomers in Svarteper compared to Longyear coal, and the higher abundance of C_{29} diasteranes in Svarteper relative to those in the Longyear coal. $29\beta a S$ and $R = C_{29} \beta a 20S$ and $20R$ diasteranes. $29\alpha aa S$ and $R = C_{29} \alpha aa 20S$ and $20R$ steranes. $29\alpha\beta\beta R$ and $S = C_{29} \alpha\beta\beta 20R$ and $20S$ steranes

The observed biodegradation susceptibility order of the Soxhlet extracts at basin margins is notably inconsistent with that of the oil seep as well as the general biodegradation susceptibility order for steranes. According to Peters *et al.* (2005),

the susceptibility of the $\alpha\beta\beta$ 20R, $\alpha\beta\beta$ 20S and aaa 20S isomers vary considerably; they seem to be depleted at nearly equal rates in some severely biodegraded oils, while in other cases, selective removal may first deplete $\alpha\beta\beta$ 20R, or $\alpha\beta\beta$ 20R and $\alpha\beta\beta$ 20S isomers together, or the aaa 20S isomer. In the samples under study, the sterane biodegradation susceptibility of the oil seep appears to be in the order of $\text{aaa } 20\text{S} + 20\text{R} > \alpha\beta\beta \text{ } 20\text{R} + 20\text{S} > \text{C}_{29} > \text{C}_{28} > \text{C}_{27}$, while that of the Longyear coals at basin margin is $\alpha\beta\beta \text{ } 20\text{S} + 20\text{R} > \text{aaa } 20\text{S} + 20\text{R}$.

Biodegradation of hopanes was assessed by comparing the m/z 191 and 177 chromatograms; this shows 25-norhopanes have been formed in the seep (Figure 6.6), and suggests severe biodegradation (stage 4+ of Wenger *et al.*, 2002). Although 25-norhopanes are absent in the extracts at all locations, depletion of regular steranes in marginal samples suggest heavy biodegradation (stage 3 of Wenger *et al.*, 2002). Microbial alteration and removal of the regular steranes from petroleum occurs after complete removal of C_{15} - C_{20} isoprenoids (Peters *et al.*, 2005); however, as observed in the CTB coals, n -alkanes are not completely removed while isoprenoids show high abundance. The following "unusual observations" with respect to biodegradation are thus noted:

- The presence of n -alkanes and isoprenoids after hopanes and steranes have been depleted/altered in the oil seep
- The depletion of steranes, while n -alkanes and isoprenoids are present in Soxhlet extracts from the marginal Longyear samples
- The perceived inconsistent depletion pathway of the sterane isomers in both the oil seep and Soxhlet extracts

Ahmed *et al.* (1999) reported unusual sequence of hydrocarbon biodegradation in Permian Moura coals of Bowen Basin of Australia, where

aromatic hydrocarbons were biodegraded more readily than *n*-alkanes $>nC_{20}$. This led Peters *et al.* (2005) to suggest that preferential degradation may be related to aqueous solubility and/or water transport through the coal matrix. The foregoing references provide a likely explanation for the inconsistent depletion pathway, and the much higher biodegradation of the upper (>80 cm) Longyear seam at basin margins (Figure 6.2).

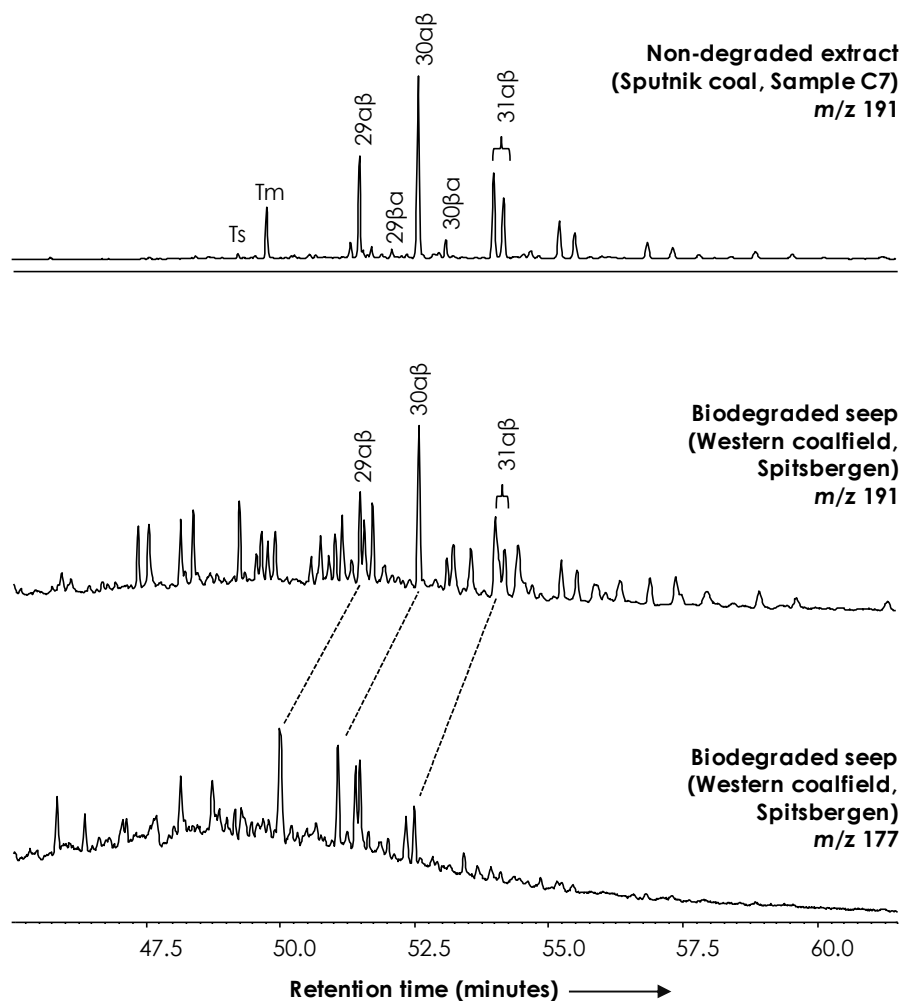


Figure 6.6. Comparing terpane distribution in the Soxhlet extract from a Sputnik coal (Sample C7) with that of the biodegraded oil seep, as both from the western coalfield of the CTB. Note: 25-norhopane (*m/z* 177) present in oil seep indicating severe biodegradation (stage 4+ of Wenger *et al.*, 2002). Ts and Tm = C_{27} 18a(H)-trisorhopane II and 17a(H)-trisorhopane. 29aβ and 30aβ = C_{29} and C_{30} 17a(H),21β(H)-hopanes. 29βa and 30βa = C_{29} and C_{30} 17β(H),21a(H)-moretanes. 31aβ to 35aβ = C_{31} to C_{35} 17a(H),21β(H)-homohopanes

The Longyear coals in the eastern CTB appear to be degraded in the order of Bassen/Lunckefjellet>Breinosa with little or no degradation in the Colesdalen coals. This trend is consistent with the direction towards basin center; i.e., increasing depth of burial and/or highest geothermal gradient (Chapter 4). Due to the inconsistent biodegradation pathways, it is impossible to assign the degree of biodegradation of these coals based on existing classification schemes.

6.2.2. Biodegradation Relative to Hydrology, Palaeoenvironment and Oil Potential

Marshall (2013) examined landscape control upon groundwater supply in Spitsbergen, and suggested that as landscape control decreased in the Firkanten Fm. (i.e. from older to younger sediments), the CTB peatlands moved from isolated raised bogs to laterally expansive minerotrophic fens. Ombrogenous high-moor peats (raised bogs) show pH values (3.3 - 4.6) lower than topogenous low-moor peats (fens) (4.8 - 6.5) (Taylor *et al.*, 1998). According to Hao and Chen (1992), marine influence prevents acidification of peatland, allowing optimum conditions for both aerobic and anaerobic decomposition. Taylor *et al.* (1998) reported that marine influence and calcium enrichment such as observed within the CTB coals (Section 6.3); results in a neutral to alkaline depositional environment, which allows bacteria to cause severe structural decomposition, leading to nitrogen and hydrogen enrichment.

Diasterane formation may be due to clay-catalysed re-arrangements or acidic conditions frequently prevalent in peat swamps (mire) (Curry *et al.*, 1994), although maturity may interfere (Peters *et al.*, 2005). The Longyear coals at Lunckefjellet and Bassen generally show the lowest values for diasterane/sterane ratios (0.12 – 0.24 and 0.12 – 0.16 respectively; Table 4.2); the fact that the

Svarteper coal, which is 12 meters above the Longyear coal at Lunckefjellet, shows much higher values (0.43 – 0.48), rules out maturity as a possible cause. It has been noted that marine influence on the CTB coals increased from the stratigraphically older to younger seams (Chapter 5); thus marine influence on the relative abundance of diasterane in the coals under study are examined below.

While working on the marine influenced Greta coals in the Sydney Basin, George *et al.* (1994) observed the highest diasterane/sterane values within the top and most marine-influenced section of the seam. Because the sulphur contents of both the Greta coals in George *et al.* (1994) (S range of 0.8 – 2.5 %) and the Longyear coals at BH15-2011 (S range of 0.5 – 2.9 %) are comparable (i.e. both coals are slightly to strongly marine influenced as per the classification of Sykes *et al.*, 2014), the relationship between diasterane/sterane and marine influence in these coals are compared (Table 6.2). A plot of S contents vs diasterane/sterane data for the Greta coals shows a clear positive relationship with moderate correlation ($R^2 = 0.56$) (Figure 6.7.A). Similarly, the S contents vs diasterane/sterane plot of the Longyear coals at BH15-2011 shows a clear positive relationship although with a strong correlation ($R^2 = 0.80$) (Figure 6.7.B). Also, the ash content vs diasterane/sterane plot of the Longyear coals shows a strong positive correlation ($R^2 = 0.82$) (Figure 6.7.C). This observation implies that flooding (marine influence) not only resulted in greater S contents, but also led to greater ash contents, which facilitated clay catalysed reactions for diasterane formation (Curry *et al.*, 1994). Unlike the Longyear coals, the Askeladden and Svarteper coals analysed, interestingly show a strong negative correlation for a plot of S contents vs diasterane/sterane ($R^2 = 0.87$) (Figure 6.8.A), but the relationship between ash content and diasterane/sterane is very poor and not clear for these coals (Figure 6.8.B).

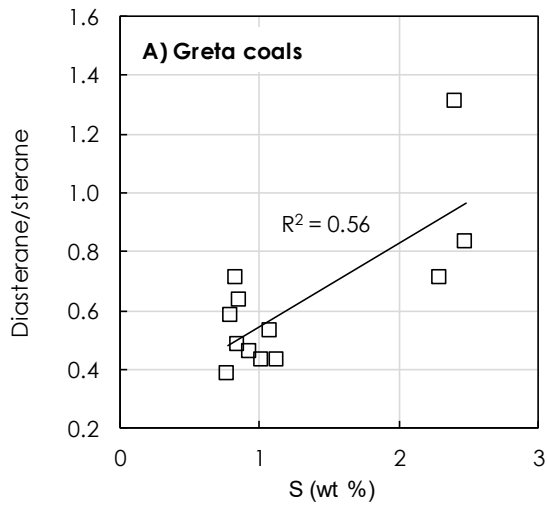


Figure 6.7.A. Sulphur vs diasterane/sterane plot of Greta coals from Sydney Basin. Data are as per George *et al.* (1994). Diasterane/sterane = $C_{29} \beta a_{20S} / C_{29} a_{aa}$

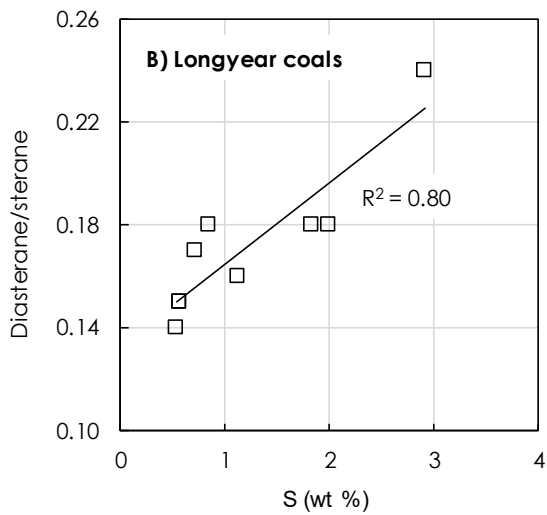


Figure 6.7.B. Sulphur vs diasterane/sterane plot of Longyear coals at Lunckefjellet BH15-2011. Diasterane/sterane = $C_{29} \beta a / C_{29} (aaa + a\beta\beta)$

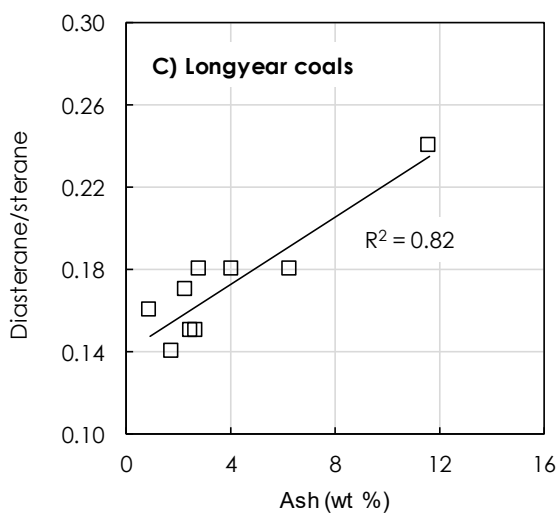


Figure 6.7.C. Ash vs diasterane/sterane plot of Longyear coals at Lunckefjellet BH15-2011. Diasterane/sterane = $C_{29} \beta a / C_{29} (aaa + a\beta\beta)$

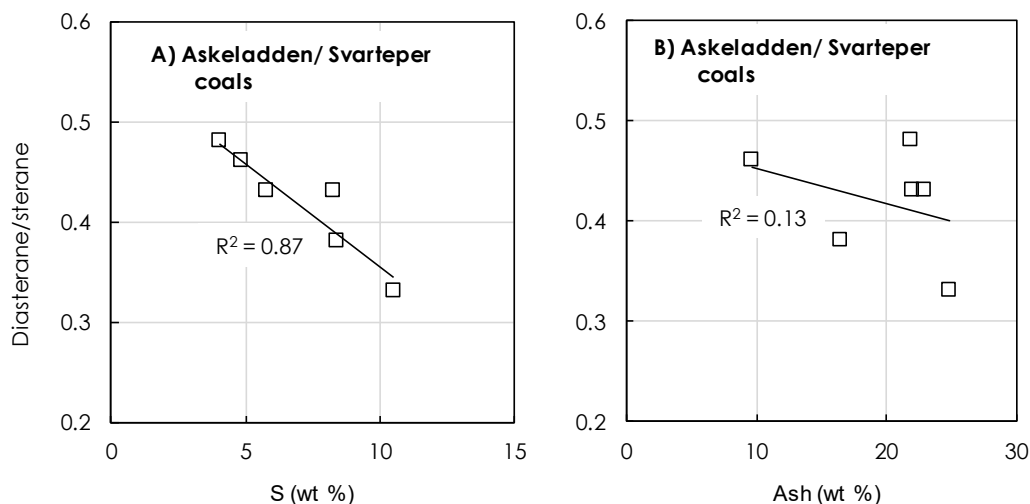


Figure 6.8. (A) Sulphur vs diasterane/sterane plot, and **(B)** Ash content vs diasterane/sterane plot, for the Askeladden and Svarteper coals from Lunckefjellet BH15-2011 and Breinosa BH4-2009 localities. Diasterane/sterane = $C_{29} \beta a / C_{29} (aaa + a\beta\beta)$.

The strong correlations seen for the Longyear coals in Figures 6.7.B and 6.7.C suggest that both marine influence and ash content exert similar levels of control (i.e. optimum pH and clay catalysed reactions) on diasterane formation within the Longyear peatland. However, marine influence appears to exert the main control on diasterane formation within the Askeladden and Svarteper peatlands because S vs diasterane/sterane show strong correlation (Figure 6.8.A), whereas ash content vs diasterane/sterane show weak/non-correlation (Figure 6.8.B). It has been noted in Chapter 5 that the Askeladden and Svarteper coals are S and ash rich, and the coals in Figure 6.8 have S and ash contents in the range of 4.0 – 17.7 and 9.7 – 30.8 % respectively, which is much higher than the S and ash contents of the Longyear coals in Figure 6.7.B and 6.7.C (0.5 – 2.9 and 0.9 – 11.6 % respectively (Table 6.2). It is therefore believed that greater marine influence not only resulted in the greater ash contents of the Askeladden and Svarteper coals, and consequently greater diasterane abundance in these coals (compared to the Longyear coals), but also resulted in higher pH (Hao and Chen, 1992) and possibly

neutral to alkaline depositional conditions (Taylor *et al.*, 1998), which is reflected in the negative correlation for Sulphur vs diasterane/sterane ratios. Thus, the Longyear seam at basin margins, due to their less marine influence (particularly within the lower section), experienced relatively lower pH conditions, which may have limited their oil potential compared to the stratigraphically younger Svarteper and Askeladden coals.

Greta Coals, Sydney Basin (George <i>et al.</i> , 1994)			CTB Coals (this study)					
Sample ID	S (%)	Diasterane/sterane	Sample ID	Seam	Location	S (%)	Ash (%)	Diasterane/sterane
a	2.40	1.31	L1	Svt	BH15-2011	5.74	22.88	0.43
c	2.48	0.83	L3	Svt	BH15-2011	4.03	21.83	0.48
e	2.29	0.71	L5	Svt	BH15-2011	4.82	9.68	0.46
g	1.13	0.43	L8	Svt	BH15-2011	8.23	22.06	0.43
j	0.84	0.71	L9	Lyr	BH15-2011	1.99	4.10	0.18
l	0.80	0.58	L11	Lyr	BH15-2011	2.91	11.60	0.24
m	0.78	0.38	L12	Lyr	BH15-2011	1.83	6.30	0.18
n	0.86	0.63	L14	Lyr	BH15-2011	1.12	0.90	0.16
o	0.85	0.48	L16	Lyr	BH15-2011	0.57	2.70	0.15
p	0.93	0.46	L18	Lyr	BH15-2011	0.57	2.50	0.15
q	1.02	0.43	L22	Lyr	BH15-2011	0.53	1.80	0.14
r	1.08	0.53	L25	Lyr	BH15-2011	0.84	2.80	0.18
-	-	-	L27	Lyr	BH15-2011	0.71	2.30	0.17
-	-	-	Br1	Ask	BH4-2009	8.35	16.44	0.38
-	-	-	Br8	Svt	BH4-2009	10.47	24.90	0.33

Table 6.2. Comparing the sulphur, ash and diasterane/sterane data from George *et al.* (1994) and this study. Diasterane/sterane data for George *et al.* (1994) = $C_{29} \beta a / C_{29} \alpha a a$. In this study, diasterane/sterane = $C_{29} \beta a / C_{29} (a a a + a \beta \beta)$.

On a hydrological context, the similar biodegradation profiles of the Longyear seam at Bassen and Lunckefjellet suggest that both areas belong to the same regional hydrological system encompassing most of the eastern margin of the CTB. This is consistent with previous report of a regional hydrological control by the Longyear peatland (Marshall, 2013). This hydrological system is believed to be structurally controlled by the trough and swell series in eastern CTB (Figure 5. of

Eiken, 1985), which parallel the NW-SE structural trend of the CTB. This section shows that microbial degradation not only occurred during peat stage and contributed to oil potential, but also occurred in the coal stage after uplift and hydrocarbon generation considering the coals are in the maturity range of 0.68 – 0.88% Ro.

6.3. Sulphur and Iron

It is generally important to investigate sulphur in coals as sulphur directly impacts their economic potential. Notably, sulphur contents in excess of 2 %, observed within some of the CTB coals is a limiting factor on the economic potential of these coals. However, the coals are perhydrous, and the perhydrous nature is sulphur driven as H₂S combines with organic matter to form organo-sulphur compounds – OSC (George *et al.*, 1994; Sandison, 2001 and references within), which in turn allows preferential preservation of hydrogen rich plant components (Sinninghe Damsté and de Leeuw, 1990; Sandison, 2001; Sandison *et al.*, 2002), and thus leading to the formation of perhydrous (oil prone) coals. Rates of deposition of sea salt and sea salt sulphate decrease rapidly inland (Gustafsson 2000; Mahowald *et al.*, 2006; Harkel, 1997) and sea spray represents a major transport mechanism (Harkel, 1997). Sulphate reducing bacteria will produce H₂S in anaerobic conditions, to levels which exceed Fe supply in order for a depositional system to allow the formation of OSC (Sandison, 2001). Therefore, the relative contents and distribution of S and Fe will reflect certain controls on S deposition, which will ultimately influence the variation of oil potential in the CTB coals, and consequently help in delineating areas of optimum hydrocarbon resource.

6.3.1. Controls on S and Fe Supply to the Firkanten Formation Coals

The sulphur and Fe contents of the coals under study are shown in Table 6.3. A scatter plot of S vs. Fe contents in the Askeladden, Svarteper, Longyear, Verkny and Sputnik coals under study show a very strong positive relationship with $R^2 = 0.92$ (Figure 6.6), which implies similar controls on both elements. It is therefore necessary to assess the controls on these elements as it will invariably influence oil potential in the CTB. Some common major elements including Al, Ca, Fe, K, Mg, Mn, Na, P, S and Ti were analysed using the ICP-AES as described in Chapter 3. To assess possible controls upon Fe and S, it is first necessary to establish which elements have similar distributions, which would imply a similar control.

Area	Location and sample type	Seam	S (ppm)	Fe (ppm)	Fe/S
Lunckefjellet	BH152011	Svarteper	59261	41727	0.69
Lunckefjellet	BH152011	Longyear	13180	9676	0.82
Lunckefjellet	BH10-2009	Svarteper	61918	48293	0.79
Lunckefjellet	BH10-2009	Longyear	28120	19354	0.55
Lunckefjellet	BH6A-2007	Svarteper	46699	31849	0.66
Lunckefjellet	BH6A-2007	Longyear	5875	4656	0.87
Bassen	Outcrop section	Longyear	8399	6988	1.01
Colesdalen	BH3-2008	Sputnik	35753	26124	0.56

Table 6.3. Bulk S and Fe contents, and Fe/S ratios of the CTB coals under study.

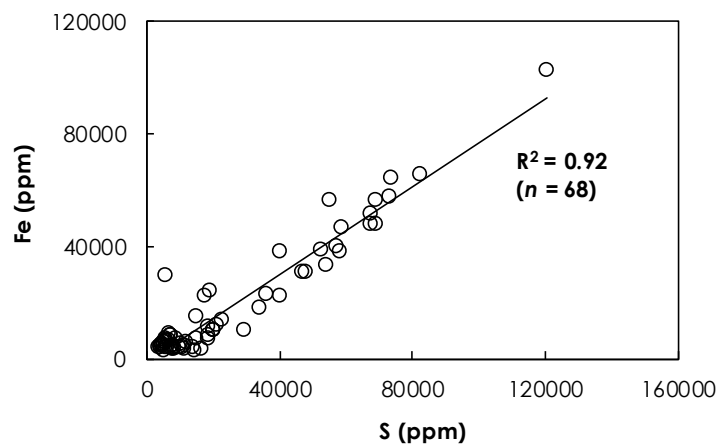


Figure 6.9. Scatter plot of S vs. Fe for the CTB coals under study. Note: samples are from the Askeladden, Svarteper, Longyear, Verkny and Sputnik seams

Assessment of relative distribution of elements was achieved through the use of correlation matrices. A correlation matrix is used to investigate the dependence between multiple variables at the same time. The result is a table containing the correlation coefficients (R) between each variable and the others (STHDA, 2015). The numerical value for R ranges from +1.0 to -1.0 and It gives us an indication of the strength of relationship. In general, $R > 0$ indicates positive relationship, $R < 0$ indicates negative relationship while $R = 0$ indicates no relationship (or that the variables are independent and not related). The closer the coefficients are to +1.0 and -1.0, the greater is the strength of the relationship between the variables. The general guidelines on strength of relationship as applied in this study is shown in Table 6.4; accepted R values range between strong to moderate relationship strengths.

R value	Strength of relationship
-1.0/1.0 to -0.7/0.7	Strong
-0.7/0.7 to -0.5/0.5	Moderate
-0.5/0.5 to -0.3/0.3	Weak
-0.3/0.3 to -0.0/0.0	Very weak or none

Table 6.4. Guideline for interpreting strength of coefficient of correlation (R) as applied in this study

6.3.1.1. *The Longyear and Sputnik Seam*

1) Lunckefjellet

The major element concentrations in the Longyear seam between 3 sampling localities at Lunckefjellet are presented in Table 6.5; similar to reports by Marshall (2013), they are dominated by Ca, Fe and S, which are probably associated with groundwater, but contain relatively lower concentrations of Al, K, Na and Ti, which are elements often associated with dust and/or clastic deposition (e.g. Lawrence and Neff, 2009; Rudnick and Gao, 2003). Phosphorous is generally

lowest and below detection in some sections; this is consistent with previous reports on the Longyear coals (e.g. Orheim *et al.*, 2007). S is notably highest within the southernmost sampling locality (BH10-2009) and indicates greater marine influence and possibly closer proximity to inferred palaeocoastline.

BH15-2011

Element	No. of Samples	% of samples measured	Mean (ppm)	Minimum (ppm)	Maximum (ppm)	Median (ppm)	STDEV (ppm)
Al	19	100	3750	381	26681	1298	6224
Ca	19	100	17125	1259	124915	3785	31061
Fe	19	100	9676	3533	23905	7264	6669
K	19	100	484	22	5374	61	1292
Mg	19	100	3094	440	15943	1574	4454
Mn	19	100	88	6	310	55	90
Na	19	100	1557	1067	2206	1453	339
P	19	100	143	BD	455	36	170
S	19	100	13180	4145	36002	8903	8914
Ti	19	100	230	21	1492	114	348

BH6A-2007

Element	No. of Samples	% of samples measured	Mean (ppm)	Minimum (ppm)	Maximum (ppm)	Median (ppm)	STDEV (ppm)
Al	8	100	1476	802	2391	1544	522
Ca	8	100	6129	2510	16038	4078	5053
Fe	8	100	4656	3583	5703	4599	736
K	8	62.5	114	57	172	114	81
Mg	8	100	1397	720	2419	1361	564
Mn	8	100	4	2	7	4	2
Na	8	25	1840	1690	1991	1840	212
P	8	12.5	596	BD	596	596	596
S	8	100	5875	3822	10481	5103	2247
Ti	8	100	193	75	411	150	118

BH10-2009

Element	No. of Samples	% of samples measured	Mean (ppm)	Minimum (ppm)	Maximum (ppm)	Median (ppm)	STDEV (ppm)
Al	4	100	3335	1647	7152	2270	2591
Ca	4	100	3080	1489	5699	2566	1820
Fe	4	100	19354	3832	56371	8606	24904
K	4	100	443	104	1262	203	552
Mg	4	100	587	366	848	567	223
Mn	4	100	16	5	43	9	18
Na	4	100	2022	1817	2292	1989	200
P	4	50	64	BD	109	64	64
S	4	100	28120	10598	68855	16514	27558
Ti	4	100	384	238	645	327	180

Table 6.5. Major element concentrations in the Longyear seam in 3 sampling localities in Lunckefjellet. Boreholes BH15-2011, BH6A-2007 and BH10-2009 respectively represent the eastern, northern and southern Lunckefjellet. (BD = below detection. 10,000 ppm = 1 %)

The correlation matrix of the Longyear coals in the eastern sampling locality of Lunckefjellet (BH15-2011) (Table 6.6) shows the elements can be generally grouped into dust/clastic deposition associated (Al, Ti and K) with $R \geq 0.77$, and the Ca, Mn and Mg group ($R \geq 0.64$) linked to groundwater influence (or marine influence for Mg - Weis *et al.*, 2002). Fe shows moderate to strong correlation with the groundwater group ($R \geq 0.64$), while S correlates strongly with both groups ($R \geq 0.75$).

In BH6A-2007 (Table 6.6), which is the northern sampling locality at Lunckefjellet, the clastic/dust associated group (Al and Ti) show weak correlation ($R = 0.33$), while Na and K were not measured. For the groundwater associated group, Mg and Mn correlate strongly ($R = 0.75$) while Ca weakly correlates with this group ($R = 0.47$). Fe only shows strong correlation with Mn ($R = 0.72$) in the groundwater group, and weak correlation with the dust/clastic group elements. S shows moderate correlation with Al ($R = 0.56$), and a weak/no correlation with other elements in the dust/clastic group. For the groundwater group elements, S shows a weak positive to moderate negative correlation.

In BH10-2009, the southern sampling locality at Lunckefjellet (Table 6.6), the clastic/dust associated group comprises Al, K, and Ti all showing very strong positive correlation ($R \geq 0.99$) with Na showing a strong negative correlation with this group ($R = -0.80$). The groundwater group comprises Mg and Mn based on a strong correlation ($R = 0.88$), while Ca shows moderate correlation with this group ($R = 0.50$). Fe and S show strong correlation with both groups ($R \geq 0.73$).

BH15-2011									
	Al	Ca	Fe	K	Mg	Mn	Na	P	S
Ca	-0.20								
Fe	0.39	0.75							
K	0.99	-0.15	0.45						
Mg	-0.24	0.96	0.75	-0.16					
Mn	-0.31	0.76	0.64	-0.29	0.74				
Na	0.13	-0.11	-0.01	0.04	-0.15	0.13			
P	0.47	-0.51	-0.34	0.42	-0.51	-0.73	0.34		
S	0.78	0.27	0.69	0.77	0.20	0.19	0.17	-0.04	
Ti	0.99	-0.23	0.36	0.98	-0.26	-0.33	0.12	0.42	0.75

BH6A-2007						
	Al	Ca	Fe	Mg	Mn	S
Ca	-0.39					
Fe	-0.02	0.22				
Mg	-0.13	0.47	0.40			
Mn	0.12	0.29	0.72	0.75		
S	0.56	-0.29	0.16	-0.53	-0.31	
Ti	0.33	0.19	0.32	0.69	0.50	0.13

BH10-2009									
	Al	Ca	Fe	K	Mg	Mn	Na	P	S
Ca	-0.29								
Fe	1.00	-0.22							
K	1.00	-0.26	1.00						
Mg	0.68	0.50	0.73	0.70					
Mn	0.95	0.02	0.97	0.96	0.88				
Na	-0.70	-0.24	-0.73	-0.70	-0.75	-0.74			
P	1.00	-0.27	1.00	1.00	0.70	0.95	-0.71		
S	1.00	-0.25	1.00	1.00	0.71	0.96	-0.73	1.00	
Ti	0.99	-0.21	0.99	0.99	0.71	0.94	-0.80	0.99	0.99

Table 6.6. Correlation matrices of major elements in the Longyear seam in 3 sampling localities at Lunckefjellet. Boreholes BH15-2011, BH6A-2007 and BH10-2009 respectively represent the eastern, northern and southern Lunckefjellet. Guidelines for strength of relationship (R value) is given in Table 6.4. **Red** = Dust/clastic associated. **Green** = Groundwater associated.

The inclusion of Fe and S in the groundwater group in eastern (BH15-2011) and southern (BH10-2009) Lunckefjellet marks a difference between these two locations and northern Lunckefjellet (BH6A-2007), which suggest the following;

- Non-inclusion of S in the groundwater group at northern Lunckefjellet implies topography and/or proximity to palaeocoastline limited the supply

of “marine influenced groundwater” to the site during the Longyear period. Consequently, there is a different control on S supply such as atmospheric marine deposition or volcanogenic supply (Todd, 1980), but atmospheric marine is more likely as the S trend from base to top of seam reflects the drop followed by rise in sea level (Figure 6.12.B) as observed in other more marine influenced localities.

2) Bassen

In Bassen, the Ca, Fe and S species are generally more abundant than the dust/clastic deposition associated elements with the exception of Al (Table 6.7); this is similar to observations at Lunckefjellet. When compared to previous studies on the Longyear seam from the Adventdalen area (Orheim *et al.*, 2007; Marshall, 2013), S values are similar but other key elements such as Al and Ca show variations (Table 6.8). For example; Al contents range between 803 – 4179 ppm in this study, between 265 – 7528 ppm in Marshall (2013), and 1433 – 7361 ppm in Orheim *et al.* (2007). This variation is likely due to sample locality and distribution, and sampling resolutions. For example, Orheim *et al.* (2007) utilised bulk samples from 3 locations in the Adventdalen area (Mines 3, 6 and 7), whereas Marshall 2013 and this study utilised higher resolution samples from one sampling locality each, which would provide a better comparison. On further examination, Marshall (2013) reported higher values of Ca and Mg compared to this study; this is believed to be due to greater groundwater interaction with underlying Cretaceous marine shales in Mine 7, as this locality is down-dip of Bassen.

The correlation matrix for the Bassen samples (Table 6.9) groups Al, Na, and K as the dust/clastic deposition associated elements ($R \geq 0.55$), and groups Ca, Mg, Mn into the groundwater associated elements ($R \geq 0.66$). Fe correlates strongly

with only Mn in the groundwater group ($R = 0.78$), but shows weak correlation with other groundwater elements and the dust/clastic group, while S shows weak/no correlation with neither the clastic/dust nor groundwater group. This is similar to observations within the Longyear seam in Mine 7 (Marshall, 2013) and northern Lunckefjellet, which suggests a different control, such as atmospheric marine deposition (sea spray). Considering sea spray also provide Mg (e.g. Ault, 2013), there is a possibility that the groundwater influence on Mg and Ca may have overwhelmed their marine signal, resulting in their weak correlation with S.

Element	No. of samples	% of Samples measured	Mean (ppm)	Minimum (ppm)	Maximum (ppm)	Median (ppm)	STDEV (ppm)
Al	13	100	1972	803	4179	1717	1025
Ca	13	100	1529	581	3204	1306	826
Fe	13	100	6988	2752	29525	4846	7005
K	13	100	106	38	203	100	46
Mg	13	100	835	130	1662	815	514
Mn	13	100	27	3	129	7	42
Na	13	100	1323	1012	1937	1185	317
P	13	75	23	BD	65	16	18
S	13	100	8399	5356	15088	6901	3368
Ti	13	100	212	67	699	135	202

Table 6.7. Major element distribution of the Longyear seam in Bassen. (10,000 ppm = 1 %)

Element	Location		
	Bassen (This study)	Mine 7 (Marshall, 2013)	Mines 3, 6 and 7 (Orheim et al., 2007)
Al	803 – 4179	265 – 7528	1433 – 7316
Ca	581 – 3204	1825 – 65357	2327 – 7749
Fe	2752 – 29525	2935 – 14170	2857 – 7939
K	38 – 203	11 – 426	71 – 575
Mg	130 – 1662	554 – 6651	ND
Mn	3 – 129	BD – 76	ND
Na	1012 – 1937	637 – 3100	ND
P	BD - 65	BD	ND
S	5356 – 15088	3679 – 13758	6236 - 15215
Ti	67 - 699	31 - 2784	153 - 3491

Table 6.8. Comparing the contents of major elements in coals of the Adventdalen area between current and previous studies. Note: elemental contents are minimum to maximum values in ppm. (ND = not determined. BD = below detection. 10,000 ppm = 1 %)

	Al	Ca	Fe	K	Mg	Mn	Na	P	S
Ca	0.58								
Fe	0.34	-0.19							
K	0.55	0.29	0.10						
Mg	0.00	0.66	-0.14	0.08					
Mn	0.73	0.26	0.78	0.48	-0.06				
Na	0.56	0.60	-0.38	0.14	0.18	-0.13			
P	0.73	0.76	0.23	0.51	0.24	0.74	0.29		
S	-0.51	0.02	-0.24	-0.24	0.25	-0.36	-0.23	-0.17	
Ti	0.36	0.34	-0.25	0.43	0.12	-0.04	0.60	0.68	-0.42

Table 6.9. Correlation matrix of major elements in the Longyear seam in Bassen. Note: Fe correlates with the groundwater group while S shows no correlation which implies control other than groundwater. Guidelines for strength of relationship (R value) is given in Table 6.4. **Red** – Dust/clastic deposition associated. **Green** – Groundwater associated

3) Colesdalen

As in the Longyear coals at Bassen and Lunckefjellet, the Sputnik coals in Colesdalen are generally dominated by Ca, Fe and S group elements (Table 6.10).

Element	No. of samples	% of Samples measured	Mean (ppm)	Minimum (ppm)	Maximum (ppm)	Median (ppm)	STDEV (ppm)
Al	8	100	12149	904	71025	2013	24261
Ca	8	100	9063	2570	20741	6985	6169
Fe	8	100	26124	3100	102368	10795	35255
K	8	100	2806	24	17645	154	6115
Mg	8	100	2166	890	7907	1376	2360
Mn	8	100	40	2	195	16	65
Na	8	100	1832	960	6068	1200	1731
P	8	87.5	115	BD	224	91	76
S	8	100	35753	13895	120493	19402	36665
Ti	8	100	640	55	3701	154	1255

Table 6.10. Major element distribution of the Sputnik seam in Colesdalen BH3-3008
BD – below detection, (10,000 ppm = 1 %)

The correlation matrix (Table 6.11.A) places Al, K, Ti and Na within the dust/clastic deposition group ($R \geq 0.99$), while Mg and Mn are within the groundwater group

(R = 0.94). Fe shows a moderate correlation with the groundwater group (R = 0.57), and weakly correlates with the dust/clastic group. S weakly correlates with both the groundwater and clastic/dust group despite the relatively high marine influence at this locality (S between 1.4 – 12.1 %; Table 6.10), which is surprising; perhaps the relatively high marine influence may be swamping the groundwater signal.

	Al	Ca	Fe	K	Mg	Mn	Na	P	S
Ca	0.00								
Fe	0.35	0.37							
K	1.00	0.00	0.35						
Mg	0.99	0.03	0.28	0.99					
Mn	0.96	0.11	0.57	0.96	0.94				
Na	0.99	-0.05	0.30	0.99	0.99	0.95			
P	0.61	0.01	0.01	0.61	0.67	0.56	0.66		
S	0.22	0.38	0.99	0.22	0.14	0.45	0.16	-0.09	
Ti	1.00	-0.01	0.35	1.00	0.99	0.96	1.00	0.61	0.22

Table 6.11.A. Correlation matrix of major elements in the Sputnik seam in Colesdalen. Note: Fe shows only a moderate correlation with the groundwater group, while S do not correlate with the groundwater group. Guidelines for strength of relationship (R value) is given in Table 6.4. Red – Dust/clastic deposition associated. Green – Groundwater associated

Further examination of the sample distribution of the 8 Sputnik coals shows that sample C6 contains 12.1 % S, whereas the S contents of the other samples range between 1.4 – 2.3 %, which suggest that the correlation matrix in Table 6.11.A may be skewed by the much higher S contents of sample C6 which is an outlier. Consequently, the correlation for the Sputnik coals was re-run without the outlier (Table 6.11.B), which subsequently groups Al, K, Na and T, into the dust/clastic group ($R^2 \geq 0.97$), while Mg and Mn are incorporated into the groundwater group ($R = 0.99$) but Ca does not correlate with this group. Unlike the initial correlation (Table 6.11.A), Fe and S strongly correlates with both the dust/clastic and

groundwater groups in the re-run correlation ($R \geq 0.97$) (Table 6.11.B), and thus indicates marine influenced groundwater control at this site.

	Al	Ca	Fe	K	Mg	Mn	Na	P	S
Ca	0.05								
Fe	0.97	0.05							
K	1.00	0.06	0.97						
Mg	0.99	0.13	0.97	0.99					
Mn	0.99	0.07	0.99	0.99	0.99				
Na	1.00	0.03	0.99	0.99	0.99	1.00			
P	0.60	0.14	0.65	0.59	0.64	0.62	0.64		
S	0.97	0.05	1.00	0.97	0.97	0.99	0.99	0.62	
Ti	1.00	0.04	0.98	1.00	0.99	0.99	1.00	0.60	0.98

Table 6.11.B. Correlation matrix of major elements in the Sputnik seam in Colesdalen after excluding an outlier (Sample C6). Note both Fe and S are incorporated in the groundwater group, and thus indicates groundwater control on both elements. Guidelines for strength of relationship (R value) is given in Table 6.4. **Red** – Dust/clastic deposition associated. **Green** –

6.3.1.2. The Svarteper Seam

As in the previous section, assessments will be done according to elements associated with groundwater (Ca, Fe and S) and those associated with dust/clastic deposition such as Al, K, Na, Ti (e.g. Lawrence and Neff, 2009; Rudnick and Gao, 2003). The concentrations of the major elements in the 3 sampled locations of Lunckefjellet is presented in Table 6.12. The samples are dominated by the groundwater based elements with relatively low amounts of dust/clastic associated elements; this is similar to observations in the Longyear seam. Fe, S and Al are notably higher than observed in the Longyear seam; this is due to the more marine influenced nature of the Svarteper seam (in the case of Fe and S) and the more ash rich nature of the Svarteper seam (in the case of Al).

BH15-2011

Element	No. of Samples	% of Samples measured	Mean (ppm)	Minimum (ppm)	Maximum (ppm)	Median (ppm)	STDEV (ppm)
Al	8	100	13548	2346	29311	11871	11052
Ca	8	100	9592	3627	28922	7324	8263.7
Fe	8	100	41727	22144	65236	39400	13162
K	8	100	2204	87	5167	1830	2089.9
Mg	8	100	1661	1372	2263	1503	355.33
Mn	8	100	191	49	951	82	308.8
Na	8	100	2114	1045	3506	2227	780.05
P	8	100	134	39	280	108	82.07
S	8	100	59261	40286	82281	57819	13119
Ti	8	100	864	246	1731	745	604.06

BH6A-2007

Element	No. of Samples	% of Samples measured	Mean (ppm)	Minimum (ppm)	Maximum (ppm)	Median (ppm)	STDEV (ppm)
Al	3	100	13161	2932	32065	4486	16390
Ca	3	100	4798	2209	6102	6084	2242.3
Fe	3	100	31849	18105	46816	30626	14394
K	3	100	2853	576	7376	605	3917.5
Mg	3	100	1316	399	2321	1226	964.33
Mn	3	100	32	19	51	25	17.385
Na	3	100	2923	1587	4814	2369	1683.1
P	2	66.7	154	BD	266	154	158.48
S	3	100	46699	34104	58904	47090	12405
Ti	3	100	952	231	2274	351	1146.7

BH10-2009

Element	No. of Samples	% of Samples measured	Mean (ppm)	Minimum (ppm)	Maximum (ppm)	Median (ppm)	STDEV (ppm)
Al	5	100	27171	3823	57001	22127	20046
Ca	5	100	3847	1098	6386	3812	2088.3
Fe	5	100	48293	33172	64570	47904	13140
K	5	100	6890	651	14437	7330	5391.9
Mg	5	100	1849	915	3526	1528	1023.4
Mn	5	100	71	25	103	96	40.18
Na	5	100	3345	1902	4174	3867	972.78
P	4	80	225	BD	358	207	112.12
S	5	100	61918	40014	73586	68799	14569
Ti	5	100	2561	425	5025	2453	1848.8

Table 6.12. Major element distribution in the Svarteper seam in Lunckefjellet. Boreholes BH15-2011, BH6A-2007 and BH10-2009 respectively represent the eastern, northern and southern Lunckefjellet. (BD – Below detection)

The correlation matrices from all three locations in Lunckefjellet are presented in Table 6.13. In the east (BH15-2011), Fe and S are incorporated into the

groundwater group alongside Ca and Mn ($R = 0.67 - 0.99$) and they show no correlation to the Al group elements.

In the north (BH6A-2007), Fe and S correlate with the groundwater group including Ca, Mg, Mn ($R = 0.55 - 0.99$), as well as with the dust/clastic deposition group including Al, K, Na, and Ti ($R = 0.71 - 1.00$).

In the south (BH10-2009), Fe correlates strongly with S ($R = 0.83$), Mg correlates strongly with Mn ($R = 0.71$), while Al, K, Na and Ti all correlate ($R = 0.67 - 0.99$). S do not correlate positively with either group possibly because the groundwater signal is overwhelmed by marine contribution. The notable difference between these elemental associations and those observed within the Longyear coals in this area is the incorporation of Fe and S into the groundwater group in the north (BH6A-2007); this indicates that:

- By the Svarteper period, elevation and/or proximity to coastline were no longer a limiting influence on the supply of seawater to northern Lunckefjellet; thus the supply of these elements to the site were being controlled, at least in part, by "marine influenced groundwater". Meaning that seawater has a farther reach in the northern/north-eastern direction during the Svarteper period compared to the Longyear period.

BH15-2011

	Al	Ca	Fe	K	Mg	Mn	Na	P	S
Ca	-0.61								
Fe	-0.44	0.68							
K	1.00	-0.59	-0.42						
Mg	0.76	-0.28	-0.58	0.74					
Mn	-0.41	0.96	0.67	-0.39	-0.18				
Na	0.86	-0.72	-0.71	0.85	0.69	-0.57			
P	0.52	-0.35	-0.01	0.52	0.10	-0.15	0.56		
S	-0.49	0.67	0.99	-0.48	-0.64	0.66	-0.70	0.05	
Ti	0.99	-0.64	-0.47	1.00	0.73	-0.45	0.85	0.49	-0.52

(B) BH6A-2007

	Al	Ca	Fe	K	Mg	Mn	Na	P	S
Ca	0.54								
Fe	0.88	0.08							
K	1.00	0.51	0.90						
Mg	0.92	0.83	0.63	0.90					
Mn	0.99	0.64	0.81	0.99	0.96				
Na	0.98	0.69	0.77	0.97	0.98	1.00			
P	-1.00	-1.00	-1.00	-1.00	-1.00	-1.00	-1.00		
S	0.83	-0.02	0.99	0.85	0.55	0.75	0.71	-1.00	
Ti	1.00	0.55	0.88	1.00	0.92	0.99	0.98	-1.00	0.82

(C) BH10-2009

	Al	Ca	Fe	K	Mg	Mn	Na	P	S
Ca	-0.41								
Fe	-0.16	-0.71							
K	0.92	-0.63	0.08						
Mg	0.98	-0.31	-0.21	0.92					
Mn	0.78	-0.85	0.49	0.87	0.71				
Na	0.67	-0.19	-0.45	0.46	0.56	0.36			
P	-0.49	0.68	-0.44	-0.86	-0.54	-0.75	0.65		
S	-0.61	-0.31	0.83	-0.47	-0.67	-0.01	-0.56	0.05	
Ti	0.87	-0.67	0.13	0.99	0.87	0.85	0.40	-0.92	-0.43

Table 6.13. Correlation matrices of major elements in the Svarteper seam in 3 sampling localities in Lunckefjellet. Boreholes BH15-2011, BH6A-2007 and BH10-2009 respectively represent eastern, northern and southern Lunckefjellet. Note: guidelines for strength of relationship (R value) is given in Table 6.3. **Red** – Dust/clastic deposition associated, **Green** – Groundwater associated

Summarily, the concentration and distribution of elements in the 3 main areas assessed (Bassen, Lunckefjellet and Colesdalen) are generally similar with minor variations; these variations are brought about by the varying contributions of groundwater, sea spray, clastic deposition and possibly dust supply. Groundwater and sea spray appear to control the supply of S to the Longyear and Sputnik peatlands, whereas S supply to the Svarteper peatland seem to be mainly groundwater controlled. In terms of Fe, groundwater appears to mainly control its supply to both peatlands, although clastic deposition seems to have also contributed, albeit to a lesser degree.

6.3.2. Marine Control on S and Fe Distribution – Implications for Oil Potential

Fe seems to have a major control on the S chemistry of the Longyear and Svarteper peatlands; sulphate reduction within organic coastal and marine sediments leads to precipitation of pyrite (FeS_2). Considering the atomic weight, the ratio of Fe to S in pyrite is 0.87, Fe/S values in excess of 0.87 is therefore required to convert available S to pyrite. This section will assess the relative abundance of Fe and S within and between seams, in relation to oil potential in areas under study.

6.3.2.1. *The Longyear and Sputnik Seams*

The bulk Fe/S ratio for all samples examined is presented in Table 6.3; lower values are generally observed in coals with greater marine influence. In Bassen where the Longyear coals are only slightly marine influenced (S content between 0.5 – 1.5 %), the bulk Fe/S ratio is 1.01; this is greater than the ratio of Fe to S in pyrite (0.87) and thus interpreted as the abundance of available Fe significantly exceeding that of S required for pyrite formation (Table 6.3; Figure 6.10.D). Majority of the available S is sequestered as pyrite and the excess Fe is deposited as Fe-carbonates (Marshall, 2013), which possibly limited oil potential (Figure 6.10.A). Fe and S show dissimilar profiles from base to top of seam (Figures 6.10.B and 6.10.C), and a weak negative correlation ($R = -0.24$, Table 6.9), which suggests limited marine control on the distribution of these elements at this site

In eastern Lunckefjellet (BH15-2011), where marine influence upon the Longyear peatland is relatively greater than in Bassen for example, the bulk Fe/S ratio (0.82) is less than the ratio of Fe to S in pyrite (Table 6.3; Figure 6.11.D); this implies that the amount of available Fe is less than that of S required for pyrite formation, and thus favours the formation of OSC (Sinninghe Damsté and de Leeuw, 1990), and

consequently favours oil potential (Figure 6.11.A). Fe and S show similar trends from seam base to top (Figures 6.11.B and 6.11.C) with good correlation ($R = 0.69$, Table 6.6) indicating significant marine control on the distribution of these elements.

In northern Lunckefjellet (BH6A-2007), where topography and/or distance from inferred palaeocoastline is believed to have limited the supply of S, the bulk Fe/S ratio (0.87) does not exceed that required for pyrite formation (Table 6.3; Figure 6.12.D), which limited oil potential (Figure 6.12.A). Although Fe and S generally increase from base to top of the seam (Figures 6.12.B and 6.12.C), both elements display very weak correlation ($R = 0.16$, Table 6.6), which indicate limited marine control on the distribution of these elements at this site.

In southern Lunckefjellet (BH10-2009) where marine influence is greatest (between 1.1 – 6.9 % S; Table 6.5) of all boreholes sampled in the Lunckefjellet area, the bulk Fe/S ratio of the Longyear coals (0.55) is significantly lower than the Fe to S ratio in pyrite (Table 6.3; Figure 6.13. D), which favours oil potential (Figure 6.13. A). Fe and S display very similar profiles (Figure 6.13.B and 6.13.C), with very strong correlation ($R = 1.0$, Table 6.6), which indicate significant marine control on their distribution.

In Colesdalen, marine sulphur input to the Sputnik peatland is relatively high (S between 1.4 – 12.1 %, Table 6.10). As observed in other locations which experienced high marine input, the bulk Fe/S ratio of the Sputnik coals (0.56) is much lower than that required for pyrite formation which favours oil potential (Figure 6.14.A). Fe and S display very similar trends (Figures 6.14.B and 6.14.C), with very strong correlation ($R \geq 0.99$, Tables 6.11.A and 6.11.B), which indicate significant marine control on their distribution.

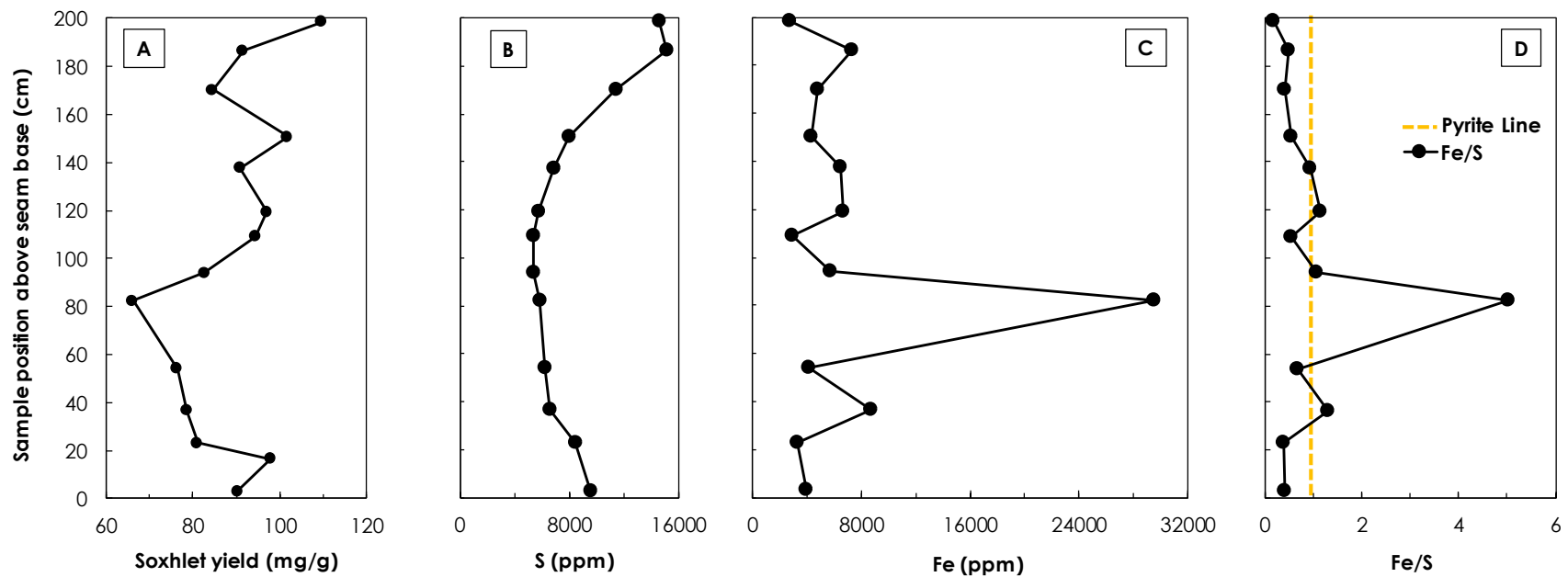


Figure 6.10. Comparing the profiles of; Soxhlet yield (dwc), S content, Fe content and Fe/S ratio, within the Longyear seam in Bassen. Pyrite line is defined as the ratio of Fe to S in pyrite (0.87). Sections to the right of the pyrite line in (D) indicate that Fe contents exceed that of S in pyrite, which correlate with low oil yield. Dissimilar profiles of Fe and S ($R = -0.24$) suggest limited marine control on the distribution of both elements at this site.

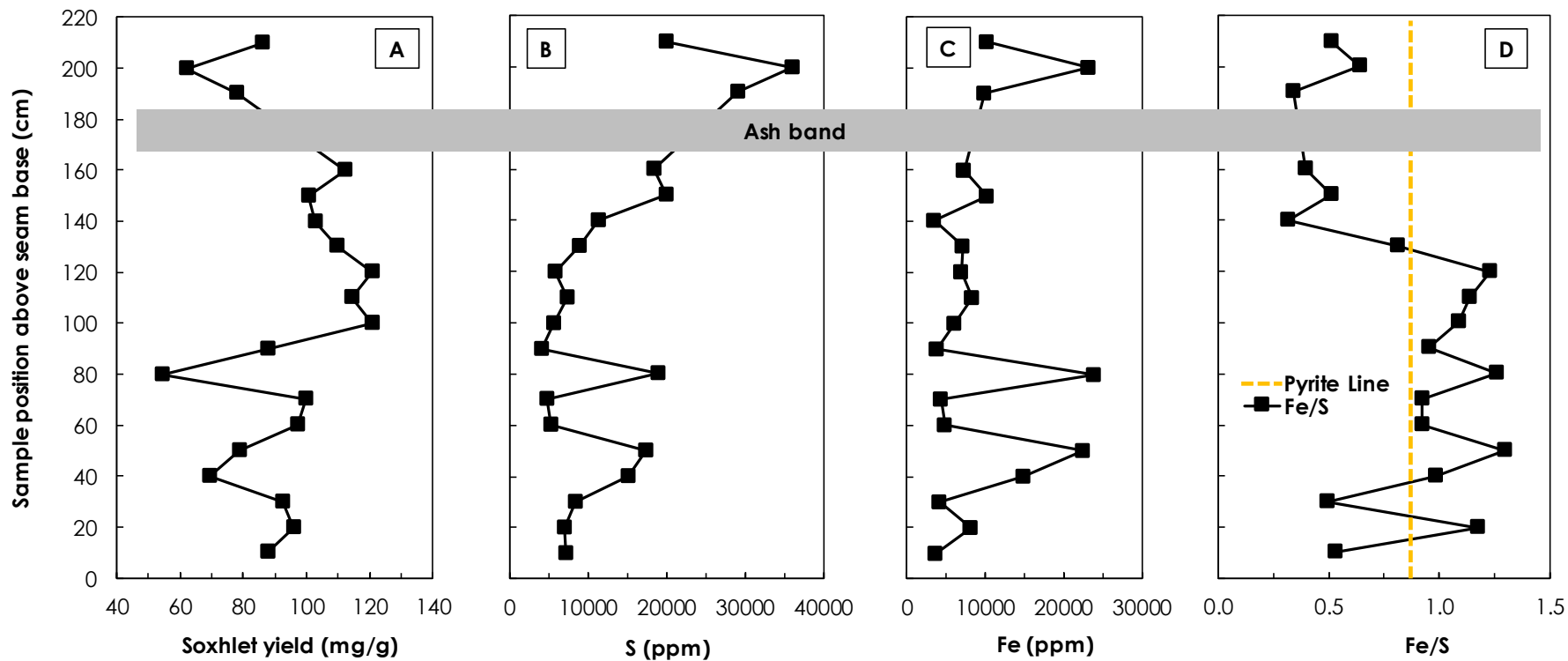


Figure 6.11. Comparing the profiles of; Soxhlet yield (dwc), S content, Fe content and Fe/S ratio, within the Longyear seam in Lunckefjellet BH15-2011. Pyrite line is defined as the ratio of Fe to S in pyrite (0.87). Sections to the right of the pyrite line in (D) indicate that Fe content exceed that of S in pyrite, which correlate with lower oil yield. Similar profiles of Fe and S ($R = 0.69$) suggest significant marine control on the distribution of both elements at this site.

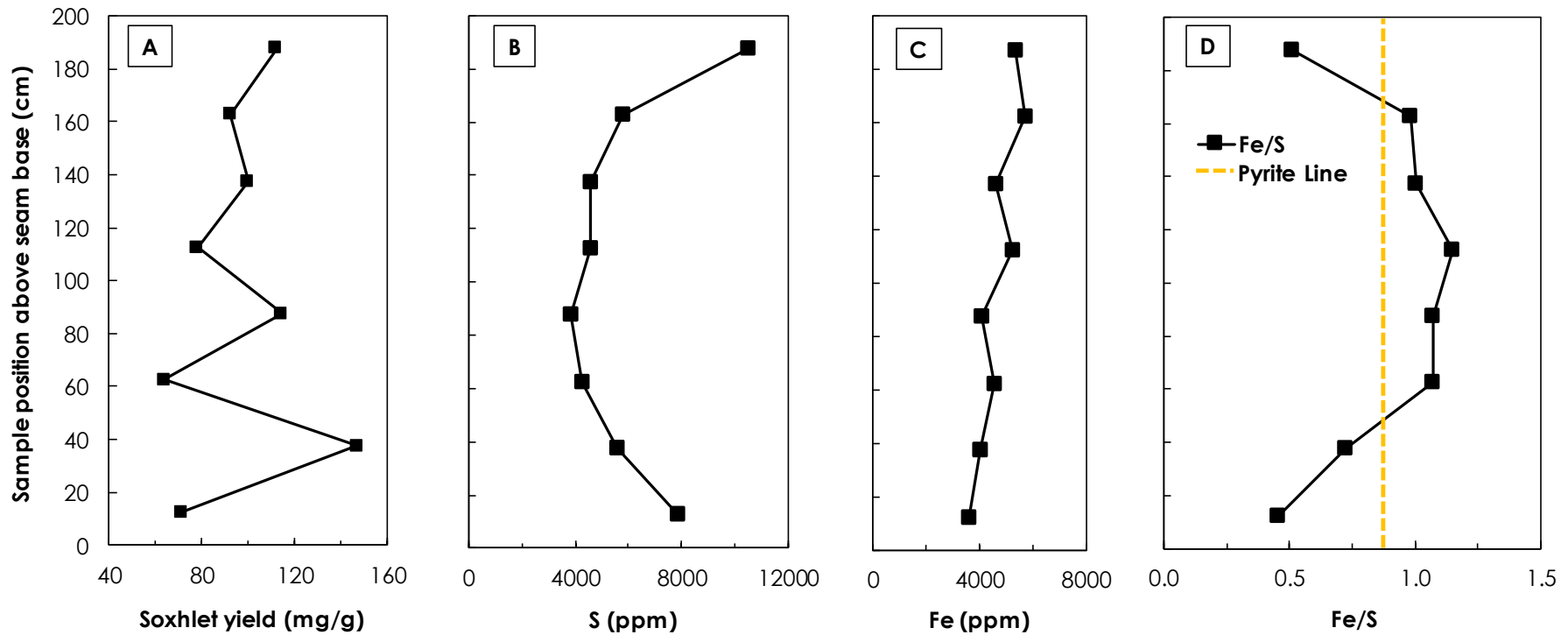


Figure 6.12. Comparing the profiles of; Soxhlet yield (dwc), S content, Fe content and Fe/S ratio, within the Longyear seam in Luncketjellet BH6A-2007. Pyrite line is defined as the ratio of Fe to S in pyrite (0.87). Sections to the right of the pyrite line in (D) indicate that Fe contents exceed that of S in pyrite, which correlate with lower oil yield. S and Fe show weak correlation ($R = 0.16$), which is indicative of limited marine control at this site.

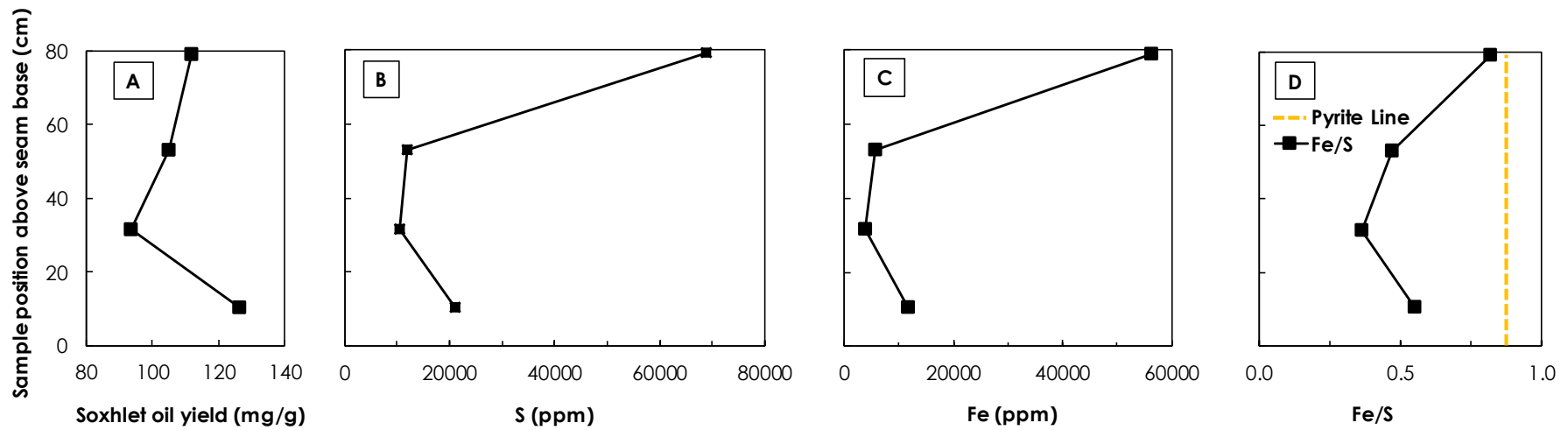


Figure 6.13. Comparing the profiles of; Soxhlet yield (dwc), S content, Fe content, Fe/S ratio, within the Longyear seam in Lunckefjellet BH10-2009. Pyrite line defined as the ratio of Fe to S in pyrite (0.87). Consistently Low Fe/S ratio is driven by marine S, which favours oil potential. Similar profile of S and Fe with very strong correlation ($R = 1.0$) is indicative of strong marine control at this site.

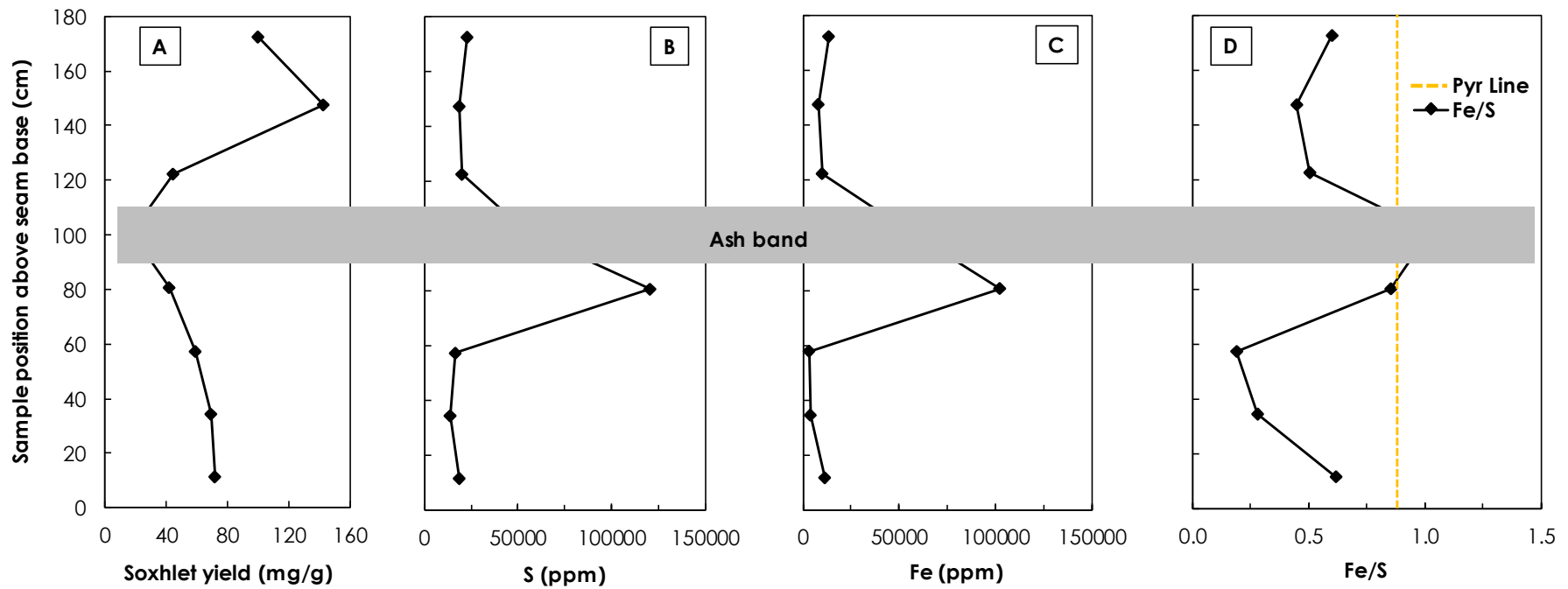


Figure 6.14. Comparing the profiles of; Soxhlet yield (dwc), S content, Fe content and Fe/S ratio, within the Sputnik seam in Colesdalen. Pyrite line defined as the ratio of Fe to S in pyrite (0.87). Very low Fe/S ratio driven by marine S, which favours oil potential. Similar profile of S and Fe ($R = 0.99$) is indicative of strong marine control at this site.

Further examination of the Soxhlet yield profiles from base to seam top shows that the fen transition associated with sea level rise is prominent in Bassen (Figure 6.10), Lunckefjellet BH15-2011 (Figure 6.11) and Colesdalen (Figure 6.14,) but absent in northern Lunckefjellet (BH6A-2007, Figure 6.12). From evidence, this is due to limited groundwater supply as controlled by the local topography and/or distance to inferred palaeocoastline in northern Lunckefjellet. Thus, groundwater may have a significant control on oil potential of the coals under study and will be examined further in Section 6.3.3. It is noted that the Fen transition is not observed in southern Lunckefjellet (BH10-2009) due to the close proximity to inferred palaeocoastline and/or vulnerability to seawater inundation, which resulted in a comparatively thinner coal (<1.0 m thick). The influence of proximity to inferred palaeocoastline is further discussed in Section 6.4.

6.3.2.2. *The Svarteper Seam*

S and Fe distributions were assessed within the Svarteper coals in Lunckefjellet. In the east (BH15-2011), Fe and S display similar profiles (Figures 6.15.B and 6.15.C) and a very strong correlation ($R = 0.99$, Table 6.13). The bulk Fe/S ratio (0.69, Table 6.3) is consistently lower than the Fe/S ratio in pyrite in all samples (Figure 6.15.D); this implies strong marine control throughout peat accumulation, which favours oil potential (Figure 6.15.A).

In southern Lunckefjellet (BH10-2009), Fe and S show strong correlation ($R = 0.83$, Table 6.13). Bulk Fe/S ratio (0.79; Table 6.3) is significantly less than that required for pyrite formation, but surprisingly increases from base to seam top beyond the pyrite line, and correlates with decreasing oil potential (Figures 6.16.A and 6.16.D). This implies an increasingly changing control on Fe supply from base to seam top, possibly due to a more clastic deposition and consequently greater ash content.

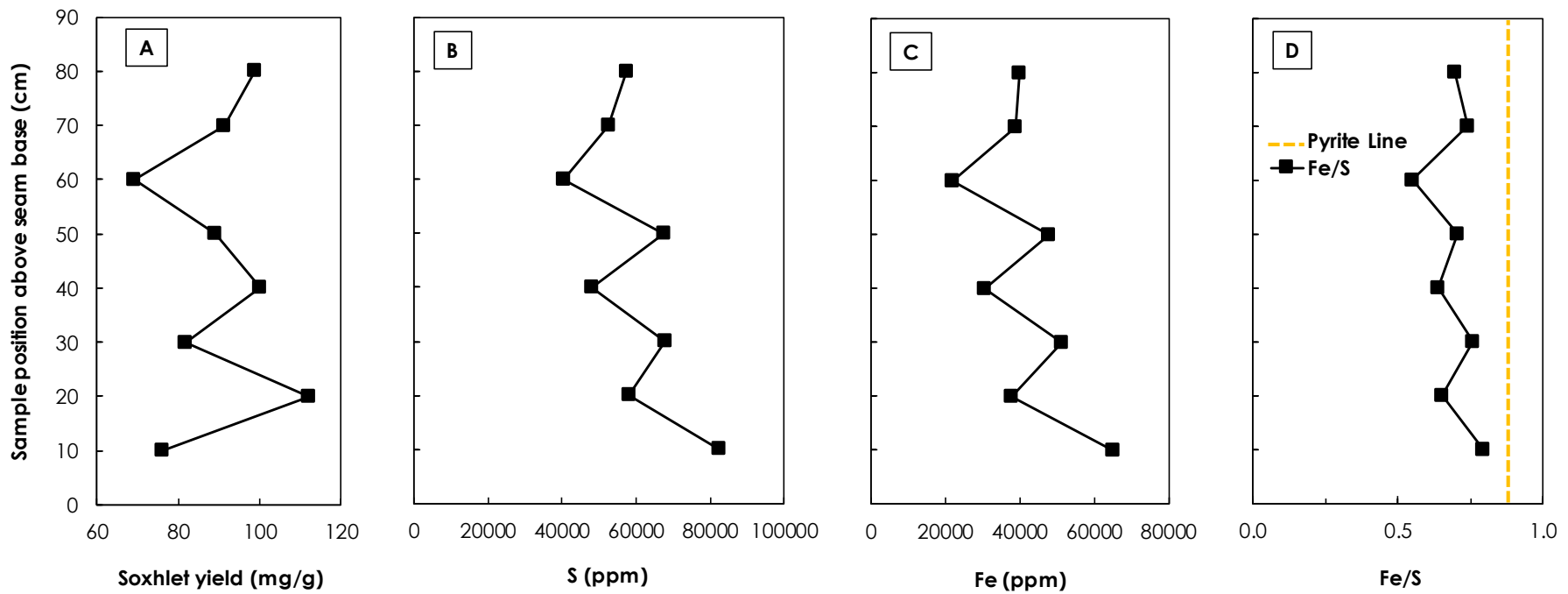


Figure 6.15. Comparing the profiles of; Soxhlet yield (dwc), S content, Fe content and Fe/S ratio, within the Svarteper seam in Lunckefjellet BH15-2011. Pyrite line is defined as the ratio of Fe to S in pyrite (0.87). Fe/S ratio is consistently less than pyrite line, which favours oil potential. S vs Fe show strong correlation ($R = 0.99$).

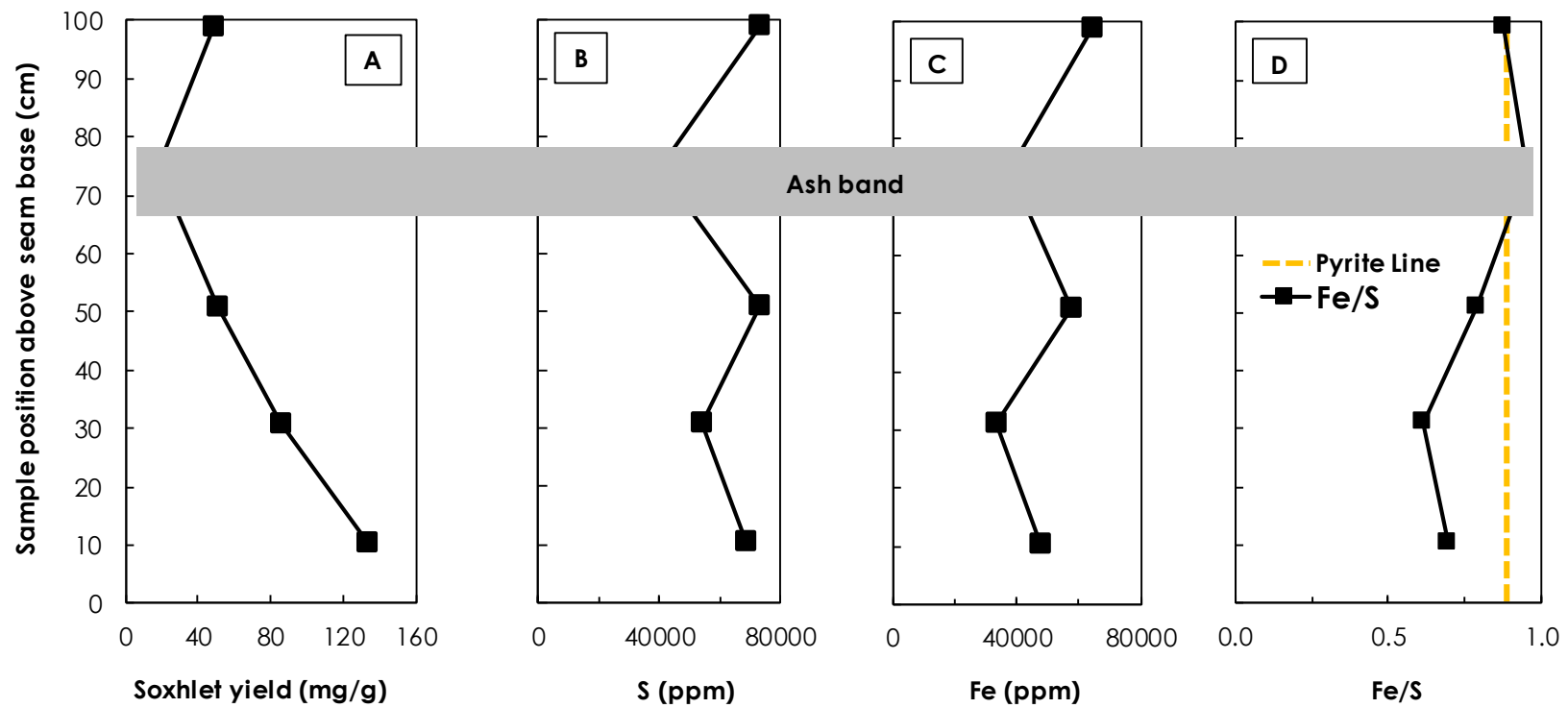


Figure 6.16. Comparing the profiles of; Soxhlet yield (dwc), S content, Fe content and Fe/S ratio, within the Svarteper seam in Lunckefjellet BH10-2009. Pyrite line is defined as the ratio of Fe to S in pyrite (0.87). Fe and S show similar trend with strong correlation ($R = 0.83$) indicating significant marine control, but Fe/S increases towards the seam top leading to decreasing in Soxhlet yield towards seam top.

Comparing Fe/S ratio, S and Soxhlet yield profiles within and between coal seams shows that higher yields positively correlates with relatively higher S and lower Fe/S values; this indicates that whilst total S content is important, the S must be available, i.e., S must be relatively more abundant than Fe. The foregoing is believed to play a significant role in limiting the hydrocarbon yields of the Longyear coals in Bassen, although maturity, and to a much lesser degree, biodegradation both appear to have some effect as shown in chapters 4 and 5, and Section 6.2 of this chapter respectively. A moderate to strong positive correlation and similar profiles from base to seam top between S and Fe such as observed within the Longyear coals in Boreholes BH15-2011, BH10-2009 and BH3-2008, implies a greater interaction between both elements in response to greater marine influence. Conversely, in areas of relatively lower marine S input, Fe and S will display weak correlations/dissimilar profiles from base to seam top (e.g. the Longyear coal in Bassen and BH6A-2007).

The contents of Fe and S relative to oil potential is compared between the Longyear coals and the stratigraphically younger Svarteper coals from the eastern, northern and southern sampling localities in Lunckefjellet. Scatter plots of Fe/S vs S contents (Figure 6.17.A) show a weak negative correlation for the Longyear coals ($R^2 = -0.2$), but a strong positive correlation for the Svarteper coals ($R^2 = 0.7$), which indicates there is relatively greater marine control on Fe supply within the Svarteper peatlands. Also, the Svarteper coals generally show lower Fe/S values, and consistently plot on the left hand side of the pyrite line (Figure 6.17.A). The relative distributions of Fe and S therefore suggest the Svarteper coals would show greater oil potential; however, this is not the case as they display similar oil potential as the Longyear coals (Figure 6.17.B). This suggests other

limiting factor(s) on oil potential are possibly having a greater effect on the Svarteper coals and will be further examined.

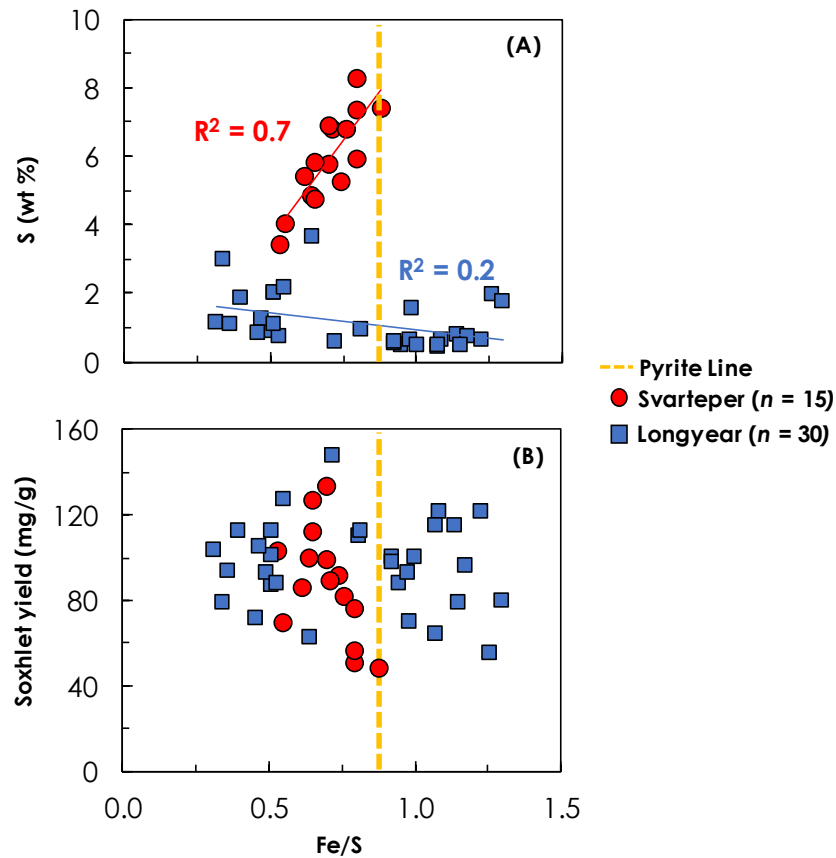


Figure 6.17. Fe and S discrimination relative to Soxhlet yield (dwc) between the Longyear and Svarteper coal seams in Lunckefjellet. (A) Greater marine S contents of the Svarteper coals results in generally lower Fe/S ratio. (B) Lower Fe/S ratio in the Svarteper coals does not result in higher oil potential. Pyrite line defined as the ratio of Fe to S in pyrite (0.87).

6.3.3. Groundwater Influence on the Oil Potential of the Firkanten Fm. Coals

It has been noted that the oil potential in northern Lunckefjellet may have been impacted by inadequate groundwater supply due to local topography (Section 6.3.1.1). Marshall (2013) examined the mineral composition of the Longyear seam in Mine 7, and reported the dominance of Ca/Fe carbonates and pyrite (FeS_2); the Ca/Fe carbonates comprises of Calcite ($CaCO_3$), Ankerite

[Ca(Fe.Mg.Mn)(CO₃)₂] and Siderite (FeCO₃). The presence of these minerals explains the positive relationships between Ca, Mg, Mn and Fe in most of the coals under study (Section 6.3.1). The Ca, Fe, and Mg group of elements represent one of the most common constituents within groundwater (Todd, 1980), and Fe and Ca are believed to be enriched by groundwater interaction with underlying Cretaceous marine shales in the CTB. Thus, groundwater may have a significant control on oil potential.

6.3.3.1. *The Longyear and Sputnik Seams*

Increased oil yields have been shown to be associated with the transition of the Longyear and Sputnik seam from a more ombrotrophic (precipitation fed) peatland to a more rheotrophic (groundwater fed) system; however, the lithophile elements (Al, Ti, Cu, Na, K) within the Longyear seam are reported to be unaffected by the transition indicating other controls (clastic deposition and/or dust supply) upon their concentration (Marshall, 2013). Thus, this section will focus on the Ca, Fe and Mg group elements.

In eastern Lunckefjellet (BH15-2011), the amounts and distribution of the Ca, Fe and Mg group of elements shows a marked change at the fen transition (~90 cm; Figure 6.18), as the elemental distribution became more stable from seam base towards the seam top. This observation is consistent with a more stable groundwater supply during fen conditions, leading to increased oil potential in the upper seam (i.e. from ~90 cm to seam top).

In northern Lunckefjellet (BH6A-2007), the fen transition is not prominent, and Ca in particular shows an erratic distribution from base to seam top (Figure 6.19). This may be due to unstable groundwater supply at this locality, although the

absolute variations in Ca concentrations are similar to the “more stable” upper Longyear seam in eastern Lunckefjellet BH15-2011 (i.e. a smaller and generally less stable groundwater catchment compared to eastern Lunckefjellet). Oil potential showed no increase from base to seam top and appear to have been inhibited by the unstable nature of groundwater supply.

In Bassen, although the greater abundance of Fe relative to S due to limited marine input is believed to have negated oil potential; the raised bog to fen transition is prominent with increasing oil potential from base to seam top as observed in eastern Lunckefjellet. This is likely due to the stable groundwater supply from base to seam top as indicated by the Ca and Mg profiles (Figure 6.20), and thus indicates the influence of stable groundwater supply on oil potential.

Groundwater Influence on oil potential was also assessed within the Sputnik coals in Colesdalen; Ca and Mg are generally stable indicating a stable groundwater supply and greater oil potential (Figure 6.21). The prominent fen transition as observed in the Longyear seam may indicate that the Sputnik coals of the western coalfield of the CTB may be a Longyear coal equivalent.

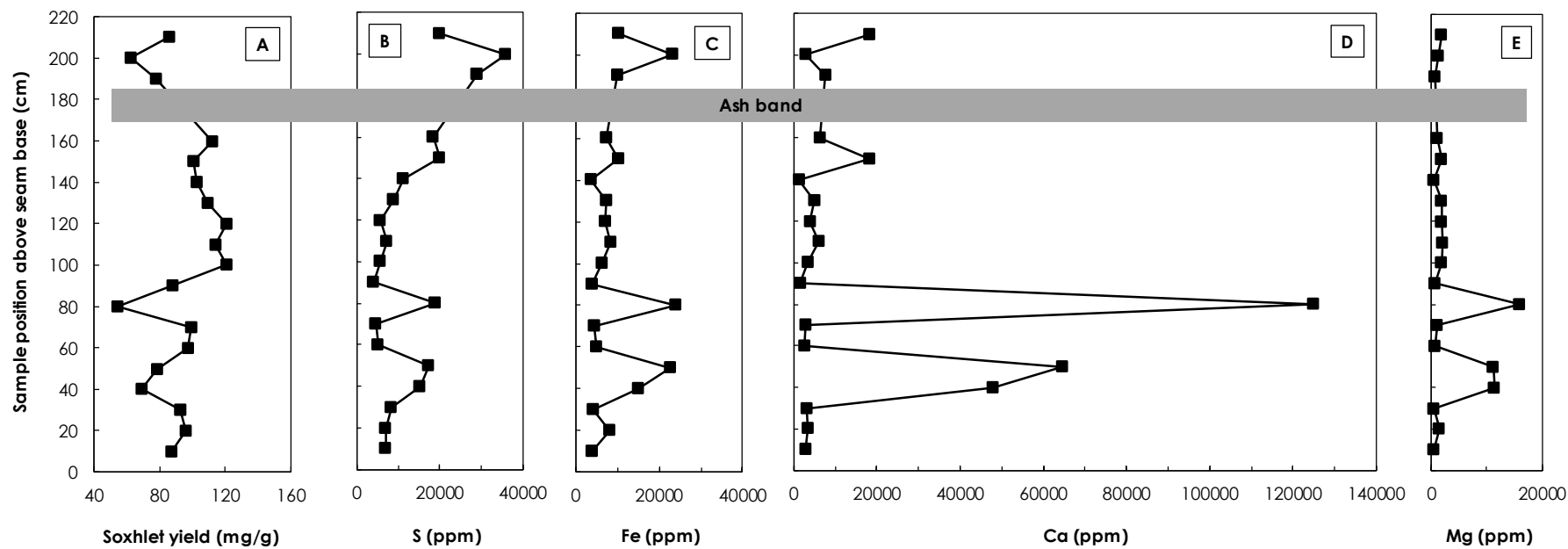


Figure 6.18. Comparing the profiles of; A) Soxhlet yield on dwc basis, B-E) Groundwater controlled elements, in the Longyear seam in eastern Lunckefjellet (BH15-2011). Note: stable elemental distribution from fen transition (~90cm) towards seam top suggests a relatively stable groundwater supply, which is believed to have facilitated greater oil potential in upper seam

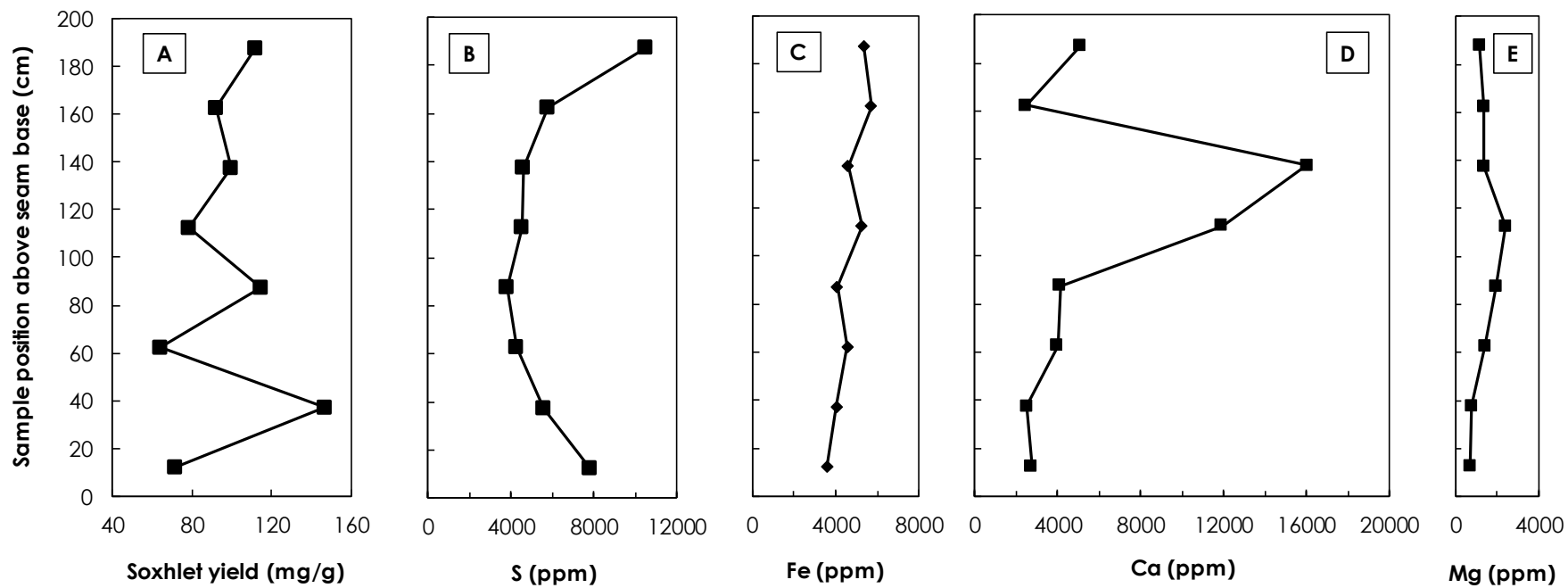


Figure 6.19. Comparing the profiles of; A) Soxhlet yield on dwc basis, B-E) Groundwater controlled elements, in the Longyear seam in northern Lunckefjellet (BH6A-2007). Note: erratic profile of Ca suggests an unstable groundwater supply which may have negatively impacted oil potential.

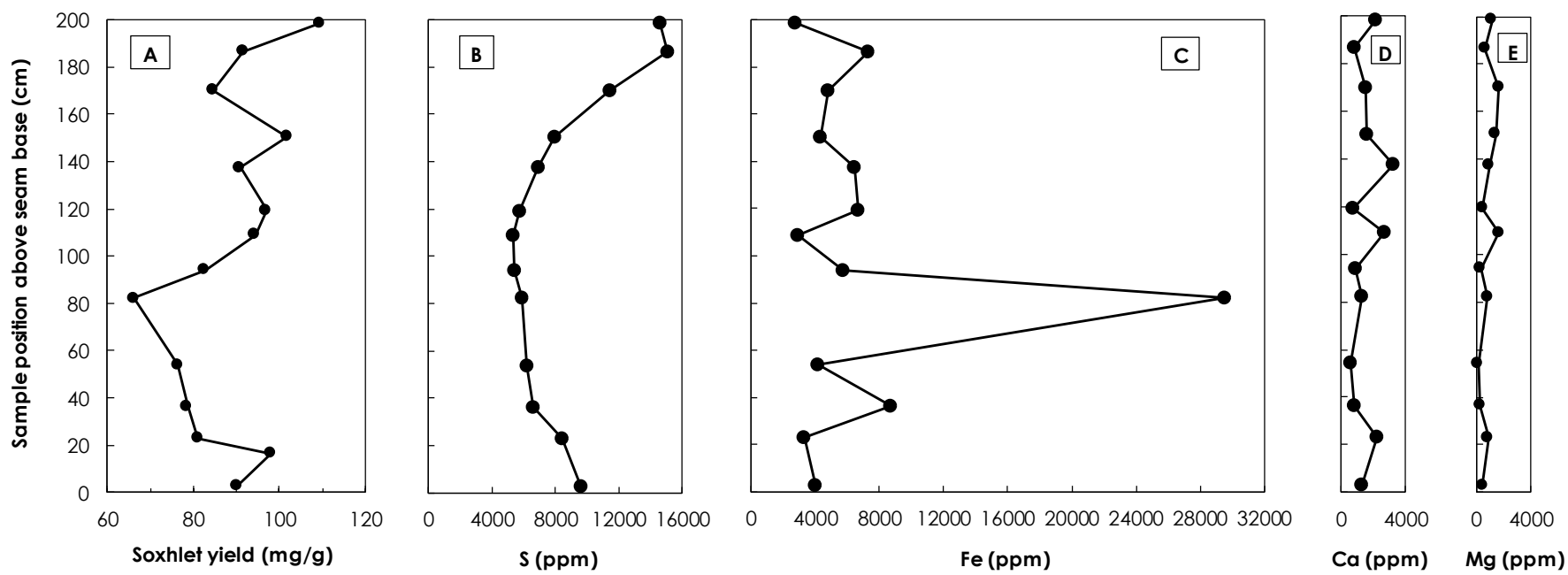


Figure 6.20. Comparing the profiles of; A) Soxhlet yield on dwc basis, B-E) Groundwater controlled elements in the Longyear seam in Bassen. Note: Ca and Mg distribution indicates stable groundwater, which is believed to have facilitated oil potential.

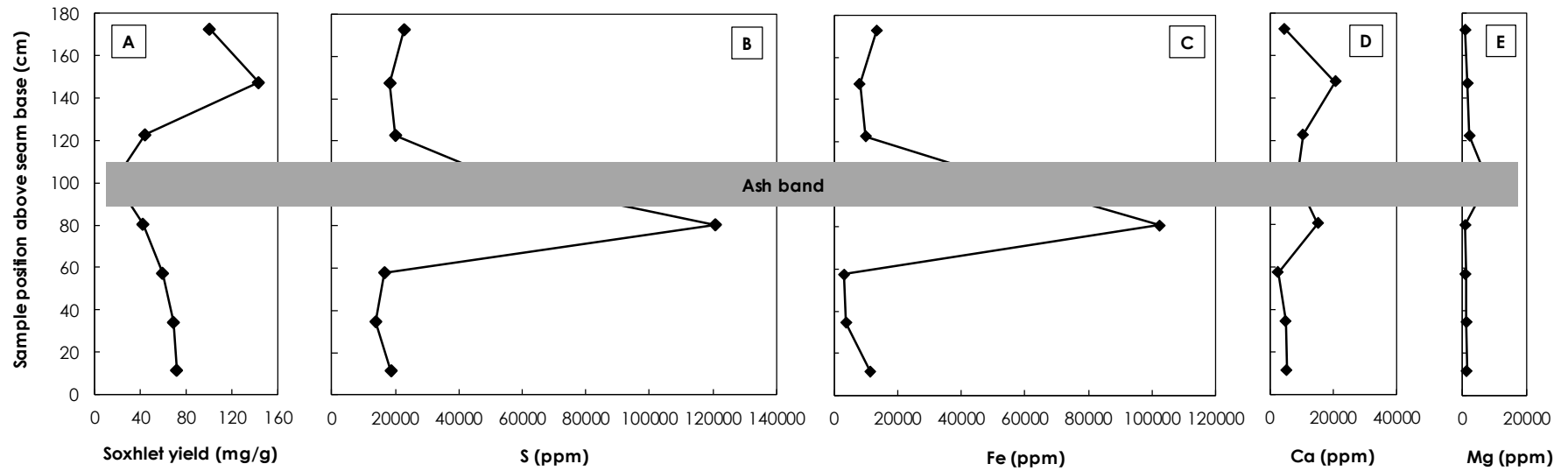


Figure 6.21. Comparing the profiles of; A) Soxhlet yield on dwc basis, B-E) Groundwater controlled elements in the Sputnik coal in Colesdalen. Note: Ca and Mg are generally stable indicating stable groundwater supply which is believed to have facilitated oil potential.

6.3.3.2. *The Svarteper Seam*

The Svarteper seams experienced a significant groundwater input to the peatland, with conditions similar to modern day coastal fens (Marshall, 2013); this implies peatland conditions (and possibly oil potential) may be similar to those observed within the more marine influenced areas of the Longyear seam. The distribution of groundwater associated elements and oil potential of the Svarteper coals in eastern Lunckefjellet (BH15-2011) is shown in Figure 6.22; Mg appear stable, while Ca appears to decrease steadily from seam base to top. S and Fe show erratic distribution alongside Soxhlet yield, and all three measurements generally decrease from base to top of seam. This indicates that other control may have a limiting influence on oil potential.

In southern Lunckefjellet (BH10-2009), Ca and Mg appear stable (Figure 6.23). S and Fe show similar but erratic profiles, while oil yield generally decreases from seam base to top. The rapid decrease in oil potential towards seam top is clearly influenced by other control, which is believed to have driven the Fe/S ratio beyond the pyrite line in Figure 6.16.D. This additional control is possibly the ash content, which will be examined in subsequent sections.

In summary, this section shows that whilst groundwater supply to the peatland is important; a stable supply will positively influence oil potential as it will ensure longer periods of favourable conditions, notably alkalinity (e.g. Hao and Chen, 1992, Marshall *et al.*, 2015a), which will sustain bigger bacteria communities leading to greater microbial degradation (Taylor *et al.*, 1998). Also, this section confirms that in addition to groundwater, clastic deposition has a greater control on the supply of Fe to the Svarteper peatland compared to the Longyear peatland.

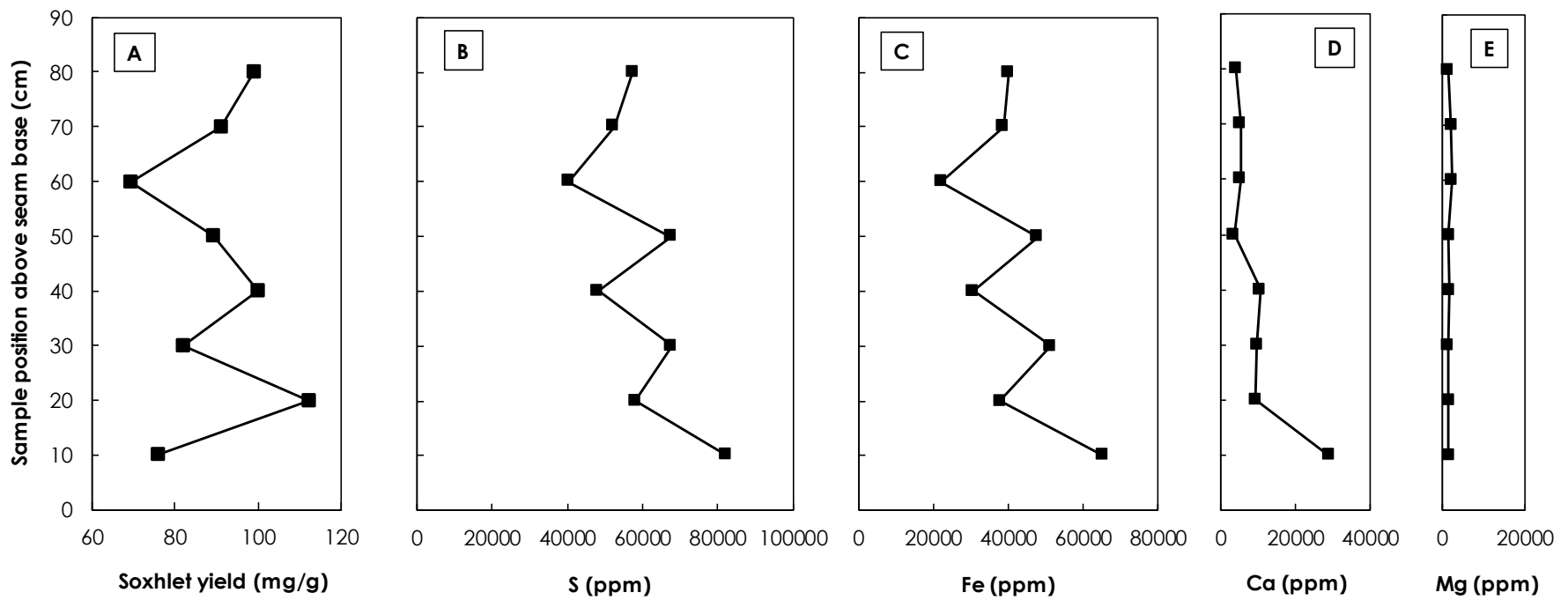


Figure 6.22. Comparing the profiles of; A) Soxhlet yield on dwc basis, B-E) Groundwater controlled elements, in the Svartepet seam in Lunckefjellet BH15-2011. Note: erratic distribution and general decrease in S and Fe, whilst Ca and Mg appears stable is an indication of other limiting influence on oil potential

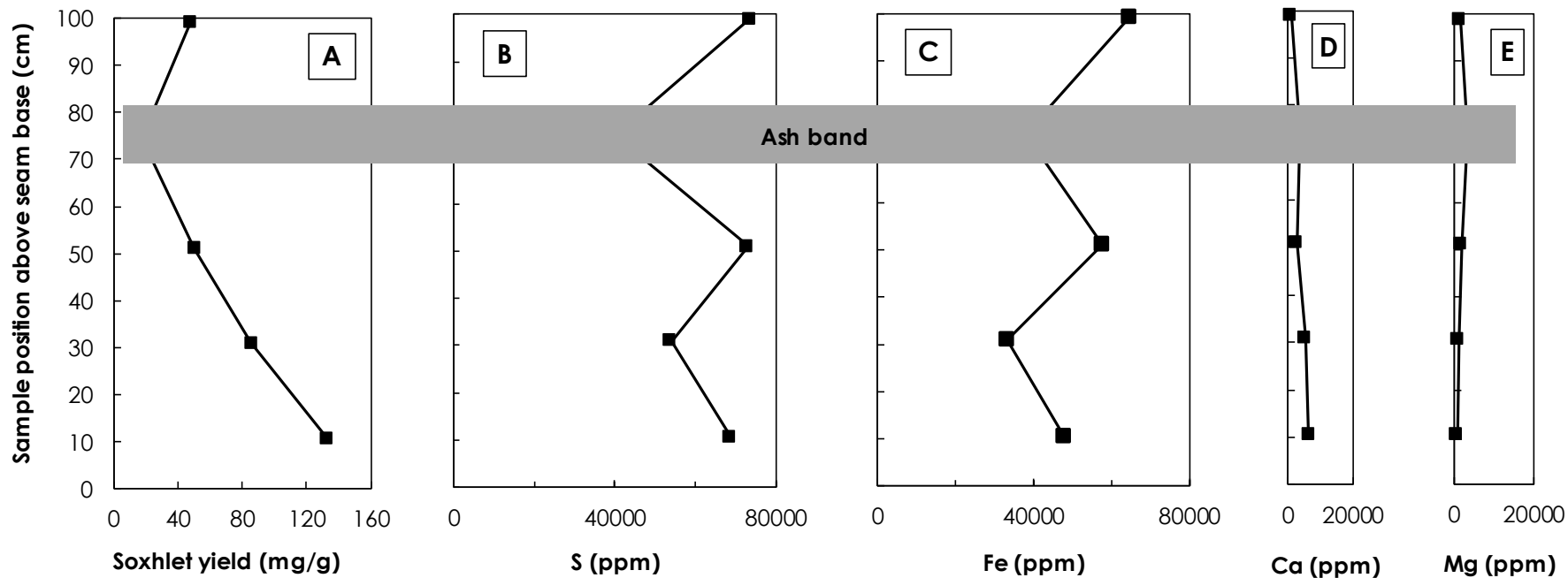


Figure 6.23. Comparing the profiles of; A) Soxhlet yield on dwc basis, B-E) Groundwater controlled elements in the Svarteper seam in southern Lunckefjellet BH10-2009. Steady decrease in Soxhlet yield towards seam top, alongside stable distribution of Ca/Mg and erratic distribution of S and Fe are all indications of other control which has a limiting influence on oil potential.

6.4. The Influence of Proximity to Inferred Palaeocoastline on Oil and Coal Potential

It has been shown that marine sulphur contents display positive variation with oil potential, and a major influence on marine S contents in coals is the proximity to palaeocoastline. A balance of “optimum proximity to inferred palaeocoastline” is required for delineation of optimum resource areas in the CTB, with optimum proximity being a distance not too close/far away from inferred palaeocoastline to allow formation of economic (sellable) coal in terms of quantity and quality. Quality will imply sufficient S contents accompanied with the right pH (alkalinity) to produce oil prone coals, but not too close to the coast to prevent excess S and ash content. For a better understanding of the economic relationship between proximity to palaeocoastline and product (i.e. coal and oil), the map of coal thickness for the Longyear seam at the eastern CTB and inferred palaeocoastline during periods of relative sea level drop and rise (Marshall, 2013) are presented in Figures 6.24.A and 6.24.B respectively. A summary of Soxhlet yield, seam thickness, S and ash contents in the eastern, southern and northern sampling localities in Lunckefjellet, and Bassen are also presented (Table 6.14; Figure 6.25), which show seam thicknesses increase, while coal quality parameters such as S and ash contents decrease in the direction away from the inferred palaeocoastline. For example, the Lunckefjellet BH10-2009 site, due to its closer proximity to the inferred palaeocoastline (Figures 6.24.A and 6.24.B) and consequently high marine S (mean S = 2.8 %), shows only slightly higher Soxhlet yields and peatland was short-lived leading to half the coal thickness and higher ash contents compared with coals in locations farther away from the inferred palaeocoastline. Thus, <95 cm coal was formed in BH10-2009, with relatively higher S contents, which is not significantly reflected in oil potential compared to the other localities farther away from the inferred palaeocoastline.

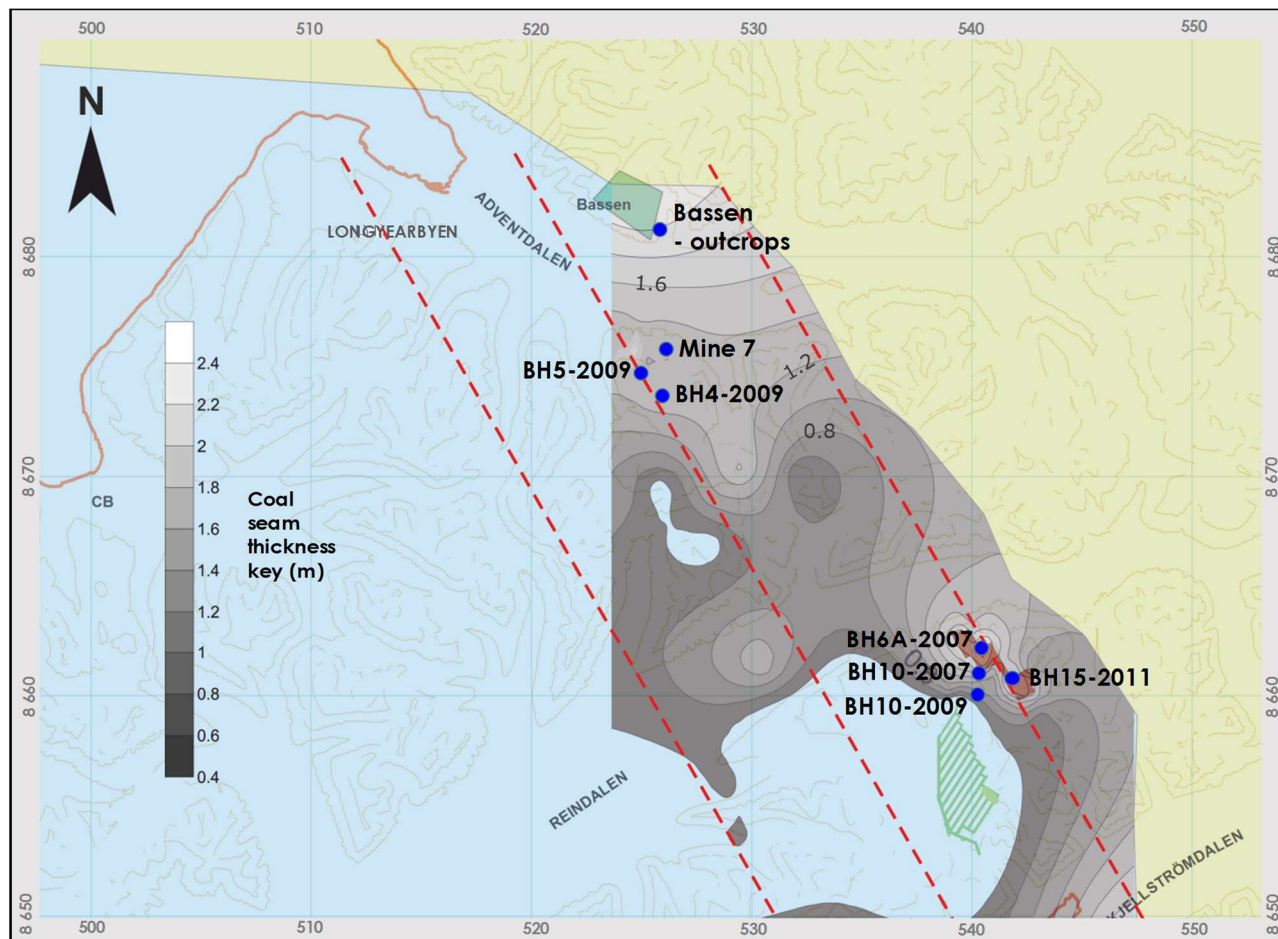


Figure 6.24.A The Longyear seam thickness map for the eastern CTB showing the influence of proximity of coal resource to the inferred palaeocoastline during period of relative sea level drop. Yellow boarder represents the limit of tertiary sedimentation. Note: Seam thickness increases away from palaeocoastline, while S and ash contents decrease. Broken red lines represent ridges, which parallel the trough and swell series in the eastern CTB (Figure 5 of Eiken, 1985). Marshall (2013) reported that these ridges exerted some control on the thickness of the Longyear coal particularly in the Lunckefjellet area where the new mine lies adjacent to the Billefjordan ridge (Modified from Marshall, 2013).

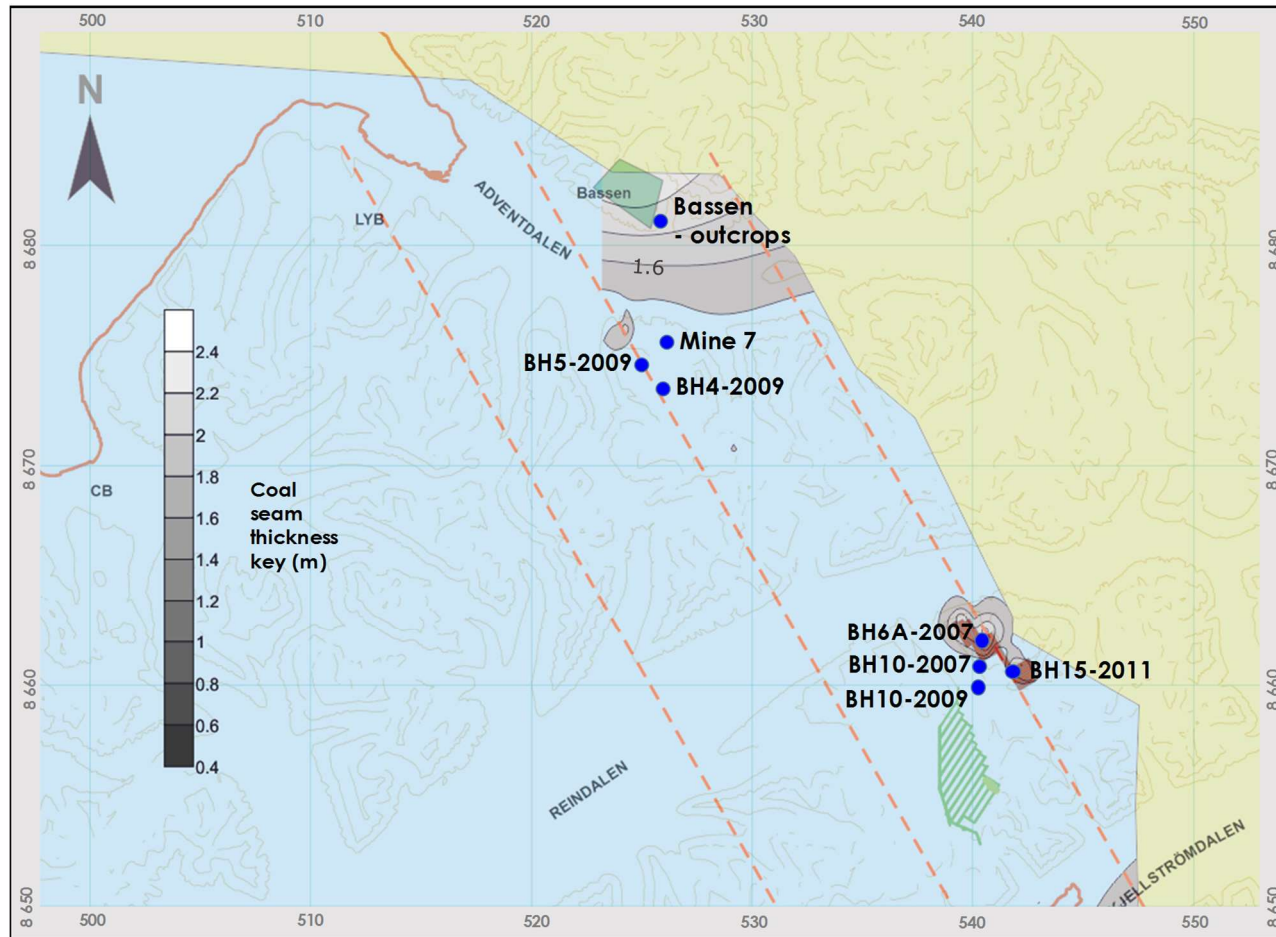


Figure 6.24.B The Longyear seam thickness map for the eastern CTB showing the influence of proximity of coal resource to inferred palaeocoastline during the period of relative sea level rise. Note: Bassen and Lunckefjellet BH6A-2007 localities were not flooded during sea level rise, and are within the inferred "optimum distance" to palaeocoastline (Modified from Marshall, 2013).

Location	Soxhlet yield (mg/g dwc)	Soxhlet yield (mg/g daf)	Seam thickness (cm)	Sulphur (%)
BH15-2011	93.2	100.7	210	1.3
BH10-2009	109.1	116.9	95	2.8
BH10-2007	105.6	111.7	160	2.4
BH6A-2007	97.4	100.7	200	0.6
Bassen	88.7	90.2	200	0.8

Table 6.14. Comparing Soxhlet yield, coal thickness and sulphur contents at Lunckefjellet and Bassen.

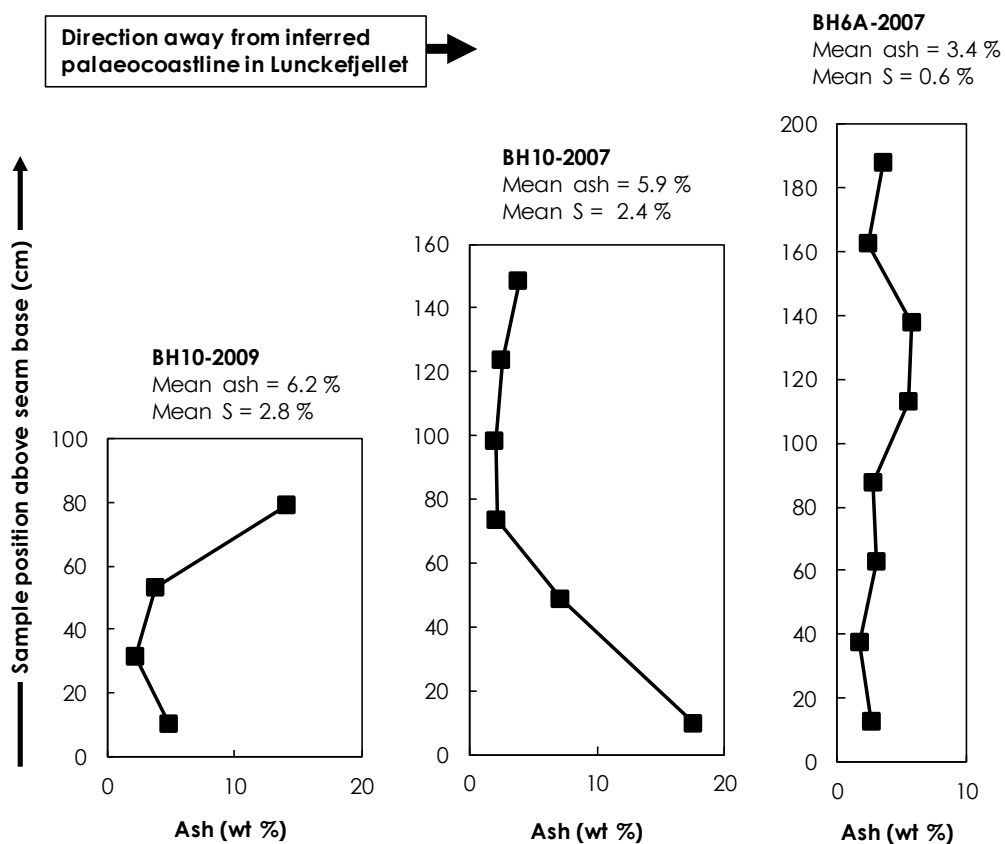


Figure 6.25. Variations in resource quality and quantity relative to the distance from inferred palaeocoastline along the Lunckefjellet N-S sampling cross section in Figure 6.24. Note: the graph heights are median values above seam base for the uppermost sample and reflects the true seam thickness which is shown in Table 6.14.

With regards to S and oil potential, Large *et al.* (2011) modelled the effect of sea salt sulphate deposition at low, medium and high latitude, which led Marshall (2013) to predict that optimum proximity to inferred palaeocoast in the CTB would

be within 2 – 4 km. This model places the Lunckefjellet BH6A-2007 and Bassen sampling localities within the optimum distance taking the periods of maximum sea level rise into consideration (Figure 6.24.B). It is noted that local topography (i.e. height above sea level) plays an important role in estimating the optimum distance. As shown in Figure 6.24.B, the BH6A-2007 site in Lunckefjellet survived flooding during sea-level rise even though inferred palaeocoastline was in closer proximity compared to Bassen where inferred palaeocoastline was much farther away. Thus, further work involving a more detailed palaeogeography model with a widespread data set (specifically using other lithologies) is required to confirm range of distance.

6.4.1. Coal Ash

It has been established that ash is one of the main coal quality issues notably affecting the Askeladden, Svarteper and Verkny coal seams, and to a much lesser extent, the Longyear and Sputnik seams. This section will firstly analyse the ash content and distribution within and between coal seams from all areas under study, and subsequently analyse the varying influence of ash content on the oil potential of the coals. The ash content for all samples under study was determined according to methods detailed in Chapter 3. The Longyear coal in Bassen show the best quality of all coals examined in terms of ash content (<2 %; Table 6.15), this is consistent with their inferred distance from palaeocoastline during sea level rise (Figure 6.24.B).

The Breinosa sampling locality (BH4-2009) on the other hand, display the highest ash content with the Askeladden, Svarteper and Longyear coals respectively showing values of 17, 40 and 25 % at this locality (Table 6.15); this implies a close

proximity to palaeocoastline as indicated by their high S contents (1.9 – 10.5 % S) and/or vulnerability to clastic deposition.

In Lunckefjellet, the ash contents of the Longyear coals range between 3 – 8 % (Table 6.15) and increases in the southerly direction from BH6A-2007 to BH10-2009. Within the Svarteper coals in Lunckefjellet, ash content range between 19 – 32 % (Table 6.15), and shows similar profile of increase in the southerly direction as the Longyear coals. This trend is consistent with the southerly tilting of the CTB (e.g. Ćmiel and Fabiańska, 2004; Nagy, 2005; Orheim *et al.*, 2007), which structurally controlled clastic deposition, and also consistent with the direction towards the inferred palaeocoastline where coals are relatively more vulnerable to flooding.

In Colesdalen, the ash contents variation between coal seams is similar to observations in the eastern coalfield as measured values of the stratigraphically younger Verkny coal (31 %) is higher than that of the older Sputnik coal (9 %) (Table 6.15).

Area	Location and sample type	Seam	No of samples	Mean (wt %)	Min (wt %)	Max (wt %)	Med (wt %)	STDEV (wt %)
Bassen	Outcrops	Longyear	32	1.8	0.8	5.3	1.4	1.0
Breinosa	BH4-2009	Askeladden	2	17.1	16.4	17.7	17.1	0.9
Breinosa	BH4-2009	Svarteper	5	38.9	24.9	52.0	42.8	11.6
Breinosa	BH4-2009	Longyear	6	24.9	7.8	64.4	18.1	20.7
Lunckefjellet	BH15-2011	Svarteper	8	18.9	9.7	28.1	21.6	6.5
Lunckefjellet	BH15-2011	Longyear	19	8.0	0.9	33.3	3.4	9.3
Lunckefjellet	BH10-2009	Svarteper	4	31.6	12.9	51.8	30.8	18.2
Lunckefjellet	BH10-2009	Longyear	4	6.2	2.2	14.2	4.3	5.4
Lunckefjellet	BH10-2007	Svarteper	2	20.4	18.3	20.7	20.4	3.0
Lunckefjellet	BH10-2007	Longyear	6	5.9	2.0	17.6	3.3	6.0
Lunckefjellet	BH6A-2007	Svarteper	3	18.5	7.3	40.2	7.9	18.8
Lunckefjellet	BH6A-2007	Longyear	8	3.4	1.7	5.8	2.9	1.5
Colesdalen	BH3-2008	Verkny	1	30.8	30.8	30.8	30.8	-
Colesdalen	BH3-2008	Sputnik	7	9.2	1.9	73.9	6.2	24.1

Table 6.15. Ash data of the Firkanten Fm. coals under study

6.4.1.1. Ash Content and Oil Potential of the CTB coals

From evidence, oil potential increases owing to increased marine S deposition, and ash content generally decrease away from inferred palaeocoastline alongside S contents. Consequently, ash content is expected to correlate (to some extent) with oil potential. A scatter plot of Soxhlet yield vs ash content for 106 coals under study shows a linear negative correlation (Figure 6.26); notably, the Askeladden, Svarteper and Verkny (A-S-V) coals show a strong negative correlation ($R^2 = 0.71$), while the Longyear and Sputnik (L-S) coals shows a weak negative correlation ($R^2 = 0.24$). This is a clear indication that ash contents of the A-S-V coals are having a greater impact on their oil potential relative to the influence of ash contents on the oil potential of the L-S coals.

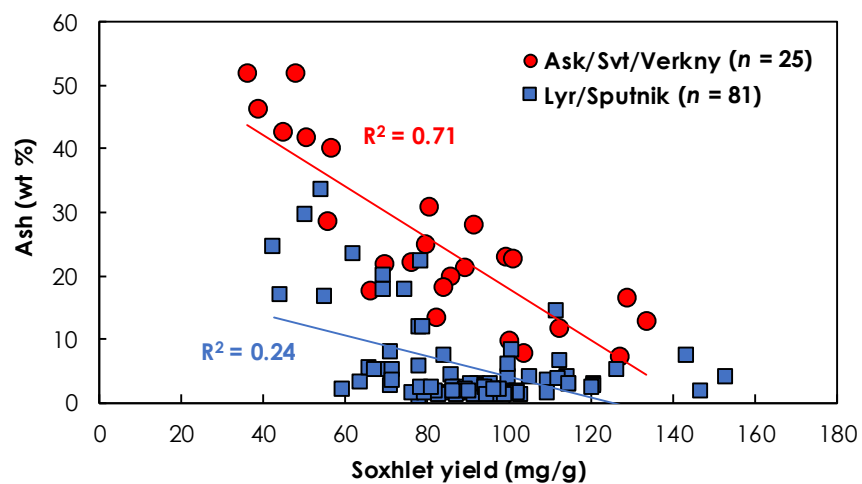


Figure 6.26. Soxhlet yield vs ash content discrimination between the Askeladden/Svarteper/Verkny and Longyear/Sputnik coals. Coals are from all other sample localities besides Mine 7. See Table 5.7 for data.

As noted in previous sections, the lower and upper L-S peatlands experienced raised-bog and “fen-like” conditions respectively, whereas the A-S-V peatlands predominantly experienced fen conditions. This implies the A-S-V coals will show similar, and possibly greater oil potential than the upper L-S coals. Within the

Upper Longyear in Lunckefjellet BH15-2011 locality (i.e. between 100 – 220 cm above seam base), Soxhlet yield increase from 10.1 % on whole coal basis, to 10.7 % on ash free basis (Figure 6.27). This is less than the increase observed within the Svarteper coals (i.e. increase from 9.0 % dwt, to 11.1 % daf; Figure 6.27) and thus indicates that the Svarteper coals in Lunckefjellet BH15-2011 may have greater oil potential than the Longyear coals.

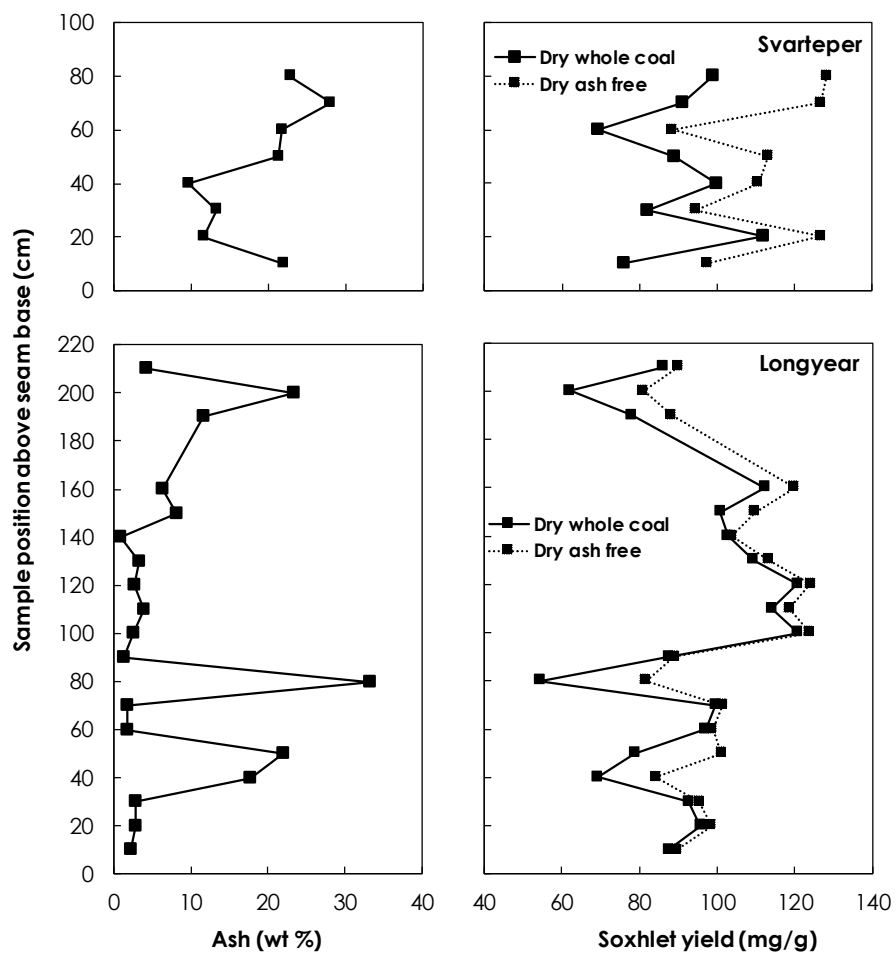


Figure 6.27. Comparing the ash and Soxhlet yield within the Svarteper seam (top) and the Longyear seam (bottom) in Lunckefjellet BH15-2011 locality.

Further examination of Figure 6.26 shows that the A-S-V coals, despite their higher ash content, have a similar range of Soxhlet yield as the L-S coals. For all 25 A-S-V

coals investigated, mean Soxhlet yield increased from 83.7 mg/g on dwc basis, to 109.6 mg/g on daf basis (Table 5.7). However, for all 81 L-S coals, mean Soxhlet yield increases from 91.0 mg/g on dwc basis, to 98.4 mg/g on daf basis. These figures represent a 30.1 % increase in soxhlet yield (i.e. from dwc to daf) for the A-S-V coals, but only an 8.1 % increase in Soxhlet yield (i.e. from dwc to daf) for the L-S coals. Thus, it is evident that the younger coals are more oil prone. It is again noted that the greater oil-prone nature of the younger coals (A-S-V) is driven by the predominantly fen conditions experienced during peat deposition, as opposed to the raised-bog to 'fen-like' conditions which characterised the L-S peatlands.

6.5. Weathering

This section examines the possible influence of weathering on the oil potential of the CTB coals. Weathering and biodegradation ultimately result in degradation; because biodegradation has been observed in some of the coals under study, and discussions in this section are relative to biodegradation, it is important to define these two terms for the purpose of clarity. Biodegradation is simply the decomposition by bacteria, while weathering involves disintegration and decomposition by physical and chemical processes (Kearey, 2001). Weathering causes the following changes in coal composition;

- Depletion of bitumen yield (Teo *et al.*, 1982).
- Decreased number of aliphatic structures (Fredericks *et al.*, 1983).
- Increased oxygen concentration (van Krevelen, 1961).
- Reduction of C and H content (Tekely *et al.*, 1987).

Oxidation is the most important process in the weathering of coal (van Krevelen, 1961), and relatively high oxygen index (OI) has been observed in the eastern

margin coals of the CTB (Figure 5.6; Tables 5.4 and 5.5). Physical weathering of coal is mainly caused by thermal diurnal changes, accompanied by the freezing of water in fractures and joints in cold climates (Ingram and Rimstidt, 1984) such as in Svalbard. According to Marchioni (1983), chemical weathering in coal is mainly promoted by oxygen, carbon dioxide, water and biota in processes including oxidation, hydration, leaching of soluble or colloidal components by water, and possibly biodegradation. The action of each agent is not well understood, but oxidation seems to be responsible for the major compositional and structural changes in the weathering of coal (van Krevelen, 1961).

6.5.1. Effects of Weathering on Bitumen Content

Martinez and Escobar (1995) in a study of 7 pairs of fresh and weathered coal samples ranging from sub-bituminous to high-volatile bituminous rank, reported difference in bitumen content of up to 1.6 % for a reduction of 14 % in organic matter contents, with at least a pair (weathered and fresh sample) showing no difference in bitumen yield. These workers attributed the reduction in the extraction yield to weathering, and consequently proposed the following;

- Weathering, especially in advanced stages, promotes leaching of the humic substances formed by oxidation. This effect is due to the rupture of the coal macromolecular structure. Following this hypothesis, the bitumen yield diminishes in a weathered coal because of the loss of small particles caused by opening of internal pores. Bitumen itself, however, would not be chemically modified. Thus, this mechanism predicts little or no change in bitumen composition with weathering.

According to Martinez and Escobar (1995), there is a decrease in saturated hydrocarbon content among weathered samples relative to the corresponding

fresh coals, and an increase in the polar components of bitumen in all the altered samples. These workers also observed differences in the *n*-alkane and isoprenoid distributions between the altered and fresh coal samples as follows:

- A remarkable decrease in the concentration of the pristane, for both incipient and advanced weathering.
- A decrease in light *n*-alkane (<C₂₀) concentrations for all the altered samples, with a corresponding increase in the heavy homologs (> C₂₄).
- All samples exposed to advanced weathering display a UCM.

Although biodegradation in crude oil deposits also causes the preferential removal of gasoline-range *n*-alkanes, leaving intact isoprenoids and other branched and cyclic compounds (Bailey *et al*, 1973a, b), Martinez and Escobar (1995) reported a decrease in pristane (Pr) and phytane (Ph), alongside *n*-alkanes due to weathering in coals. These workers postulated that the steric effects of Pr and Ph are relatively low in comparison with other branched hydrocarbons, and consequently, these compounds may be leached from coals together with *n*-alkanes of similar molecular weight. While investigating the leaching behaviour of alkanes via laboratory experiments, Karamalidis and Voudrias (2007) showed that the leaching of Pr and Ph is greater than the leaching of *n*-alkanes in the *n*C₁₀ – *n*C₄₀ range, which supports the inference that isoprenoids may be leached alongside *n*-alkanes from coals.

With regards to the CTB coals, the relatively high OI at Bassen (Table 5.4, Figure 5.6) may suggest weathering within the outcrop samples, although this is also believed to be due to relatively greater terrestrial deposition at the eastern/north-eastern margin of the basin (Chapter 5). Soxhlet extracts could not be used to ascertain weathering at Bassen due to non-access to fresh samples from this area

for comparison. In terms of alkanes, some samples from Bassen and other locations in the eastern/north-eastern margin of the CTB show very high abundance of isoprenoids relative to the *n*-alkanes in their bitumen extracts (Table 4.1); as weathering would generally deplete isoprenoids alongside *n*-alkanes (albeit some *n*-alkanes would go first) (Martinez and Escobar, 1995; Karamalidis and Voudrias, 2007), this is therefore an indication that these coal samples are not significantly weathered, and the oil potential of the Bassen outcrops in particular are not significantly diminished by weathering.

6.6. Summary and Conclusions

This chapter utilised a combination of organic biomarker analysis, inorganic elemental analysis and coal ash contents to evaluate possible controls on oil potential. This led to the establishment of a number of additional parameters for oil potential to support the delineation of optimum resource areas in the CTB. The conclusions are;

- The Longyear coals in the eastern CTB appear to be degraded in the order of Bassen/Lunckefjellet > Breinosa, while the Colesdalen coals do not show evidence of biodegradation. This trend is consistent with the direction towards increasing depth of burial and/or highest geothermal gradient as inferred in Chapter 4. Considering biodegradation is postulated to have occurred both during peat stage and after uplift, the greater biodegradation seen in the eastern CTB may be related to meteoric water movement.
- Within seams, greater biodegradation appears to correlate with increased oil potential; this feature is more pronounced at basin margins and decreases towards basin center, and thus suggests that the eastern CTB

coals may be more oil-prone than coals from the western CTB. This is consistent with results of coal maceral analysis (Chapter 5). Biodegradation pathway is inconsistent with the general biodegradation susceptibility order as sterane depletion commenced while *n*-paraffins and isoprenoids are still present. The inferred biodegradation susceptibility order for steranes is $C_{29} > C_{28} > C_{27}$. The degree of biodegradation of the CTB coals could not be assigned based on existing classification schemes due to the inconsistent biodegradation pathways; a more quantitative assessment is therefore recommended, perhaps as described in Figure 16.12 of Peters *et al.* (2005).

- The relative abundance of Fe and S significantly influences the oil potential of the CTB coals as lower Fe/S ratio correlates with greater oil potential. Groundwater and sea spray appear to control the supply of S to the Longyear and Sputnik peatlands, whereas S supply to the Svarteper peatland seems to be mainly groundwater controlled. In terms of Fe, groundwater appears to mainly control its supply to the Longyear and Sputnik peatlands but clastic deposition has a greater control on its supply to the Svarteper peatland compared to the Longyear peatland. Considering the Fe/S ratio required for pyrite formation is 0.87, the Fe/S ratio >1.0 measured in the Longyear coals in Bassen appears to significantly limit their oil potential, in addition to thermal maturity. The bulk Fe/S ratio of 0.71 and 0.75 respectively measured for the Svarteper and Longyear coals in Lunckefjellet, coupled with the generally higher levels of microbial degradation in the eastern margin of the CTB (Chapter 5), resulted in their relatively high oil potential. In Colesdalen, the coals display relatively high marine influence and consequently low Fe/S ratio (0.56) which led to a high oil potential.

- The distribution of the Ca, Fe and Mg indicates that hydrological stability significantly influences oil potential. A smaller/less stable groundwater catchment would generally be less oil-prone compared to a large/more stable groundwater catchment. Stable hydrology will ensure longer periods of favourable conditions (alkalinity), which will sustain bigger bacteria communities and lead to greater degradation and oil potential.
- Analysis of optimum proximity to inferred palaeocoastline places the Bassen and Lunckefjellet BH6A-2007 sampling localities within the optimum distance of 2 – 4 km. However, local topography plays an important role in estimating the optimum distance. Consequently, further work involving a more detailed palaeogeographic model with a widespread data set and high resolution sampling incorporating other lithologies, is required to confirm range of distance.
- Ash contents >50 % significantly limits oil potential. The oil potential of the younger coal seams (Askeladden, Svarteper and Verkny) is significantly limited by their high ash content compared to the Longyear and Sputnik coals.
- The oil potential of the Bassen outcrops and the CTB coals in general is not significantly affected by weathering. Thus, assessments based on the Bassen outcrops in this study are considered reliable.
- The major controls on the oil-potential of the investigated coals are:
 - a) Thermal maturity
 - b) High bacteria degradation
 - c) Marine sulphur deposition (S > 0.5 %)
 - d) Fe/S ratio <0.87

- e) Optimum pH levels (alkalinity)
- f) Stable hydrology
- g) Ash content $\leq 30\%$

CONCLUSIONS AND FUTURE WORK

7.1. Overall Conclusions

This study is aimed at investigating the maturity, oil source rock and retorting potential of perhydrous coals in the Central Tertiary Basin (CTB) in Spitsbergen. In addition, it has considered the controls on the oil potential of the coals to provide measures that could be used to determine the optimum resource areas in the basin. Investigated samples include drill cores, mine sections and outcrops from the Askeladden, Svarteper, Longyear and Svea coal seams from the eastern coalfield, and drill cores from the Verkny and Sputnik coals seams in the western coalfield of the basin. The aims of this study formed the focus of Chapters 4, 5 and 6, and the main conclusions are summarised below.

1) Maturity of the CTB Coals

Inferred VR gaps within the Firkanten Fm. coals are due to suppression of VR by bitumen impregnation and hydrogen enrichment of vitrinites; evidences include a general decrease in VR towards the top of the Longyear seam which correlates with increasing oil potential, and a generally strong negative correlation of VR vs. HI (R^2 up to 0.78). VR at the eastern/north-eastern basin margins appear to be more suppressed compared to samples down-dip and towards basin center. T_{max} and formation of aromatics also appear suppressed in these coals, and therefore should be used in conjunction with other techniques towards estimating the true VR. The VR suppression effect was corrected by using the Lo (1993) method (LoVR), which shows that all samples are within the oil generation window, with estimated thermal maturities of 0.68, 0.78, 0.80 and 0.88% R_o in the Bassen, Lunckefjellet, Breinosa and Colesdalen areas respectively. LoVR values indicate peak temperatures of around 104 °C in Bassen, 116 °C in Lunckefjellet, 118 °C in

Breinosa and 125 °C in the Colesdalen area. Coalification gradients in the Adventdalen sub-region equate to 0.37 R_o /km, with an estimated geothermal gradient of approximately 55 °C/km. Peak burial depths in the Adventdalen sub-region range from 1.9 km in the Bassen area (up-dip), to 2.2 km in the Breinosa area (down-dip). This indicates overall overburden erosion estimates are in the range of 0.9 – 1.2 km in Adventdalen. In Lunckefjellet, peak burial depth is around 2.1 km which implies missing overburden of 1.1 km. In more central areas of the basin such as Colesdalen, peak burial depths are considerably higher at around 2.3 km with missing overburden estimate of 1.4 km. These results suggest that burial and subsequent uplift and erosion were perhaps lower than previously thought. Consequently, the sediment load from Svalbard to the Barents Shelf in the Late Tertiary may be much less than previously thought.

2) Oil Source Rock and Retorting Potential of the CTB Coals

Coal maceral analysis indicates that the oil potential of the investigated Firkanten Fm. coals is mainly due to perhydrous detrovitrinites but other vitrinites including collotelinite, in addition to liptinites, appear to have significantly contributed. Maceral analysis also indicates that the eastern CTB coals may be more oil-prone than coals from the western parts of the basin, and oil-proneness between seams is in the order of Askeladden>Svarteper>Longyear.

The coals are enriched in Type II and a mixture of Types II/III kerogens with HI values between 150 - 410 mg HC/g TOC. HI values generally increase towards the inferred palaeocoastline, and between coal seams, HI values appear to be in the order of Askeladden>Svarteper>Longyear>Svea indicating oil potential increases from the stratigraphically older to younger seams. HI distributions between areas and between seams are consistent with sulfur contents, and reflect the positive

influence of marine sulfur on perhydrous coal formation. The TOC contents of the coals are high with values between 44.5 – 89.8 %, and the S₂ contents are also high with values between 109 – 368 mg/g, and thus indicating excellent potential for oil generation.

The mean S₁ contents of the coals are 6.8, 11.8, 15.0 and 14.5 mg/g for the Bassen, Lunckefjellet, Breinosa and Colesdalen samples respectively, and reflect increasing maturity from Bassen, through Lunckefjellet, to Breinosa and Colesdalen. The Bassen coals are yet to generate significant volumes of oil, the Lunckefjellet coals are at peak oil generation/onset of expulsion, while the Breinosa and Colesdalen coals are already expelling oil. However, all samples have low PI values (<0.10), which suggest that significant amounts of oil have not been expelled. The inference that the Bassen and Lunckefjellet coals are yet to generate and/or expel significant volumes of oil is consistent with the relatively greater VR suppression observed in coals from these areas. These results indicate that the Lunckefjellet coals will give the best indication of the maturity at which oil expulsion occurs in the CTB; consequently, future work which attempts to assess the maximum oil potential should be focused on coals from this area.

The upper Longyear seam has higher oil potential than the lower Longyear seam. This is consistent with greater sulphur contents associated with sea level rise, which resulted in a transition from raised-bog conditions in the lower Longyear, to fen-like conditions in the upper Longyear. Notably, the Sputnik coal seam in Colesdalen, representing the western coalfield of the CTB displays similar fen transition observed in Bassen, Breinosa and Lunckefjellet; thus it may be a Longyear seam equivalent.

In investigated areas, maximum retorting yields range between 90 mg/g dwc in Bassen, and 240 mg/g dwc in Lunckefjellet. Highest bulk estimate is 160 mg/g dwc in Lunckefjellet. At Breinosa and Colesdalen, bulk yields of 140 and 100 mg/g dwc were respectively measured, while lowest bulk yield (80 mg/g dwc) was measured at Bassen. Residual coke ranges between 60 – 75 % of starting material in all areas. With a maximum coal resource of 3,300 Mt, of which 600 Mt is recoverable in the CTB (Orheim, 1982), maximum hydrocarbon resource via retorting would range between 3,188 – 5,394 Mbbl in place, with 580 – 981 Mbbl recoverable by mining. In areas where conventional mining is not possible perhaps because the seams are not up to required thickness, in-situ techniques may be applied.

3) Controls on the Oil Potential of the CTB Coals

In summary, the major controls on the oil potential of the investigated coals are:

- Thermal maturity (true VR of around 0.78% R_o)
- Marine sulfur contents ≥0.5 %
- Fe/S ratio significantly <0.87
- Stable hydrology (i.e. relatively large/stable groundwater catchment)
- Optimum pH levels (alkalinity)
- Relative distance to inferred palaeocoastline and local topography
- Ash content ≤30 %

7.2. Future Work

Recommended future works are discussed based on specific aspects below.

1) Maturity of the CTB Coals

It has been noted that the island of Spitsbergen was exposed to volcanic activities (Section 4.1), there was however no access to a petroleum system modelling software in this study. Consequently, the thermal history that accounts for both the predicted geothermal gradients and the VR data could not be determined. Thus, future work assessing and comparing the geothermal history between the eastern (basin margins) and western CTB (basin center) with the aid of a petroleum system modelling software, would be beneficial. From this PhD study, important geochemical/petrographic information is now available for the western coalfield, where little or no previous work existed. The proposed future work will take advantage of the data from both areas, and in addition, incorporate samples from the youngest coal seam in the western coalfield (Nidzny coal) which were unavailable in this study. This study will provide a thermal history and enable the maturity and oil potential to be predicted to assist the further assessment of oil potential within the CTB.

2) Oil-Prone Macerals and Oil potential of the CTB coals

Coal maceral analysis indicates that the oil potential of the Firkanten Fm. coals is mainly due to perhydrous detrovitrinites. However, other vitrinites including collotelinite, in addition to liptinites, appear to have significantly contributed (Chapter 5). Thus, future work incorporating a geochemical and statistical approach will allow identification of individual vitrinitic and liptinitic macerals which may have significantly contributed to the oil potential of these coals. This

will help in the further characterisation of the CTB coals and provide more understanding of high latitude oil-prone coals in general.

3) Hydrological Stability and Oil Potential of the CTB Coals

Analysis of groundwater character relative to oil potential shows that smaller/less stable groundwater catchments may be less oil-prone compared to a large/more stable groundwater catchment (Chapter 6); thus a detailed groundwater classification scheme for stable/unstable catchments relative to oil potential will provide information that will help in delineating optimum hydrocarbon resource areas in the basin.

4) Retorting Potential of the CTB Coals

Retorting yields from current method are notably limited by swelling of the coals within the reactor vessel leading to blockage of sweep gas flow. Hence, further work involving other methods such as the Grey-King assay, is required to fully measure the retorting potential in these coals. One of the advantages of the retorting technique is the reduction of sulphur contents in the products relative to the feedstock, but this objective was not achieved because the semi-coke is in a sand mixture (i.e. coal was pre-mixed with sand to avoid sweep gas blockage), which could not be properly separated and there was no access to a suitable elemental analysis technique during this period of work. Thus, the sulfur contents of the semi-coke, preferably from a retorting method that will allow gas analysis, needs to be assessed. Also, analysis of the semi-coke and sand mixture from this study could be achieved with suitable techniques such as sulfur coulometry.

5) Resource Estimates

It is noted in Section 5.7.4 that hydrocarbon resource estimates for the CTB as a whole unit is based on coal resource estimates from over 30 years ago, and includes the relatively less oil-prone Svea seam (Orheim, 1982). Thus the true estimates may be considerably closer to, and possibly less than the lower range noted in Table 5.14. Therefore, more detailed estimates, which take into account up to date coal production figures, would be necessary for any future planning for exploration of the oil potential of these coals.

REFERENCES

Abdullah, W., Murchison, D., Jones, J. M., Telnaes, N. and Gjelberg, J. (1988) Lower Carboniferous coal deposition environments on Spitsbergen, Svalbard. *Organic Geochemistry*, **13**(4-6), 953-964.

Ahmed, M., Smith, J. W. and George, S. C. (1999) Effects of biodegradation on Australian Permian coals. *Organic Geochemistry*, **30**, 1311-1322.

Akinlua, A., Ajayi, T. R. and Adeleke, B. B. (2006) Niger delta oil geochemistry: insight from light hydrocarbons. *Journal of Petroleum Science and Engineering*, **50**, 308-314.

Alexander, R., Kagi, R. I., Woodhouse, G. W. (1981) Geochemical correlation of Windalia oil and extracts of winning group (Cretaceous) potential source rocks, Barrow Subbasin, Western Australia. *American Association of Petroleum Geologists Bulletin*, **65**, 235-250.

Axelson D. E. and Parkash S. (1986) ¹³C solid state NMR of Alberta subbituminous macerals. *Fuel Science and Technology International*, **4**, 45-85.

Bailey, N. J. L., Jobson, A. M. and Rogers, M. A. (1973a) Bacterial degradation of crude oils: Comparison of field and experimental data. *Chemical Geology*, **11**, 203-221.

Bailey, N. J. L., Krouse, H. R., Evans, C. R. and Rogers, M. A. (1973b) Alteration of crude oil by waters and bacteria - evidence from geochemical and isotope studies. *American Association of Petroleum Geologists Bulletin*, **57**, 1276-1290.

Banerjee, A., Sinha, A. K., Jain, A. K., Thomas, N. J., Misra, K. N. and Chandra, K. (1998) A mathematical representation of Rock-Eval hydrogen index vs T_{max} profiles. *Organic Geochemistry*, **28** (1/2), 43-55.

Barker, C. (1974) Pyrolysis techniques for source rock evaluation. *American Association of Petroleum Geologists Bulletin*, **58**, 2349-2361.

Barker, C. E. and Goldstein, R. H. (1990) Fluid-inclusion technique for determining maximum temperature in calcite and its comparison to the vitrinite reflectance geothermometer. *Geology*, **18**, 1003-1006.

Barker, C. E., Lewan, M. D. and Pawlewicz, M. J. (2007) The influence of extractable organic matter on vitrinite reflectance suppression: a survey of kerogen and coal types. *International Journal of Coal Geology*, **70** (1-3), 67-78.

Barker, C. E. and Pawlewicz, M. J. (1994) Calculation of vitrinite reflectance from thermal histories and peak temperatures, a comparison of methods. In: Mukhopadhyay, P. K. and Dow, W. G. (eds.) *Vitrinite reflectance as a maturity parameter, applications and limitations*. Washington, D.C: *American Chemical Society Symposium Series*, **570**, 216-229.

Barker, C. E., Pawlewicz, M. J., Lewan, M. D. Carlson, C. L. and Webbers, A. (2004) Update on the influence of extractable organic matter on vitrinite reflectance: implications to liquid hydrocarbon or bitumen impregnation as a suppression mechanism. *Abstracts of the 21st Annual Meeting of the Society for Organic Petrology*, **Vol. 21**, Sydney, Australia, 27 September – 1 October, 2004.

Bechtel, A., Gruber, W., Sachsenhofer, F., Gratzer, R., Lucke, A. and Puttman, W. (2002a) Depositional environment of the Late Miocene lignite (Alpine Foreland Basin): insights from petrography, organic geochemistry and stable carbon isotopes. *International Journal of Coal Geology*, **54** (3), 153-180.

Bechtel, A., Markic, M., Sachsenhofer, R. F., Jelen, B., Gratzer, R., Lucke, A., and Puttman, W. (2004) Paleoenvironment of the upper Oligocene Trbovlje coal seam (Slovenia). *International Journal of Coal Geology*, **57**(1), 23-48.

Bectel, A., Sachsenhofer, R. F., Kolcon, I., Gratzer, R., Otto, A. and Puttmann, W. (2002b) Organic geochemistry of the Lower Miocene Oberdorf lignite (Styrian Basin, Austria): its relation to petrography, palynology and palaeoenvironment. *International Journal of Coal Geology*, **50** (1), 31-57.

Bechtel, A., Sachsenhofer, R. F., Markic, M., Gratzer, R., Lucke, A. and Puttman, W. (2003) Paleoenvironmental implications from biomarker and stable isotope investigations on the Pliocene Velenje lignite seam (Slovenia). *Organic Geochemistry*, **34** (9), 1277-1298.

Bechtel, A., Sachsenhofer, R. F., Zdravkov, A., Kostova, I. and Gratzer, R. (2005) Influence of floral assemblage, facies and diagenesis on petrography and organic geochemistry of the Eocene Bourgas coal and the Miocene Maritza-East lignite (Bulgaria). *Organic Geochemistry*, **36** (11), 1498-1522.

Behar, F., Lewan, M. D., Lorant, F. and Vandenbroucke, M. (2003) Comparison of artificial maturation of lignite in hydrous and nonhydrous conditions. *Organic Geochemistry*, **34** (4), 575-600.

Behar, F., Pelet, R. and Roucache, J. (1984) Geochemistry of asphaltenes. *Organic Geochemistry*, **7**, 587-595.

Bergmann, U., Mullins, O. and Cramer, S. P. (2000) X-ray raman spectroscopy of carbon in asphaltene: light element characterization with bulk sensitivity. *Analytical Chemistry*, **72**, 2609-2612.

Bertrand, P., Behar, F. and Durand, B. (1986) Composition of potential oil from humic coals in relation to their petrographic nature. *Organic Geochemistry*, **10**, 601-608.

Bestougeff, M. A. (1967) Petroleum hydrocarbons. In: Nagy, B. and Colombo, U. (eds.) *Fundamental aspects of petroleum geochemistry*. Amsterdam: Elsevier. 77-108.

Bishop, A. N. and Abbot, G. D. (1995) Vitrinite reflectance and molecular geochemistry of Jurassic sediments: the influence of heating by Tertiary dykes (northwest Scotland). *Organic Geochemistry*, **22** (1), 165-177.

Blanc, P. and Connan, J. (1992) Generation and expulsion of hydrocarbons from a Paris Basin Toarcian source rock: an experimental study by confined-system pyrolysis. *Energy and Fuels*, **6** (5), 666-677.

Bojeson-Koefoed, J. A., Kalkreuth, W., Petersen, H. I. and Piasecki, S. (2012) A remote coal deposit revisited: Middle Jurassic coal at Kulhøj, western Germania Land, northeast Greenland. *International Journal of Coal Geology*, **98**, 50-61.

Borhema, C. J., Crick, I. H. and Powell, T. G. (1988) Alternative calibration of the Methylphenanthrene Index against vitrinite reflectance: Application to maturity measurements on oils and sediments. *Organic Geochemistry*, **12** (3), 289-294.

Boreham, C. J., Horsfield, B. and Schenk, H. J. (1999) Predicting the quantities of oil and gas generated from Australian Permian coals, Bowen Basin using pyrolytic methods. *Marine and Petroleum Geology*, **16**, 165-188.

Boreham, C. J. and Powell, T. G. (1993) Petroleum source rock potential of coal and associated sediments: qualitative and quantitative aspects. In: Law, B. E. and Rice, D. D. (eds.) Hydrocarbons from coal. *American Association of Petroleum Geologists Studies in Geology*, **38**, 133-157.

Bost, F. D., Frontera-Suau, R., McDonald, T. J., Peters, K. E. and Morris, P. J. (2001) Aerobic biodegradation of hopanes and norhopanes in Venezuelan crude oils. *Organic Geochemistry*, **32**, 105-114.

Bostick, N. H. (2011) Measured reflectance suppressed by thin-film interference of crude oil smeared on glass - as on vitrinite in coal or petroliferous rocks. *The Society of Organic Petrology Newsletter*, **28** (2), 12-15.

Braathen, A., Bælum, K., Christiansen, H. H., Dahl, T., Eiken, O., Elvebakk, H., Hansen, F., Hanssen, T. H., Jochmann, M., Johansen, T. A., Johnsen, H., Larsen, L., Lie, T., Mertes, J., Mørk, A., Mørk, M. B., Nemeč, W., Olaussen, S., Oye, V., Rød, K., Titlestad, G. O., Tveranger, J. and Vagle, K. (2012) The Longyearbyen CO₂ Lab of Svalbard, Norway - initial assessment of the geological conditions for CO₂ sequestration. *Norwegian Journal of Geology*, **92**, 353-976.

Breitmaier, E. and Bauer, G. (1984) *¹³C NMR Spectroscopy: A working Manual with exercises*. **Vol 3**. Switzerland: Hardwood Academic Publishers GmbH.

Bulter, I. B. and Rickard, D. (2000) Framboidal pyrite formation via the oxidation of iron (II) monosulfide by hydrogen sulphide. *Geochimica et Cosmochimica Acta*, **64**, 2665-2672.

Carr, A. D. (2000) Suppression and retardation of vitrinite reflectance, part 1. Formation and significance for hydrocarbon generation: *Journal of Petroleum Geology*, **23**, 313-343.

Carr, A. D., Snape, C. E., Meredith, W., Uguna, C., Scotchman, I. C. and Davis, R. C. (2009) The effect of water pressure on hydrocarbon generation reactions: some inferences from laboratory experiments. *Petroleum Geoscience*, **15**, 17–26.

Carr, A. D. and Williamson, J. E. (1990) The relationship between aromaticity, vitrinite reflectance and maceral composition of coals - implications for the use of vitrinite reflectance as a maturation parameter. *Organic Geochemistry*, **16**, 313-323.

Casareo, F. E., George, S. C., Batts, B. D. and Conaghan, P. J. (1996) The effects of varying tissue preservation on the aliphatic hydrocarbons within a high-volatile bituminous coal. *Organic Geochemistry*, **24** (8/9), 785-800.

Chou, C-L. (2012) Sulfur in coals: A review of geochemistry and origins. *International Journal of Coal Geology*, **100**, 1–13.

Claypool, G. E. and Reed, P. R. (1976) Thermal analysis technique for source rock evaluation: Quantitative estimate of organic richness and effects of lithologic variation. *American Association of Petroleum Geologists Bulletin*, **60**, 608-626.

Clayton, J. L. and Bostick, N. H. (1986) Temperature effects on kerogen and on molecular and isotopic composition of organic matter in Pierre Shale near an igneous dike. *Organic Geochemistry*, **10**, 135-143.

Clementz, D. M., Demaison G. J. and Daly, A. R. (1979) Well site geochemistry by programmed pyrolysis. *Proceedings of the 11th Annual Offshore Technology Conference, Houston, OTC 3410*, **vol 1**, 465-470.

Ćmiel, S. R. and Fabianska, M. J. (2004) Geochemical and petrographic properties of some Spitsbergen coals and dispersed organic matter. *International Journal of Coal Geology*, **57**, 77-97.

Connan, J. (1984) Biodegradation of crude oils in reservoirs. In: Brooks, J. and Welte, D. (eds.) *Advances in petroleum geochemistry*. London: Academic Press. **Vol. 1**. 299-335.

Connan J., Le Tran, K. and van der Weide, B. (1975) Alteration of petroleum in reservoirs. In: Proceedings of 9th world petroleum congress, Tokyo. *Applied Science Publication*, **2**, 171-178.

Corcoran, D. and Clayton, G. (1999) Interpretation of vitrinite reflectance profiles in the central Irish sea area: implications for the timing of organic maturation. *Journal of Petroleum Geology*, **22**, 261-286.

Cranwell, P. A. (1982) Lipids of aquatic sediments and sedimenting particulates. *Progress in Lipid Research*, **21**, 271-308.

Crelling, J. C. (1987) Separation, identification and characterisation of single coal maceral types. In: Moulijn, J. A., Nater, K. A. and Chermin, H. A. G. (eds.) *Proceedings of the 1987 international conference on coal science, Maastricht, The Netherlands*. The Netherlands: Elsevier Science Publishers, 119-122.

Crelling, J. C., Skorupska, N. M. and Marsh, H. (1988) Reactivity of coal macerals and lithotypes. *Fuel*, **67**, 781-785.

Cronoble, J. M. (1969) Geothermal gradients and application to petroleum geology. *The Mountain Geologist*, **6** (1), 27-39.

Curry, D. J., Emmet, J. K. and Hunt, J. W. (1994) Geochemistry of aliphatic-rich coals in the Cooper Basin, Australia and Taranaki Basin, New Zealand: implications for the occurrence of potentially oil-generative coals. In: Scott, A. C. and Fleet, A. J. (eds.) *Coal and coal-bearing strata as oil-prone source rocks? Geological Society Special Publication*, **77**. London: The Geological Society. 149-182.

Dallmann, W. K. (1993) Notes on the stratigraphy, extent and tectonic implications of the Minkinfjellet Basin, Middle Carboniferous of central Spitsbergen. *Polar Research*, **12**, 153-160.

Dallmann, W. K., Midbø, P. S., Nøttvedt, A. and Steel, R. J. (1999) Tertiary lithostratigraphy. In: Dallmann, W. K. (ed.) Lithostratigraphic Lexicon of Svalbard. Norsk Polarinstitut, Tromsø, 318 pp

Dallmann, W. K., Ohta, Y. and Andresen, A. (1988) Tertiary tectonics of Svalbard. *Extended abstracts from symposium held in Oslo 26 and 27 April 1988*. Oslo: Norsk Polarinstitut. Rapport **46**.

Davidson R. M. (1986) Nuclear magnetic resonance studies of coal. Coal Research, London. Report No. **ICTIS/TR32**, IEA.

Davis, M. R., Abbott, J. M. and Gaines, A. F. (1985) Chemical structures of telocollinites and sporinites. Differentiation between telocollinites and sporinites by the aromatic structures present in their pyridine extracts. *Fuel*, **64**, 1362-1369.

Diessel, C. F. K. (1986) On the correlation between coal facies and depositional environments, in *Advances in the study of the Sydney Basin: Proceedings of the 20th Newcastle Symposium*, The University of Newcastle, *Publication* **246**, 19-22.

Diessel, C. F. K. (1992) *Coal-bearing depositional systems*. Berlin: Springer-Verlag.

Diessel, C. F. K. and Gammidge, L. (1998) Isometamorphic variations in the reflectance and fluorescence of vitrinite - a key to depositional environment. *International Journal of Coal Geology*, **36**, 167-222.

Dinneen, G. U. (1976) Developments in petroleum science: Chapter 9 - Retorting technology of oil shale. *Oil Shale*, **5**, 181-198.

Domine, F. (1991) High pressure pyrolysis of *n*-hexane, 2,4-dimethylpentane and 1-phenylbutane. Is pressure an important geochemical parameter? *Organic Geochemistry*, **17** (5), 619-634.

Douglas, A. G., Sinninghe Damste', J. S., Fowler, M. G., Eglinton, T. I. and de Leeuw, J. W. (1991) Unique distributions of hydrocarbons and sulphur compounds by flash pyrolysis from the fossilized alga *Gloeocapsomorpha prisca*, a major constituent in one of four Ordovician kerogens. *Geochimica et Cosmochimica Acta*, **55**, 275-291.

Durand, B. and Paratte, M. (1983) Oil potential of coals: a geochemical approach. In: Brooks, J. (ed.) *Petroleum geochemistry and exploration of Europe. Geological Society Special Publication*, **12**. Boston: Blackwell Scientific Publications. 255-265.

Eiken, O. (1985) Seismic mapping of the Post-Caledonian strata in Svalbard. *Polar Research*, **3** (2), 167-176.

Enguehard, F., Kressmann, S. and Domine, F. (1990) Kinetics of dibutylether pyrolysis at high pressure: experimental study. *Organic Geochemistry*, **16** (1-3), 155-160.

Faix, O., Mozuch, M. D. and Kent Kirt, T. (1985) Degradation of Gymnosperm (Guaiacyl) vs. Angiosperm (Syringyl/Guaiacyl) Lignins by *Phanerochaete chrysosporium*. *Holzforschung - International Journal of the Biology, Chemistry, Physics and Technology of Wood*, **39** (4), 203-208.

Farrimond, P., Bevan, J. C. and Bishop, A. N. (1996) Hopanoid hydrocarbon maturation by an igneous intrusion. *Organic Geochemistry*, **25** (3-4), 149-164.

Fifield, F. W. and Kealey, D. (2000) *Principles and practice of analytical chemistry*. 5th edition. Cambridge: Blackwell Science.

Fleet, A. J. and Scott, A. C. (1994) Coal and coal-bearing strata as oil-prone source rocks: an overview. In: Scott, A. C. and Fleet, A. J. (eds.) Coal and coal-bearing strata as oil-prone source rocks? *Geological Society Special Publication*, **77**. London: The Geological Society. 1-8.

Fredericks, P., Warbrooke, P. and Wilson, M. (1983) Chemical changes during natural oxidation of a high volatile bituminous coal. *Organic Geochemistry*, **5**, 89-97.

George, S. C. (1992) Effect of igneous intrusion on the organic geochemistry of a siltstone and an oil shale horizon in the Midland Valley of Scotland. *Organic Geochemistry*, **18** (5), 705-723.

George, S. C., Smith, J. W. and Jardine, D. R. (1994) Vitrinite reflectance suppression in coal due to a marine transgression: a case study of the organic geochemistry of the Greta Seam, Sydney Basin. *Australian Petroleum Exploration Association Journal*, **34**(1), 241-255.

Grantham, P. J. (1986) Sterane isomerisation and moretane/hopane ratios in crude oils derived from Tertiary source rocks. *Organic Geochemistry*, **9**, 293-304.

Grob, L. R. and Barry, E. F. (2004) *Modern practice of gas chromatography*. 4th edition. New Jersey: John Wiley and Sons Inc.

Gustafsson, M. E. R. and Franzen, L. G. (2000) Inland transport of marine aerosols in southern Sweden. *Atmospheric Environment*, **34**, 313-325.

Halpern, H. I. (1995) Development and applications of light-hydrocarbon based star diagrams. *American Association of Petroleum Geologists Bulletin*, **79**, 801-815.

Han, Z. and Kruger, M. A. (1999) Classification of torbanite and cannel coal II. Insights from pyrolysis-GC/MS and multivariate statistical analysis. *International Journal of Coal Geology*, **38**, 203-218.

Hao, F. and Chen, J. Y. (1992) The cause and mechanism of vitrinite reflectance anomalies. *Journal of Petroleum Geology*, **15**, 419-434.

Harkel, M. J. (1997) The effects of particle-size distribution and chloride depletion of sea-salt aerosols on estimating atmospheric deposition at a coastal site. *Atmospheric Environment*, **31** (3), 417-427.

Harland, W. B., Anderson, L. M., Manasrah, D., Butterfield, N. J., Challinor, A., Doubleday, P. A., Dowdeswell, E. K., Dowdeswell, J. A., Geddes, I., Kelly, S. R. A., Lesk, E. L., Spencer, A. M. and Stephens, C. F. (1997) The Geology of Svalbard. *Geological Society Memoir*, **17** (IXXI), 1-521.

Harland, W. B., Pickton, C. A. G., Wright, N. J. R., Croxton, C. A., Smith, D. G., Cutbill, J. L. and Henderson, W. G. (1976) Some coal bearing strata in Svalbard. *Norsk Polarinstitutt Skrifter*, **164**, Oslo.

Hartgers, W. A., Sinninghe Damsté, J. S. and de Leeuw, J. W. (1992) Identification of C₂-C₄ alkylated benzenes in flash pyrolyzates of kerogens, coals and asphaltenes. *Journal of Chromatography A*, **606** (2), 211-220.

Hjelle, A. (1993) The Geology of Svalbard. Norsk Polarinstitutt, Oslo, **163**.

Hoel, A. (1925) The coal deposits and coal mining of Svalbard (Spitsbergen and Bear Island) Norsk Polarinstitutt Skrifter **6**, Oslo.

Horsfield, B. (1985) Pyrolysis studies in petroleum exploration. In: Brooks, J. and Welte, D. (eds.) *Advances in petroleum geochemistry*. **Vol. 1**. New York: Academy Press. 247-298.

Horsfield, B. (1989) Practical criteria for classifying kerogens: Some observations from pyrolysis-gas chromatography. *Geochimica et Cosmochimica Acta*, **53**, 891-901.

Horstad, I., Larter, S. R. and Mills, N. (1991) A Quantitative Model of biological petroleum degradation within the Brent Group Reservoir in the Gullfaks Field, Norwegian North Sea. *Organic Geochemistry*, **19**, 107-117.

Howell, V. J. Connan, J. and Aldridge A. K. (1984) Tentative identification of demethylated tricyclic terpanes in nonbiodegraded and slightly biodegraded crude oils from the Los Llanos Basin, Colombia. *Organic Geochemistry*, **6**, 83-92.

Hsu, C. S. and Drinkwater, D. (2001) Gas chromatography - mass spectrometry in the petroleum industry. In: Niessen, W. M. A (ed.) *Current practice of gas chromatography - mass spectrometry*. **Vol. 86**. New York: Marcel Dekker Inc. Chromatographic Science Series.

Hunt, J. M. (1991) Generation of gas and oil from coal and other terrestrial organic matter. *Organic Geochemistry*, **17**, 673-680.

Hunt, J. M. (1995) *Petroleum geochemistry and geology*. 2nd edition. New York: W. H. Freeman and Company.

Ingram G. R. and Rimstidt J. D. (1984) Natural weathering of coal. *Fuel*, **63**, 292-296.

International Committee for Coal and Organic Petrology - ICCP (1998) The new vitrinite classification (ICCP System 1994). *Fuel*, **77** (5) 349-358.

International Organisation for Standardisation (ISO) (2009) Methods for the petrographic analysis of coals - Part 3: Method of determining maceral group composition - ISO 7404-3:2009, ISO, Geneva.

International Organisation for Standardisation (ISO) (2009) Methods for the petrographic analysis of coals - Part 3: Method of determining maceral group composition - ISO 7404-5:2009, ISO, Geneva.

Iglesias, J. M., del Rio, J. C., Laggoun-Défarge, F., Cuesta, M. J. and Suárez-Ruiz, I. (2002) Control of the chemical structure in perhydrous coals by FTIR and Py-GC/MS. *Journal of Analytical and Applied Pyrolysis*, **62** (1), 1-34.

Ignasiak, T., Kemp-Jones, A. V. and Strausz, O. P. (1977) The molecular structure of Athabasca asphaltenes. Cleavage of the carbon sulphur bonds by radical ion electron transfer reactions. *Organic Chemistry*, **42**, 312-320.

Ikan, R., Baedeker, M. J. and Kaplan, I. R. (1975) Thermal alteration experiments on organic matter in recent marine sediments - II. Isoprenoids. *Geochimica et Cosmochimica Acta*, **39**, 187-194.

Isaksen, G. H., Curry, D. J., Yeakel, J. D. and Jenssen, A. I. (1998) Controls on the oil and gas potential of humic coals. *Organic Geochemistry*, **29**, 23-44.

Jamtveit, B., Hammer, Ø., Andersson, C., Dysthe, D. K., Heldmann, J. and Fogel, M. L. (2006) Travertines from the Troll thermal springs, Svalbard. *Norwegian Journal of Geology*, **86**, 387-395.

Jones, J. M. and Creany, S. (1977) Optical character of thermally metamorphosed coals of northern England. *Journal of Microscopy*, **109**, 105-118.

Jones, R. B., Robertson, S. D., Claque, A. D. H., Wind, R. A., Duijvestijn, M. J., Van Der Lugt, C., Vriend J. and Smidt J. (1986) Dynamic nuclear polarization ^{13}C n.m.r. of coal. *Fuel*, **65**, 520-525.

Kalinowski, A. and Gurba, L. (2014) Vitrinite reflectance suppression in the northern Denison Trough, Bowen Basin, QLD Australia. *Abstracts of the 31st Annual Meeting of the Society for Organic Petrology*, **Vol. 31**, Sydney, Australia, 27th September – 3rd October, 2004.

Kalkreuth, W., Steller, M., Wieschenkamper, I. and Ganz, S. (1991) Petrographic and chemical characterisation of Canadian and German coals in relation to utilization potential. *Fuel*, **70**, 683-694.

Karamalidis, A. K. and Voudrias, E. A. (2007) Cement-based stabilization/solidification of oil refinery sludge: Leaching behaviour of alkanes and PAHs. *Journal of Hazardous Materials*, **148**, 122-135.

Kearey, P. (2001) *The new penguin dictionary of geology*. 2nd edition. London: Penguin Books.

Killops, S. D., Gunnell, R. H., Suggate, R. P., Sykes, R., Peters, K. E., Walters, C., Woolhouse, A. D., Weston, R. J. and Boudou, J. P. (1998) Predicting generation and expulsion of paraffinic oil from vitrinite rich coals. *Organic Geochemistry*, **29** (1-3), 1-21.

Killops, S., Jarvie, D., Sykes, R. and Funnell, R. (2002) Maturity-related variation in the bulk-transformation kinetics of a suite of compositionally related New Zealand coals. *Marine and Petroleum Geology*, **19**, 1151-1168.

Killops, S. D. and Killops, V. J. (1993) *Introduction to organic geochemistry*. New York: John Wiley and Sons.

Killops, S. and Killops, V. (2005) *Introduction to Organic Geochemistry*. 2nd edition. Malden: Blackwell Publishing.

Killops S. D., Woodhouse A. D., Weston., R. J. and Cook, R. A. (1994) A geochemical appraisal of oil generation in the Taranaki Basin, New Zealand. *American Association of Petroleum Geologists Bulletin*, **78** (10), 1560-1585.

Kvalheim, O. M., Christy, A. A., Telnæs, N. and Bjorseth, A. (1987) Maturity determination of organic matter in coals using the methylphenanthrene distribution. *Geochemica et Cosmochimica Acta*, **55**, 1883-1888.

Laban, K. L. and Atkins, B. P. (1999) The determination of minor and trace element associations in coal using a sequential microwave digestion procedure. *International Journal of Coal Geology*, **4** (41), 351-369.

Lafargue, E., Espitalié, J., Marquis, F. and Pillot, D. (1998) Rock-Eval 6 applications in hydrocarbon exploration, production and in soil contamination studies. *Oil and Gas Science and Technology - Revue de l'Institut Francais du Petrole*, **53**, 421-437.

Lajunen, L. H. J. and Peramaki, P. (2004) *Spectrochemical analysis by atomic absorption and emission*. 2nd edition. Cambridge: The Royal Society of Chemistry.

Lambert Jr., J. M., Simkovich, G. and Walker Jr., P. L. (1998) The kinetics and mechanism of the pyrite-to-pyrrhotite transformation. *Metallurgical and Materials Transactions B*, **29**, 385-396.

Large, D. J., Marshall, C., Meredith, W., Snape, C. E. and Spiro, B. F. (2011) Potential to generate oil prone coal source rocks in arctic environments. *Search and Discovery Article #40806*.

Larter, S. R. and Douglas, A. G. (1982) Pyrolysis methods in organic geochemistry: An overview. *Journal of Analytical and Applied Pyrolysis*, **4**, 1-19.

Larter, S., Huang, H., Adams, J., Bennett, B., Jokanola, O., Oldenburg, T., Jones, M., Head, I., Riediger, C. and Fowler, M. (2006) The controls on the composition of biodegraded oils in the deep subsurface: Part II - Geological controls on subsurface biodegradation fluxes and constraints on reservoir-fluid property prediction. *American Association of Petroleum Geologists Bulletin*, **90** (6), 921-938.

Lawrence, C. R. and Neff, J. C. (2009) The contemporary physical and chemical flux of aeolian dust: a synthesis of direct measurements of dust deposition. *Chemical Geology*, **267**, 46-63.

Lewan, M. D., Winters, J. C. and McDonald, J. H. (1979) Generation of oil-like pyrolyzates from organic-rich shales. *Nature*, **203**, 897-899.

Lo, H. B. (1993) Correction criteria for the suppression of vitrinite reflectance in hydrogen-rich kerogens: preliminary guidelines. *Organic Geochemistry*, **20** (6), 653-657.

Love, G. D., Snape, C. E., Carr, A. D., Cocksedge, M. and Law, G. (1991) A sequential extraction/hydrogenation procedure to differentiate between physically trapped and covalently bound alkanes in coals and kerogens. In: Manning, D. (ed.) *Organic geochemistry. Advances and applications in energy and the natural environment*. Manchester University Press, 436-438.

Love, G. D., Snape, C. E., Carr, A. D. and Houghton, R. C. (1996) Changes in molecular biomarker and bulk skeletal parameters of vitrinite concentrates as a function of rank. *Energy and Fuels*, **10**, 149-157.

Love, G. D., Snape, C. E., Carr, A. D. and Houghton, R. C. (1995) Release of covalently-bound alkane biomarkers in high yields from kerogen via catalytic hydrolysis. *Organic Geochemistry*, **23** (10), 981-986.

Lundegard, P. and Knott, J. R. (2001) Polar organics in crude oil and their potential impacts on water quality. *Petroleum Hydro-carbons and Organic Chemicals in the Ground Water Conference Proceeding*, 1380144 Houston, Texas NGWA/APL.

Lüthje, C. J. (2009) *Transgressive Development of Coal-bearing Coastal Plain to Shallow Marine Setting in a Flexural Compressional Basin, Paleocene, Svalbard, Arctic Norway*. PhD Thesis, University of Bergen, Norway.

MacGregor, D. S. (1994) Coal-bearing strata as source rocks - a global overview. In: Scott, A. C. and Fleet, A. J. (eds.) Coal and coal-bearing strata as oil-prone source rocks? *Geological Society Special Publication*, **77**. London: The Geological Society. 107-116

Mackenzie, A. S. (1984) Application of biological markers in petroleum geochemistry. In: Brooks, J. and Welte, D. H. (eds.) *Advances in petroleum geochemistry*. **Vol. 1**. London: Academy Press. 115-214.

Mackenzie, A. S., Patience, R. L., Maxwell, J. R., Vandenbroucke, M and Durand, B. (1980) Molecular parameters of maturation in the Toarcian shales, Paris Basin, France – I. Changes in the configuration of acyclic isoprenoid alkanes, steranes and triterpanes. *Geochemica et Cosmochimica Acta*, **44**, 1709-1721.

Mahowald, N. M., Lamarque, J. F., Tie, X. X. and Wolff, E. (2006) Sea-salt aerosol response to climate change: Last glacial maximum, preindustrial and doubled carbon dioxide climates. *Journal of Geophysical Research: Atmospheres*, **111** (D5), 1984-2012.

Major, H. and Nagy, J. (1972) Geology of the Adventdalen map area. Norsk Polarinstitut, Oslo.

Majorowicz, J. A. and Jessop, A. M. (1981) Regional heat flow patterns in the Western Canadian Sedimentary Basin. *Tectonophysics*, **74** (3-4), 209-238.

Marchioni, D. (1983) The detection of weathering in coal by petrographic, rheologic and chemical methods. *International Journal of Coal Geology*, **2**, 231-259.

Manum, S. and Throndsen, T. (1978) Rank of coal and dispersed organic matter and its geological bearing in the Spitsbergen Tertiary. *Norsk Polarinstitutt Arbok*, 159-177.

Marshall, C. J. (2013) Palaeogeographic development and economic potential of the coal-bearing Palaeocene Todalen Member, Spitsbergen. Ph.D. Thesis, University of Nottingham, United Kingdom.

Marshall, C., Large, D. J., Meredith, W., Snape, C. E., Uguna, C., Spiro, B. F., Orheim, A., Jochmann, M., Mokogwu, I., Wang, Y. and Friis, B. (2015a) Geochemistry and petrology of Palaeocene coals from Spitsbergen - Part 1: oil potential and depositional environment. *International Journal of Coal Geology*, **143**, 22-33.

Marshall, C., Uguna, J., Large, D. J., Meredith, W., Jochmann, M., Friis, B., Vane C., Spiro, B. F., Snape, C. E. and Orheim, A. (2015b) Geochemistry and petrology of Palaeocene coals from Spitzbergen - Part 2: maturity variations and implications for local and regional burial models. *International Journal of Coal Geology*, **143**, 1-10.

Martinez, M. and Escobar, M. (1995) Effect of coal weathering on some geochemical parameters. *Organic Geochemistry*. *Organic Geochemistry*, **23** (3), 253-261.

McCarthy, K., Rojas, K., Niemann, M., Palmowski, D., Peters, K. and Stankiewicz, A. (2011) Basic petroleum geochemistry for source rock evaluation. *Oilfield Review*, **23** (2), 32-43.

Meredith, W., Russell, C. A., Cooper, M., Snape, C. E., Love, G. D., Fabbri, D. and Vane, C. H. (2004) Trapping hydropyrolysate on silica and their subsequent thermal desorption to facilitate rapid fingerprinting by GC-MS. *Organic Geochemistry*, **35** (1) 73-89.

Michels, R., Landais, P., Philp, R. P. and Torkelson, B. E. (1994) Effects of pressure on organic matter maturation during confined pyrolysis of Woodford kerogen. *Energy and Fuels*, **8** (3), 741-754.

Michels, R., Landis, P., Philp, R. P. and Torkelson, B. E. (1995) Influence of pressure and the presence of water on the evolution of the residual kerogen during confined, hydrous, and high-pressure hydrous pyrolysis of Woodford shale. *Energy and Fuels*, **9** (2), 204-215.

Miknis, F. P., Sullivan, M., Bartuska, V. J., Maciel, G. E. (1981) Cross-polarization magic-angle spinning ¹³C NMR spectra of coals of varying rank. *Organic Geochemistry*, **3**, 19-28.

Moi, R. (2008) Oil-prone Carboniferous coals (Tettegras Fm.) from the Finnmark Platform: Implications for an alternative and new Petroleum System based on oil generative coals of the Billefjord Group in the Barents Region. MSc. Thesis, University of Oslo, Norway.

Mokogwu, I. (2011) Generation and migration of oil from perhydrous Longyear coal. MSc. Thesis, University of Nottingham, United Kingdom.

Moldowan, J. M., Fago, F. J., Carlson, R. M. K., Young, D. C., Duvne, G. A., Clardy, J., Schoell, M., Pillinger, C. T. and Watt, D. S. (1991) Rearranged hopanes in sediments and petroleum. *Geochimica et Cosmochimica Acta*, **55**, 3333-3353.

Monthioux, M., Landais, P. and Durand, B. (1986) Comparison between extracts from natural and artificial maturation series of Mahakam delta coals. *Organic Geochemistry*, **10** (1-3), 299-311.

Monthioux, M., Landais, P. and Monin, J.-C. (1985) Comparison between natural and artificial maturation series of humic coals from the Mahakam delta, Indonesia. *Organic Geochemistry*, **8** (4), 275-292.

Mukhopadhyay, P. K. and Dow, W. G. (eds.) (1994) Vitrinite reflectance as a maturity parameter: applications and limitations. Washington, D.C: American Chemical Society Symposium Series, **570**, 294 pp.

Nagy, J. (2005) Delta-influenced foraminiferal facies and sequence stratigraphy of Paleocene deposits in Spitsbergen. *Palaeogeography, Palaeoclimatology, Palaeoecology*, **222**, 161-179.

Newman, J., Price, L. C. and Johnston, I. H. (1997) Hydrocarbon source potential and maturation in Eocene New Zealand vitrinite-rich coals. *Journal of Petroleum Geology*, **20**, 137-163.

Niessen, W. M. A. (2001) Principles and instrumentation of gas chromatography – mass spectrometry. In: Niessen W. M. A. (ed.) *Current practice of gas chromatography - mass spectrometry*. **Vol 86**. New York: Marcel Dekker Inc.

Nøttvedt A. (1985) Askeladden Delta Sequence (Palaeocene) on Spitsbergen – sedimentation and controls on delta formation. *Polar Research*, **3 n.s.**, 21-48.

Nøttvedt, A., Cecchi, M., Gjelberg, J. G., Kristensen, S. E., Lønøy, A., Rasmussen, A., Rasmussen, E., Skott, P. H., Van Veen, P. M. (1993) Svalbard – Barents Sea correlation: a short review. In: Vorren, T., Bergsager, E., Dahl-Stamnes, Ø. A., Holter, E., Johansen, B., Lie, E. and Lund, T. B. (eds.) *Arctic Geology and Petroleum Potential*. *Norwegian Petroleum Society Special publication*, **no.2**, 363-375.

NPI (2015) Norwegian Polar Institute. <http://toposvalbard.npolar.no/> (Last accessed 10th October, 2015).

OC (2015) Oil Converter.

<http://www.thecalculatorsite.com/conversions/substances/oil.php> (Last assessed 25th September, 2015).

OD (2015) Oxford Dictionaries

<http://www.oxforddictionaries.com/definition/english/coke> (Last accessed 25th August, 2015).

Orem, W. H. and Finkelman, R. B. (2003) Coal Formation and Geochemistry. In: Mackenzie, F. T. (ed.) *Treatise on Geochemistry*. London: Elsevier. 191-222.

Orheim, A. (1982) Undiscovered Tertiary coal resources of Svalbard: an assessment using Monte Carlo methods. In: Embry, A. F. and Balkwill, H. R. (eds.) Arctic geology and geophysics. *Canadian Society of Petroleum Geology*, 399-414.

Orheim, A., Bleg, G., Brække, T., Horseide, V. and Stenvold, J. (2007) Petrography and geochemical affinities of Spitsbergen Palaeocene coals, Norway. *International Journal of Coal Geology*, **70**, 116-136.

Paech, H. J. and Koch, J. (2001) Coalification in Post-Caledonian sediments on Spitsbergen. In: Tessensohn F. (ed.) Intra-Continental Fold Belts CASE 1: West Spitsbergen, Stuttgart. *Geologisches Jahrbuch Reihe B, Polar Issue*, **No. 7**, 505-530.

Pande, A., Uniyal, A. K. and Chandra., K. (1994) Genetic correlation of biodegraded crude oils from Lower Assam, India using biomarker compositions. *Organic Geochemistry*, **21** (8-9), 971-977.

Pecsok, R. L., Shields, L. D., Cairns, T. and McWilliam, I. G. (1968) *Modern methods of chemical analysis*. 2nd edition. Canada: John Wiley and Sons.

Pepper, A. S. and Corvi, P. J. (1995a) Simple kinetic models of petroleum formation. Part I: Oil and gas generation from kerogen. *Marine and Petroleum Geology*, **12**, 291-319.

Pepper, A. S. and Corvi, P. J. (1995b) Simple kinetic models of petroleum formation. Part III: Modelling an open system. *Marine and Petroleum Geology*, **12**, 417-452.

Peters, K. E. (1986) Guidelines for evaluating petroleum source rock using programmed pyrolysis. *American Association of Petroleum Geologists Bulletin*, **70** (3), 318-329.

Peters, K. E. and Moldowan, J. M. (1991) Effects of source, thermal maturity and biodegradation on the distribution and isomerisation of homohopanes in petroleum. *Organic Geochemistry*, **17**, 47-61.

Peters, K. E. and Moldowan, J. M. (1993) *The biomarker guide: interpreting molecular fossils in petroleum and ancient sediments*. New Jersey: Prentice-Hall Incorporated.

Peters, K. E., Walters, C. C. and Moldowan, J. M. (2005) *The biomarker guide: biomarkers and isotopes in petroleum exploration and earth history*. 2nd edition. New York: Cambridge University Press.

Petersen, H. I. (2002) A re-consideration of the "oil window" for humic coal and kerogen type III source rocks. *Journal of Petroleum Geology*, **25**, 407-431.

Petersen, H. I. (2005) Oil generation from coal source rocks: the influence of depositional conditions and stratigraphic age. *Geological Survey of Denmark and Greenland, Bulletin 7*, 9-12.

Petersen, H. I. (2006) The petroleum generation potential and effective oil window of humic coals related to coal composition and age. *International Journal of Coal Geology*, **67** (4), 221-248.

Petersen, H. I. Lindström, S., Nytoft, H. P. and Rosenberg, P. (2009) Composition, peat-forming vegetation and kerogen paraffnicity of Cenozoic coals: relationship to variations in the petroleum generation potential (Hydrogen Index). *International Journal of Coal Geology*, **78**, 119–134

Petersen, H. I. and Nytoft, H. P. (2006) Oil generation capacity of coals as a function of coal age and aliphatic structure. *Organic Geochemistry*, **37**, 558-583.

Petersen, H. I. and Rosenberg, P. (1998) Reflectance retardation (suppression) and source rock properties related to hydrogen-enriched vitrinite in Middle Jurassic coals, Danish North Sea. *Journal of Petroleum Geology*, **21**, 247-263.

Petersen, H.I. and Vosgerau, H. (1999) Composition and organic maturity of Middle Jurassic coals, North-East Greenland: evidence for liptinite-induced suppression of huminite reflectance. *International Journal of Coal Geology*, **41**, 257-274.

Petrov, A. A. (1987) *Petroleum hydrocarbons*. Berlin Heidelberg: Springer-Verlag

Philp, R. P. (1994) Geochemical characteristics of oils derived predominantly from terrigenous source materials. In: Scott, A. C. and Fleet, A. J. (eds.) Coal and coal-bearing strata as oil-prone source rocks? *Geological Society Special Publication*, **77**. London: The Geological Society. 71-92.

Powell, T. G. and Boreham, C. J. (1994) Terrestrially sourced oils: where do they exist and what are our limits of knowledge? – a geochemical perspective. In: Scott, A. A. and Fleet, A. J. (eds.) Coal and coal-bearing strata as oil-prone

source rocks? *Geological Society Special Publication*, **77**. London: The Geological Society. 11-29.

Price, L. C. (1980) Crude oil degradation as an explanation of the depth rule. *Chemical Geology*, **28**, 1-30.

Price, L. C. (1985) Examples, causes and consequences of vitrinite reflectance suppression in hydrogen-rich organic matter - a major unrecognised problem. *American Association of Petroleum Geologists Bulletin (Abstract)*, **69** (2), 298.

Price, P. L., Sullivan, T. and Alexander, R. (1987) The nature and occurrence of oil in Seram, Indonesia. *Proceedings of the Indonesian Petroleum Association, Sixteenth Annual Convention*, **Vol 1**. Indonesian Petroleum Association, Jakarta, 141-173.

Price, L. C. and Wenger, L. M. (1992) The influence of pressure on petroleum generation and maturation as suggested by aqueous pyrolysis. *Organic Geochemistry*, **19** (1-3), 141-159.

Pugmire, R. J., Zilm, K. W., Wolfenden, W. R., Grant, D. M., Dyrkacy, G. R., Bloomquist, C. A. A. and Horwitz, E. P. (1982) Carbon-13 NMR spectra of macerals separated from individual coals. *Organic Geochemistry*, **4**, 79-84.

Qin, K., Huang, D., Li, L. and Guo, S. (1993) Oil and gas potential of macerals as viewed by C-13 NMR spectroscopy. *Organic Geochemistry*, poster sessions from the 16th International Meeting on Organic Geochemistry, Stavanger, 1993. Falch, Oslo. 758-762.

Radke, M. (1988) Application of aromatic compounds as maturity indicators in source rocks and crude oils. *Marine and Petroleum Geology*, **5**, 224–236.

Radke, M., Garrigues, P. and Willsch, H. (1990) Methylated dicyclic and tricyclic aromatic hydrocarbons in crude oils from the Handil field, Indonesia. *Organic Geochemistry*, **15**, 17-34.

Radke, M., Wehe, D. H. and Willsch, H. (1982a) Geochemical study on a well in the Western Canada Basin: relation of the aromatic distribution pattern to maturity of organic matter. *Geochimica et Cosmochimica Acta*, **46**, 1-10.

Radke, M., Willsch, H., Leythaeuser, D. and Teichmüller, M. (1982b) Aromatic components of coal: relation of distribution pattern to rank. *Geochimica et Cosmochimica Acta*, **46**, 1831-1848.

Radke, M. and Welte D. H. (1983) The Methylphenanthrene Index (MPI): a maturity parameter based on aromatic hydrocarbons. In: Bjoroy, M. *et al* (eds.) *Advances in Organic Geochemistry*. Wiley: Chichester. 504-512.

Raiswell, R. and Berner, R. A. (1985) Pyrite formation in euxinic and semi-euxinic sediments. *American Journal of Science*, **285**, 710-724.

Rasmussen, E. and Fjeldskaar, W. (1996) Quantification of the Pliocene-Pleistocene erosion of the Barents Sea from present-day bathymetry. *Global and Planetary Change*, **12**, 119-133.

Raymond, A. C. and Murchison, D. G. (1988) Development of organic maturation in the thermal aureoles of sills and its relation to sediment compaction. *Fuel*, **67**, 1599-1608.

Reed, W. E. (1977) Molecular Composition of Weathered Petroleum and Composition with its Possible Source. *Geochimica et Cosmochimica Acta*, **41**, 237-247.

Reeckmann, S. A., Duddy, I. R. and Gleadow, A. J. (1985) Igneous intrusions in porous sandstone sequences - widespread thermal effects measured by fission track annealing and vitrinite reflectance. *Abstract of the American Association of Petroleum Geologists Meeting*, **69** (2). 299-300.

Robertson, E. C. (1988) Thermal properties of rocks. US Department of the Interior Geology, Open-File Report 88-441.

Rudnick, R. L. and Gao, S. (2003) The composition of the continental crust. In: Rudnick, R. L. (ed.) *Treatise on geochemistry*. **Vol. 3**. Oxford: Elsevier. 1-64.

Rullkötter, J. and Wendisch, D. (1982) Microbial alteration of 17a(H)-hopane in Madagascar asphalts: removal of C-10 methyl group and ring opening. *Geochimica et Cosmochimica Acta*, **46**, 1543-1553.

Rullkötter, J., Spiro, B. and Nissenbaum, A. (1985) Biological marker characteristics of oils and asphalts from carbonate source rocks in a rapidly subsiding graben, Dead Sea, Israel. *Geochimica et Cosmochimica Acta*, **49** (6), 1357-1370.

Russell, N. J., Wilson, M. A., Pugmire, R. J. and Grant, D. M. (1983) Preliminary studies on the aromaticity of Australian coals: solid state n.m.r. techniques. *Fuel*, **62** (5), 601-605.

Rybach, L. (1984) The paleogeothermal conditions of the Swiss molasses basin: implications for hydrocarbon potential. *Rev. Inst. Franç. Pétrole*, **39**, 143-146.

Salvigsen, O. and Høgvard, K. (2007) Gygrekjelda, a new warm spring in Bockfjorden, Svalbard. *Polar Research*, **27**, 107-109.

Sandison, C. M. (2001) The organic geochemistry of marine-influenced coals. Ph.D. Thesis, Curtin University of Technology, Perth.

Sandison, C. M., Alexander, R., Kagi, R. I. and Boreham, C. J. (2002) Sulfurisation of lipids in a marine-influenced lignite. *Organic Geochemistry*, **33** (9), 1053-1077.

Sandercock, R. G. (1975) Non-recovery coke ovens. In: Cook, A. C. (ed.) Australian black coal – its occurrence, mining, preparation and use. *Australian Institute of Mining and Metallurgy*, Illawarra Branch, 224-231.

Saxby, J. D. and Shibaoka, M. (1986) Coal and coal macerals as source rocks for oil and gas. *Applied Geochemistry*, **1**, 25-36.

Schenk, H. J. and Dieckmann, V. (2004) Prediction of petroleum formation: the influence of laboratory heating rates on kinetic parameters and geological extrapolations. *Marine and Petroleum Geology*, **21**, 79-95

Schutter, S. (2010) Hydrocarbons associated with igneous rocks (North America and Worldwide). *Houston Geological Society Bulletin*, **Vol. 52** (7), 24- 27.

Scott, A. C. (2000) The pre-Quaternary history of fire. *Palaeogeography, Palaeoclimatology, Palaeoecology*, **164**, 281-329.

Scott, A. C. (2002) Coal petrology and the origin of coal macerals: a way ahead? *International Journal of Coal Geology*, **50**, 119-134.

Scott, A. C. and Fleet, A. J. (eds.) *Coal and coal-bearing strata as oil-prone source rocks? Geological Society Special Publication*, **77**. London: The Geological Society.

Scott, A. C., Cripps, J., Nichols, G. and Collinson, M. E. (2000) The taphonomy of charcoal following a recent heathland fire and some implications for the interpretation of fossil charcoal deposits. *Palaeogeography, Palaeoclimatology, Palaeoecology*, **164**, 1-31.

Scott, A. C. and Glasspool, I. J. (2007) Observations and experiments on the origin and formation of inertinite group macerals. *International Journal of Coal Geology*, **70**, 53-66.

Seifert, W. K. and Moldowan, J. M. (1978) Applications of steranes, terpanes and monoaromatics to the maturation, migration and source of crude oils. *Geochimica et Cosmochimica Acta*, **42**, 77-95.

Seifert, W. K. and Moldowan, J. M. (1979) Effect of biodegradation on steranes and terpanes in crude oils. *Geochimica et Cosmochimica Acta*, **43**, 111-126.

Seifert, W. K. and Moldowan, J. M. (1980) The Effect of Thermal Stress on Source-Rock Quality as Measured by Hopane Stereochemistry. *Physics and Chemistry of the Earth*, **12**, 229-237

Seifert, W. K. and Moldowan, J. M. (1986) Use of Biological Markers in Petroleum Exploration. In: R. B. Johns (ed.) *Methods in Geochemistry and Geophysics*. Vol 24. Amsterdam: Elsevier.

Shanmugam, G. (1985) Significance of coniferous rain forests and related organic matter in generating commercial quantities of oil, Gippsland Basin, Australia. *American Association of Petroleum Geologists Bulletin*, **69**, 1241-1254.

Sharp, J. M. Jr. and Domenico, P. A. (1976) Energy transport in thick sequences of compacting sediments. *Geological Society of America Bulletin*, **87**, 390-400.

Shen, J-C. and Huang, W-L. (2007) Biomarker distributions as maturity Indicators in coals, coaly shales, and shales from Taiwan. *Terrestrial, Atmospheric and Oceanic Sciences*, **8** (4), 739-755.

Simanzhenkov, V. and Idem, R. (2003) *Crude oil chemistry*. Florida: CRC Press.

Sinninghe Damsté, J. S. and de Leeuw, J. W. (1990) Analysis, structure and geochemical significance of organically-bound sulfur in the geosphere: state of the art and future research. *Organic Geochemistry*, **16**, 1077-1101.

Sinninghe Damsté, J. S., de Las Heras, F. X. C. and de Leeuw, J. W. (1992) Molecular analysis of sulphur-rich brown coals by flash pyrolysis-gas chromatography-mass spectrometry. *Journal of Chromatography A*, **607**, 361–376.

Sinninghe Damsté, J. S., de Las Heras, X. C., van Bergen, P. F. and de Leeuw, J. W. (1993) Characterization of Tertiary Catalan lacustrine oil shales: discovery of extremely organic sulphur-rich Type I kerogens. *Geochimica et Cosmochimica Acta*, **57**, 389-415.

Sinninghe Damsté, J. S., Eglinton, T. I., de Leeuw, J. W. and Schenck, P. A. (1989) Organic sulphur in macromolecular sedimentary organic matter: I. Structure and origin of sulphur-containing moieties in kerogen, asphaltenes and coal as revealed by flash pyrolysis. *Geochimica et Cosmochimica Acta*, **53**, 873–889.

Snowdon, L. R. (1995) Rock-Eval T_{max} suppression: documentation and amelioration. *American Association of Petroleum Geologists Bulletin*, **79**, 1337-1348.

Stach, E. (1982) The macerals of coal. In: Stach, E., Mackowsky, M.-Th., Teichmüller, M., Taylor, G. H., Chandra, D. and Teichmüller, R. (eds.) *Stach's textbook of coal petrology*. 3rd edition. Berlin-Stuttgart: Gebruder Borntraeger. 87-140.

Stach, E., Mackowsky, M.-Th., Teichmüller, M., Taylor, G. H., Chandra, D. and Teichmüller, R. (eds.) (1982) *Stach's textbook of coal petrology*. 3rd edition. Berlin-Stuttgart: Gebruder Borntraeger.

Steel, R., Dalland, A., Kalgraff, K. and Larsen V. (1981) The Central Tertiary Basin of Spitsbergen: sedimentary development of a sheared margin basin: Geology of the North Atlantic Borderland. *Canadian Society of Petroleum Geologists Memoir*, **7**, 647-664.

Steel, R. J. and Worsley, D. (1984) Svalbard's post-Caledonian strata – an atlas of sedimentological patterns and palaeogeographic evolution. In: Spencer, A. M. (ed.) Habitat of hydrocarbons on the Norwegian continental margin. London: Graham and Trotman. 109-135

STHDA (2015) Statistical tools for high-throughput data analysis. <http://www.sthda.com/english/wiki/correlation-matrix-a-quick-start-guide-to-analyze-format-and-visualize-a-correlation-matrix-using-r-software> (Last accessed 15th October, 2015)

Stephens, J. F., Leow, H. M., Gilbert, T. D. and Philp, R. P. (1985) Investigation of the relationship between coal maturity and aromaticity: Characteristics of sodium dichromate oxidation products of Australian vitrinite concentrates. *Fuel*, **64**, 1537-1541.

Stout, S. A. (1994) Chemical heterogeneity among adjacent coal microlithotypes - implications for oil generation and primary migration from humic coal. In: Scott, A. C. and Fleet, A. J. (eds.) Coal and coal-bearing strata as oil-prone source rocks? *Geological Society Special Publication*, **77**. London: The Geological Society. 93-106.

Suggate, R. P. (2000) The Rank (Sr) scale: its basis and its applicability as a maturity index for all coals. *New Zealand Journal of Geology and Geophysics*, **43**, 521-553.

Suggate, R. P. and Dickinson, W. W. (2004) Carbon NMR of coals: the effects of coal type and rank. *International Journal of Coal Geology*, **57** (1), 1-22.

Svendsen, H., Beszczynska-Møller, A., Hagen, J. O., Lefauconnier, B., Tverberg, V., Gerland, S., Ørbæk, J. B., Bischof, K., Papucci, C., Zajaczkowski, M., Azzolini, R., Bruland, O., Wiencke, C., Winther, J-G. and Dallmann, W. (2002) The physical environment of Kongsfjorden–Krossfjorden, an Arctic fjord system in Svalbard. *Polar Research*, **21**, 133-166.

Sykes, R. (2001) Depositional and rank controls on the petroleum potential of coaly source rocks. In: Hill, K. C. and Bernecker, T. (eds.) Eastern Australasian Basins Symposium, a Refocused Energy Perspective for the Future. *Petroleum Exploration Society of Australia Special Publication*, 591–601.

Sykes, R. and Snowdon, L. R. (2002) Guidelines for assessing the petroleum potential of coaly source rocks using Rock-Eval pyrolysis. *Organic Geochemistry*, **33**, 1441-1455.

Sykes, R., Snowdon, L. R., Johansen, P. E., Killops, S. D., Chagué-Goff, C., Bartram, K. M. and Markwitz, A. (2004) Effects of marine influence on the petroleum generation characteristics of humic coals: Eocene Mangahewa Formation, Taranaki Basin. Abstracts of the 21th Annual Meeting of the Society for Organic Petrology, **vol 21**, Sydney, New South Wales, Australia, 27 September – 1 October, 2004.

Sykes, R., Volk, H., George, S. C., Ahmed, M., Higgs, K. E., Johansen, P. E. and Snowdon, L. R. (2014) Marine influence helps preserve the oil potential of coaly source rocks: Eocene Mangahewa Formation, Taranaki Basin, New Zealand. *Organic Geochemistry*, **66**, 140-163.

Tangedal, O. (2011) 3D architecture and hydrocarbon potential of a pre-uplift Billefjorden Basin. MSc. Thesis, University of Bergen, Norway.

Tarafa, M. E., Hunt, J. M and Ericson, I. (1983) Effect of hydrocarbon volatility and adsorption on source-rock pyrolysis. *Journal of Geochemical Exploration*, **18**, 75-85.

Taylor, G. H., Teichmüller, M., Davis, A., Diessel, C. F. K., Littke, R. and Robert, P. (eds.) (1998) *Organic petrology*. Berlin: Gebrüder Borntraeger.

Teichmüller, M. (1989) The genesis of coal from the viewpoint of coal petrology. *International Journal of Coal Geology*, **12**, 1-87.

Teichmüller, M. and Durand, B. (1983) Fluorescence microscopical rank studies on liptinites and vitrinites in peat and coals, and comparison with results of the rock-eval pyrolysis. *International Journal of Coal Geology*, **2**, 197-230.

Teichmüller, M. and Teichmüller, R. (1967) Diagenesis of coal (coalification). In: Larsen, G. and Chilingar, G. V. (eds.) *Diagenesis in sediments*. Amsterdam: Elsevier. 391-415.

Teichmüller, M. and Teichmüller, R. (1982) The geological basis of coal formation. In: Stach, E., Mackowsky, M.-Th., Teichmüller, M., Taylor, G. H., Chandra, D. and Teichmüller, R. (eds.) *Stach's textbook of coal petrology*. 3rd edition. Berlin-Stuttgart: Gebruder Borntraeger. 5-86.

Tekely, P., Nicole, D., Delpuech, J., Totino, E. and Muller, J. (1987) Chemical structure changes in coals after low-temperature oxidation and demineralization by acid treatments as revealed by high resolution solid state ^{13}C NMR. *Fuel Processing Technology*, **15**, 225-231.

Templeton, D. M. (1994) Inductively coupled plasma-atomic emission spectrometry (ICP-AES) and inductively coupled plasma-mass spectrometry (ICP-MS). In: Seiler G. H., Sigel, A. and Sigel, H. (eds.) *Handbook on metals in clinical and analytical chemistry*. New York: Marcel Dekker, Inc. 167-178.

Teo, K., Finora, S. and Leja, J. (1982) Oxidation states in surface and buried coal from the Fjording River Deposit. *Fuel*, **61**, 71-76.

Tessensohn, F. (2001) Intra-continental fold belts. Case 1: West Spitsbergen. *Geologisches Jahrbuch*. Stuttgart: Schweizerbart.

Thompson, S., Cooper, B. S., Morley, R. J. and Barnard, P. C. (1985) Oil generating coals. In: Thomas, B. M., et al. (eds.) *Petroleum Geochemistry in Exploration of the Norwegian Shelf*. London: Graham and Trotman. 59-73.

Thronsdalen, T. (1982) Vitrinite reflectance studies of coals and dispersed organic matter in tertiary deposits in the Advent-Dalen Area, Svalbard. *Polar Research*, 77-91.

Tissot, B., Califet-Debyser, Y., Deroo, G. and Oudin, J. L. (1971) Origin and evolution of hydrocarbons in Early Toarcian shales, Paris Basin, France. *American Association of Petroleum Geologists Bulletin*, **55**, 2177-2193.

Tissot, B. P. and Welte, D. H. (1984) *Petroleum formation and occurrence*. 2nd edition. Berlin: Springer-Verlag.

Tissot, B. P., Pelet, R. and Ungerer, Ph. (1987) Thermal history of sedimentary basins, maturation indices, and kinetics of oil and gas generation. *AAPG Bulletin*, **71**, 1445-1466.

Todd, D.K (1980) *Groundwater hydrology*. 2nd edition. New York: Wiley.

Todd, S. P., Dunn, M. E. and Barwise, A. J. G. (1997) Characterizing petroleum charge systems in the tertiary of SE Asia. In: Fraser, A. J., Matthews, S. J. and Murphy, R. W. (eds.) *Petroleum Geology of Southeast Asia. Geological Society Special Publication*, **126**, 25-47.

Treiman, A. H. (2012) Eruption age of the Sverrefjellet volcano, Spitsbergen Island, Norway. *Polar Research*, **31**, 17320, DOI: 10.3402/polar.v31i0.17320.

Uguna, C. N., Carr, A. D., Snape, C. E. and Meredith, W. (2015) High pressure water pyrolysis of coal to evaluate the role of pressure on hydrocarbon

generation and source rock maturation at high maturities under geological conditions. *Organic Geochemistry*, **78**, 44-51.

Uguna, C. N, Carr, A. D., Snape, C. E., Meredith, W. and Castro-Diaz, M. (2012) A laboratory pyrolysis study to investigate the effect of water pressure on hydrocarbon generation and maturation of coals in geological basins. *Organic Geochemistry*, **52**, 103-113.

USGS (2015) United States Geological Survey.

minerals.cr.usgs.gov/gips/na/5process.html (Last assessed 15th September, 2015)

USOCR - U.S. Office of Coal Research (1967) Methods of analysing and testing coal and coke. *Bureau of Mines, Bulletin* **638**, 1-83.

van Koeverden, J. H., Karlsen, D. A. and Backes-Owe, K. (2011) Carboniferous non marine source rocks from Spitsbergen and Bjørnøya; comparison with the Western Arctic. *Journal of Petroleum Geology*, **34** (1), 53-66.

van Koeverden, J. H., Karlsen, D. A., Schwark, L., Chpitsglouz, A. and Backer-Owe, K. (2010) Oil-prone lower Carboniferous coals in the Norwegian Barents Sea; implications for a Palaeozoic petroleum system. *Journal of Petroleum Geology*, **33** (2), 155-181.

van Krevelen, D. W. (1961) Coal: typology-chemistry-physics-constitution. Amsterdam: Elsevier Science.

van Krevelen, D. W. (1984) Organic geochemistry - old and new. *Organic Geochemistry*, **6**, 1-10.

Volkman, J. K., Alexander, R., Kagi, R. I. and Woodhouse, G. W. (1983) Demethylated hopanes in crude oils and their applications in petroleum geochemistry. *Geochimica et Cosmochimica Acta*, **47** (4), 785-794.

Vu, T. T. A., Zink, K. G., Mangelsdorf, K., Sykes, S., Wilkes, H. and Horsfield, B. (2009) Changes in bulk properties and molecular compositions within New Zealand Coal Band solvent extracts from early diagenetic to catagenetic maturity levels. *Organic Geochemistry*, **40**, 963-977.

Wang, Y. (2011) Oil generative potential of perhydrous coals from the Arctic Svalbard archipelago. MSc. Thesis, University of Nottingham, United Kingdom.

Ward, C. R. (1984) *Coal geology and coal technology*. Boston: Blackwell Scientific Publications. 1-40.

Weis, D., Shotyck, W., Rieley, J., Paige, S., Gloor, M., Reese, S. and Martinez-Coritzas, A. (2002) The geochemistry of major and selected trace elements in a forested peat bog, Kalimantan SE Asia and its implications for past atmospheric dust deposition. *Geochim. Cosmochim Acta*, **66** (13), 2307-2323.

Wenger, L. M. and Baker, D. R. (1987) Variations in vitrinite reflectance with organic facies - Examples from Pennsylvanian cyclothems of the Midcontinent, U.S.A. *Organic Geochemistry*, **11**, 411-416.

Wenger, L. M., Davis, C. L. and Isaksen, G. H. (2002) Multiple controls on petroleum biodegradation and impact on oil quality. *SPE Reservoir Evaluation and Engineering*, **5**, 375-383.

Weres, O., Newton, A. S. and Tsao, L. (1988) Hydrous pyrolysis of alkanes, alkenes, alcohols and ethers. *Organic Geochemistry*, **12** (5), 433-444.

Wignall, P. B., Newton, R. and Brookfield, M. E. (2005) Pyrite framboid evidence for oxygen-poor deposition during the Permian-Triassic crisis in Kashmir. *Palaeogeography Palaeoclimatology Palaeoecology*, **216**, 183-188.

Wilkes, H., Boreham, C., Harms, G., Zengler, K. and Rabus, R. (2000). Anaerobic degradation and carbon isotopic fractionation of alkylbenzenes in crude oil by sulphate-reducing bacteria. *Organic Geochemistry*, **31** (1), 101-115.

Wilkins, R. W. T. and George, G. C. (2002) Coal as a source rock for oil: a review. *International Journal of Coal Geology*, **50**, 317-361.

Wilkins, R. W. T., Wilmshurst, J. R., Russell, N. J., Hladky, G., Ellacott, M. V. and Buckingham, C. (1992) Fluorescence alteration and the suppression of vitrinite reflectance. *Organic Geochemistry*, **18** (5), 629-640.

Worsley, D., Aga, O. J., Dalland, A., Elverhøi, A. and Thon, A. (1986) The Geological History of Svalbard, Evolution of an Arctic Archipelago. Stavanger: Den norske states oljeselskap. A.S.

Xie, W., Stanger, R., Wall, T. F., Lucas, J. A. and Mahoney, M. R. (2015) Associations of physical, chemical with thermal changes during coking as coal heats – Experiments on coal maceral concentrates. *Fuel*, **147**, 1-8.

Zilm, K. W., Pugmire, R. J., Larter, S. R., Allan J. and Grant D. M. (1981) Carbon-13 CP/MAS spectroscopy of coal macerals. *Fuel*, **60**, 717-722.

APPENDICES

1. Sample Distribution

Sample ID	Area	Location and sample type	Seam	Median drill depth (m)	Median height above seam base (cm)	Core length (cm)	Comment
Ba1	Bassen	Outcrop section	Longyear	-	198.50	7.0	Coal
Ba2	Bassen	Outcrop section	Longyear	-	192.00	6.0	Coal
Ba3	Bassen	Outcrop section	Longyear	-	186.50	5.0	Coal
Ba4	Bassen	Outcrop section	Longyear	-	181.50	5.0	Coal
Ba5	Bassen	Outcrop section	Longyear	-	176.00	6.0	Coal
Ba6	Bassen	Outcrop section	Longyear	-	170.00	6.0	Coal
Ba7	Bassen	Outcrop section	Longyear	-	162.50	9.0	Coal
Ba8	Bassen	Outcrop section	Longyear	-	155.50	5.0	Coal
Ba9	Bassen	Outcrop section	Longyear	-	150.50	5.0	Coal
Ba10	Bassen	Outcrop section	Longyear	-	144.50	7.0	Coal
Ba11	Bassen	Outcrop section	Longyear	-	137.50	7.0	Coal
Ba12	Bassen	Outcrop section	Longyear	-	130.50	7.0	Coal
Ba13	Bassen	Outcrop section	Longyear	-	124.50	5.0	Coal
Ba14	Bassen	Outcrop section	Longyear	-	119.25	5.5	Coal
Ba15	Bassen	Outcrop section	Longyear	-	113.75	5.5	Coal
Ba16	Bassen	Outcrop section	Longyear	-	109.00	4.0	Coal
Ba17	Bassen	Outcrop section	Longyear	-	105.00	4.0	Coal
Ba18	Bassen	Outcrop section	Longyear	-	100.00	6.0	Coal
Ba19	Bassen	Outcrop section	Longyear	-	94.00	6.0	Coal
Ba20	Bassen	Outcrop section	Longyear	-	88.00	6.0	Coal
Ba21	Bassen	Outcrop section	Longyear	-	82.25	5.5	Coal
Ba22	Bassen	Outcrop section	Longyear	-	76.25	6.5	Coal
Ba23	Bassen	Outcrop section	Longyear	-	60.00	6.0	Coal
Ba24	Bassen	Outcrop section	Longyear	-	54.00	6.0	Coal
Ba25	Bassen	Outcrop section	Longyear	-	48.50	5.0	Coal
Ba26	Bassen	Outcrop section	Longyear	-	43.00	6.0	Coal
Ba27	Bassen	Outcrop section	Longyear	-	36.50	7.0	Coal
Ba28	Bassen	Outcrop section	Longyear	-	29.50	7.0	Coal
Ba29	Bassen	Outcrop section	Longyear	-	23.00	6.0	Coal
Ba30	Bassen	Outcrop section	Longyear	-	16.50	7.0	Coal
Ba31	Bassen	Outcrop section	Longyear	-	9.50	7.0	Coal
Ba32	Bassen	Outcrop section	Longyear	-	3.00	6.0	Coal
Br1	Breinosa	BH4-2009	Askeladden	-298.44	46.50	19	Coal
Br2	Breinosa	BH4-2009	Askeladden	-298.55	35.00	4	Mudstone
Br3	Breinosa	BH4-2009	Askeladden	-298.74	16.50	33	Coal
Br4	Breinosa	BH4-2009	Svarteper	-300.19	107.00	24	Ash rich coal
Br5	Breinosa	BH4-2009	Svarteper	-300.43	83.00	24	Ash rich coal
Br6	Breinosa	BH4-2009	Svarteper	-300.67	59.00	24	Ash rich coal
Br7	Breinosa	BH4-2009	Svarteper	-301.05	35.00	24	Ash rich coal
Br8	Breinosa	BH4-2009	Svarteper	-301.15	11.50	23	Ash rich coal
Br9	Breinosa	BH4-2009	Unknown	-313.78	24.00	24	Coal
Br10	Breinosa	BH4-2009	Longyear	-314.53	136.00	20	Coal
Br11	Breinosa	BH4-2009	Longyear	-314.73	116.00	20	Coal
Br12	Breinosa	BH4-2009	Longyear	-314.94	95.50	21	Coal
Br13	Breinosa	BH4-2009	Longyear	-315.15	74.50	21	Coal
Br14	Breinosa	BH4-2009	Longyear	-315.33	56.00	16	Mudstone
Br15	Breinosa	BH4-2009	Longyear	-315.49	40.00	16	Mudstone
Br16	Breinosa	BH4-2009	Longyear	-315.65	24.00	16	Coal
Br17	Breinosa	BH4-2009	Longyear	-315.81	8.00	16	Coal
Br18	Breinosa	BH5-2009	Askeladden	-	33	-	Coal
Br19	Breinosa	BH5-2009	Svarteper	-	93	-	Coal
Br20	Breinosa	BH5-2009	Svarteper	-	72	-	Coal
Br21	Breinosa	BH5-2009	Svea	-	125	-	Coal
Br22	Breinosa	BH5-2009	Svea	-	100	-	Coal
Br23	Breinosa	BH5-2009	Svea	-	50	-	Coal
Br24	Breinosa	BH5-2009	Svea	-	7.5	-	Coal
Br25	Breinosa	Mine 7 section	Longyear	-	147	-	Coal
Br26	Breinosa	Mine 7 section	Longyear	-	142	-	Coal
Br27	Breinosa	Mine 7 section	Longyear	-	135	-	Coal
Br28	Breinosa	Mine 7 section	Longyear	-	117	-	Coal
Br29	Breinosa	Mine 7 section	Longyear	-	105	-	Coal
Br30	Breinosa	Mine 7 section	Longyear	-	101	-	Coal
Br31	Breinosa	Mine 7 section	Longyear	-	90	-	Coal
Br32	Breinosa	Mine 7 section	Longyear	-	83	-	Coal
Br33	Breinosa	Mine 7 section	Longyear	-	75	-	Coal
Br34	Breinosa	Mine 7 section	Longyear	-	66	-	Coal
Br35	Breinosa	Mine 7 section	Longyear	-	63	-	Coal
Br36	Breinosa	Mine 7 section	Longyear	-	55	-	Coal
Br37	Breinosa	Mine 7 section	Longyear	-	49	-	Coal

Br38	Breinosa	Mine 7 section	Longyear	-	40	-	Coal
Br39	Breinosa	Mine 7 section	Longyear	-	29	-	Coal
Br40	Breinosa	Mine 7 section	Longyear	-	25	-	Coal
Br41	Breinosa	Mine 7 section	Longyear	-	18	-	Coal
Br42	Breinosa	Mine 7 section	Longyear	-	5	-	Coal
Br43	Breinosa	Mine 7 section	Longyear	-	Bulk	-	Coal
L1	Lunckefjellet	BH15-2011	Svarteper	-246.0	80.00	10	Coal
L2	Lunckefjellet	BH15-2011	Svarteper	-246.1	70.00	10	Coal
L3	Lunckefjellet	BH15-2011	Svarteper	-246.2	60.00	10	Coal
L4	Lunckefjellet	BH15-2011	Svarteper	-246.3	50.00	10	Coal
L5	Lunckefjellet	BH15-2011	Svarteper	-246.4	40.00	10	Coal
L6	Lunckefjellet	BH15-2011	Svarteper	-246.5	30.00	10	Coal
L7	Lunckefjellet	BH15-2011	Svarteper	-246.6	20.00	10	Coal
L8	Lunckefjellet	BH15-2011	Svarteper	-246.7	10.00	10	Coal
L9	Lunckefjellet	BH15-2011	Longyear	-258.3	210.00	10	Coal
L10	Lunckefjellet	BH15-2011	Longyear	-258.4	200.00	10	Coal
L11	Lunckefjellet	BH15-2011	Longyear	-258.5	190.00	10	Coal
L12	Lunckefjellet	BH15-2011	Longyear	-258.8	160.00	10	Coal
L13	Lunckefjellet	BH15-2011	Longyear	-258.9	150.00	10	Coal
L14	Lunckefjellet	BH15-2011	Longyear	-259	140.00	10	Coal
L15	Lunckefjellet	BH15-2011	Longyear	-259.1	130.00	10	Coal
L16	Lunckefjellet	BH15-2011	Longyear	-259.2	120.00	10	Coal
L17	Lunckefjellet	BH15-2011	Longyear	-259.3	110.00	10	Coal
L18	Lunckefjellet	BH15-2011	Longyear	-259.4	100.00	10	Coal
L19	Lunckefjellet	BH15-2011	Longyear	-259.5	90.00	10	Coal
L20	Lunckefjellet	BH15-2011	Longyear	-259.6	80.00	10	Coal
L21	Lunckefjellet	BH15-2011	Longyear	-259.7	70.00	10	Coal
L22	Lunckefjellet	BH15-2011	Longyear	-259.8	60.00	10	Coal
L23	Lunckefjellet	BH15-2011	Longyear	-259.9	50.00	10	Coal
L24	Lunckefjellet	BH15-2011	Longyear	-260.00	40.00	10	Coal
L25	Lunckefjellet	BH15-2011	Longyear	-260.1	30.00	10	Coal
L26	Lunckefjellet	BH15-2011	Longyear	-260.2	20.00	10	Coal
L27	Lunckefjellet	BH15-2011	Longyear	-260.3	10.00	10	Coal
L28	Lunckefjellet	BH10-2009	Svarteper	-54.25	99.00	22	Ash rich coal
L29	Lunckefjellet	BH10-2009	Svarteper	-54.50	74.50	27	Mudstone
L30	Lunckefjellet	BH10-2009	Svarteper	-54.73	51.00	20	Coal
L31	Lunckefjellet	BH10-2009	Svarteper	-54.93	31.00	20	Coal
L32	Lunckefjellet	BH10-2009	Svarteper	-55.14	10.50	21	Coal
L33	Lunckefjellet	BH10-2009	Longyear	-69.71	79.00	30	Coal
L34	Lunckefjellet	BH10-2009	Longyear	-69.97	53.00	22	Coal
L35	Lunckefjellet	BH10-2009	Longyear	-70.19	31.50	21	Coal
L36	Lunckefjellet	BH10-2009	Longyear	-70.40	10.50	21	Coal
L37	Lunckefjellet	BH10-2007	Svarteper	-236.38	85.50	35	Coal
L38	Lunckefjellet	BH10-2007	Svarteper	-237.03	20.50	41	Coal
L39	Lunckefjellet	BH10-2007	Longyear	-247.06	148.50	25	Coal
L40	Lunckefjellet	BH10-2007	Longyear	-247.31	123.50	25	Coal
L41	Lunckefjellet	BH10-2007	Longyear	-247.56	98.50	25	Coal
L42	Lunckefjellet	BH10-2007	Longyear	-247.81	73.50	25	Coal
L43	Lunckefjellet	BH10-2007	Longyear	-248.06	48.50	25	Coal
L44	Lunckefjellet	BH10-2007	Longyear	-248.45	9.50	19	Coal
L45	Lunckefjellet	BH6A-2007	Svarteper	-210.36	110.50	39	Coal
L46	Lunckefjellet	BH6A-2007	Svarteper	-210.75	71.50	39	Coal
L47	Lunckefjellet	BH6A-2007	Svarteper	-211.29	17.00	34	Coal
L48	Lunckefjellet	BH6A-2007	Longyear	-223.03	187.50	25	Coal
L49	Lunckefjellet	BH6A-2007	Longyear	-223.28	162.50	25	Coal
L50	Lunckefjellet	BH6A-2007	Longyear	-223.53	137.50	25	Coal
L51	Lunckefjellet	BH6A-2007	Longyear	-223.78	112.50	25	Coal
L52	Lunckefjellet	BH6A-2007	Longyear	-224.03	87.50	25	Coal
L53	Lunckefjellet	BH6A-2007	Longyear	-224.28	62.5	25	Coal
L54	Lunckefjellet	BH6A-2007	Longyear	-224.53	37.50	25	Coal
L55	Lunckefjellet	BH6A-2007	Longyear	-224.78	12.50	25	Coal
C1	Colesdalen	BH3-2008	Verkny	-258.18	16.00	16	Pyrite rich coal
C2	Colesdalen	BH3-2008	Sputnik	-274.13	172.50	25	Coal
C3	Colesdalen	BH3-2008	Sputnik	-274.38	147.50	25	Coal
C4	Colesdalen	BH3-2008	Sputnik	-274.63	122.50	25	Coal
C5	Colesdalen	BH3-2008	Sputnik	-274.84	101.00	18	Mudstone
C6	Colesdalen	BH3-2008	Sputnik	-275.05	80.50	23	Coal
C7	Colesdalen	BH3-2008	Sputnik	-275.28	57.50	23	Coal
C8	Colesdalen	BH3-2008	Sputnik	-275.51	34.50	23	Coal
C9	Colesdalen	BH3-2008	Sputnik	-275.74	11.50	23	Coal
S1	Svea Nord	Mine section	Svea	-	183.0	-	Coal
S2	Svea Nord	Mine section	Svea	-	127.0	-	Coal
S3	Svea Nord	Mine section	Svea	-	83.0	-	Coal
S4	Svea Nord	Mine section	Svea	-	81.5	-	Coal
S5	Svea Nord	Mine section	Svea	-	7.0	-	Coal
S6	Svea Nord	Mine section	Svea	-	Bulk	-	Coal
P1	Pyramiden	Outcrop	-	-	-	-	Coal